Design and development of bioresponsive *pseudo*glucosinolates, non-cytotoxic coumarins with antibiofilm properties and studies towards the synthesis of [13]cytochalasans

Aishi Chakrabarti

GÖTEBORGS UNIVERSITET

Department of Chemistry and Molecular Biology

University of Gothenburg

2024

DOCTORAL THESIS

Submitted for fulfillment of the requirements for the degree of

Doctor of Philosophy in Natural Sciences

Design and development of bioresponsive *pseudo*glucosinolates, non-cytotoxic coumarins with antibiofilm properties and studies towards the synthesis of [13]cytochalasans

Aishi Chakrabarti

ISBN: 978-91-8115-032-2 (PRINT)
ISBN: 978-91-8115-033-9 (PDF)

Department of Chemistry and Molecular Biology

Division of Organic and Medicinal Chemistry

SE-41390 Göteborg

Sweden

This thesis is dedicated to

my beloved parents

Acknowledgements

First and foremost, I would like to express my deepest gratitude to my supervisor, Prof. Dr. Philipp Klahn, for granting me the opportunity to pursue my PhD in his group and for his unwavering trust, guidance, and encouragement throughout these four years. His constant support provided me with an excellent and collaborative environment to grow as a researcher. Thank you for motivating me to keep striving and for helping me become a better scientist.

I am sincerely grateful to my examiner, Prof. Dr. Morten Grötli, for his patience, understanding, and invaluable guidance during my PhD journey. Your support has been instrumental in shaping my work. I would also like to thank my co-supervisor, Prof. Dr. Carl Johan Wallentin, for his active involvement and insightful contributions to my research.

I extend my heartfelt thanks to my opponent, Prof. Dr. Hans-Günther Schmalz, and the members of my thesis committee, Prof. Dr. Berit Olofsson, Prof. Dr. Henrik Sundèn, and Dr. Charlotte Johansson for dedicating their time to evaluate my work and for attending my defense in Gothenburg.

I am deeply thankful to all my research collaborators in Germany and Sweden for their invaluable contributions to my projects. Being part of the Cytolabs consortium was a privilege, and I am grateful for the opportunity to engage in such exciting research.

Special thanks go to the Swedish National NMR Center (SNC) for NMR measurements and the Proteomics Facility at the University of Gothenburg for HRMS analyses. I also want to express my gratitude to Dr. Kerstin Ibrom and Ms. Petra Holba-Schulz for their assistance with NMR measurements, and to Dr. Ulrich Papke for HRMS support at TU Braunschweig.

I would like to thank everyone in the Schulz, Lindel and Wertz group at TU-Braunschweig for their help and everyone at CMB for their warm welcome to the University of Gothenburg and all their help. I had so much fun during our Merck challenges. Thank you, Oscar, for your help.

I would like to thank everyone at the Klahn lab for such a collaborative atmosphere in the lab and all the laughs and fun conversations. Thank you, Claire, Charity and Mervic for making my time both in Braunschweig and Gothenburg so memorable. It would not be possible to do this without your friendship and support. I will always remember our impromptu vacations and our elaborate thanksgiving dinners. You guys truly made this journey so much fun.

I want to thank Ganesh, Rahul, Shivangi, Yogesh and Bhaskar for creating a home away from home. Thank you for making my time in Gothenburg such fun. Cheers to all the fun vacations, movie nights and home cooked meals and most importantly giving me a sense of community. Thank you to all my friends back in India, especially Somsuddha for her blind support and sheer commitment to this friendship.

Lastly, I would like to extend my heartiest appreciation and gratitude to my family, especially my parents, Chirantan and my sister for constantly checking in on me and always believing in me. Without your love and appreciation, I could never have done this. Your constant support and reassurance truly made this possible.

Abstract

The main aim of this thesis was the development of multifunctional *pseudo*glucosinolates (*ps*GSLs) and artificial multivalent glucosinolates (mv-GSLs) as ITC releasing prodrugs. They were utilized as imaging, enzyme labelling and controlled drug delivery tools. Beyond that it also dealt with the development of 6,7-dihydroxycoumarins as non-cytotoxic antibiofilm agents. Lastly, studies towards the total synthesis of [13]cytochalasans (chaetoglobosin B and D) were conducted.

The first chapter focused on the exploration and expansion of the utility of glucosinolate (GSL) inspired compounds for diverse biochemical and therapeutic applications. The first project within this chapter involved the development of enzyme-responsive *pseudo*glucosinolates (*ps*GSLs) as prodrugs for the controlled release of isothiocyanates (ITCs). Incorporating nitroreductase (NTR) and azoreductase (AzoR)-responsive masking groups and a polyethylene glycol (PEG) chain enhanced solubility and functionality of the probes. Further attachment of fluorophores enabled imaging of enzymatic activation. Synthesized via multistep routes, *ps*GSLs demonstrated successful ITC release upon enzymatic cleavage, confirmed by LC-MS and covalent binding of the ITCs were confirmed by SDS-PAGE analysis. *In vivo* validation in *C. elegans* further highlighted the covalent binding of ITCs. These results showcase the potential of *ps*GSLs as flexible tools for imaging, and enzyme dependent labelling of biomolecules.

The second project within this chapter investigated the design and synthesis of *ps*GSL-based antimicrobial prodrugs for controlled drug release upon enzymatic activation. Antibiotics were attached to the *ps*GSL thiohydroximate unit via carbamates, replacing the *O*-sulfonate group. LC-MS analysis showed release of antibiotics upon activation of the antimicrobial prodrugs by nitroreductase (NTR). Although the conversions were slow and incomplete, proof-of-principle for the activity of these probes was provided. Photo-cleavable *ps*GSLs were also developed to bypass enzymatic incompatibility by incorporating *o*-nitrobenzyl moiety for UV-activated drug release at 365 nm. Additionally, azide groups in the *ps*GSL structure allowed for fluorophore attachment or immobilization on surfaces, enabling potential applications as imaging agents or antimicrobial coatings.

The third project within this chapter is introducing the first artificial multivalent glucosinolates (mv-GSLs). Compounds which bear more than one glycosidic thiohydroximate-*O*-sulfonate moiety, potentially amplifying the bioactivities observed for natural monovalent antetypes. Multistep synthesis and biochemical evaluation of mv-GSLs, featuring aliphatic and aromatic cores, were conducted. Myrosinase from *Sinapis alba* efficiently released multivalent isothiocyanates (mv-ITCs) for selected substrates, while specifier protein AtNSP3 facilitated only partial conversion to nitriles. Further optimization of the structures and developing a bigger panel of compounds could facilitate better conversion efficiency with myrosinase.

The second chapter focused on the synthesis and bio evaluation of novel 6,7-dihydroxycoumarin-5-carboxylates (**DHCou** and **4-MeDHCou**) as non-cytotoxic antibiofilm agents. These compounds were synthesized through multistep route in 11% and 8% overall yield respectively. Biological evaluation revealed significant retention of biofilm inhibition activity, with 4-MeDHCou demonstrating efficacy against *Staphylococcus aureus* and *Candida albicans*, while **DHCou** selectively inhibited *C. albicans* biofilms. Importantly, both derivatives exhibited no cytotoxicity against mammalian cell lines, unlike their parent compounds, esculetin (**II-2**) and 4-methylesculetin (**II-29**). Therefore, incorporation of a carboxylate moiety at the C5 position successfully produced compounds with reduced cytotoxicity and retained biofilm activity. These results establish a basis for further exploration of dihydroxycoumarin

derivatives as antibiofilm agents, with potential applications in developing artificial siderophores or antimicrobial drug conjugates.

The third chapter focused on the studies towards the total synthesis of [13]cytochalasans chaetoglobosin B and D. Efforts toward the total synthesis of chaetoglobosin D were centered on the construction of its isoindolone core (**III-148**) and macrocyclic fragment (**III-149**). Initial strategies faced significant challenges, including unsuccessful attempts to form the *Wittig* salt (**III-145**) during the construction of the macrocyclic fragment as well as decomposition of intermediates (**III-122**, **III-128a**, **III-128b**) during *Diels-Alder* reactions for construction of the isoindolone core. These drawbacks necessitated a shift to the synthesis of chaetoglobosin B, employing a revised strategy. Key precursors, diene **III-163** and dienophile **III-171**, were synthesized via multistep routes, though the processes were hindered by low yields and issues with product selectivity, such as inseparable E/Z-isomer mixtures and material loss during intermediate preparation. While the assembly of the isoindolone core (**III-173**) and macrocyclic fragment (**III-180**) was not completed, a new synthetic pathway was proposed, incorporating intramolecular *Diels-Alder* reactions and optimized strategies for coupling and protecting intermediates. Future efforts could refine these routes, improve yields, and enable the total synthesis of chaetoglobosin B and related compounds. This work lays a foundation for advancing synthetic methodologies toward complex natural products.

Sammanfattning

Huvudsyftet med denna avhandling var utvecklingen av multifunktionella *pseudo*glukosinolater (*ps*GSL) och artificiella multivalenta glukosinolater (mv-GSL) som prodrugs för frisättning av isotiocyanater (ITC). Dessa användes som verktyg för avbildning, enzymmärkning och kontrollerad läkemedelsleverans. Utöver detta behandlade arbetet också utvecklingen av 6,7-dihydroxykumarin som icke-cytotoxiska antibiofilmbildande ämnen. Slutligen genomfördes studier mot totalsyntes av [13]cytochalasaner (chaetoglobosin B och D).

Det första kapitlet fokuserade på att undersöka och utöka användningen av glukosinolat (GSL)-inspirerade föreningar för olika biokemiska och terapeutiska tillämpningar. Det första projektet inom detta kapitel innefattade utvecklingen av enzymresponsiva pseudoglukosinolater (*ps*GSL) som prodrugs för kontrollerad frisättning av isotiocyanater (ITC). Genom att inkorporera nitroreduktas (NTR)- och azoreduktas (AzoR)-responsiva skyddsgrupper samt en polyetylenglykolkedja (PEG) förbättrades lösligheten och funktionaliteten hos proberna. Vidare möjliggjorde påkoppling av fluorescerande grupper avbildning av enzymaktivering. *ps*GSL framställdes via flerstegssyntes och visade framgångsrik frisättning av ITC vid enzymatisk klyvning, vilket bekräftades genom LC-MS och SDS-PAGE-analys. Validering av systemet i modelldjuret *C. elegans* underströk ytterligare föreningarnas förmåga att binda kovalent. Dessa resultat visar potentialen hos *ps*GSL som flexibla verktyg för avbildning och enzymberoende märkning av biomolekyler.

Det andra projektet inom kapitlet undersöktes design och syntes av *ps*GSL-baserade antimikrobiella prodrugs för kontrollerad läkemedelsfrisättning vid enzymatisk aktivering. Antibiotika kopplades till *ps*GSLs tiohydroximatenhet via karbamater, där *O*-sulfonatgruppen ersattes. LC-MS-analys visade frisättning av antibiotika vid aktivering av de antimikrobiella prodrugs av nitroreduktas (NTR). Även om omvandlingarna var långsamma och ofullständiga, gavs ett principbevis för aktivitet hos dessa prober. Fotoklyvbara *ps*GSL utvecklades också för att kringgå enzyminkompatibilitet genom att inkludera o-nitrobensylgrupper för UV-aktiverad läkemedelsfrisättning vid 365 nm. Dessutom möjliggjorde azidgrupper i *ps*GSL-strukturen koppling av fluoroforer eller immobilisering på ytor, med potentiella tillämpningar som avbildningsreagenser eller antimikrobiella beläggningar.

Det tredje projektet i kapitlet introducerade de första artificiella multivalenta glukosinolatföreningarna (mv-GSL). Dessa föreningar innehåller fler än en glykosidisk tiohydroximat-*O*-sulfonatgrupp, vilket potentiellt förstärker bioaktiviteten jämfört med naturliga monovalenta föregångare. Multistegsyntes och biokemisk utvärdering av mv-GSL med alifatiska och aromatiska kärnor genomfördes. Myrosinas från *Sinapis alba* frisatte effektivt multivalenta isotiocyanater (mv-ITC) för utvalda substrat, medan specifikationsprotein AtNSP3 endast delvis omvandlade dem till nitriler. Vidare optimering av strukturerna och utveckling av ett större panel av föreningar skulle kunna förbättra omvandlingseffektiviteten med myrosinas.

Det andra kapitlet fokuserade på syntes och biologisk utvärdering av nya 6,7-dihydroxykumarin-5-karboxylater (**DHCou** och **4-MeDHCou**) som icke-cytotoxiska antibiofilmbildande ämnen. Det andra kapitlet fokuserade på syntes och biologisk utvärdering av nya 6,7-dihydroxykumarin-5-karboxylater (**DHCou** och **4-MeDHCou**) som icke-cytotoxiska antibiofilmbildande ämnen. Dessa föreningar syntetiserades via en flerstegsmetod med en total utbyte på 11 % respektive 8 %. Biologisk utvärdering visade att aktiviteten för biofilmshämning bibehölls signifikant, där **4-MeDHCou** visade effekt mot *Staphylococcus aureus* och *Candida albicans*, medan **DHCou** selektivt hämmade biofilmer av *Candida albicans*. Viktigt är att båda derivaten inte visade någon cytotoxicitet mot däggdjurscellinjer, till skillnad från deras modersubstanser, esculetin (**II-2**) och 4-metyleskuletin (**II-29**). Införandet av en karboxylatgrupp på C5-positionen resulterade framgångsrikt i föreningar med minskad cytotoxicitet

och bibehållen biofilmsaktivitet. Dessa resultat utgör en grund för vidare utforskning av dihydroxykumarin-derivat som antibiofilmbildande ämnen, med potentiella tillämpningar för att utveckla artificiella sideroforer eller antimikrobiella läkemedelskonjugat.

Det tredje kapitlet fokuserade på studier mot totalsyntes av [13]cytochalasanerna chaetoglobosin B och D. Ansträngningarna för totalsyntes av chaetoglobosin D koncentrerades på konstruktionen av dess isoindolon-kärna (**III-148**) och dess makrocykliska fragment (**III-149**). Initiala strategier stötte på betydande utmaningar, inklusive misslyckade försök att bilda Wittig-saltet (**III-145**) under konstruktionen av det makrocykliska fragmentet samt nedbrytning av intermediärer (**III-122**, **III-128a**, **III-128b**) under *Diels-Alder* reaktioner för att skapa isoindolon-kärnan. Dessa hinder gjorde det nödvändigt att skifta fokus till syntes av chaetoglobosin B genom en reviderad strategi. Huvudföreningarna dien **III-163** och dienofil **III-171**, syntetiserades via flerstegssyntes. Detta gjordes trots låga utbyten och problem med produktselektivitet, såsom oskiljbara E:Z-isomerblandningar, och materialförlust under förberedelse av intermediat.

Trots att sammansättningen av isoindolon-kärnan (**III-173**) och det makrocykliska fragmentet (**III-180**) inte slutfördes, föreslogs en ny syntesväg som inkluderade intramolekylära *Diels-Alder* reaktioner och optimerade strategier för koppling och skydd av intermediärer. Framtida insatser kan förbättra dessa syntesvägar, öka utbytena och möjliggöra totalsyntes av chaetoglobosin B och relaterade föreningar. Detta arbete lägger grunden för att avancera syntesmetoder för komplexa naturprodukter.

List of publications and manuscripts

I. **Bioresponsive *pseudo*glucosinolates (*ps*GSLs) release Isothiocyanates (ITCs) in the Presence of Nitroreductases**
Aishi Chakrabarti,[#] Claire C. Jimidar,[#] Charity S. G. Ganskow,[#] Mervic D. Kagho,[#] Lorenz Wiese, Michael Zollo, Ulrike Beutling, Leona C. Cesar, Julia Morud, Mark Brönstrup, Stephan A. Sieber, Stephan M. Hacker and Philipp Klahn,* ChemRxiv **2024**, 10.26434/chemrxiv-2024-f8x8z-v2. Preprint, manuscript submitted. [#] Shared first authors.

II. **Synthesis and evaluation of *pseudo*glucosinolates (*ps*GSLs) releasing isothiocyanates (ITCs) in the presence of azoreductases**
Aishi Chakrabarti,[#] Charity S. G. Ganskow,[#] Mervic D. Kagho,[#] Claire C. Jimidar, Lorenz Wiese, Ulrike Beutling, Margarita Seeger, Anett Schallmey, Mark Brönstrup and Philipp Klahn,* *Manuscript,* **2024**. [#] Shared first authors.

III. **Design, synthesis and evaluation of *pseudo*glucosinolate (*ps*GSLs)-*O*-carbamates as bio- and photoresponsive building blocks for molecular drug release systems**
Aishi Chakrabarti, Katharina Pfeiffer, Neslihan Beyazit, Silvana Smits, Stella Nyström, Anne Farewell and Philipp Klahn,***Manuscript,* **2024.**

IV. **Synthesis and evaluation of artificial multivalent glucosinolates (mv-GSLs) releasing multivalent isothiocyanates (ITCs)**
Aishi Chakrabarti,[#] Claire. C. Jimidar,[#] Hedda Schrey, Hoaxuan Zeng, Wera Collisi, Marc Stadler and Philipp Klahn,* *Manuscript,* **2024**. [#] Shared first authors.

V. **Design of non-cytotoxic 6,7-dihydroxycoumarin-5-carboxylates with antibiofilm activity against *Staphylococcus aureus* and *Candida albicans***
Aishi Chakrabarti,[#] Robert Zscherp,[#] Anna P. Lehmann, Hedda Schrey, Hoaxuan Zeng, Wera Collisi and Philipp Klahn,* [#] Shared first authors.
Org. Biomol. Chem. **2023**, *21*, 4744 - 4749.

Author's contributions

I. Contributed to the design and development of the synthesis of NTR responsive *ps*GSL probes (**psGSL$_{PEG}$(NO$_2$)-N$_3$**, **psGSL$_{PEG}$(NO$_2$)-DNSA**), interpreted results and contributed to writing respective parts of the manuscript.

II. Contributed to the design and development of the synthesis of AzoR responsive *ps*GSL probes(**psGSL$_{PEG}$(Azo)-N$_3$**, **psGSL$_{PEG}$(Azo)-BODIPY**), performed fluorescence turn on assays, interpreted results and contributed to writing respective parts of the manuscript.

III. Contributed to the design and development of the synthesis of all analogues of ***ps*GSL-*O*-carbamates** Developed enzymatic and photocleavable evaluation of the probes, interpreted results and wrote the manuscript draft.

IV. Contributed to the design and development of the synthesis of mv-GSLs (**I-161a-e**). Performed qualitative evaluation of the compounds, interpreted results and wrote the manuscript draft.

V. Contributed to the design and development of the synthesis of 6,7-dihydroxycoumarin-5-carboxylates (**DHCou** and **4-MeDHCou**) and wrote respective parts of the manuscript.

Abbreviations

A.baumannii	*Acinetobacter baumannii*
AAC	Aminoglycoside-*N*-acetlyacetyl transferase
ACN	Acetonitrile
ADP	Adenosine diphosphate
AITC	Allyl isothiocyanate
Ala	Alanine
AMR	Antimicrobial resistance
ANT	Aminoglycoside-*O*-nucleotidyl transferases
APH	Aminoglycoside-*O*-phosphotransferases
Arg	Arginine
ATP	Adenosine triphosphate
AzoR	Azoreductase
B. subtilis	*Bacillus subtilis*
BCAT	Branched chain amino acid transferase
BITC	Benzyl isothiocyanate
Boc	*tert*-ButoxycarbonylButoxy carbonyl
BSA	Bovine serum albumin
C. albicans	*Candida albicans*
C. elegans	*Caenorhabditis elegans*
C. violaceum	*Chromobacterium violaceum*
DCI	Carbonyl diimidazole
CH_2Cl_2	Dichloromethane
CsF	Caesium fluoride
CuAAC	Copper-(I) catalyzed azide-alkyne cycloaddition
CYP	Cytochrome P450
DAMP	Damage-associated molecular patterns
DAR	Diels-Alder reaction
DGC	Diguanylate cyclases
DMF	Dimethylformamide
DNA	Deoxyribonucleic acid
E. coli	*Escherichia coli*
EDC·HCl	1-Ethyl-3-(3-dimethylaminopropyl)carbodiimide hydrochloride
EPS	Extracellular polymeric substances
ESP	Epithiospecifier protein
F-actin	Filamentous actin
f-GSL	Fluorescent glucosinolates
FMN	Flavin mononucleotide
FMO	Flavin monooxygenase
G-actin	Globular actin
GC-MS	Gas chromatography-mass spectometry
GDP	Gross domestic product
Gln	Glutamic acid
Glu	Glutamine
GMP	Guanylate monophosphate
GSL	Glucosinolate
GT	Glucotransferase
GTR	Glucosinolate transport receptor
HEPES	4-(2-hydroxyethyl)-1-piperazineethanesulfonic acid
His	Histidine
HIV	Human immunodeficiency virus

HOBt	Hydroxy benzotriazole
IBX	2-Iodoxybenzoic acid
Ile	Isoleucine
IPMDH	Isopropyl malate dehydrogenase
IPMP	Isopropyl malate isomerase
ITC	Isothiocyanate
LC-MS	Liquid chromatography-mass spectrometry
Leu	Leucine
M. hiemalis	*Mucor hiemalis*
M. smegmatis	*Mycobacterium smegmatis*
MAM	Methylthioalkylmalate synthase
MDR	Multidrug resistant
MeOH	Methanol
MES	2-Morpholinoethanesulphonic acid
Met	Methionine
MRSA	Methicillin resistant *Staphylococcus aureus*
mv-CN	Multivalent nitrile
mv-GSL	Multivalent glucosinolate
mv-ITC	Multivalent isothiocyanate
NADH	Nicotinamide adenine dinucleotide
NHS	*N*-hydroxy succinimide
NMP	1-(1-naphthylmethyl)-piperazine
NRPS-PKS	Nonribosoimal peptide synthetase-polyketide synthase
NSP	Nitrile specifier protein
NTR	Nitroreductase
o-HPA	*o*-hydroxyphenyl acetaldehyde
o-HPAA	*o*-hydroxyphenyl acetic acid
o-HPLA	*o*-hydroxyphenyl lactic acid
o-HPPA	*o*-hydroxyphenyl propionic acid
P. aeruginosa	*Pseudomonas aeruginosa*
P. anomala	*Pichia anomala*
PAMP	Pathogen-associated molecular patterns
PAβN	Phenyl-arginine β-naphthylamide
PBP	penicillin binding proteins
PDE	Phosphodiesterase
PEG	Polyethylene glycol
PEITC	Phenylethyl isothiocyanate
Phe	Phenylalanine
*ps*GSL	*pseudo*glucosinolates
QS	Quorum sensing
R. glutinis	*Rhodoturula glutinis*
RNA	Ribonucleic acid
S. aureus	*Staphylococcus aureus*
S. pombe	*Schizosaccharomyces pombe*
SAM	*S*-adenyosyladenosyl-L-methionine
Ser	Serine
SOT	Sulfurtransferase
TBDPSCl	*tert*-Butyldiphenylsilyl chloride
TBSCl	*tert*-Butyldimethylsilyl chloride
TEMPO	2,2,6,6-Tetramethylpiperidinyloxyl2,2,6,6-tetramethylpiperidin-1-yl)oxidanyl
TFP	Thiocyanate forming protein
THF	Tetrahydrofuran

TLR	Toll-like receptors
TRIS	Tris(hydroxymethyl)aminomethane
Trp	Tryptophane
Tyr	Tyrosine
UV	Ultraviolet
Val	Valine
VRSA	Vancomycin-resistant *Staphylococcus aureus*

Table of Contents

I. Synthesis and evaluation of artificial glucosinolates as bioresponsive tool compounds

I-1. From plant defense to human health: An overview of glucosinolate function and application.

I-1.1. Natural glucosinolates

Glucosinolates (GSLs) are a large group of naturally occurring secondary metabolites found in plants of the economically valuable *Brassicaceae* family which includes cabbage, broccoli, horseradish, cauliflower, white or black mustard. These compounds are part of the natural plant-herbivore defense system.[1–3] GSLs are characterized by a glycosidic thiohydroximate-*O*-sulfonate moiety, which features an alkyl, aryl, or indolyl side chain. The structural diversity of the R group (Figure I-1) arises from the biosynthetic amino acid precursor of the GSL.[4–6] Naturally occurring GSLs can be distributed over three main classes:

1. aliphatic GSLs, in which the sidechain is derived from Alanine (Ala), Methionine (Met), Isoleucine (Ile), Valine (Val) or Leucine (Leu),
2. aromatic GSLs, in which the side chain is derived from Tyrosine (Tyr) and Phenylalanine (Phe),
3. and lastly indolyl GSLs in which the sidechain is derived from Tryptophane (Trp).[5]

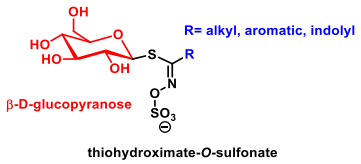

Figure I-1: Core structure of glucosinolates.

The distribution and concentration of GSLs are dependent on the part of the plant (e. g. roots, leaves or seeds), the developmental stage of the plant and other external factors like temperature or soil type.[7] For example in *Arabidopsis thaliana* the seeds and fruit were found to have the highest diversity of GSLs whereas young leaf florets had higher GSL concentration than older leaves.[8] In case of kale, low temperatures showed a reduction in GSL content.[9] Studies with *Raphanus sativus* indicated that GSL concentrations were higher in young leaves, likely due to the dilution effect caused by leaf expansion.[10] GSLs are stored in the vacuoles of sulfur rich *S*-cells, which exist in the periphery of vascular bundles in plant tissue.[11] Hydrolysis of GSLs is catalyzed by β-thioglucosidases, otherwise known as myrosinases, which are present in myrosin cells. They are distributed along leaf vasculature as seen in *Arabidopsis thaliana*.[7,12]

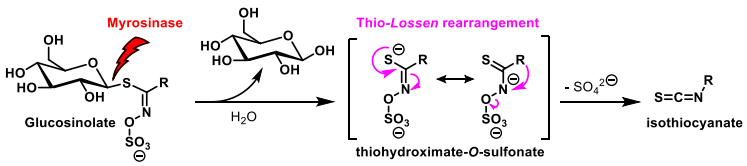

Scheme I-1: GSL-myrosinase defense system in *Brassicaceae* family.

GSLs are part of the natural herbivore defense system. Upon tissue damage, through chewing or herbivore feeding, GSL and myrosinase get mixed and the thioglucosidic bond in the GSLs are hydrolyzed (Scheme I-1) by these β-thioglucosidases, leading to the formation of an unstable thiohydroximate-*O*-sulfonate aglycone.[1,13,14] This aglycone undergoes a thio-*Lossen* rearrangement to form an isothiocyanate (ITC) as the active species, which predominantly act as a feeding deterrent against herbivores.[15,16]

I-1.1.2. Biosynthesis of Glucosinolates

Given the interesting role of GSLs in the natural plant defense system, significant research has been conducted to elucidate the biosynthetic pathway of GSLs in plants. This research identifies three main stages in the formation of GSLs (Scheme I-2).[5,17] The first stage is the chain elongation via insertion of a methylene group into the aliphatic amino acid side chain, the second stage involves metabolic transformations for the development of the core structure and the third stage includes secondary modifications of the amino acid side chain.[18,19]

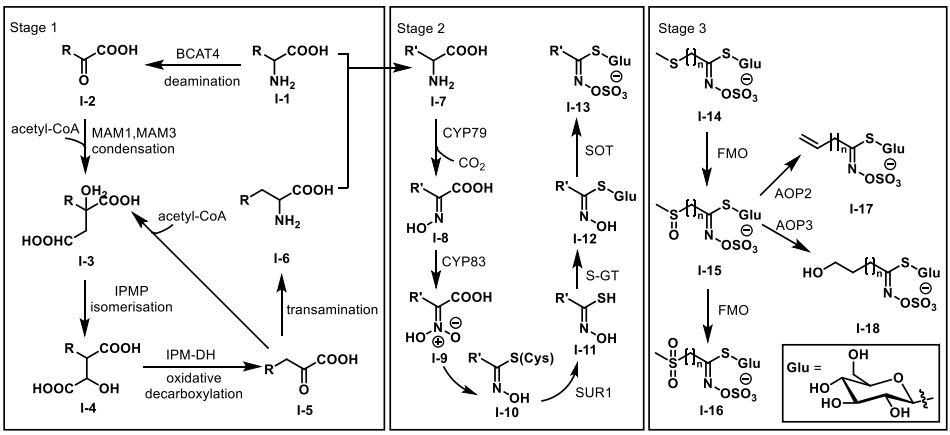

Scheme I-2: Biosynthetic pathway for formation of GSLs in plants.

The process of chain elongation is initiated via deamination of the parent amino acid **I-1** by a branched chain amino acid transferase (BCAT) giving the 2-oxo-acid **I-2** This then undergoes condensation with acetyl-CoA in the presence of a methylthioalkylmalate synthase (MAM) to give the corresponding 2-malate derivative **I-3**. Depending on the number of elongation cycles, different MAM synthases catalyze this step.[19] An isomerization in the presence of an isopropyl malate isomerase (IPMP) gives the 3-malate derivative **I-4**.[20,21] It is then transformed to the methylene elongated 2-oxo acid **I-5** via a oxidative decarboxylation in the presence of a isopropyl malate dehydrogenase (IPM-DH).[22,23] A final transamination gives the elongated amino acid **I-6**. From this stage it can re-enter the methylene insertion pathway or go straight to the GSL core formation step.

In the second stage, the methylene elongated amino acid **I-7** is oxidized to the corresponding aldoxime **I-8**, which is catalyzed by different enzyme families depending on the amino acid precursor.[17] For aromatic GSLs having Phe and Tyr , the oxidation to aldoxime is catalyzed by cytochrome P450 dependent monooxygenases from the CYP79 family.[24–26] For indoylyl GSLs having Trp the formation of indole acetaloxime is also the first step in their biosynthesis.[17] This is catalyzed by plasma membrane

bound peroxidases.[27] For aliphatic GSLs the oxidation to aldoxime for all chain elongated Met derivatives are catalyzed by CYP79F1 and CYP79F2 specifically catalyzes transformations of only long chain Met derivatives.[28,29] The aldoxime **I-8** is then oxidized further into an activated nitrile or aci-nitro substrate **I-9** by cytochrome P450 of the CYP83 family,[30–33] followed by subsequent non-enzymatic conjugation with cysteine[34] or glutathione[35] as a sulfur donor to give **I-10**. The formation of thiohydroximate **I-11** from *S*-alkyl thiohydroximate **I-10** is catalyzed by SUR1, which is a *C-S* lyase.[36] Further, *S*-glucosylation of thiohydroximate **I-11**, catalyzed by glucotransferases (S-GT) of the UGT74 family gives the desulfoglucosinolate **I-12**.[37,38] Finally, the desulfoGSL is sulfated by sulfotransferases (SOT) to produce the core structure of glucosinolates **I-13**.[39]

Further structural diversity is introduced in the final stage which involves secondary modifications to the side chain or the glucose moiety of GSLs. They can undergo a variety of transformations namely, glucosylation, desaturation, methoxylation, oxidation, sulfation and hydroxylation.[40] The chain elongated GSLs derived from Met are especially subject to further transformations.[5] Both short and long chain aliphatic GSLs can undergo *S*-oxygenation to produce alkylsulfinyl GSL **I-15** and alkylsulfonyl GSLs **I-16**. This step is catalyzed by $FMO_{GS\text{-}OX1\text{-}5}$, which is a *Brassicaceae* specific sub group of flavin monooxygenases (FMO).[41,42] The *S*-oxygenated species can undergo further modification to a corresponding alkenyl GSL **I-17**, catalyzed by AOP2,[43] or a hydroxyalkyl GSL **I-18** catalyzed by AOP3,[44] which are 2-oxoglutarate dependent dioxygenases.[45] The late stage biosynthesis contributes to the structural diversity of naturally occurring GSLs.[5]

I-1.1.3. Enzymic hydrolysis in GSL-myrosinase system

GSLs are most commonly known to form ITCs as the active moiety upon exposure to myrosinase. After cleavage of the thioglucosidic bond by myrosinase, the unstable aglycone undergoes a thio-*Lossen* rearrangement to produce ITCs as the active metabolite. This is the natural herbivore defense mechanism employed by plants of the *Brassicaceae* family (Scheme I-1).[1,46,47]

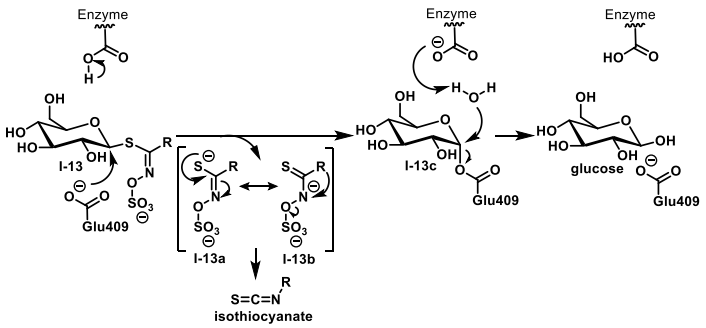

Scheme I-3: Schematic representation of myrosinase catalytic activity.

Myrosinase has been reported to show similarities with *O*-glycosidases with the exception that one of the acid/base glutamic acid residues is replaced by glutamine.[48] It can be concluded that the mechanism of myrosinase will be similar to that of *O*-glycosidases, involving the retention of the anomeric configuration followed by a hydrolysis with double displacement.[49] Firstly, the glucose moiety recognition is brought about by formation of six hydrogen bonds. The glycosyl-enzyme complex disrupts the salt bridge between Glu409 and Arg95. Glu409 then changes its conformation and

covalently binds to the anomeric carbon center of **I-13** (Scheme I-3). The sulphate group is also responsible for site recognition through interaction with Arg194 and Arg259 residues. Next, the aglycone moiety is eliminated as **I-13a**, which tautomerizes to **I-13b** and undergoes thio-*Lossen* rearrangement to form ITC. Meanwhile, an enzymic residue abstracts a proton from a water molecule facilitating the nucleophilic attack on the anomeric carbon center of **I-13c** leading to deglycosylation and subsequent release of a glucose molecule.[50]

Many plants in the *Brassicaceae* family contain specifier proteins as auxiliary components of the GSL myrosinase system. In order to circumvent the feeding deterrence property, certain insects employ specifier proteins to transform the ITCs into other metabolites. For example the cabbage white butterfly (*Pieris rapae*) uses nitrile specifier protein to redirect the unstable aglycone towards formation of nitriles and excrete them.[51] Besides nitriles the unstable aglycone moiety is capable to form various other metabolites like epithiocyanates, and thiocyanates in presence of specifier proteins (Scheme I-4).

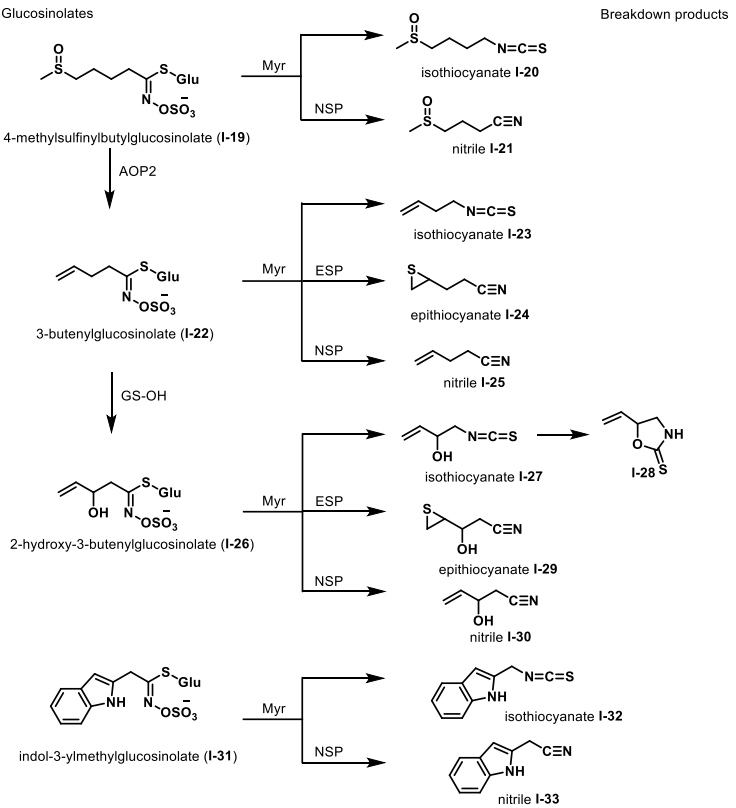

Scheme I-4: Examples of glucosinolate breakdown products in presence Myrosinase (Myr), nitrile specifier protein (NSP) and epithio specifier protein (ESP).[52]

Specifier proteins, first discovered in *Crambe abyssnica*,[53] are able to impact hydrolysis products without having any direct hydrolytic activity.[52] Epithiospecifier proteins (ESPs) expressed in *Escherichia coli*. were able to catalyze the hydrolysis of alkenyl GSL **I-26** to epithiocyanates **I-29**, non-alkenyl GSL **I-**

19 to nitrile **I-21** and indole GSLs **I-31** into nitrile **I-33**.[54–56] Moreover, nitrile specifier proteins isolated from *Arabidopsis thaliana* (AtNSPs), were able to redirect hydrolysis towards nitriles irrespective of the GSL sidechain.[57,58] Thiocyanate forming proteins (TFPs) responsible for formation of thiocyanates are limited to sinigrin (**I-45**) (Figure I-5) and few other aromatic GSLs and quite rare.[47,59–61]

I-1.1.4. Bioactivities of glucosinolate breakdown products

The breakdown products of GSLs have a plethora of bioactivities. ITCs primarily act as a feeding deterrent towards soil borne as well as plant pathogens and pests.[15,16] Since most ITCs from naturally occurring GSLs are volatile, they show potential to be used as bio fumigants against plant pathogens.[62] Additionally, volatile allyl isothiocyanate (AITC) (**I-49**) originating from sinigrin (**I-45**) present in *Brassica napus* was found to attract a pollen-feeding sap beetle (*Meligethes aeneus*), and the seed weevil, (*Ceuthorhynchus assimilis*).[63] GSL rich green manures made from seed meal of *Brassicaceae* used in rotation show activity against pathogens as well as suppression of weed formation.[64,65] Seed waste water of *Boscia senegalensis* rich in methyl ITCs show allelopathic activity leading to disruption in germination of weeds.[66]

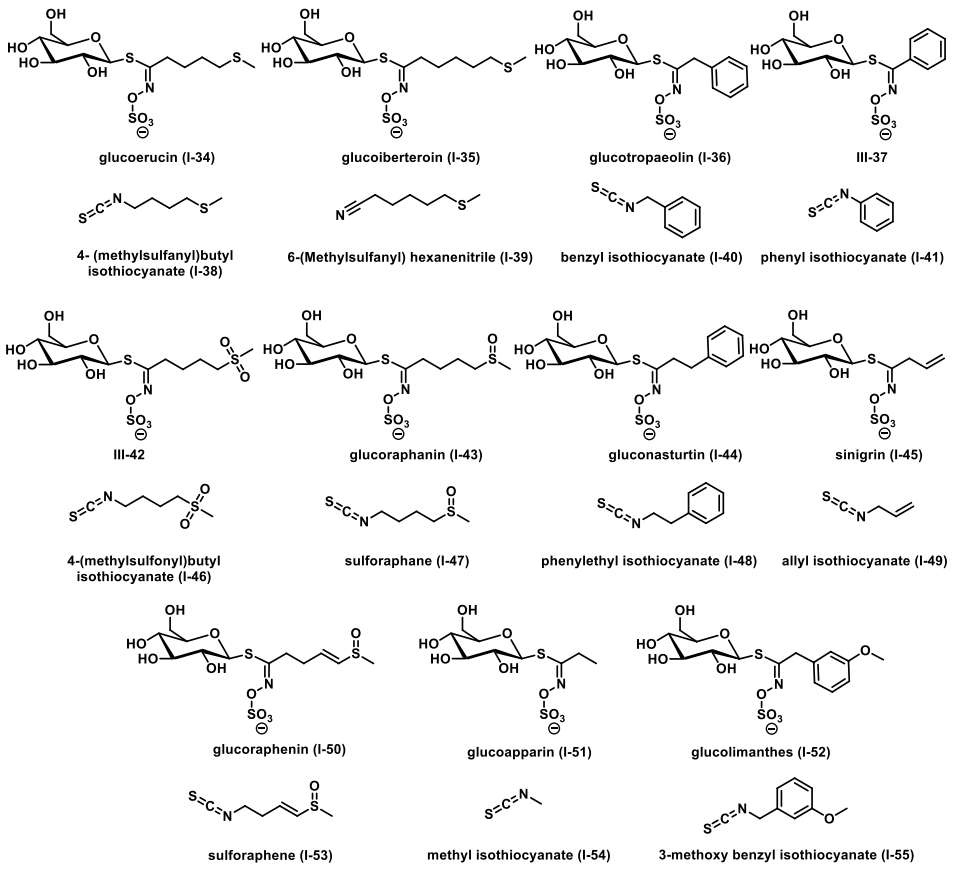

Figure I-2: Selected naturally occurring GSLs and their respective ITCs.

The antimicrobial activity of GSL derived ITCs (Figure I-2) have also been well investigated.[67–69] Volatile extracts containing 4-(methylsulfanyl)butyl isothiocyanate (**I-38**) from glucoerucin (**I-34**), sulforaphane (**I-47**) from glucoraphanin (**I-43**), 4-(methylsulfonyl)butyl isothiocyanate (**I-46**) were shown to inhibit growth in *Escherichia coli*, *Pseudomonas aeruginosa* and *Staphylococcus aureus.*[69–74] Allyl isothiocyanate (AITC) (**I-49**) and phenylethyl isothiocyanate (PEITC) (**I-48**) were shown to disrupt intracellular potassium transport in *Escherichia coli* and *Staphylococcus aureus*.[67] AITC and benzyl isothiocyanate (BITC) (**I-40**) also showed antimicrobial activity against Methicillin resistant *Staphylococcus aureus* (MRSA)[75] and *Campylobacter. Jejuni*,[76] along with increased antimicrobial activity against biofilm forming multidrug resistant (MDR) *Pseudomonas aeruginosa*.[77] Phenyl isothiocyanate (PITC) (**I-41**) derived from *Sinapsis alba* seeds showed growth inhibitory activity against intestinal bacteria like *Clostridium difficile* and *Clostridium perfringens*.[78] For *Mycobacterium tuberculosis*, 6-(Methylsulfanyl) hexanenitrile (**I-39**) from glucoberteroin (**I-35**) showed selective antimicrobial activity against MDR stains.[62]

ITCs also show anti-cancer activity for example, AITC (**I-49**) from sinigrin (**I-45**) derived from mustard seeds showed inhibition of cell proliferation in human bladder cancer cell lines (UM-UC-3) by arresting the cell cycle.[79] BITC (**I-40**) extracts from *Carica papaya* also showed anti-proliferative activity against lunger cancer cell lines (H69)[80] Furthermore, methyl isothiocyanate (MITC) (**I-54**) from glucoapparin (**I-51**) showed antiproliferative activity on human adenocarcinoma cell lines (HT29) by inhibition of the nuclear factor κB (NF-κB),[81]causing morphological changes, cell apoptosis and general cytotoxicity.[82–88] The observed effects maybe dose dependent or even heightened via synergistic effect of various compounds [80,89,90]

Additionally, sulforaphane (**I-47**) and sulforaphene (**I-52**) (Figure I-2) have been widely studied for its antioxidant, anti-inflammatory, and chemoprotectiveproperties, demonstrating efficacy against various types of cancer, such as prostate, breast, liver, and colon cancer.[91] For example, sulforaphene derived from radish seeds were shown to induce apoptosis in esophageal cancer cells (Eca109).[92] Sulforaphene (**I-52**), extracted from *Raphanus sativus* seeds, have been shown to reduce colitis symptoms in model mice and strengthen the epithelial barrier by covalently binding to a conserved cysteine residue within the NES (nuclear export signal) binding site of CRM1.[83] It also showed significant growth inhibition of breast cancer cell lines (MCF-7) and hepatocarcinoma cells (Hep-G2)[82] Sulforaphane (**I-47**) has shown to inhibit DNA replication causing double strand breaks in prostate cancer cells (PC-3).[93] It has detoxifying effects and enzyme metabolization such as inhibition of cyclooxygenase 2 in colon cancer cell lines (HT-29).[94] It has also been shown to upregulate glutathione-S-transferase in rat prostate cancer cell lines.[95–97] Additionally, prolonged ingestion of sulforaphane rich broccoli has been shown to have reduced risk of prostate cancer,[98] chemoprotective activity in melanoma patients,[99] reduction in serum insulin and increased insulin resistance in type II diabetes patients, decreased risk of cardiovascular diseases[100] and enhanced bronchoconstrictor effect against major or mild asthma.[101] Sulforaphane has also been reported to reduce UV-B induced inflammation in mouse models.[102] Furthermore, 3-methoxybenzyl isothiocyanate (**I-55**) from glucolimanthes (**I-52**) extracted from *Limmanthes alba* also show photoprotective and chemoprotective properties against UV-B radiation.[102]

I-1.1.5. Synthesis of GSLs

The wide range of biological activities of GSLs and their derived ITCs make GSLs interesting target compounds for synthesis. The synthesis of GSLs has been explored by a limited number of research

groups, where they have approached the retrosynthetic disconnection in two major routes (Scheme I-5). It can be classified as the oxime disconnection route, which is the most predominantly used route, and the anomeric carbon disconnection route.

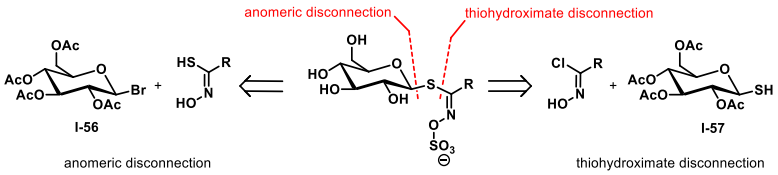

Scheme I-5: Retrosynthetic analysis of GSLs.

The synthesis of GSLs was pioneered by the work of *Ettlinger* and *Lundeen*, where they synthesized glucotropaeolin (**I-36**) (Scheme I-6).[103] The synthesis was initiated with the generation of a *Grignard* reagent from benzyl chloride (**I-58**), which was then reacted with carbon disulfide and hydroxylamine to give thiohydroxamic acid **I-59** in an overall yield of 33% over three steps. A nucleophilic substitution on the anomeric carbon of α-bromoglucopyranose tetraacetate (**I-57**) under basic conditions provided thiohydroximate **I-60** in 47% yield. Lastly *O*-sulfation of the thiohydroximate **I-60** with sulfur trioxide-pyridine complex, followed by deprotection of the acetate group in presence of methanolic ammonia and purification through anion exchange resin gave glucotropaeolin (**I-36**) in 46% yield and an overall yield of 7% over 7 steps. Although this was the first reported synthetic route for any GSL, it had its own drawbacks, namely poor overall yield of 7%, the poor yield of 33% of thiohydroxamic acid **(I-59**) due to the instability and decomposition while purification,[104] and the low yielding nucleophilic substitution at the anomeric carbon. Thus, this particular disconnection route has not been explored further.

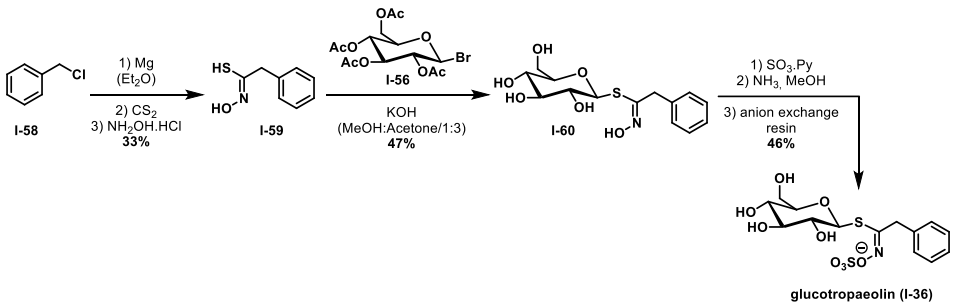

Scheme I-6: Synthesis of glucotropaeolin by *Ettinger* and *Lundeen*.[103]

The more commonly used thiohydroximate disconnection can be further subdivided into the nitronate, nitrovinyl and aldoxime routes based on the formation of the oxime intermediate (Scheme I-7).

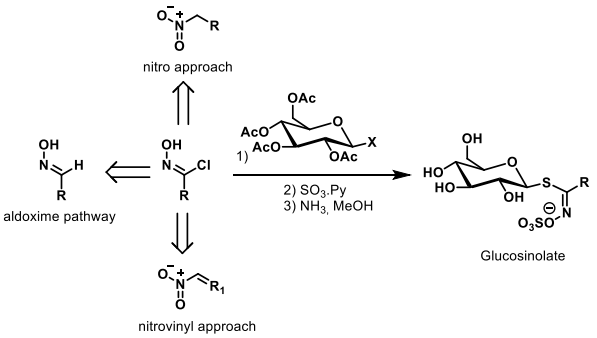

Scheme I-7: Different approaches towards synthesis of thiohydroximate.

The nitronate route was first explored by *Benn* and *Ettlinger* in 1965 for the synthesis of sinigrin **(I-45)** (Scheme I-8).[103] The synthesis was initiated with 4-nitro-but-1-ene (**I-61**) which was converted into nitronate **I-62** to facilitate the subsequent nucleophilic chlorination in presence of lithium chloride and HCl to give chloro oxime **I-63**. This avoided any side reactions via possible formation of reactive halonium species with the double bond in the alkenyl side chain. Then **I-63** was coupled with the 1-thio-β-D-glucose tetraacetate (**I-57**) under basic conditions to give thiohydroximate **I-64**. A final *O*-sulfonation with sulfur trioxide pyridine complex to form the thiohydroximate-*O*-sulfonate and subsequent deprotection of the acetate groups with methanolic ammonia led to the formation of sinigrin (**I-45**).

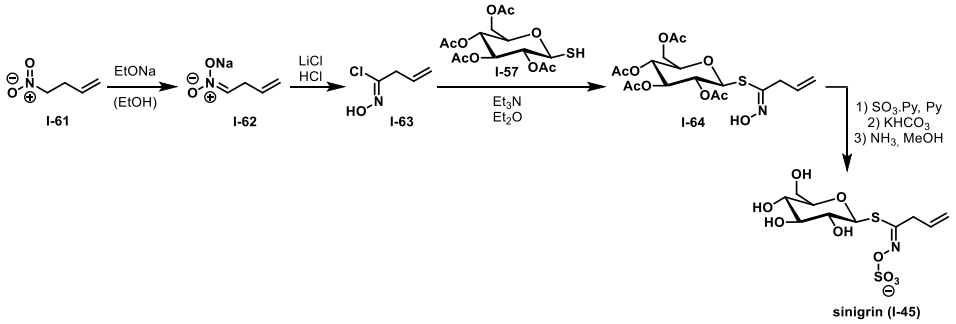

Scheme I-8: Synthesis of sinigrin by *Benn* and *Ettinger*.[103]

Later in 1968, a similar approach was taken for the synthesis of progrotin (**I-69**) and epiprogroitin (**I-70**) *by Kjaer et al*. (Scheme I-9),[105] where a nitronate **I-66** was synthesized from **I-65** in presence of ethanoate. Then the nucleophilic addition of chlorine was facilitated by thionyl chloride to give **I-67**. Next, 1-thio-β-D-glucose tetraacetate (**I-57**) was coupled to **I-67** to give thiohydroximate **I-68**. Finally, *O*-sulfonation and deprotection of acetate groups gave a racemic mixture of progrotin (**I-69**) and epiprogroitin (**I-70**).

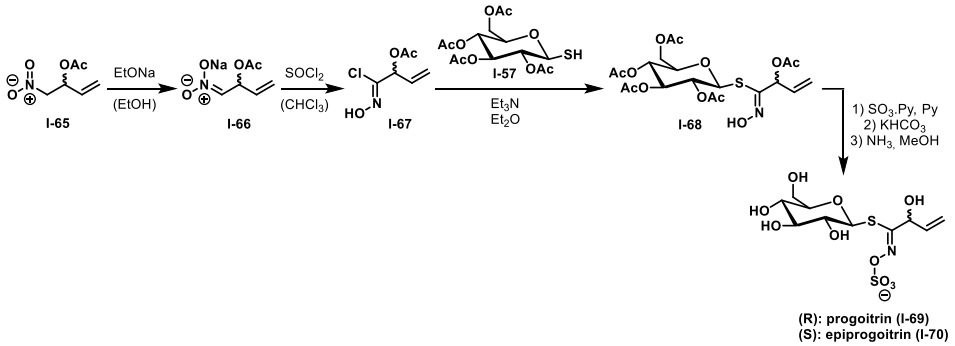

Scheme I-9: Synthesis of progoitrin and epiprogoitrin by *Kjaer et al*.[105]

The nitrovinyl route is a more recent development pioneered by *Kulkarni*, who developed an efficient one step conversion of nitrovinyl substrates (**I-72**) into chloro oxime (**I-73**) (Scheme I-10).[106] In this route aldehydes **I-71** are effectively converted to corresponding nitrovinyl derivatives **I-72**. It is then activated with *Lewis* acid titanium tetrachloride in presence of triethysilane as the hydride source, to generate the chloro oxime **I-73** in good yields. **I-73** is then coupled with **I-57** under basic conditions followed by *O*-sulfonation and deprotection of acetate groups to give the desired GSLs.

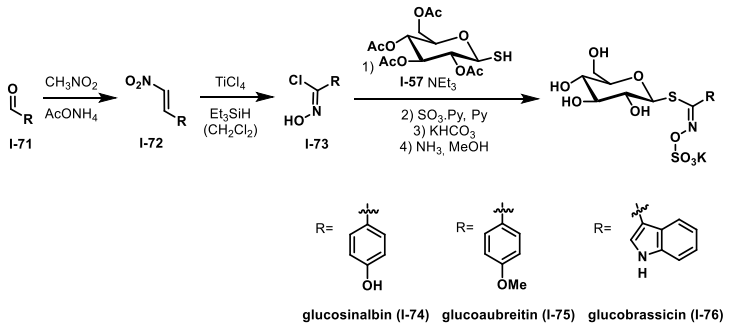

Scheme I-10: Synthesis of glucosinalbin and glucoaubreitin via nitrovinyl pathway by *Rollin et al*.[107]

This route was utilized by *Rollin et al.* for the synthesis of aromatic GSLs glucosinalbin (**I-74**) and glucoaubretin (**I-75**) (Scheme I-10).[107] Indolyl GSL glucobrassicin (**I-76**) was also prepared with the same method (Scheme I-10).[107] The free proton of the indole had to be protected as an acetate for optimal results under harsh conditions of the *Kulkarni* method.[108,109] The nitrovinyl route is not only an improvement regarding yields as compared to the nitronate route but also provides an efficient one pot step for conversion of vinyl nitrates to chloro oximes.

Nevertheless, the aldoxime route is the most used in the field of glucosinolate synthesis (Scheme I-11), which was developed by *Benn* and co-workers in the 1960s, who synthesized various aliphatic GSLs like glucoapparin (**I-51**)[110] and glucoputranjivin (**I-80**)[111] as well as aryl aliphatic GSLs like glucotropaelin (**I-36**),[112] glucosinalbin (**I-74**) and glucoaubreitin (**I-75**).[113] In this route a chloro oxime intermediate (**I-78**) is synthesized from a corresponding oxime (**I-77**) via radical chlorination in the presence of *N*-bromo succinimide *in situ* and subsequently coupled with 1-thio-β-D-glucose tetraacetate (**I-57**) in the

presence of triethylamine to give the (Z)-thiohydroximate (**I-79**) with complete stereo control. Further *O*-sulfonation followed by removal of acetate groups leads to GSL formation.

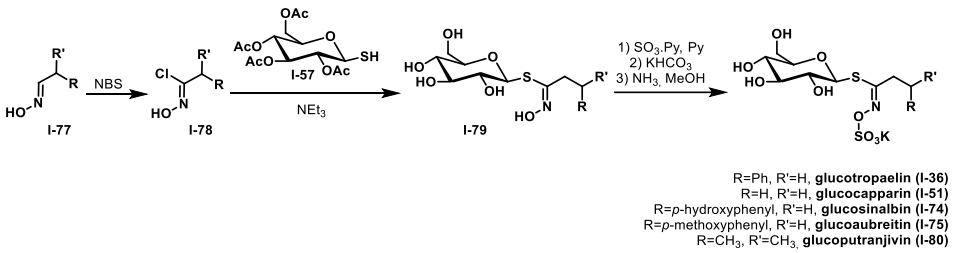

Scheme I-11: Synthesis of selected GSLs by *Benn et al*. via aldoxime route.

I-1.1.6 Artificial glucosinolates

The synthesis of naturally occurring GSLs were significantly developed from 1960s-1980s. To further explore the structural diversity and biological properties of GSLs, the synthesis of various artificial GSLs were developed following that period. For example, one of the first reports of such an artificial GSL was that of radio labelled glucobrassin in 1993 by *Chevolleau et al.*, synthesized via the nitrovinylation route (Scheme I-12).[114] 5-bromoindole (**I-81**) was coupled to (*E*)-*N,N*-dimethyl-2-nitroethen-1-amine (**I-82**) to give 5-bromo-3-(2-nitrovinyl)indole (**I-83**) which was then converted to its corresponding chloro oxime (**I-84**) in 3 steps. Then the coupling with **I-57** followed by *O*-sulfonation gave thiohydroximate-*O*-sulfonate **I-85**. Finally, palladium-catalyzed tritiolysis followed by removal of acetate groups gave radiopure tritium labelled glucobrassicin (**I-86**). It was then used to study the enzymatic, thermal and chemical breakdown of indole GSLs.[115]

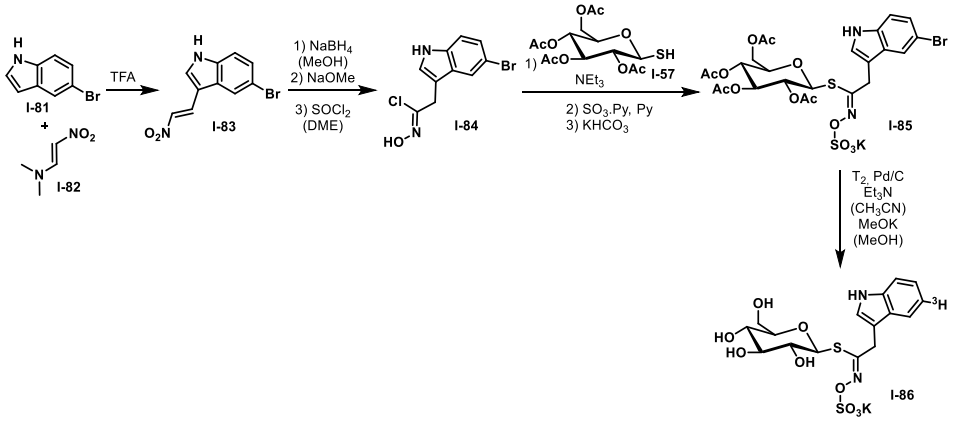

Scheme I-12: Synthesis of tritium-labelled glucobrassicin by *Chevolleau et al*.[114]

Further structural diversity was explored by modifications in the pyranose moiety to investigate the GSL-myrosinase defense system. For example, deoxyglucosinolates (Figure I-3) were synthesized to evaluate the significance of hydroxyl groups on the glucose.[116] Synthetic derivatives, including 2-, 3-, 4-, and 6-deoxyglucotropaeolins and their glucobrassicin analogs, were utilized to demonstrate that the absence of a hydroxy group at the C-2 position results in the inhibition of myrosinase activity.[117]

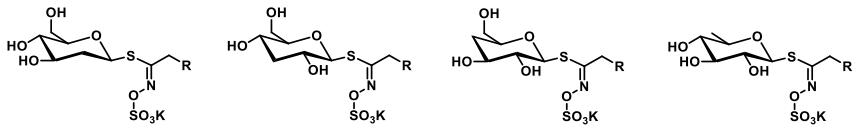

Figure I-3: Examples of deoxy GSLs.

Modifications at the anomeric carbon center of the glucose moiety gave rise to further GSL analogues (Figure I-4) like α-GSL analogues of glucotropaelin (**I-36e**) and glucobrassicin (**I-76e**), which have a α-D-pyranose instead of the usual β-D-pyranose.[118] Seleno analogues (Figure I-4) of glucotropaeolin (**I-36f**) and glucocapparin (**I-51a**) were also synthesized and shown to be hydrolyzed by myrosinase.[119,120]

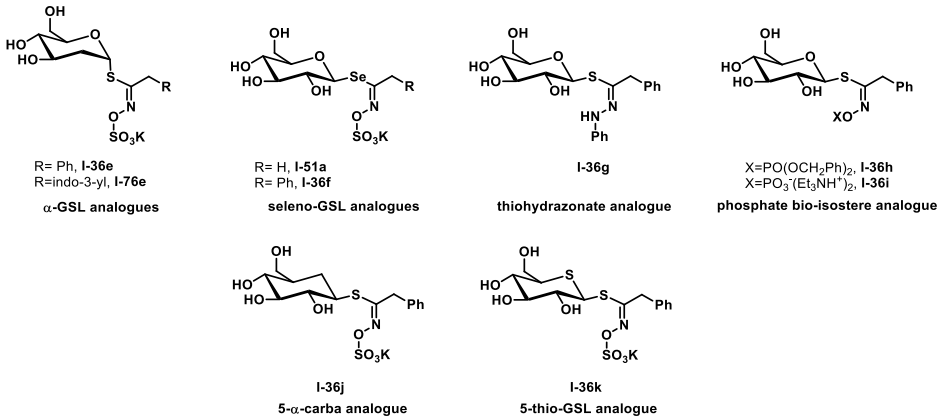

Figure I-4: Examples of artificial GSLs.

Additionally, GSLs having a non-natural aglycone (Figure I-3) were also synthesized like thiohydrazonates (**I-36g**) where the *O*-sulfonate is replaced with a hydrazone moiety,[121] phosphate biostere (**I-36h**, **I-36i**) where the *O*-sulfonate is replaced with different phosphonates and was shown to be recognized as a substrate for myrosinase.[122] 5α-carba-GSL (**I-36j**)[123] and non-hydrolysable 5-thio-GSL (**I-36k**) were synthesized to study the effect of removal of the oxygen at C5 of the pyranose moiety on substrate recognition and inhibitory effects on myrosinase.[124]

More recent reports of artificial GSLs include the synthesis of bifunctional GSL-mannoside glycoconjugates by *Tatibouët et al.* in 2018 (Scheme I-13).[125] Here, they have combined the structural recognition by myrosinase as well as interaction with lectin due to the conjugated FimH ligand. The synthesis started with glycosylation of *p*-bromophenol (**I-87**) with either **I-57** or **I-95** to give per-acetylated mannose derivatives **I-88a** and **I-88b**. A palladium catalyzed *Suzuki-Miyaura* coupling with boronate **I-94** and subsequent *Henry* condensation afforded the nitrovinyl derivatives **I-90** and **I-90b**, which was previously developed in their group.[126] The nitrovinyl derivative **I-90** was then subjected to *Kulkarni* conditions to form the thiohydroximate **I-91**. Next, the *O*-sulfonation and subsequent deprotection of the acetyl groups under basic conditions gave the final conjugates **I-92** and **I-93**. The FimH ligand didn't disrupt hydrolysis with myrosinase while retaining good affinity and recognition towards lectin. This opened the potential of artificial GSLs having further interesting bioactivity.

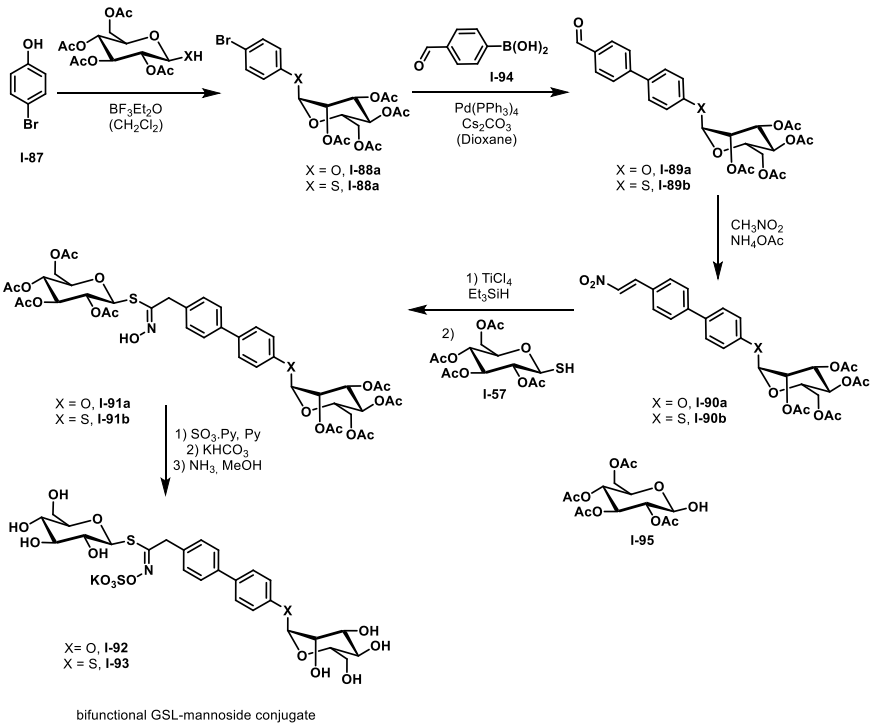

Scheme I-13: Synthesis of bifunctional GSL-mannose conjugate by *Tatibouet et al.*

In 2019, further development was made by *Klahn et al*. by synthesizing a fluorescent GSL via aldoxime route and utilizing copper(I)-mediated azide-alkyne click chemistry (CuAAC) (Scheme I-14).[1] The synthesis was initiated from 4-chlorobutanol (**I-96**) undergoing substitution with an azide to give **I-97**. Further oxidation with IBX gave aldehyde **I-98** followed by formation of azido-oxime **I-99**. Next, it was coupled with the 1-thio-β-D-glucose tetraacetate (**I-57**) under basic conditions, followed by formation of thiohydroximate-*O*-sulfonate and removal of the acetate groups with methanolic ammonia to give **GSL-N_3**. Finally, a copper catalyzed click reaction with **I-100** gave **GSL-BODIPY**. It was shown to be a good substrate for myrosinase as well as specifier protein AtNSP3 from *Arabidopsis thaliana*.

In a collaborative effort *Klahn, Nour Eldin, Tatibouët* and coworkers developed novel fluorescent GSLs (Scheme I-15) which were shown to be actively transported via glucosinolate transporters (GTR). The probes **GSL-B-DNS** and **GSL-B-NBD** were synthesized from oxime-*O*-sulfonate **I-95**, where the azide moiety was first reduced to give corresponding amine **I-96**. A nucleophilic substitution with the respective fluorescent dyes **I-102a** and **I-103** gave the final compounds **GSL-B-DNS** and **GSL-B-NBD** in 55% and 71% yield respectively. **GSL-A-DNS** was synthesized from **GSL-N_3** via copper catalyzed click with **I-97** in 18% yield. These probes were transported through GTR1 and GTR2 and were competing for a common binding site. Such probes could also be used as tracers for monitoring GSL transport *in vivo*.

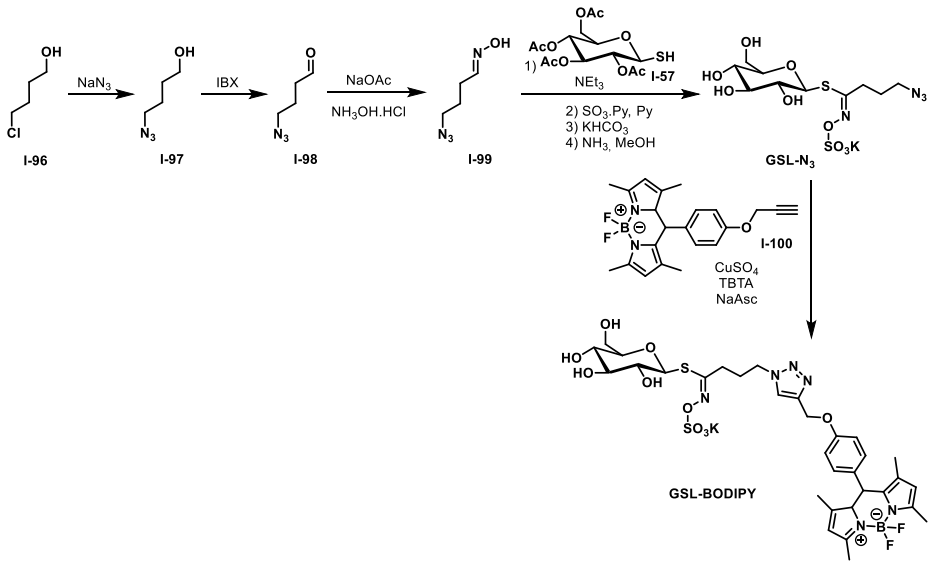

Scheme I-14: Synthesis of fluorescent glucosinolate GSL-BODIPY by *Klahn et al*.

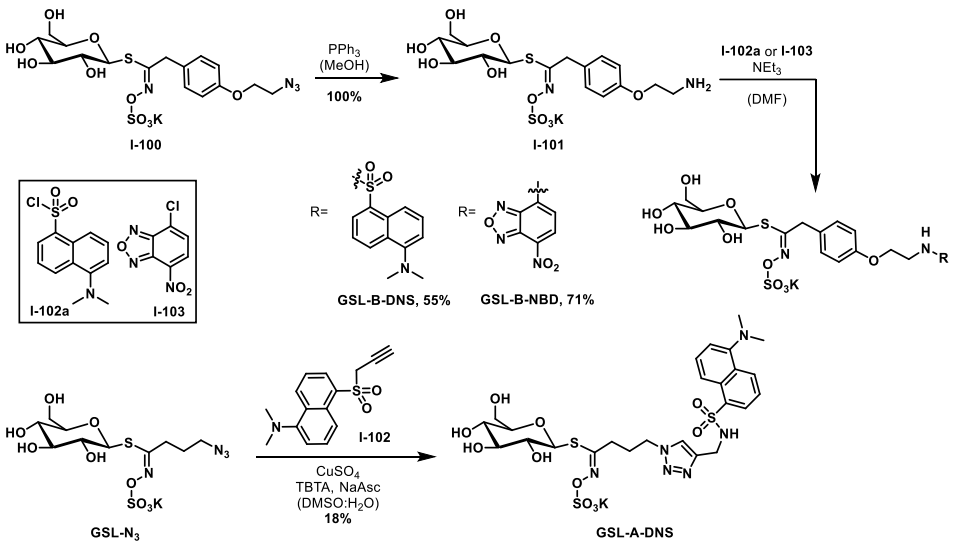

Scheme I-15: Synthesis of fluorescent GSL as GTR active probes.

The biological activities of the breakdown products of GSLs, especially ITCs, have been well established.[15,16,128–132,62,63,75,77,78,91,103,127] However, a critical challenge remains in fully utilizing the biological potential of ITCs due to their poor pharmacokinetics, including sensitivity to hydrolysis and strong electrophilicity, which limits their stability and bioavailability.[133–135] Therefore, GSLs as natural prodrugs of ITCs have been explored as synthetic targets. These efforts have led to extensive synthesis of both natural[94,136–138] and artificial GSLs.[114,116,120–122,125,139–141] However, the application of these natural ITC-prodrugs are limited to plant systems as mammals do not express myrosinase. This

highlights the need for synthetic prodrugs to be responsive to non-canonical enzymes and thereby mimic the natural GSL-myrosinase system while overcoming these limitations. Addressing these gaps in knowledge and technology is essential to unlocking the therapeutic potential of ITCs and expanding the scope of applications for GSL derivatives in medicine and agriculture.

I-2. Aims and Objectives

I-2.1. Development of nitroreductase and azoreductase responsive *pseudo*glucosinolates (*ps*GSLs)

Isothiocyanates (ITCs) exhibit a diverse array of bioactivities, yet their potential as therapeutic agents are constrained by their inherent instability, as they are prone to hydrolysis and react readily with nucleophilic targets due to their high electrophilicity. To address these limitations, nature employs glucosinolates (GSLs) as prodrugs for ITCs. GSLs enable controlled ITC release through enzymatic hydrolysis by myrosinase, a thioglucosidase enzyme found in plants. However, the absence of myrosinase in mammalian systems restricts the application of natural GSLs in therapeutic contexts.

Inspired by nature's design, the concept of *pseudo*glucosinolates (*ps*GSLs) was developed as a prodrug strategy to mimic the enzymatic release of ITCs by leveraging non-canonical enzymes as triggers. The design of artificial GSLs was envisaged, in which the thioglycosidic trigger was substituted with a chemically masked *para*-aminobenzylthiol unit (Scheme 16).[142] Upon enzymatic or chemical removal of the masking group, *ps*GSLs were intended to undergo an auto-immolative 1,6-elimination of the free *p*-aminobenzylthiol moiety. This process would lead to the formation of an aromatic iminium ion and a thiohydroximate-*O*-sulfonate intermediate, followed by the eventual generation of ITCs through a thio-*Lossen* rearrangement. Thereby, *ps*GSLs could serve as prodrugs and tool compounds for ITC release, with their responsiveness designed to be adaptable to different non-canonical enzymes and chemical triggers.

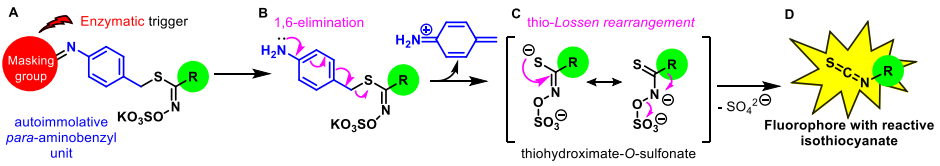

Scheme I-16: Bioresponsive mechanism of the release of ITCs from *ps*GSLs. **A**: enzymatic action on psGSL masking group, **B**: auto-immolative 1,6-elimination of the *p*-aminobenzylthiol moiety, **C**: thio-*Lossen* rearrangement of the thiohydroximate-*O*-sulfonate intermediate, **D**: release of ITC.

To prove the design and concept of *ps*GSLs, nitroreductase (NTR, NfsB from *E. coli*) and azoreductase (AzoR from *E. coli*) were specifically chosen as enzymatic targets for this work. NfsB produced by *E. coli* belongs to the family of flavin-based oxidoreductases that catalyze the reduction of nitro compounds to amines through stepwise transformations involving nitroso and hydroxylamine intermediates, utilizing nicotinamide adenine dinucleotide hydrogen (NADH) and flavin cofactors.[143] This enzymatic mechanism allows bacteria to metabolize toxic nitro-aromatic compounds.[144] NTR-responsive *p*-aminobenzyl derived masking groups strategies have previously been explored to synthesize fluorescent probes for detection of *E. coli*. and *S. aureus* related bacterial infections.[145] It has also been used to synthesize NTR-responsive prodrugs for localized drug release in hypoxic cellular conditions.[146] AzoR, on the other hand, catalyzes the reduction of azo bonds in the presence of NADH and flavin cofactors.[147] AzoR has been exploited in designing prodrugs that target gut microbiota.[148,149]

For the design of NTR responsive *ps*GSLs the usual thioglucosidase trigger was substituted by a *p*-nitro benzyl moiety (Scheme I-17B). A similar strategy utilizing a self-immolative *p*-amino benzyl moiety for the design of possible prodrugs was reported in 1981.[150] It was expected that upon enzymatic removal of the masking group in presence of NfsB, the probe would undergo breakdown as previously described

in Scheme I-16, resulting in the formation of ITCs as the active metabolite. Furthermore by attaching a fluorophore via click chemistry on the thiohydroximate side chain, as previously developed in the *Klahn* group,[1] it was expected to produce a fluorescent ITC after enzymatic activity. This could then be used for labelling nucleophilic targets such as proteins.

Similarly, for development of AzoR responsive prodrugs, the β-D-pyranose moiety would be substituted with an azobenzene moiety (Scheme I-17B). It would then undergo breakdown as shown in Scheme I-16, where the reduced masked azo trigger would undergo 1,6-elimination producing an aromatic iminium ion and a thiohydroximate-*O*-sulfonate intermediate followed by a thio-*Lossen* rearrangement to produce an ITC. The primary aim of this work was to synthesize the planned *ps*GSLs and provide proof of principle for the possible enzymatic cleavage in presence of NfsB and AzoR respectively. It was envisaged to further explore the possible applications such as labeling of proteins via covalent binding of the resulting fluorescent ITCs.

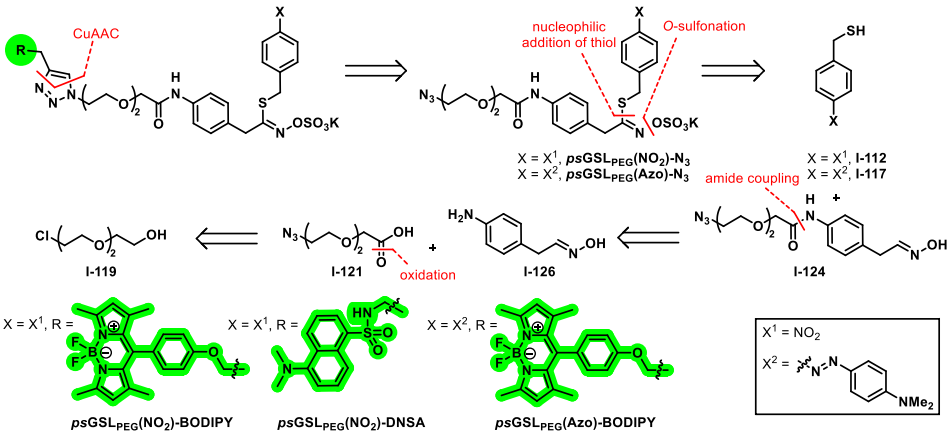

Scheme I-17A: Retrosynthesis of NTR and AzoR responsive *ps*GSLs.

The proposed synthesis was designed (Scheme I-17A) with the incorporation of a polyethylene glycol (PEG) chain into the aglycone, to enhance the water solubility of the envisioned probes, leveraging the well-established property of PEG chains to increase the hydrophilicity of drug conjugates.[151] The fluorescent *ps*GSLs were intended to be synthesized via a copper(I)-mediated click reaction between ***ps*GSL$_{PEG}$(NO$_2$)-N$_3$** and ***ps*GSL$_{PEG}$(Azo)-N$_3$** with a fluorophore containing a terminal alkyne (Scheme I-17A). The precursor ***ps*GSL$_{PEG}$(NO$_2$)-N$_3$** and ***ps*GSL$_{PEG}$(Azo)-N$_3$** was planned to be synthesized through nucleophilic substitution of the oxime **I-124** with the corresponding thiol (**I-112**, **I-117**). The intermediate oxime **I-124** was to be derived from commercially available 2-(2-(2-chloroethoxy)ethoxy)ethan-1-ol (**I-119**) via substitution with sodium azide, followed by IBX oxidation and subsequent hydroxylamine formation.

The retrosynthesis of both the NTR-and AzoR-responsive masking groups were planned as shown in Scheme I-17B. For the NTR-responsive unit, *p*-nitrobenzyl thiol (**I-112**) was envisioned to be synthesized from *p*-nitrophenol (**I-109**) in three steps. Similarly, for the AzoR-responsive unit, (E)-(4-((4-(dimethylamino)phenyl)diazenyl)phenyl)methanethiol (**I-117**) was planned to be synthesized from commercially available *p*-aminobenzyl alcohol (**I-113**) in a four-step process. This included the formation of the diazonium intermediate from aniline (**I-113**), followed by reaction with N,N'-

dimethylaniline to yield the diazo compound (**I-114**), which would then undergo conversion to the thiol derivative in three subsequent steps.

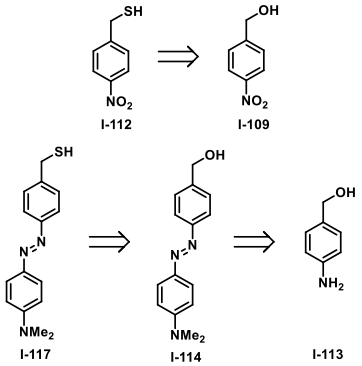

Scheme I-17B: Retrosynthesis of NTR and AzoR responsive masking groups

I-2.2. Development of *ps*GSL based antimicrobial prodrugs

The aim of this part was to expand the structural scope of *ps*GSLs and explore if the *O*-sulfonate moiety in *ps*GSLs could be replaced by an antimicrobial drug attached via carbamate formation as shown in Scheme I-18. It was envisaged that upon exposure to NTR, the *p*-nitrobenzyl moiety would be reduced to the corresponding *p*-aminobenzyl moiety (Scheme I-18A), which would then undergo a self-immolative 1,6-elimination to form an unstable thiohydroximate-*O*-carbamate moiety (Scheme I-18B)

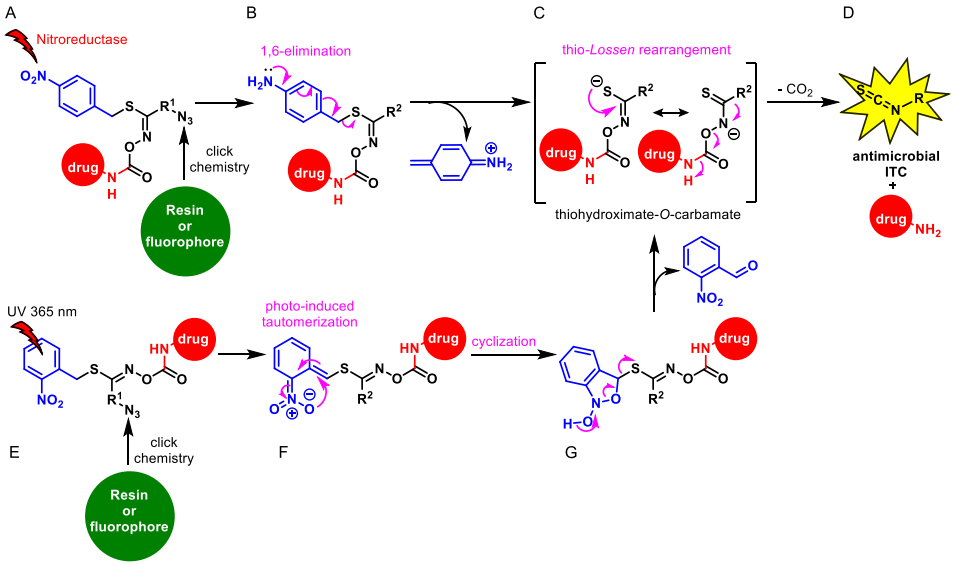

Scheme I-18: Drug activation of *ps*GSL based antimicrobial prodrugs. **A:** enzymatic action of NTR on *ps*GSL based antimicrobial prodrugs, **B**: auto-immolative 1,6-elimination of the *p*-aminobenzylthiol moiety, **C**: thio-*Lossen* rearrangement of the thiohydroximate-*O*-sulfonate intermediate, **D**: release of

ITC and drug, **E:** irradiation of 365 nm on *ps*GSL based antimicrobial prodrugs, **F:** photo-induced tautomerization and subsequent cyclization, **G:** elimination of *o*-nitrobenzaldehyde.

It was expected that the intermediate would undergo a thio-*Lossen* rearrangement thereby releasing an ITC and the antimicrobial drug (Scheme I-18C-D). This would enable the controlled release of antibiotics in the presence of an enzyme such as NTR. We envisioned that these probes held the potential to study the synergistic effect of antibiotics along with the released ITC on different pathogens. Such compounds could serve as linkers in antimicrobial hybrid drugs or siderophore drug conjugates.[152]

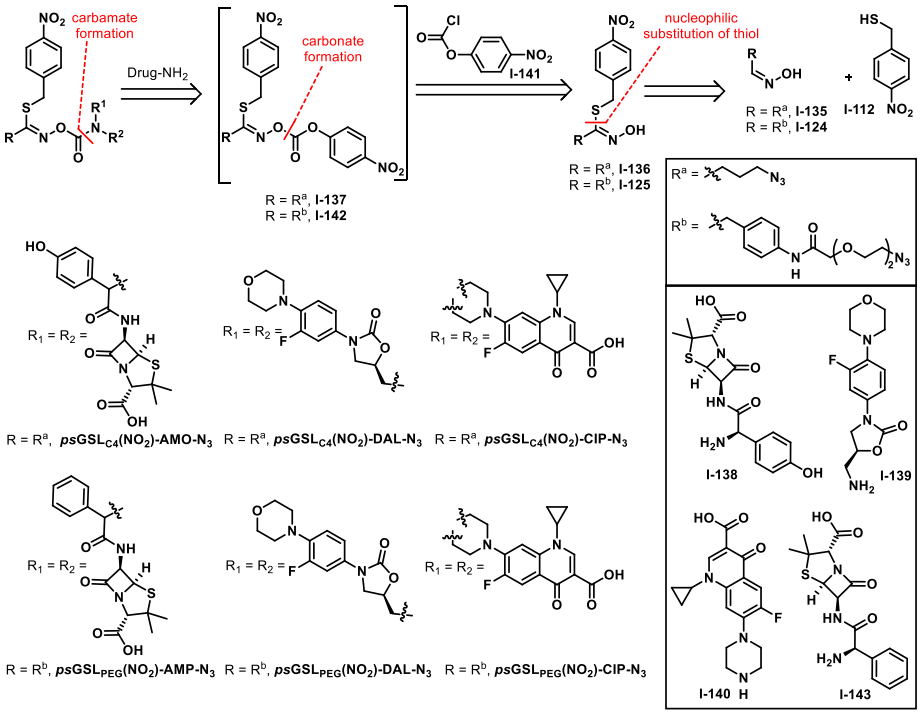

Scheme I-19A: Retrosynthesis of NTR responsive *ps*GSL based antimicrobial prodrugs

The proposed synthesis of NTR responsive *ps*GSL based antimicrobial prodrugs were designed as shown in (Scheme I-19A). The *ps*GSL based antimicrobial prodrugs ***ps*GSL$_{C4}$(NO$_2$)-AMO-N$_3$**, ***ps*GSL$_{C4}$(NO$_2$)-DAL-N$_3$** and ***ps*GSL$_{C4}$(NO$_2$)-CIP-N$_3$**, bearing a C4 backbone were intended to be synthesized via a carbamate formation from an intermediary carbonate (**I-137**) in the presence of the respective antibiotics, amoxicillin (**I-138**), deacetyl linezolid (**I-139**) and ciprofloxacin (**I-140**) respectively. The carbonate (**I-137**) was planned to be accessed from oxime **I-135** and thiol **I-122** by first formation of a thiohydroximate followed by formation of carbonate **I-137** with *p*-nitrobenzyl chloroformate (**I-141**). The *ps*GSL based antimicrobial prodrugs ***ps*GSL$_{PEG}$(NO$_2$)-AMO-N$_3$**, ***ps*GSL$_{PEG}$(NO$_2$)-DAL-N$_3$** and ***ps*GSL$_{PEG}$(NO$_2$)-CIP-N$_3$**, bearing a PEG linker were designed to produce more hydrophilic analogues. The planned synthesis was similar where a nucleophilic substitution with thiol **I-122** on oxime **I-124** would form a thiohydroximate, which would be transformed into carbonate **I-142** in presence of **I-144**. A final

carbamate formation with ampicillin (**I-143**), deacetyl linezolid (**I-139**) and ciprofloxacin (**I-140**) would give the prodrugs.

Furthermore, the development of photocleavable *ps*GSL based antimicrobial prodrugs were also planned where the *p*-nitrobenzyl group was replaced with a photocleavable *o*-nitro benzyl moiety (Scheme I-18). It was expected that irradiation of UV light at 365nm would initiate a photo-induced tautomerization (Scheme 18E-F), facilitating a cyclization leading to the formation of an intermediary five membered ring (Scheme I-18G). Further elimination of *o*-nitrobenzaldehyde would give an unstable thiohydroximate-*O*-carbonate, which would undergo a subsequent thio-*Lossen* rearrangement to release the antibiotic and ITC (Scheme I-18C-D). This would allow further expansion of the functionality of *ps*GSLs to potentially not be affected by substrate binding affinity or steric hindrance in the active site of enzymes.

For the synthesis of the UV (365 nm) sensitive *ps*GSL based antimicrobial drug conjugates ***ps*GSL$_{C4}$(*o*-NO$_2$)-CIP-N$_3$** and ***ps*GSL$_{C4}$(*o*-NO$_2$)-DAP-N$_3$** were designed as previously described. A carbamate formation from an intermediary carbonate (**I-137**) in the presence of the respective antibiotics, daptomycin and ciprofloxacin (**I-140**). The carbonate (**I-137**) was planned to be accessed from oxime **I-135** and commercially available photocleavable *o*-nitobenzylthiol (**I-146**) by first formation of a thiohydroximate followed by formation of carbonate **I-145** with *p*-nitrobenzylchloroformate (**I-141**).

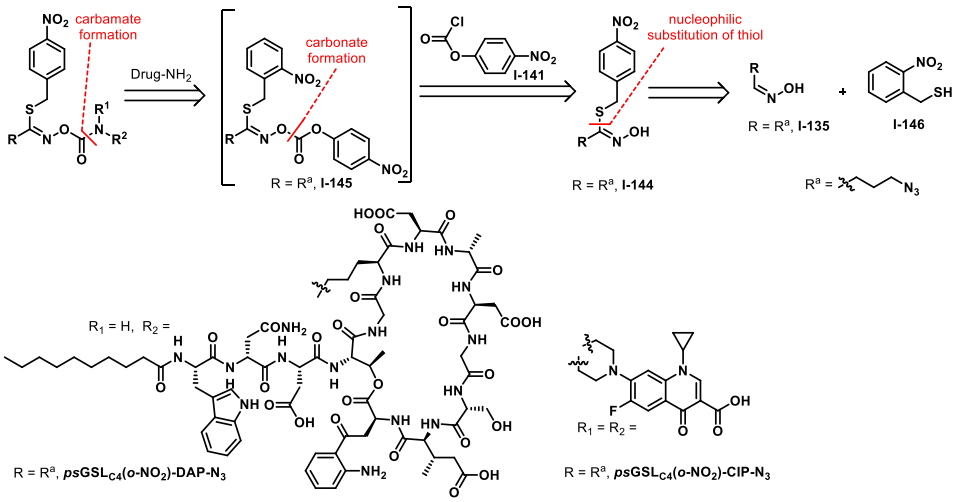

Scheme I-19B*:* Retrosynthesis of UV (365 nm) responsive *ps*GSL based antimicrobial prodrugs.

Moreover, the terminal azide in the GSL side chain of all probes was planned to be used to attach either a fluorophore for imaging purposes or they could be immobilized onto surfaces enabling the development of potential antimicrobial surfaces.

I-2.3. Development of multivalent glucosinoltes (mv-GSLs)

Considering the interesting biological activities of ITC, there has been some significant development in the field of artificial glucosinolates. Previous developments in the *Klahn* lab have shown the synthesis of f-GSLs (Scheme I-14), which are still accepted as myrosinase substrates. Furthermore, selected f-GSLs developed at the *Klahn* lab in collaboration with *Tatibouët et al.* (Scheme I-20) have also been

shown to be actively transported through GTR1 and GTR2. In 2000, *Rollin et al.* reported the first synthesis of glucomoringin (**I-104**) which is a major GSL found in *Moringa oleifera* (Figure I-5). It had an additional sugar moiety on the side chain of glucosinalbin (**I-74**) (Scheme I-10) Later in 2010, they expanded on the structural diversity to produce various other *O*-glycosylated derivatives (Figure I-5). They utilized a nitrovinyl derivative (**I-103**) to generate glucomorigin (**I-104**), galactose derivative (**I-106**), glucose derivative (**I-106**), mannose derivative (**I-107**) and cellobiose derivative (**I-108**).

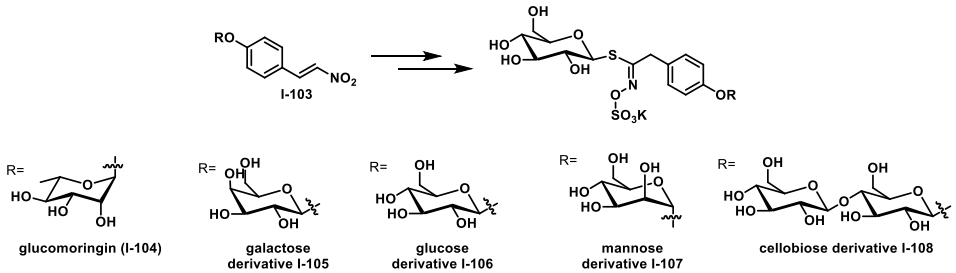

Figure I-6: Structures of *O*-glycosylated derivatives of glucosinalbin by *Rollin* et al.

These structures having an additional sugar moiety was the inspiration for the development of multivalent glucosinolates (mv-GSLs) where it was planned to introduce an additional β-D-pyranose moieties on bivalent or trivalent oxime-*O*-sulfonate backbones. It was envisioned that upon enzymatic cleavage of the thio-glucosidase bond by myrosinase, it would generate either a bivalent or trivalent unstable aglycone which would then undergo thio-*Lossen* rearrangement to give multivalent ITCs as active metabolites as shown in Scheme I-18.

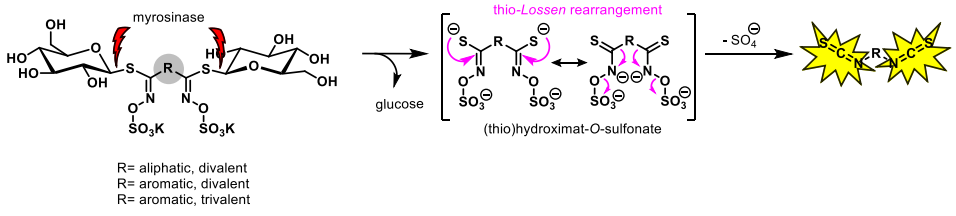

Scheme I-20: Breakdown mechanism of mv-GSLs.

The retrosynthesis of the mv-GSLs were planned as shown in Scheme I-21. The mv-GSLs (**I-161a-e**) would be accessed via a nucleophilic substitution by tetra-*O*-acetyl-1-thio-β-D-glucopyranose (**I-57**) to an intermediary chloro oxime obtained from the respective oximes (**I-158a-e**). The oximes (**I-158a-e**) would be accessed from commercially available bis or tri aldehydes (**I-157a-e**).

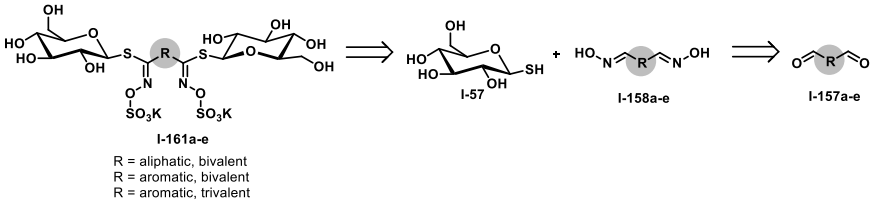

Scheme I-21: Retrosynthesis of mv-GSLs

It was planned to provide proof-of-principle of enzymatic cleavage of the mv-GSLs with myrosinase from *Sinapsis alba*. Beyond that, it is known that within the *Brassicaceae* family, many plants produce specifier proteins (SPs) as auxiliary components of the glucosinolate (GSL) metabolic pathway.[52,61,153] These proteins guide the enzymatically released aglycone toward the formation of less reactive metabolites, including nitriles,[57,58] epithionitriles[56] and thiocyanates.[47,61]. Interestingly, specialized herbivores such as *Pieris rapae* larvae (cabbage white butterfly, *Lepidoptera Pieridae*) utilize nitrile specifier proteins (NSPs) to bypass the GSL-myrosinase defense system, allowing them to feed on *Brassicales* plants.[51] Therefore, for this work it was also planned to evaluate the potential of these mv-GSLs to form multivalent nitriles in presence of nitrile specifier protein (AtNSP3) obtained from *Arabidopsis thaliana.* This would provide an insight into the functionality of these mv-GSLs as propesticides. Furthermore, it was envisaged to investigate whether these multivalent ITCs had any enhanced biological properties like antimicrobial activity or activity against biofilms. This would broaden the scope to explore the potential applications of mv-GSLs.

I-3. Results and Discussion

I-3.1 Development of bioresponsive glucosinolates (*ps*GSLs) releasing isothiocyanantes (ITCs) in the presence of nitroreductases and azoreductases.

As previously discussed in section I-2.1., the primary aim of this work was the synthesis of novel *pseudo*glucosinolates (*ps*GSLs) as enzyme-responsive prodrugs and to utilize them for evaluation of controlled release of ITCs. The synthetic strategy centered on the incorporation of nitroreductase (NTR)- and azoreductase (AzoR)-responsive masking groups into the *ps*GSL backbone. A PEG chain was integrated to enhance hydrophilicity, improving the water solubility of the resulting prodrugs. The *ps*GSLs were designed to also include a fluorophore, enabling monitoring of ITC release via fluorescence imaging. The synthesis involves multistep routes, including the preparation of NTR- and AzoR-responsive thiol intermediates (**I-112**, **I-117**), and the subsequent assembly of *ps*GSLs via nucleophilic substitution and copper(I)-mediated click reactions. This work aimed to establish a proof-of-concept for enzymatic activation of the synthesized *ps*GSLs while laying the groundwork for their application in bioimaging and drug delivery.

I-3.1.1 Synthesis of NTR and AzoR responsive *ps*GSLs

To prepare the NTR and AzoR masking groups the respective thiols **I-112** and **I-117** were synthesized respectively as shown in Scheme I-22. The synthesis for the NTR responsive thiol was initiated by subjecting *p*-nitrobenzyl alcohol (**I-109**) to an *Appel* reaction in the presence of tetrabromo methane and triphenyl phosphine to form the corresponding *p*-nitrobenzyl bromide (**I-110**) in 95% yield. A nucleophilic substitution of the bromide in **I-110** in presence of potassium thioacetate provided **I-111** in 97% yield. A final cleavage of the thioacetate moiety under acidic conditions in presence of methanolic HCl provided the desired thiol **I-112** in 97% yield and a good overall yield of 89% over 3 steps.

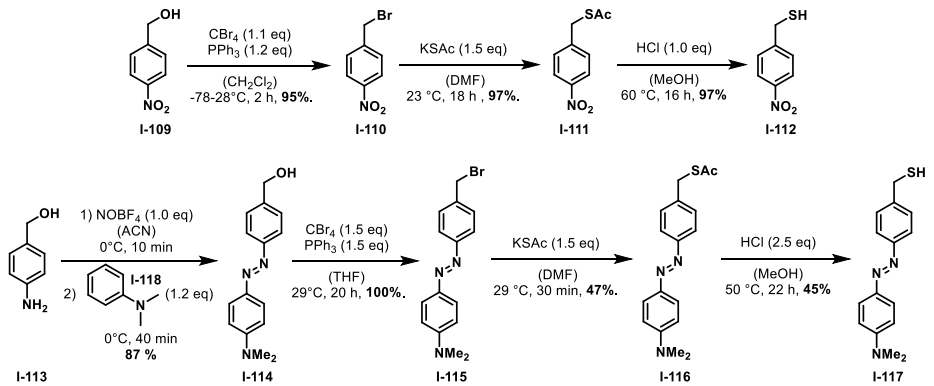

Scheme I-22: Synthesis of NTR and AzoR responsive thiols.

The AzoR-responsive thiol was synthesized starting from *p*-aminobenzyl alcohol (**I-113**), where a diazotation in the presence of nitrosonium tetrafluoroborate in acetonitrile at 0°C and subsequent coupling with *N*,*N*-dimethylaniline (**I-118**) in a diazo coupling gave azobenzene (**I-114**) in 87% yield over two steps. The substitution of the primary alcohol of **I-114** with an *Appel*-type reaction gave the corresponding bromide(**I-115**) in quantitative yield. Next, a nucleophilic substitution of the bromide in

presence of potassium thioacetate gave the corresponding thioacetate **I-116** in 47% yield. Finally, cleavage of thioacetate moiety with methanolic HCl in degassed methanol gave the desired thiol with the azobenzene moiety **I-117** in 45% yield and an overall yield of 18% over 4 steps. The thiols **I-112** and **I-117** were stored at -20°C under argon to prevent further disulfide formation.

The synthesis of the azido oxime **I-124** backbone (Scheme I-23) was initiated from commercially available 2-(2-(2-chloroethoxy)ethoxy)ethanol (**I-119**) where a nucleophilic substitution in presence of NaN_3 at 110°C gave the corresponding azide **I-120** in 95%. Subsequent *Jones* oxidation led to the formation carboxylic acid **I-121** in 92% yield. Next, an amide coupling via pre activation of **I-121** with isobutyl chloroformate followed by nucleophilic attack with 2-(4-aminophenyl)ethanol (**I-127**) gave **I-122** in 63% yield. Subsequent oxidation of **I-123** with IBX gave aldehyde **I-124** in 86% yield, which was swiftly transformed into the corresponding oxime **I-124** in presence of hydroxylamine hydrochloride and sodium acetate in 98% yield and an overall yield of 46% over 5 steps.

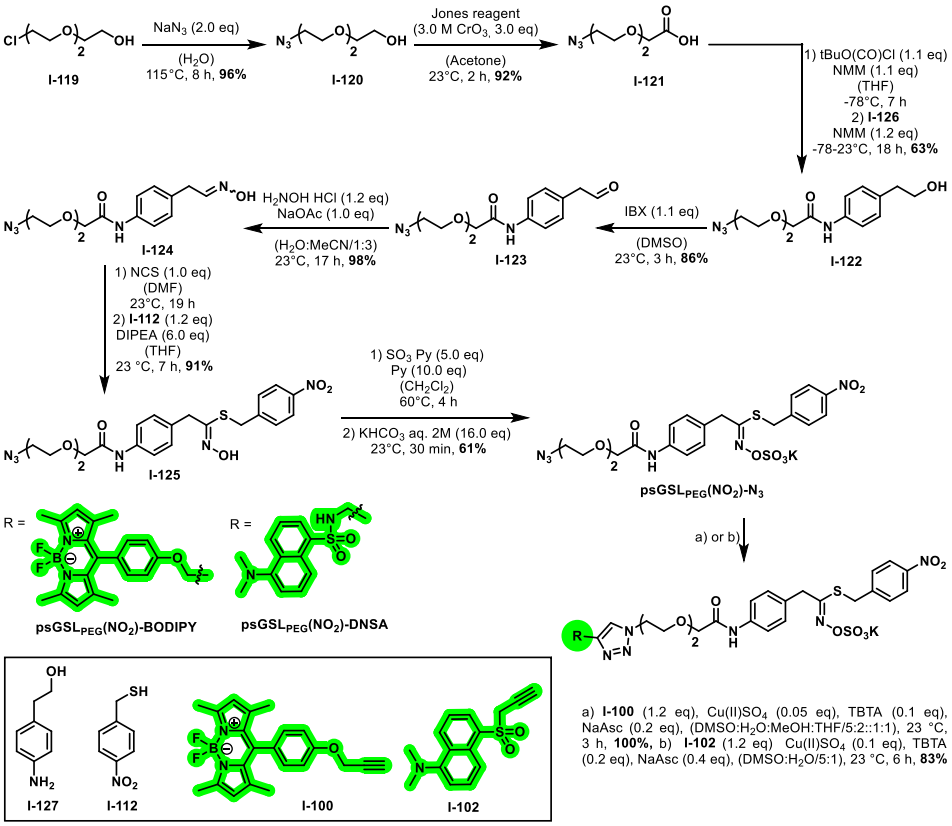

Scheme I-23: Synthesis of NTR responsive ***ps*GSL *ps*GSL$_{PEG}$(NO$_2$)-DNSA** and ***ps*GSL$_{PEG}$(NO$_2$)-BODIPY**.

For the preparation of NTR responsive *ps*GSL probes (Scheme I-23), an *in-situ* transformation of hydromixate **I-124** to an intermediate chloro oxime, followed by subsequent substitution with thiol **I-112** under basic conditions gave thiohydroximate **I-125** in 68% yield. Treatment of **I-125** with sulfur trioxide-pyridine complex and aqueous potassium bicarbonate solution gave access to ***ps*GSL$_{PEG}$(NO$_2$)-**

N_3 in form of its potassium salt in 57% yield. Finally, a copper mediated click reaction (CuAAC) with dansylamide dye **I-102** and BODIPY dye **I-100**, both bearing a terminal alkyne, provided access to ***ps*GSL$_{PEG}$(NO$_2$)-DNSA** and ***ps*GSL$_{PEG}$(NO$_2$)-BODIPY**, in 83% and quantitative yield respectively.

Similarly, for the preparation of AzoR responsive *ps*GSL probe (Scheme I-24), an *in situ* transformation of previously synthesized oxime **I-124** to an intermediate chloro oxime, followed by subsequent substitution with thiol **I-117** under basic conditions gave thiohydroximate **I-126** in 93% yield. Treatment of **I-125** with sulfur trioxide-pyridine complex and aqueous potassium bicarbonate solution gave access to ***ps*GSL$_{PEG}$(Azo)-N$_3$** in form of its potassium salt in 60% yield. Finally, a copper mediated click reaction (CuAAC) with BODIPY dye **I-100**, bearing a terminal alkyne, provided access to ***ps*GSL$_{PEG}$(Azo)-BODIPY** in 78% yield.

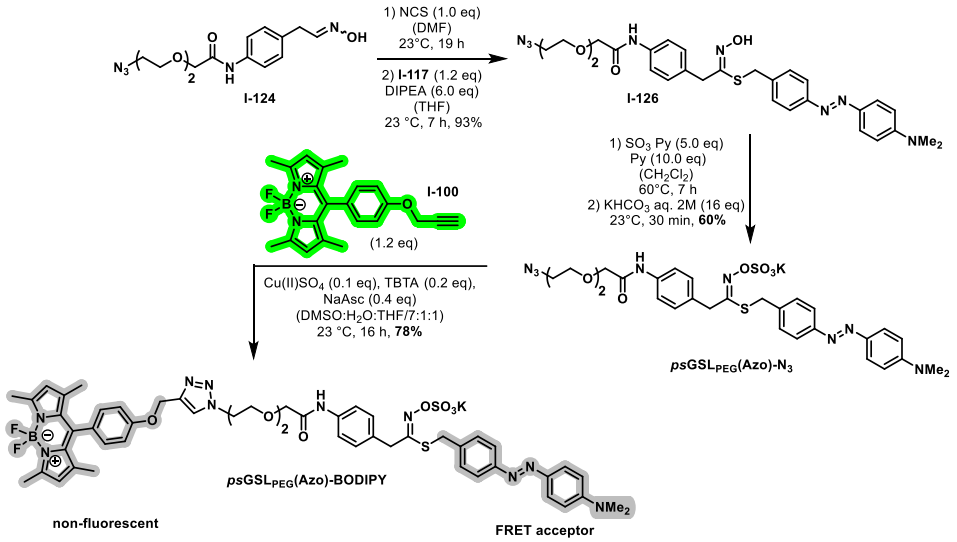

Scheme I-24: Synthesis of AzoR responsive ***ps*GSL$_{PEG}$(Azo)-BODIPY**.

I-3.1.2 Evaluation of NTR- and AzoR-responsive *ps*GSLs

The biochemical and biological evaluation of the NTR- and AzoR-responsive *ps*GSLs was planned and performed by my colleagues Dr. Charity S. G. Ganskow and Dr. Claire C. Jimidar in collaboration with Dr. Julia Morud Lekholm (University of Gothenburg), Prof. Dr. Anett Schallmey (TU Braunschweig), Prof. Dr. Mark Brönstrup (Helmholtz Center for Infection Research), as well as Dr. Stephan Hacker (Leiden University) and Prof. Dr. Stephan Sieber (Technische Universität München). However, I was involved in the evaluation of fluorescence turn on for the AzoR-responsive probe and the overall interpretation of the results and to provide the complete picture of the project a summary of the results will be presented in this work.

I-3.1.2.1 LC-MS analysis of ITC release from breakdown of NTR responsive *ps*GSL$_{PEG}$(NO$_2$)-N$_3$ and *ps*GSL$_{PEG}$(NO$_2$)-DNSA

The evaluation of NTR-responsive ***ps*GSL$_{PEG}$(NO$_2$)-N$_3$** using NfsB from *E. coli*. with cofactors FMN and NADH. LC-MS analysis (Figure I-7) confirmed its conversion to ITC **I-128** (Figure I-7, A: structure, B2: R_t = 4.10 min, and C3: mass 358 m/z for $[M+Na]^+$ and 336 m/z for $[M+H]^+$) and hydroxylamine **I-127** (Figure

I-7, A: structure, B2: R_t = 2.63 min, and C2: mass 553 m/z for $[M-K]^-$). Upon treatment with aqueous ammonia, both intermediates rapidly formed the corresponding thiourea **I-129** (Figure I-7, A: structure, B3: R_t = 2.33 min, and C4: mass 375 m/z for $[M+Na]^+$, 353 m/z for $[M+H]^+$, 705 m/z for $[2M+H]^+$, and 727 m/z for $[2M+Na]^+$), providing further evidence of successful enzymatic activation and subsequent ITC release.

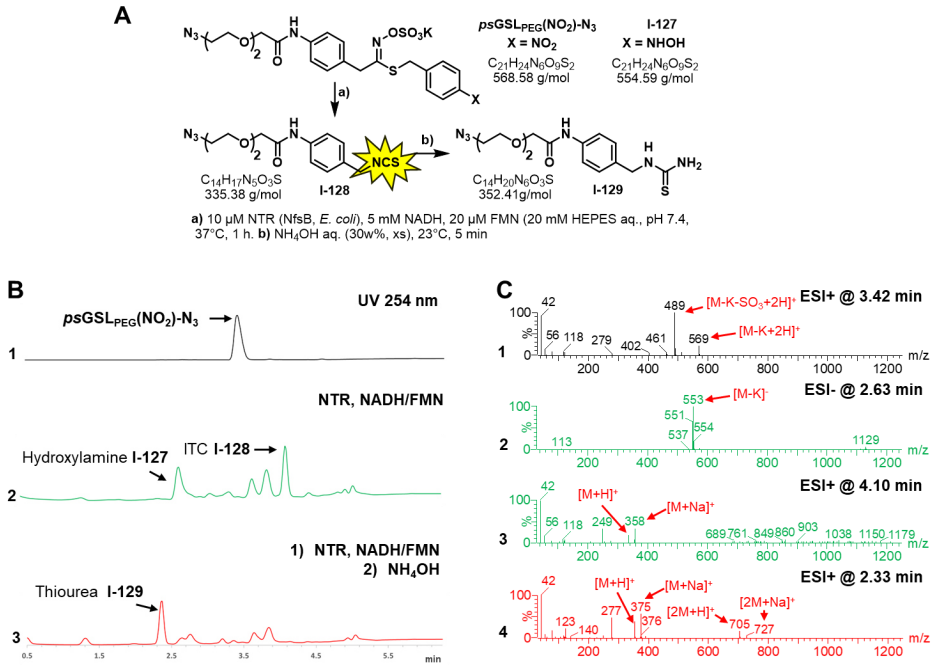

Figure I-7: LC-MS analysis after incubation of ***ps*GSL$_{PEG}$(NO$_2$)-N$_3$** with nitroreductase (NTR) NfsB from *E. coli* and subsequent derivatization with NH_4OH solution. **A:** Structures of ***ps*GSL$_{PEG}$(NO$_2$)-N$_3$**, ITC **I-128**, thiourea **I-129** and hydroxylamine **I-127**. **B:** UV chromatogram at 254 nm of (B1) pure ***ps*GSL$_{PEG}$(NO$_2$)-N$_3$** (500 µM) in HEPES buffer (20 mM, pH 7.4), (B2) incubation of ***ps*GSL$_{PEG}$(NO$_2$)-N$_3$** (500 µM) with NfsB (10 µM), NADH (5 mM) and FMN (20 µM) in HEPES buffer (20mM, pH 7.4) after 1 h at 37°C and (B3) A2 and addition of aqueous NH_4OH solution (30 w%, 10 µL). **C:** ESI+ or ESI- mass analysis at (C1) 3.42 min of B1, (C2 and C3) 4.10 min and 2.63 min of B2 and (C4) 2.33 min of B3.

Additionally, control experiments were performed as shown in Figure I-8. Incubation of ***ps*GSL$_{PEG}$(NO$_2$)-N$_3$** in the absence of NfsB (Figure I-8, 1) and incubation of ***ps*GSL$_{PEG}$(NO$_2$)-N$_3$** in absence of NfsB followed by subsequent addition of excess of aqueous ammonia (Figure I-8, 3) showed no conversion. Similarly, incubation of ***ps*GSL$_{PEG}$(NO$_2$)-N$_3$** in absence of cofactors NADH and FMN(Figure I-8, 2) as well as with subsequent addition of excess aqueous ammonia (Figure I-8, 4) did not show any conversion.

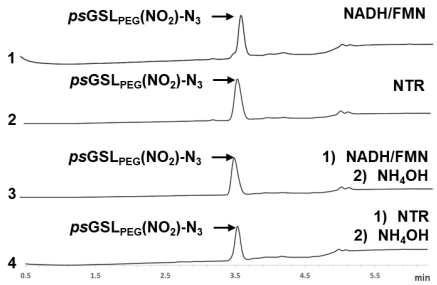

Figure I-8: UV chromatogram of control experiments of incubation of ***ps*GSL$_{PEG}$(NO$_2$)-N$_3$** in absence of NTR (1 and 4) or the cofactors NADH and FMN (2 and 3).

The conversion of ***ps*GSL$_{PEG}$(NO$_2$)-N3** in the presence of NfsB and FMN/NADH was monitored over 2 hours, revealing a rapid initial reduction to hydroxylamine **I-127**, with minimal formation of ITC **I-128** as detected by LC-MS (Figure I-9, A2). Upon treatment with aqueous ammonia, both intermediates were converted to thiourea **I-129**, confirming a 1,6-elimination from hydroxylamine **I-127** and subsequent ITC formation (Figure I-9, A3). Over time, hydroxylamine **I-127** was gradually consumed, leading to the formation of ITC **I-128** (Figure I-9, B), consistent with the stepwise nitro reduction mechanism catalyzed by NTRs.

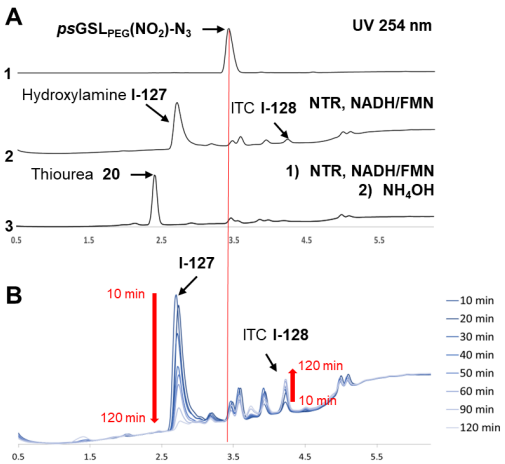

Figure I-9: LC-MS analysis after incubation of ***ps*GSL$_{PEG}$(NO$_2$)-N$_3$** with nitroreductase (NTR) NfsB from E. coli and subsequent derivatization with NH_4OH solution. **A:** UV chromatogram at 254 nm of (A1) pure ***ps*GSL$_{PEG}$(NO$_2$)-N$_3$** (500 µM) in HEPES buffer (20 mM, pH 7.4), (A2) incubation of ***ps*GSL$_{PEG}$(NO$_2$)-N$_3$** (500 µM) with NfsB (10 µM), NADH (5 mM) and FMN (20 µM) in HEPES buffer (20mM, pH 7.4) after 10 min at 37°C and (A3) A2 and addition of aqueous NH_4OH solution (30 w%, 5 µL) at 23°C. **B:** UV chromatogram at 254 nm of the conversion of ***ps*GSL$_{PEG}$(NO$_2$)-N$_3$** (500 µM) in presence of NfsB (10 µM), NADH (5 mM) and FMN (20 µM) in HEPES buffer (20mM, pH 7.4) over the course of 2 h at 37°C (at t = 10, 20, 30, 40, 50, 60, 90, 120 min).

Similarly, the fluorophore-labeled compound ***ps*GSL$_{PEG}$(NO$_2$)-DNSA** (Figure I-10, A: structure, B1: R_t 3.85 min; C1: mass 857 m/z for $[M-K+2H]^+$ and 777 m/z for $[M-K-SO_3+2H]^+$) was shown to release its corresponding ITCs upon incubation with NfsB, FMN, and NADH (Figure I-10). LC-MS analysis confirmed

the formation of ITC **I-131a** (Figure I-10, A: structure, B2: R_t 4.65 min; C3: mass 646 m/z for $[M+Na]^+$ and 624 m/z for $[M+H]^+$) and hydroxylamine **I-130a** (Figure I-10, A: structure, B2: R_t 3.25 min; C2: mass 842 m/z for $[M-K]^-$ and 761 m/z for $[M-K-SO_3]^-$), with subsequent rapid conversion to thiourea **I-132a** (see Figure I-10, A: structure, B3: R_t = 3.32 min; C4: mass 641 m/z for $[M+H]^+$ and 663 m/z for $[M+Na]^+$) upon addition of aqueous ammonia, demonstrating successful enzymatic cleavage and ITC release.

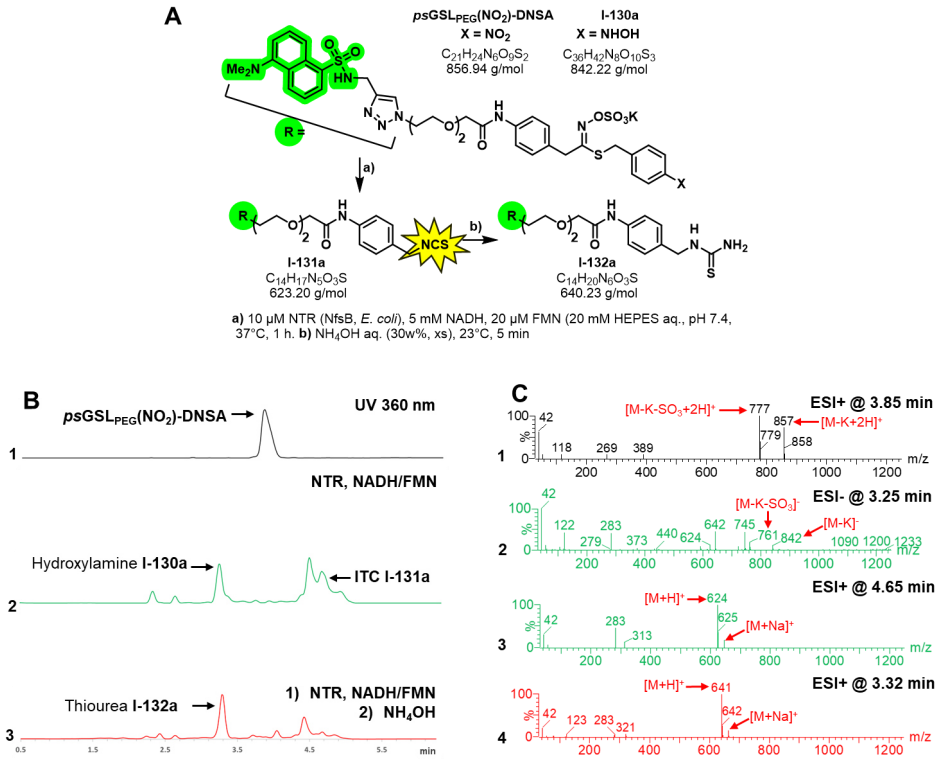

Scheme I-10: LC-MS analysis after incubation of ***ps*GSL$_{PEG}$(NO$_2$)-DNSA** with nitroreductase (NTR) NfsB from E. coli and subsequent derivatization with NH_4OH solution. **A:** Structures of ***ps*GSL$_{PEG}$(NO$_2$)-DNSA**, ITC **I-131a**, thiourea **I-132a** and hydroxylamine **I-130a**. **B:** UV chromatogram at 254 nm of (B1) pure ***ps*GSL$_{PEG}$(NO$_2$)-DNSA** (500 µM) in HEPES buffer (20 mM, pH 7.4), (B2) incubation of ***ps*GSL$_{PEG}$(NO$_2$)-DNSA** (500 µM) with NfsB (10 µM), NADH (5 mM) and FMN (20 µM) in HEPES buffer (20mM, pH 7.4) after 1 h at 37°C and (B3) A2 and addition of aqueous NH_4OH solution (30 w%, 10 µL) at 23°C. **C:** ESI+ or ESI- mass analysis at (C1) 3.85 min of B1, (C2 and C3) 3.25 min and 4.65 min of B2 and (C4) 3.32 min of B3.

I-3.1.2.2 Analysis of covalent binding of ITCs from NTR responsive *ps*GSL$_{PEG}$(NO$_2$)-DNSA, *ps*GSL$_{PEG}$(NO$_2$)-BODIPY

The covalent binding of the resulting ITCs to enzyme NfsB was evaluated by an SDS-PAGE analysis on the reaction mixtures of ***ps*GSL$_{PEG}$(NO$_2$)-DNSA** and ***ps*GSL$_{PEG}$(NO$_2$)-BODIPY** incubated with NfsB, FMN, and NADH (Figure I-11, A). Fluorescent bands at the height of the enzyme were observed when the gel was excited at 366 nm for both reactions, indicating covalent labeling of NfsB (MW: 24,727 Da, Uniprot P38489, with a His6-tag). Additionally, fluorescent small molecules, likely ITC derivatives, were detected

in the flow-through (Figure I-11, C for structures). Similarly covalent binding with bovine serum albumin (BSA, 69.3 kDa, Uniprot P02769) (Figure I-11, B) was observed.

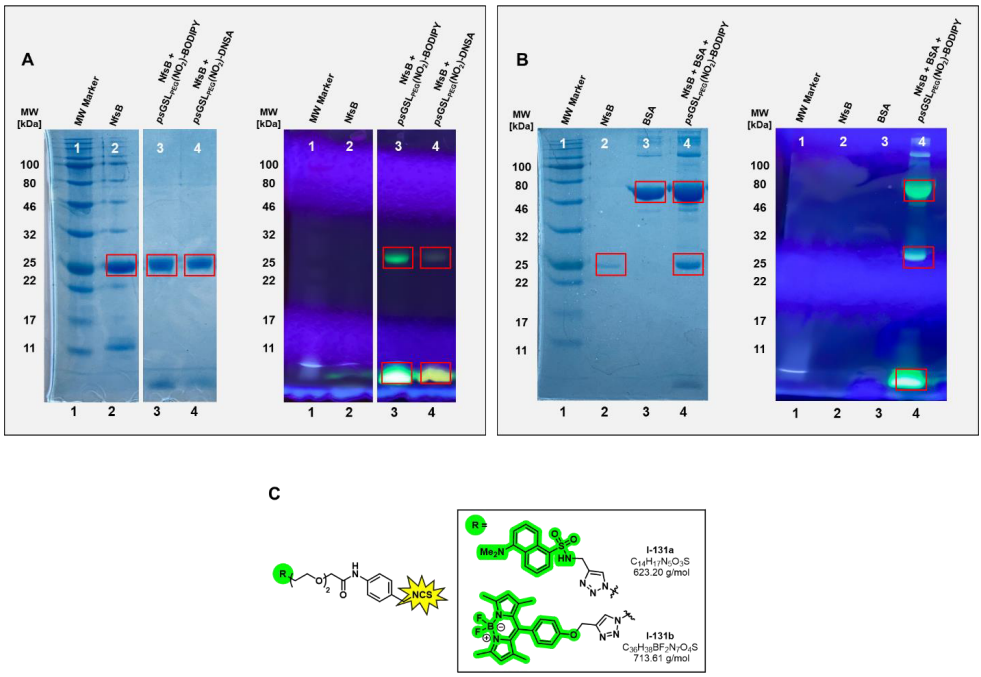

Figure I-11: A: SDS-PAGE gel analysis of the conversion of ***ps*GSL$_{PEG}$(NO$_2$)-BODIPY** and ***ps*GSL$_{PEG}$(NO$_2$)-DNSA** in the presence of nitroreductase (NTR) NfsB from *E. coli*, left: visible light/Coomassie blue™ stain, right: UV light (366 nm), (1) molecular weight marker (3 µL, 2 mg/mL), (2) nitroreductase NfsB (10 µL, 2 mg/mL), (3) 10 µL of ***ps*GSL$_{PEG}$(NO$_2$)-BODIPY** (500 µM) with NfsB (10 µM), NADH (5 mM) and FMN (20 µM) in HEPES buffer (20mM, pH 7.4) after 2 h at 37°C, (4) 10 µL of ***ps*GSL$_{PEG}$(NO$_2$)-DNSA** (500 µM) with NfsB (10 µM), NADH (5 mM) and FMN (20 µM) in HEPES buffer (20mM, pH 7.4) after 2 h at 37°C. **B:** SDS-PAGE gel analysis of the labelling of bovine serum albumin (BSA) with ***ps*GSL$_{PEG}$(NO$_2$)-BODIPY** in the presence of nitroreductase (NTR) NfsB from *E. coli*, left: visible light/Coomassie blue™ stain, right: UV light (366 nm), (1) molecular weight marker (3 µL, 2 mg/mL), (2) nitroreductase NfsB (10 µL, 0.5 mg/mL), (3) BSA (10 µL, 2 mg/mL), (4) 10 µL of ***ps*GSL$_{PEG}$(NO$_2$)-BODIPY** (500 µM) with NfsB (10 µM), NADH (5 mM) and FMN (20 µM) in HEPES buffer (20mM, pH 7.4) and BSA (2 mg/mL) after 2 h at 37°C. **C:** Structures of ITCs **I-131a** and **I-131b**.

Lastly, the covalent binding of ITC formation mediated by NfsB, formed during the conversion of fluorescent ***ps*GSL$_{PEG}$(NO$_2$)-BODIPY**. was investigated *in vivo* in *Caenorhabditis elegans (C. elegan)* worms via fluorescence microscopy imaging at 488 nm. The fluorescent signal was strongest in the presence of NfsB from *E. coli* and co-factors NADH and FMN, with localization primarily in the intestinal lumen membrane (Figure I-12, C). In the absence of NfsB, a weak signal was observed in a few worms, likely due to endogenous NTR activity. No specific signal was detected after 24 hours in control conditions, indicating presence of unbound compound (Figure I-12, A). These results provide an initial proof of concept of release of ITCs in presence of NTR (NfsB from *E. coli.*). Furthermore, the released ITCs were shown to covalently label proteins both *in vitro* and *in vivo*.

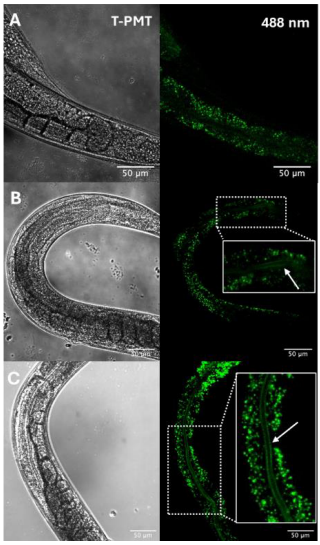

Figure I-12: Fluorescence microscopy imaging of C. elegans 24 h after an initial pre-incubation step with ***ps*GSL$_{PEG}$(NO$_2$)-BODIPY** for 1 h. **A**: pre-incubation with ***ps*GSL$_{PEG}$(NO$_2$)-BODIPY** at 23°C (but no NfsB or co-factors). **B *ps*GSL$_{PEG}$(NO$_2$)-BODIPY** at 23°C and 2 h incubation with co-factors NADH and FMN at 23°C (but no NfsB). **C:** 1 h pre-incubation with ***ps*GSL$_{PEG}$(NO$_2$)-BODIPY** at 23°C and 2 h incubation with external nitro-reductase (NfsB) from *E. coli* and co-factors NADH and FMN at 23°C. All conditions included washing out of excessive unconsumed and unbound ***ps*GSL$_{PEG}$(NO$_2$)-BODIPY** for 2 h with M9 buffer as well as 24 h incubation on NGM plates in presence of OP50 *E. coli.*

I-3.1.2.3 LC-MS analysis of ITC release from breakdown of AzoR responsive *ps*GSL$_{PEG}$(Azo)-N$_3$

AzoR being not commercially available had to be sourced from *E. coli* strain BL21 (DE3) by overexpressing AzoR upon treatment with pET28 plasmid and isolation via a His-Trap-Ni column.[154] The purified protein was diluted in TRIS buffer pH 7.4 and stored at -30°C for further use.

The enzymatic cleavage of AzoR-responsive ***ps*GSL$_{PEG}$(Azo)-N$_3$** was evaluated by incubating the compound with AzoR from *E. coli* and cofactors NADH and FMN. ***ps*GSL$_{PEG}$(Azo)-N$_3$** (Figure I-13, A: structure, B1: R_t = 4.85 min; C1: mass 693 m/z for $[M\text{-}K+H+Na]^+$, 671 m/z for $[M\text{-}K+2H]^+$, and 591 m/z for $[M\text{-}K\text{-}SO_3+H]^+$) was converted to the corresponding ITC **I-128** (Figure I-13, A: structure, B2: R_t = 4.22 min; C2: mass 358 m/z for $[M+Na]^+$ and 336 m/z for $[M+H]^+$), which was further converted into thiourea **I-127** (Figure I-13, A: structure, B3: R_t = 2.33 min; C3: mass 375 m/z for $[M+Na]^+$ and 353 m/z for $[M+H]^+$). upon addition of aqueous ammonia. These results confirm the successful enzymatic breakdown of the *ps*GSL probe.

Control experiments (Figure I-14) confirmed the specificity of the reaction. Incubation of ***ps*GSL$_{PEG}$(Azo)-N$_3$** without NfsB (Figure I-14, 1) or without cofactors NADH and FMN (Figure I-14, 2), as well as in both conditions followed by the addition of aqueous ammonia (Figure I-14, 3 and 4), showed no conversion, indicating that the enzymatic cleavage requires both NfsB and cofactors.

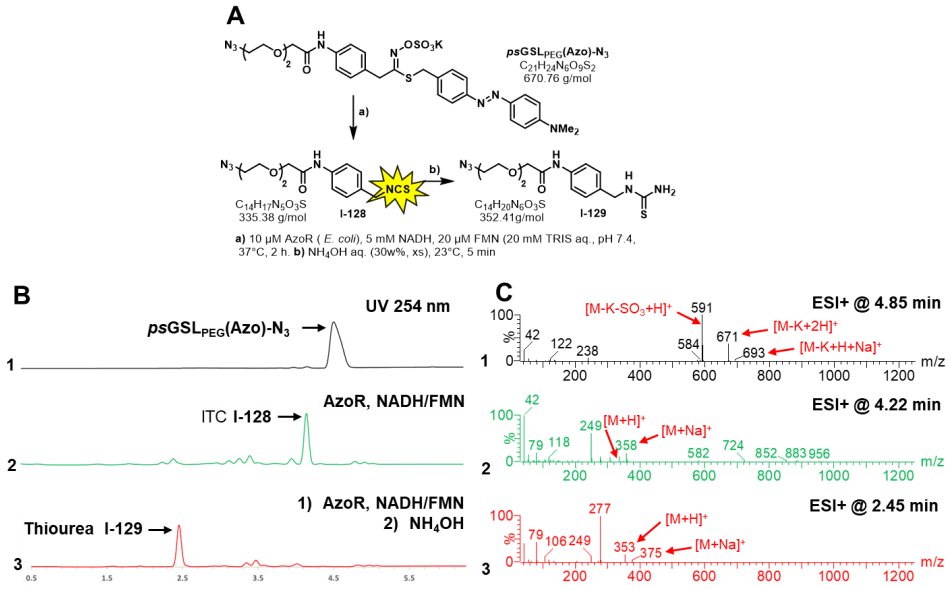

Figure I-13: LC-MS analysis after incubation of ***ps*GSL$_{PEG}$(Azo)-N$_3$** with azoreductase AzoR from E. coli and subsequent derivatization with NH_4OH solution. **A:** Structures of ***ps*GSL$_{PEG}$(Azo)-N$_3$**, ITC **I-128** and thiourea **I-129**. **B:** UV chromatogram at 254 nm of (B1) pure ***ps*GSL$_{PEG}$(Azo)-N$_3$** (500 µM) in TRIS buffer (20 mM, pH 7.4), (B2) incubation of ***ps*GSL$_{PEG}$(Azo)-N$_3$** (500 µM) with AzoR (10 µM), NADH (5 mM) and FMN (20 µM) in TRIS buffer (20mM, pH 7.4) after 2 h at 37°C and (B3) A2 and addition of aqueous NH_4OH solution (30 w%, 10 µL) at 23°C. **C:** ESI+ mass analysis at (C1) 4.85 min of B1, (C2) 4.22 min of B2 and (C3) 2.45 min of B3.

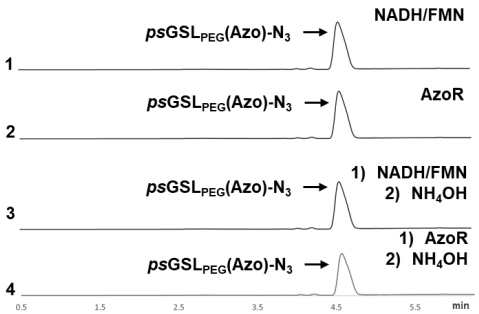

Figure I-14: UV chromatogram of control experiments of incubation of ***ps*GSL$_{PEG}$(Azo)-N$_3$** in absence of AzoR (1 and 4) or the cofactors NADH and FMN (2 and 3).

I-3.1.2.4 UV analysis of fluorescence turn on of AzoR responsive *ps*GSL$_{PEG}$(Azo)-BODIPY

The fluorescence of the BODIPY moiety in ***ps*GSL$_{PEG}$(Azo)-BODIPY** is quenched due to the overlap between the emission band of BODIPY and the absorption band of the azobenzene moiety, facilitated by Förster resonance energy transfer (FRET). As a result, the dissociation of the azobenzene moiety

upon incubation with azoreductase was expected to produce a fluorescent ITC, resulting in a fluorescent "turn-on" effect.

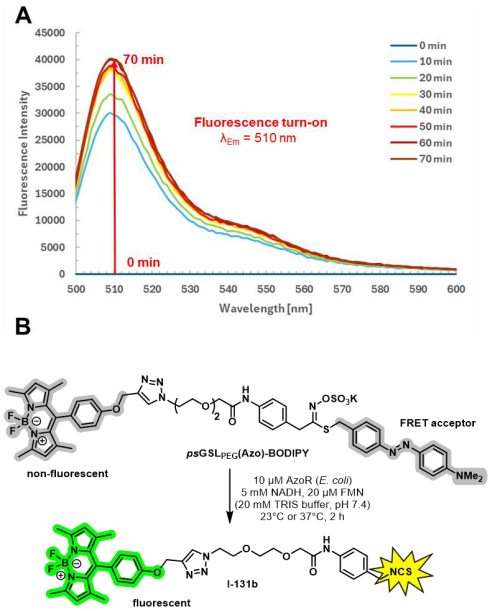

Figure I-15: **A:** Fluorescence turn-on of ***ps*GSL$_{PEG}$(Azo)-N$_3$** in the presence of AzoR: Aliquots of the incubation of ***ps*GSL$_{PEG}$(Azo)-N$_3$** (500 µM) with AzoR (10 µM), NADH (5 mM) and FMN (20 µM) in TRIS buffer (20mM, pH 7.4) at 37°C, were diluted in TRIS buffer and fluorescence emission was measured at t = 0, 10, 20, 30, 40, 50 and 60 min at 511 nm upon excitation at 495 nm. **B:** Structure of ITC **I-131b**.

This hypothesis was tested by incubating ***ps*GSL$_{PEG}$(Azo)-BODIPY** (500 µM) with AzoR (10 µM), NADH (5 mM), and FMN (20 µM) in TRIS buffer (20 mM, pH 7.4) at 37°C. Aliquots of 6 µL were taken at t = 0, 10, 20, 30, 40, 50, and 60 minutes, diluted in 3 mL of a 3:1 mixture of CH_2Cl_2:MeOH, and fluorescence emission was measured at 511 nm with excitation at 495 nm (Figure I-15, A). Already after 10 min a significant fluorescence increasing over time was observed, indicating that the FRET acceptor unit azobenzene was cleaved and the fluorescent ITC **I-131b** was released (Figure I-15, B).

I-3.1.2.5 Analysis of covalent binding of ITC from AzoR responsive *ps*GSL$_{PEG}$(Azo)-BODIPY

The covalent binding of the resulting ITCs to enzyme NfsB was evaluated by an SDS-PAGE analysis on the reaction mixture of ***ps*GSL$_{PEG}$(NO$_2$)-BODIPY** incubated with AzoR, FMN, and NADH (Figure I-16, A). Fluorescent bands at the height of the enzyme were observed when the gel was excited at 366 nm for both reactions, indicating covalent labeling of NfsB (MW: 24,727 Da, Uniprot P38489, with a His6-tag). Additionally, fluorescent small molecules, presumably corresponding to the fluorescent ITCs **I-131b** (or its hydrolysis product; Figure I-16, C), were detected in the flow-through. Beyond the labeling of NfsB, a fluorescent band was clearly observed for the same height as BSA (Figure I-16, B), thereby demonstrating that bovine serum albumin (BSA, 69.3 kDa, Uniprot P02769), added to the reaction mixture, was efficiently covalently labeled with ***ps*GSL$_{PEG}$(Azo)-BODIPY** in the presence of AzoR.

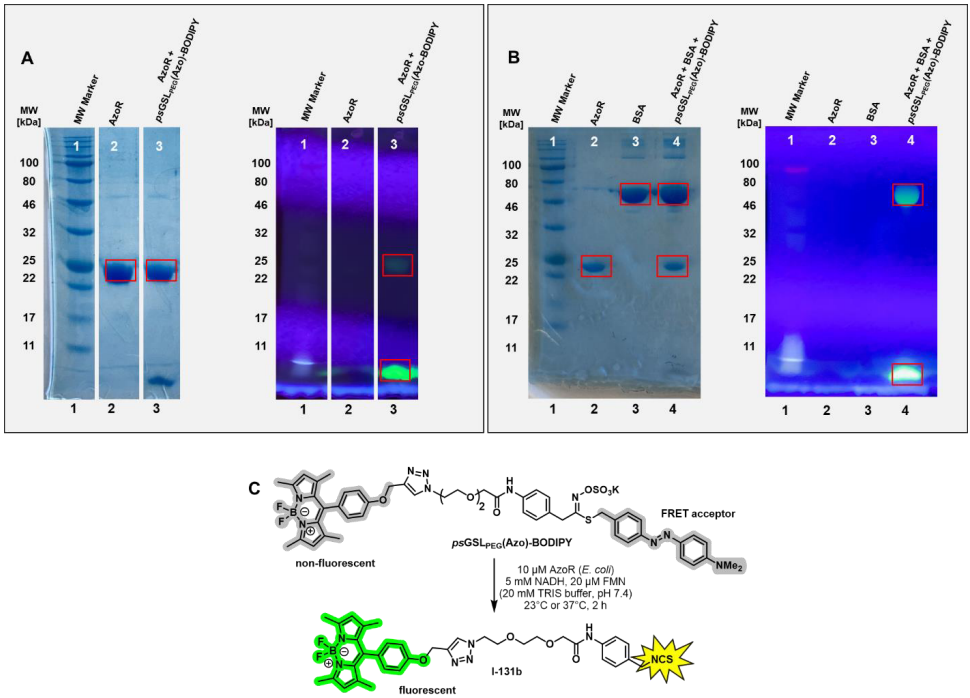

Figure I-16: **A:** SDS-PAGE gel analysis of the conversion of ***ps*GSL$_{PEG}$(Azo)-BODIPY** in the presence of azoreductase AzoR from E. coli, left: visible light/Comassi blue™ stain, right: UV light (366 nm), (1) molecular weight marker (3 µL, 2 mg/mL), (2) azoreductase AzoR (10 µL, 2 mg/mL), (3) 10 µL of ***ps*GSL$_{PEG}$(Azo)-BODIPY** (500 µM) with AzoR (10 µM), NADH (5 mM) and FMN (20 µM) in TRIS buffer (20mM, pH 7.4) after 2 h at 37°C. **B:** SDS-PAGE gel analysis of the labelling of bovine serum albumin (BSA) with ***ps*GSL$_{PEG}$(Azo)-BODIPY** in the presence of azoreductase AzoR from E. coli, left: visible light/Coomassie blue™ stain, right: UV light (366 nm), (1) molecular weight marker (3 µL, 2 mg/mL), (2) azoreductase AzoR (10 µL, 0.5 mg/mL), (3) BSA (10 µL, 2 mg/mL), (4) 10 µL of ***ps*GSL$_{PEG}$(Azo)-BODIPY** (500 µM) with AzoR (10 µM), NADH (5 mM) and FMN (20 µM) in TRIS buffer (20mM, pH 7.4) and BSA(2 mg/mL) after 2 h at 37°C.

I-3.2. Development of *ps*GSL based antimicrobial prodrugs

As discussed in section I-2.2., the main aim of this project was to investigate the structural diversity of *ps*GSL-based antimicrobial prodrugs and explore controlled drug release upon enzymatic activation. The sulfonate group in *ps*GSLs would be replaced with an antibiotic, linked via a carbamate bond. Upon NTR-mediated reduction, the nitro group would be converted to an amine, leading to a 1,6-elimination that releases the drug and an ITC. The project also focused on designing photo-cleavable *ps*GSL prodrugs that could be activated by UV light (365 nm). This would be achieved through the substitution of the NTR-responsive *p*-nitrobenzyl moiety with a photocleavable *o*-nitrobenzyl moiety. Additionally, azide groups in the psGSL side chain were planned to facilitate the attachment of fluorophores for imaging or immobilization onto resin beads for the development of antimicrobial surfaces. These strategies aim to enable the study of synergistic effect of ITCs and antibiotics and advance the potential of antimicrobial drug delivery

I-3.2.1. Docking studies of *ps*GSL$_{C4}$(NO$_2$)-CIP-N$_3$ with NTR (NfsB from *E. coli.)*

Before synthesizing the *ps*GSLs based antimicrobial prodrugs, one of the probes ***ps*GSL$_{C4}$(NO$_2$)-CIP-N$_3$** was evaluated *in silico* as a potential substrate for NTR by docking it into the active site of NfsB from *E. coli*. (PDB:1OON) using SeeSAR software.[155] The co-crystal structure of the dinitrobenzamide prodrug **I-133** with NTR from *E. coli* (PDB:1OON) was used as a reference (Figure I-17A).[156] In the case of **I-133** a hydrogen bonding network was observed for the nitro moiety interacting with FMN and a Thr^{41} residue which in turn is hydrogen bonded with a water molecule (H_2O^{440}), which is again hydrogen bonded with a Asn^{117} residue. The water molecule also is bound to proton of the amid moiety in **I-133**. A second hydrogen bonding network is observed for the diol moiety with Arg^{107}. Beyond that lipophilic interactions were observed with FMN, Phe^{70} and Ala^{116}.

Next the sulfonate analogue **I-134** of *ps*GSL based prodrug was docked into the active site of NTR (Figure I-17B). The previously observed hydrogen bonding network of the nitro moiety with FMN and Thr^{41} was there along with hydrogen bonding interaction of the terminal nitrogen of the azide moiety in **I-134** and a Lys^{14} residue. Although there was a decrease in the hydrogen bonding, lipophilic interactions increased as Phe^{70} interacted with the sulfur atom in **I-134**.

Finally, docking of ***ps*GSL$_{C4}$(NO$_2$)-CIP-N$_3$** showed consistent hydrogen bonding interaction of FMN and Thr^{41} with the nitro moiety (Figure I-17C). The hydrogen bonding interaction of the azide moiety was shifted to the first nitrogen. Furthermore, there was a significant increase in lipophilic interactions of the ciprofloxacin core with Phe^{70}, along with its previously observed interaction with sulfur. Beyond that the rest of the ciprofloxacin core was outside the binding pocket. The consistent hydrogen bonding observed for the nitro moiety and increased lipophilic interaction with the ciprofloxacin core could suggest that ***ps*GSL$_{C4}$(NO$_2$)-CIP-N$_3$** was a suitable substrate for NTR.

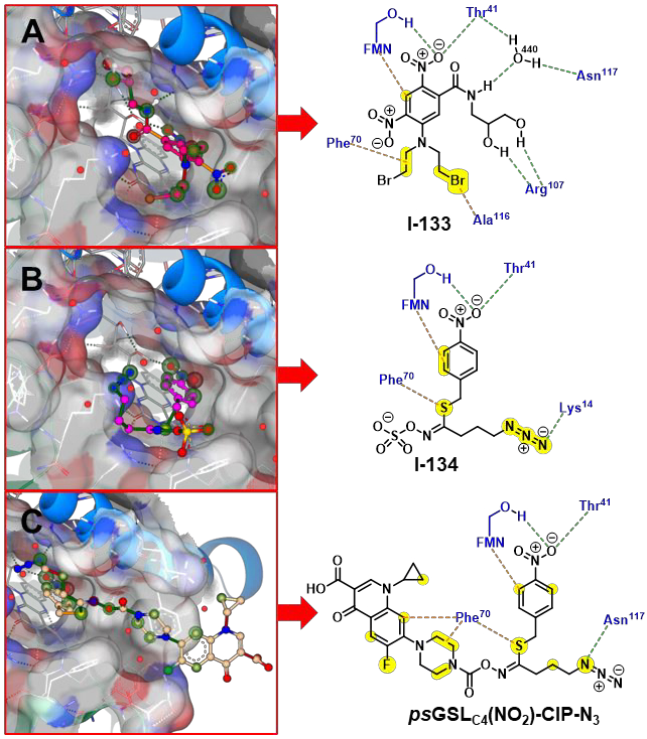

Figure I-17: **A**: 3D-illustration of the co-crystal structure and binding interactions of the dinitrobenzamide prodrug **I-133** in the active center of NTR from *E. coli*. (PDB:1OON).[156] **B:** Docking of *ps*GSL-*O*-sulfonate analogue **I-134** onto NTR from *E.coli*. (PDB:1OON)[156] and illustrations of the binding interactions. **C**: Docking of ***ps*GSL$_{C4}$(NO$_2$)-ClP-N$_3$** onto NTR from *E.coli* (PDB:1OON)[156] and illustrations of the binding interactions. The docking was performed and 3D-illustration were generated with SeeSAR version 14.0.0; BioSolveIT GmbH, 2024, www.biosolveit.de/SeeSAR.[155] Green spheres around atoms indicate overall favorable contributions to ΔG(Hyde), red spheres around atoms indicate overall unfavorable contributions to ΔG(Hyde).[157] Hydrogen bridges are indicated by dotted green lines. Light grey illustration represents surface of the binding pocket with elements surrounding the bound mv-GSL in red (oxygen), blue (nitrogen) and yellow (sulfur). Grey shadows represent unoccupied space in the binding pocket.

I-3.2.2. Synthesis of *ps*GSL based antimicrobial prodrugs

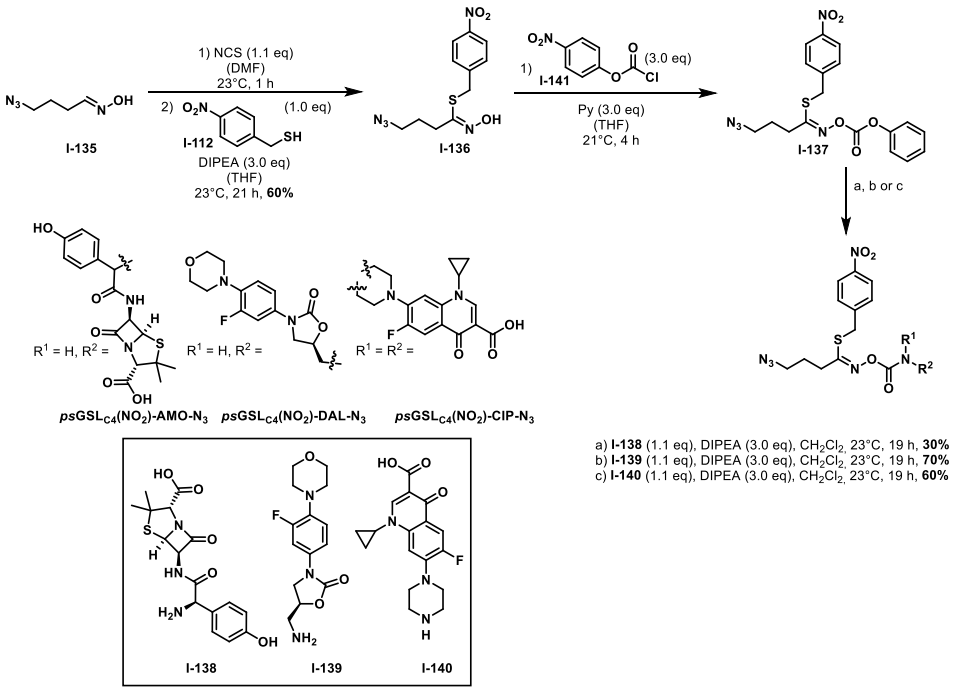

Scheme I-25: Synthesis of *ps*GSL based antimicrobial prodrugs bearing a C4 backbone.

For the synthesis of the *ps*GSL based antimicrobial prodrugs bearing a C4 backbone (Scheme I-25), oxime **I-135** was used and was previously synthesized in our lab. An *in-situ* conversion of **I-135** in the presence of *N*-chlorosuccinimide under light exclusion gave an intermediate chloro oxime followed by a nucleophilic addition of *p*-nitrobenzyl thiol (**I-122**) under basic conditions to give thiohydroximate **I-136** in 60% yield. Next **I-136** was converted to an intermediate carbonate in the presence of *p*-nitrobenzylchloroformate (**I-141**) to give **I-137** and subsequently converted to the corresponding carbamates ***ps*GSL$_{C4}$(NO$_2$)-AMO-N$_3$** in presence of amoxicillin (**I-138**) in 30% yield, ***ps*GSL$_{C4}$(NO$_2$)-DAL-N$_3$** in presence of deacetyl linezolid (**I-139**) in 70% yield and ***ps*GSL$_{C4}$(NO$_2$)-CIP-N$_3$** in presence of ciprofloxacin (**I-140**) in 60% yield respectively.

For the synthesis of the more hydrophilic *ps*GSL based antimicrobial prodrugs bearing a PEG linker (Scheme I-26) oxime **I-124** was used and synthesized as previously shown and described in Scheme I-23. Similarly, an *in-situ* conversion of oxime **I-124** in the presence of *N*-chlorosuccinimide under light exclusion gave an intermediate chloro oxime, followed by a nucleophilic addition of *p*-nitrobenzyl thiol (**I-122**) under basic conditions to give thiohydroximate **I-125** in 60% yield. Next **I-125** was converted to an intermediate carbonate in the presence of *p*-nitrobenzyl chloroformate (**I-141**) to give **I-142** and subsequently converted to the corresponding carbamates ***ps*GSL$_{PEG}$(NO$_2$)-AMP-N$_3$** in presence of ampicillin (**I-143**) in 42% yield, ***ps*GSL$_{PEG}$(NO$_2$)-DAL-N$_3$** in presence of deacetyl linezolid (**I-139**) in 71% yield and ***ps*GSL$_{PEG}$(NO$_2$)-CIP-N$_3$** in presence of ciprofloxacin (**I-140**) in 30% yield respectively.

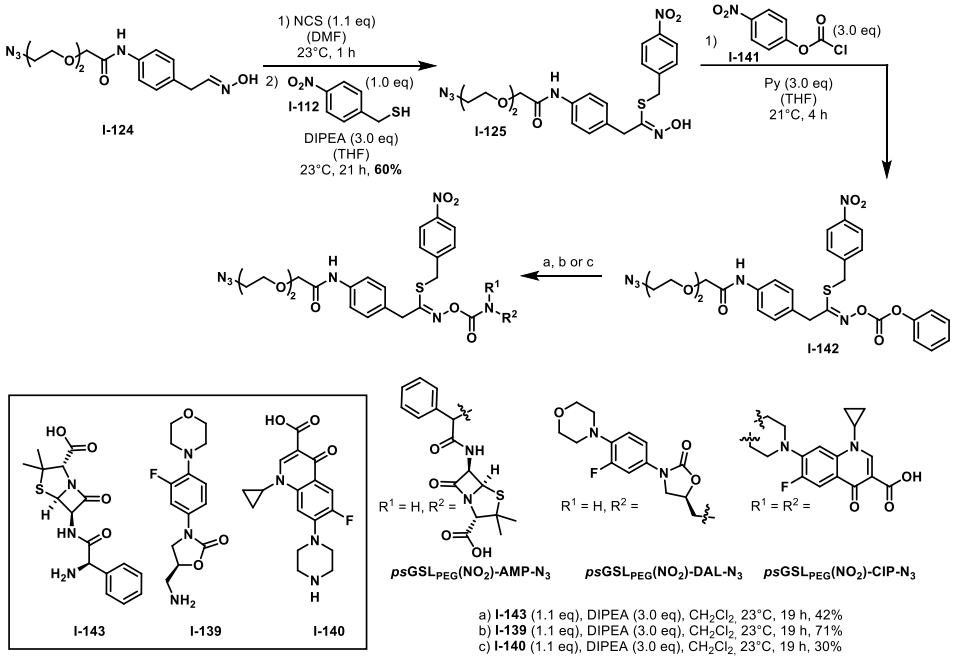

Scheme I-26: Synthesis of *ps*GSL based antimicrobial prodrugs bearing a PEG linker.

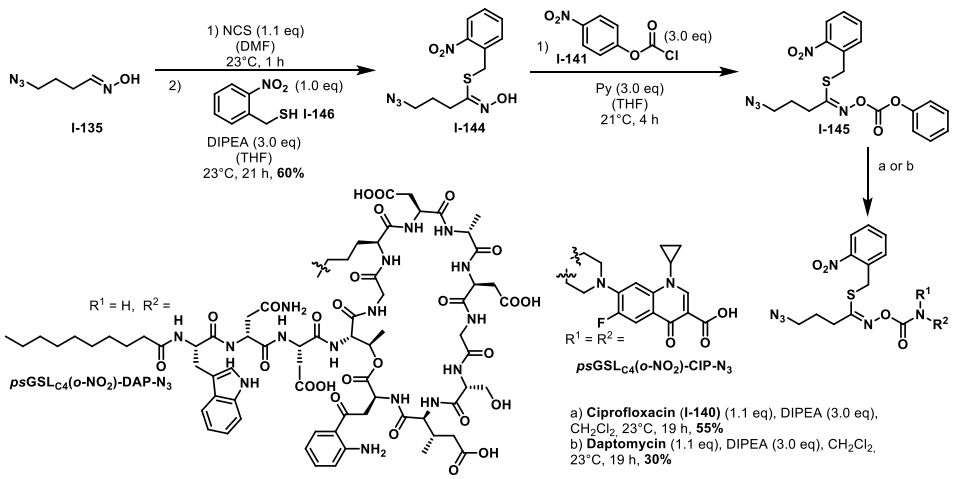

Scheme I-27: Synthesis of photo-responsive *ps*GSL based antimicrobial prodrugs.

Similarly, two *ps*GSL based UV (365 nm) sensitive antimicrobial prodrugs were also synthesized as described before (Scheme I-27). Oxime **I-135** was used and was previously synthesized in our lab. An *in-situ* conversion of **I-135** in the presence of *N*-chlorosuccinimide under light exclusion gave an intermediate chloro oxime followed by a nucleophilic addition of *o*-nitrobenzyl thiol (**I-146**) under basic conditions to give thiohydroximate **I-144** in 60% yield. Next, **I-144** was converted to an intermediate carbonate in the presence of *p*-nitrobenzyl chloroformate (**I-141**) to give **I-145** and subsequently

converted to the corresponding carbamates ***ps*GSL$_{C4}$(*o*-NO$_2$)-CIP-N$_3$** in presence of ciprofloxacin (**I-140**) in 55% yield and ***ps*GSL$_{C4}$(*o*-NO$_2$)-DAP-N$_3$** in 30% yield respectively.

I-3.2.3. Evaluation of *ps*GSL based antimicrobial prodrugs

I-3.2.3.1. LC-MS analysis of the breakdown of *ps*GSL based antimicrobial probes with the C4 backbone in presence of NTR.

With the synthesized *ps*GSL-based antimicrobial conjugates in hand, they were evaluated for the controlled released of the antibiotics and resulting ITCs upon NTR activity based on the protocol developed in our lab.[158] For this firstly, 5 mM of each of the *ps*GSL-based antimicrobial probes with the C4 backbone (***ps*GSL$_{C4}$(NO$_2$)-AMO-N$_3$**, ***ps*GSL$_{C4}$(NO$_2$)-DAL-N$_3$** and ***ps*GSL$_{C4}$(NO$_2$)-CIP-N$_3$**) were incubated with 10 µM NTR (NfsB from *E. coli*.) in presence of cofactors 5 mM NADH and 20 µM FMN at 37°C for 2h, 24 h and 48 h respectively.

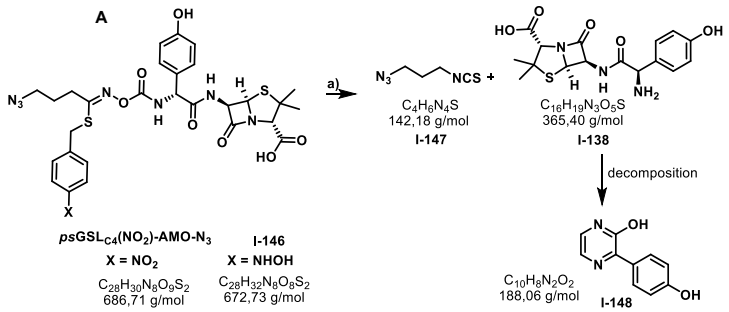

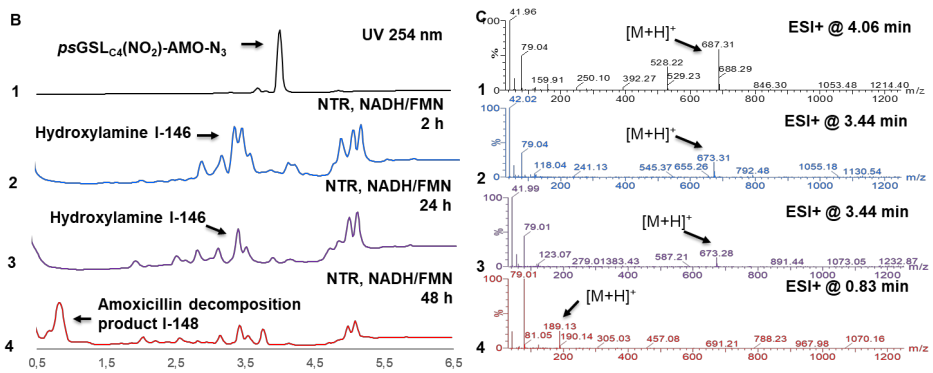

Figure I-18: LC-MS analysis after incubation of ***ps*GSL$_{C4}$(NO$_2$)-AMO-N$_3$** with nitroreductase NfsB from *E. coli*. **A:** Structures of ***ps*GSL$_{C4}$(NO$_2$)-AMO-N$_3$**, hydroxylamine **I-146**, ITC **I-147** amoxicillin (**I-138**) and degradation product of amoxicillin **I-148**. **B:** UV chromatogram at 254 nm of (B1) pure ***ps*GSL$_{C4}$(NO$_2$)-AMO-N$_3$** (500 µM) in HEPES buffer (20 mM, pH 7.4), (B2) incubation of ***ps*GSL$_{C4}$(NO$_2$)-AMO-N$_3$** (500 µM) with NfsB (10 µM), NADH (5 mM) and FMN (20 µM) in HEPES buffer (20mM, pH 7.4) after 2 h at 37°C and (B3) incubation of ***ps*GSL$_{C4}$(NO$_2$)-AMO-N$_3$** (500 µM) with NfsB (10 µM), NADH (5 mM) and FMN (20 µM) in HEPES buffer (20mM, pH 7.4) after 24 h at 37°C and (B4) incubation of ***ps*GSL$_{C4}$(NO$_2$)-AMO-N$_3$** (500 µM) with NfsB (10 µM), NADH (5 mM) and FMN (20 µM) in HEPES buffer (20mM, pH 7.4) after

48 h at 37°C. **C:** ESI+ mass analysis at (C1) 4.06 min of B1, (C2) 3.44 min of B2, (C3) 3.44 min of B3 and(C4) 0.83 min of B4.

***ps*GSL$_{C4}$(NO$_2$)-AMO-N$_3$** (Figure I-18, A: structure B1: R_t 4.06 min and C1: mass 687.31 m/z for $[M+H]^+$) was converted by NfsB and the formation of the corresponding hydroxylamine **I-146** (Figure I-18, A: structure, B2: R_t = 3.44 min, and C3: mass 673.31 m/z for $[M+H]^+$) was observed after 2 h of incubation. Therefore, incubation time was increased to 24 h but again only hydroxylamine **I-146** (Figure I-18, A: structure, B2: R_t = 3.44 min, and C3: mass 673.31 m/z for $[M+H]^+$) was observed. When incubation time was increased to 48 h ***ps*GSL$_{C4}$(NO$_2$)-AMO-N$_3$** was completely consumed but only a degradation product of amoxicillin **I-148** (Figure I-18, A: structure, B2: R_t = 0.83 min, and C3: mass 189.83 m/z for $[M+H]^+$) was observed. In all cases ITC formation was not detected via LC-MS analysis. The formation of hydroxylamine **I-146** confirms the conversion of ***ps*GSL$_{C4}$(NO$_2$)-AMO-N$_3$** by NTR although the reaction with this substrate was slow. The released amoxicillin seemed to be unstable under these conditions as only the degradation product **I-148** was observed.[159] Overall the conversion was not straightforward and led to formation of many unidentified side products.

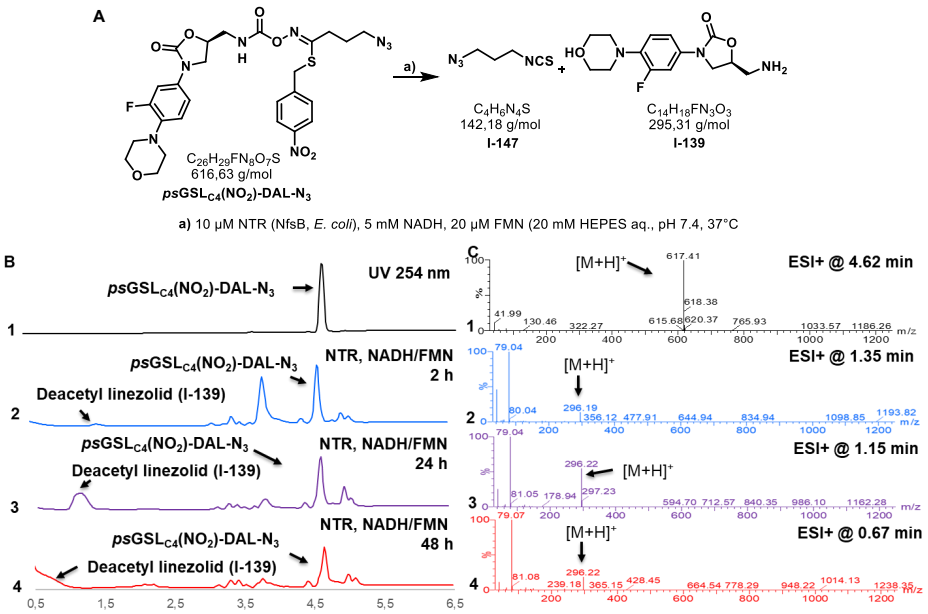

Figure I-19: LC-MS analysis after incubation of ***ps*GSL$_{C4}$(NO$_2$)-DAL-N$_3$** with nitroreductase NfsB from *E. coli*. **A:** Structures of ***ps*GSL$_{C4}$(NO$_2$)-DAL-N$_3$**, ITC **I-147** and deacetyl linezolid (**I-139**). **B:** UV chromatogram at 254 nm of (B1) pure ***ps*GSL$_{C4}$(NO$_2$)-DAL-N$_3$** (500 µM) in HEPES buffer (20 mM, pH 7.4), (B2) incubation of ***ps*GSL$_{C4}$(NO$_2$)-DAL-N$_3$** (500 µM) with NfsB (10 µM), NADH (5 mM) and FMN (20 µM) in HEPES buffer (20mM, pH 7.4) after 2 h at 37°C, (B3) incubation of ***ps*GSL$_{C4}$(NO$_2$)-DAL-N$_3$** (500 µM) with NfsB (10 µM), NADH (5 mM) and FMN (20 µM) in HEPES buffer (20mM, pH 7.4) after 24 h at 37°C and (B4) incubation of ***ps*GSL$_{C4}$(NO$_2$)-DAL-N$_3$** (500 µM) with NfsB (10 µM), NADH (5 mM) and FMN (20 µM) in HEPES buffer (20mM, pH 7.4) after 48 h at 37°C. **C:** ESI+ mass analysis at (C1) 4.62 min of B1, (C2) 1.35 min of B2, (C3) 1.15 min of B3 and(C4) 0.67 min of B4.

***ps*GSL$_{C4}$(NO$_2$)-DAL-N$_3$** (Figure I-19, A: structure B1: R_t 4.62 min and C1: mass 617.41 m/z for $[M+H]^+$) was partially converted by NfsB and the formation of traces of released deacetyl linezolid (**I-139**) (Figure

I-19, A: structure, B2: R_t = 1.35 min, and C3: mass 296.19 m/z for $[M+H]^+$) along with the residual peak for ***ps*GSL$_{C4}$(NO$_2$)-DAL-N$_3$** was observed after 2 h of incubation. Therefore, incubation time was increased to 24 h and an increase in the amount of released drug **I-139** (Figure I-19, A: structure, B2: R_t = 1.55 min, and C3: mass 296.22 m/z for $[M+H]^+$) was observed. When incubation time was increased to 48 h ***ps*GSL$_{C4}$(NO$_2$)-DAL-N$_3$** was still not completely consumed and the UV peak for **I-139** shifted towards the injection peak (Figure I-19, A: structure, B2: R_t = 0.67 min, and C3: mass 296.22 m/z for $[M+H]^+$), therefore the amount of drug released could not be understood properly. In all cases ITC formation was not detected via LC-MS analysis. The formation of released drug **I-139** confirmed the partial and slow conversion of ***ps*GSL$_{C4}$(NO$_2$)-DAL-N$_3$** by NTR and the probe seemed to be stable under these reaction conditions.

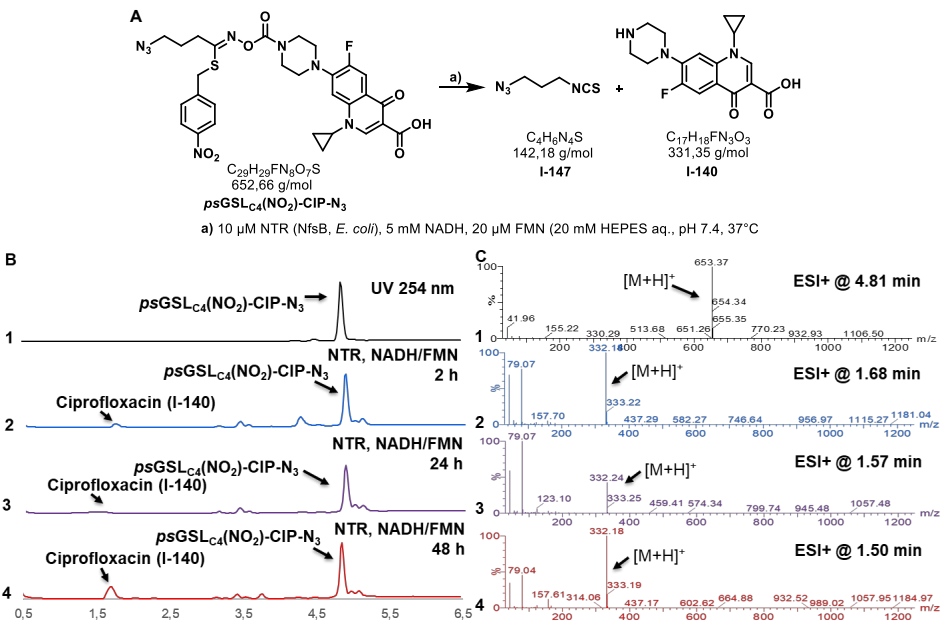

Figure I-20: LC-MS analysis after incubation of ***ps*GSL$_{C4}$(NO$_2$)-CIP-N$_3$** with nitroreductase NfsB from *E. coli*. **A:** Structures of ***ps*GSL$_{C4}$(NO$_2$)-CIP-N$_3$**, ITC **I-137** and ciprofloxacin (**I-140**). **B:** UV chromatogram at 254 nm of (B1) pure ***ps*GSL$_{C4}$(NO$_2$)-CIP-N$_3$** (500 µM) in HEPES buffer (20 mM, pH 7.4), (B2) incubation of ***ps*GSL$_{C4}$(NO$_2$)-CIP-N$_3$** (500 µM) with NfsB (10 µM), NADH (5 mM) and FMN (20 µM) in HEPES buffer (20mM, pH 7.4) after 2 h at 37°C, (B3) incubation of ***ps*GSL$_{C4}$(NO$_2$)-CIP-N$_3$** (500 µM) with NfsB (10 µM), NADH (5 mM) and FMN (20 µM) in HEPES buffer (20mM, pH 7.4) after 24 h at 37°C and (B4) incubation of ***ps*GSL$_{C4}$(NO$_2$)-CIP-N$_3$** (500 µM) with NfsB (10 µM), NADH (5 mM) and FMN (20 µM) in HEPES buffer (20mM, pH 7.4) after 48 h at 37°C. **C:** ESI+ mass analysis at (C1) 4.81 min of B1, (C2) 1.68 min of B2, (C3) 1.57 min of B3 and(C4) 1.50 min of B4.

Similarly, ***ps*GSL$_{C4}$(NO$_2$)-CIP-N$_3$** (Figure I-20, A: structure B1: R_t 4.81 min and C1: mass 653.37 m/z for $[M+H]^+$) was partially converted by NfsB and the formation of traces of released ciprofloxacin (**I-140**) (Figure I-20, A: structure, B2: R_t = 1.68 min, and C3: mass 332.18 m/z for $[M+H]^+$) along with the residual peak for ***ps*GSL$_{C4}$(NO$_2$)-CIP-N$_3$** was observed after 2 h of incubation. Therefore, incubation time was increased to 24 h but no change in the amount of released drug **I-140** (Figure I-20, A: structure, B2: R_t = 1.55 min, and C3: mass 332.24 m/z for $[M+H]^+$) was observed. When incubation time was increased

to 48 h ***ps*GSL$_{C4}$(NO$_2$)-CIP-N$_3$** was still not completely consumed but the amount of released ciprofloxacin (**I-156**) clearly increased (Figure I-20, A: structure, B2: R_t = 1.50 min, and C3: mass 332.18 m/z for $[M+H]^+$). In all cases ITC formation was not detected via LC-MS analysis. The formation of released drug **I-140** confirmed the partial and slow conversion of ***ps*GSL$_{C4}$(NO$_2$)-CIP-N$_3$** by NTR. In conclusion, the *ps*GSL-based antimicrobial prodrugs with the C4 backbone were not the most optimal substrates for NfsB obtained from *E. coli.*

I-3.2.3.2. LC-MS analysis of the breakdown of *ps*GSL based antimicrobial probes with a PEG linker in presence of NTR.

Given the previously observed results, 5 mM of each of the *ps*GSL based antimicrobial probes with the PEG linker (***ps*GSL$_{PEG}$(NO$_2$)-AMP-N$_3$**, ***ps*GSL$_{PEG}$(NO$_2$)-DAL-N$_3$** and ***ps*GSL$_{PEG}$(NO$_2$)-CIP-N$_3$**) were incubated with 10 µM NTR (NfsB from *E. coli*.) in presence of cofactors 5 mM NADH and 20 µM FMN at 37°C for 2h and 48 h respectively.

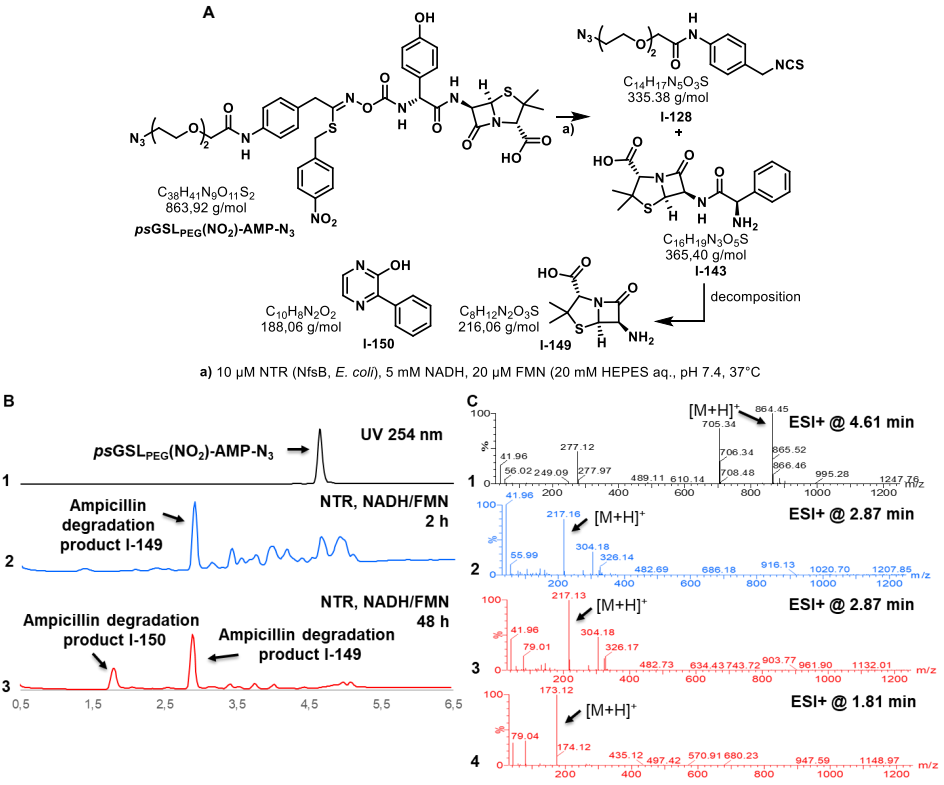

Figure I-21: LC-MS analysis after incubation of ***ps*GSL$_{PEG}$(NO$_2$)-AMP-N$_3$** with nitroreductase NfsB from *E. coli*. **A:** Structures of ***ps*GSL$_{PEG}$(NO$_2$)-AMP-N$_3$**, ITC **I-128** ampicillin (**I-143**)and ampicillin degradation products **I-149** and **I-150**. **B:** UV chromatogram at 254 nm of (B1) pure ***ps*GSL$_{PEG}$(NO$_2$)-AMP-N$_3$** (500 µM) in HEPES buffer (20 mM, pH 7.4), (B2) incubation of ***ps*GSL$_{PEG}$(NO$_2$)-AMP-N$_3$** (500 µM) with NfsB (10 µM), NADH (5 mM) and FMN (20 µM) in HEPES buffer (20mM, pH 7.4) after 2 h at 37°C and (B3) incubation of ***ps*GSL$_{PEG}$(NO$_2$)-AMP-N$_3$** (500 µM) with NfsB (10 µM), NADH (5 mM) and FMN (20 µM) in

HEPES buffer (20mM, pH 7.4) after 48 h at 37°C **C:** ESI+ mass analysis at (C1) 4.61 min of B1, (C2) 2.87 min of B2, (C3) 2.87 min of B3 and(C4) 1.81 min of B3.

***ps*GSL$_{PEG}$(NO$_2$)-AMP-N$_3$** (Figure I-21, A: structure B1: R_t 4.61 min and C1: mass 864.45 m/z for $[M+H]^+$) was converted by NfsB and the formation of a possible corresponding degradation product **I-149** (Figure I-21, A: structure, B2: R_t = 2.87 min, and C3: mass 217.16 m/z for $[M+H]^+$) of ampicillin was observed after 2 h incubation. No hydroxylamine or ITC formation was observed. Increasing the incubation time to 48 h, another degradation product **I-150** of ampicillin[160] (Figure I-21, A: structure, B2: R_t = 1.81 min, and C3: mass 173.18 m/z for $[M+H]^+$) was observed along with the previously formed degradation product **I-149** (Figure I-21, A: structure, B2: R_t = 2.87 min, and C3: 217.16 mass m/z for $[M+H]^+$) while ***ps*GSL$_{PEG}$(NO$_2$)-AMP-N$_3$**was completely consumed. The formation of the degradation product was consistent with the previously observed amoxicillin conjugate ***ps*GSL$_{C4}$(NO$_2$)-AMO-N$_3$**. As the incubation times were longer the ITC formed could have covalently bound to NfsB as previously shown by us.[158]

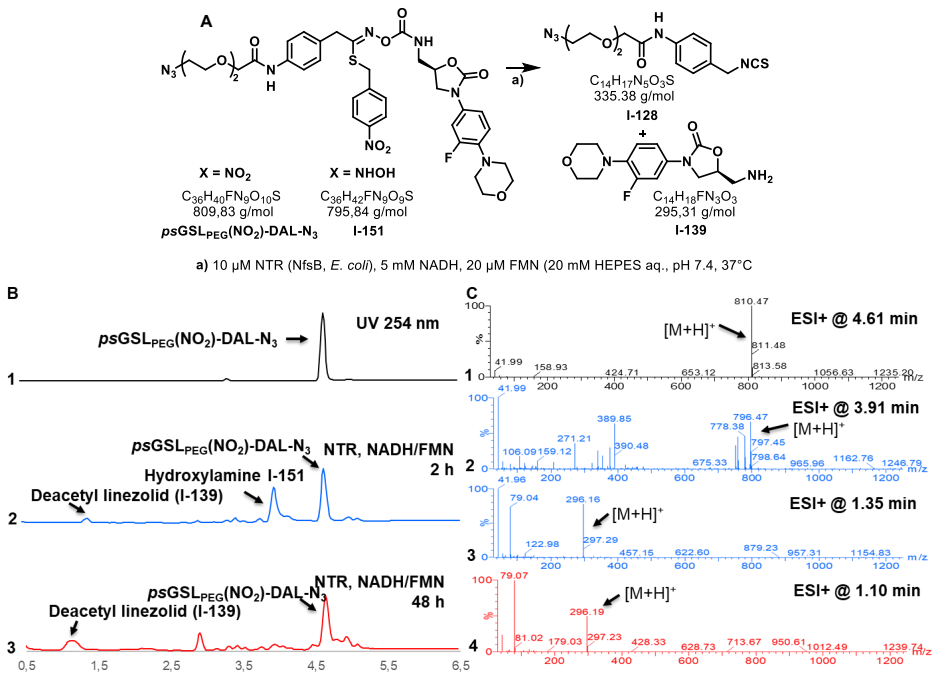

Figure I-22: LC-MS analysis after incubation of ***ps*GSL$_{PEG}$(NO$_2$)-DAL-N$_3$** with nitroreductase NfsB from *E. coli*. **A:** Structures of ***ps*GSL$_{PEG}$(NO$_2$)-DAL-N$_3$**, ITC **I-128**, hydroxylamine **I-151**, deacetyl linezolid (**I-139**). **B:** UV chromatogram at 254 nm of (B1) pure ***ps*GSL$_{PEG}$(NO$_2$)-DAL-N$_3$** (500 µM) in HEPES buffer (20 mM, pH 7.4), (B2) incubation of ***ps*GSL$_{PEG}$(NO$_2$)-DAL-N$_3$** (500 µM) with NfsB (10 µM), NADH (5 mM) and FMN (20 µM) in HEPES buffer (20mM, pH 7.4) after 2 h at 37°C and (B3) incubation of ***ps*GSL$_{PEG}$(NO$_2$)-DAL-N$_3$** (500 µM) with NfsB (10 µM), NADH (5 mM) and FMN (20 µM) in HEPES buffer (20mM, pH 7.4) after 48 h at 37°C **C:** ESI+ mass analysis at (C1) 4.61 min of B1, (C2) 3.91 min of B2, (C3) 1.35 min of B2 and(C4) 1.10 min of B3.

***ps*GSL$_{PEG}$(NO$_2$)-DAL-N$_3$** (Figure I-22, A: structure B1: R_t 4.61 min and C1: mass 810.47 m/z for $[M+H]^+$) was partially converted by NfsB and the formation of the corresponding hydroxylamine **I-151** (Figure I-

22, A: structure, B2: R_t = 3.44 min, and C3: mass 796.47 m/z for $[M+H]^+$) and a small amount of deacetyl linezolid (**I-139**) (Figure I-22, A: structure, B2: R_t = 1.35 min, and C3: mass 296.16 m/z for $[M+H]^+$) was observed after 2 h of incubation. When, incubation time was increased to 48 h and hydroxylamine **I-151** was not observed and there was an increase in the amount of released **I-155**.(Figure I-22, A: structure, B2: R_t = 1.10 min, and C3: mass 296.19 m/z for $[M+H]^+$) was observed along with the non-converted ***ps*GSL$_{PEG}$(NO$_2$)-DAL-N$_3$**. In all cases ITC formation was not detected via LC-MS analysis. The formation of hydroxylamine **I-151** and corresponding release of deacetyl linezolid (**I-139**) confirms the slow and incomplete conversion of ***ps*GSL$_{C4}$(NO$_2$)-DAL-N$_3$** by NTR.

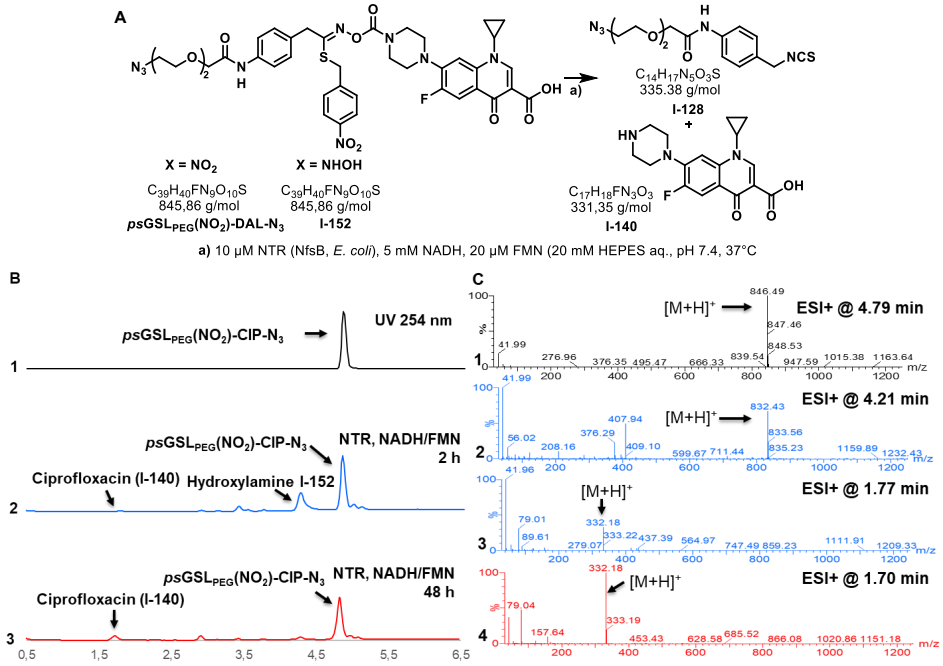

Figure I-23: LC-MS analysis after incubation of ***ps*GSL$_{PEG}$(NO$_2$)-CIP-N$_3$** with nitroreductase NfsB from *E. coli*. **A:** Structures of ***ps*GSL$_{PEG}$(NO$_2$)-CIP-N$_3$**, ITC **I-128**, hydroxylamine **I-152**, ciprofloxacin (**I-140**). **B:** UV chromatogram at 254 nm of (B1) pure ***ps*GSL$_{PEG}$(NO$_2$)-CIP-N$_3$** (500 µM) in HEPES buffer (20 mM, pH 7.4), (B2) incubation of ***ps*GSL$_{PEG}$(NO$_2$)-CIP-N$_3$** (500 µM) with NfsB (10 µM), NADH (5 mM) and FMN (20 µM) in HEPES buffer (20mM, pH 7.4) after 2 h at 37°C and (B3) incubation of ***ps*GSL$_{PEG}$(NO$_2$)-CIP-N$_3$** (500 µM) with NfsB (10 µM), NADH (5 mM) and FMN (20 µM) in HEPES buffer (20mM, pH 7.4) after 48 h at 37°C **C:** ESI+ mass analysis at (C1) 4.79 min of B1, (C2) 4.21 min of B2, (C3) 1.77 min of B2 and(C4) 1.70 min of B3.

***ps*GSL$_{PEG}$(NO$_2$)-CIP-N$_3$** (Figure I-23, A: structure B1: R_t 4.79 min and C1: mass 846.49m/z for $[M+H]^+$) was partially converted by NfsB and the formation of the corresponding hydroxylamine **I-152** (Figure I-23, A: structure, B2: R_t = 4.21 min, and C3: mass 832.43 m/z for $[M+H]^+$) and a small amount of ciprofloxacin (**I-140**) (Figure I-23, A: structure, B2: R_t = 1.77 min, and C3: mass 332.18 m/z for $[M+H]^+$) was observed after 2 h of incubation. When, incubation time was increased to 48 h and hydroxylamine **I-152** was not observed and there was an increase in the amount of released **I-140**.(Figure I-23, A: structure, B2: R_t = 1.70 min, and C3: mass 332.18 m/z for $[M+H]^+$) was observed along with the non-

converted ***ps*GSL$_{PEG}$(NO$_2$)-CIP-N$_3$**. In all cases ITC formation was not detected via LC-MS analysis. The formation of hydroxylamine **I-165** and corresponding release of ciprofloxacin (**I-140**) confirms the slow and incomplete conversion of ***ps*GSL$_{PEG}$(NO$_2$)-CIP-N$_3$** by NTR.

I-3.2.3.3. LC-MS analysis of the breakdown of UV (365 nm) *ps*GSL based antimicrobial probes

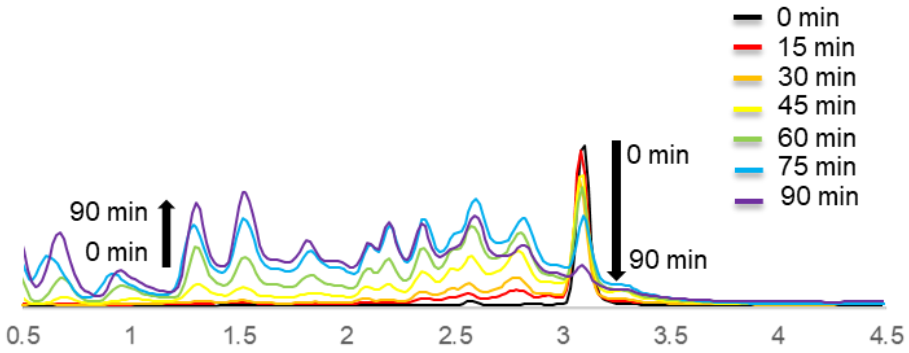

Figure I-24: UV chromatogram at 254 nm of the conversion of ***ps*GSL$_{C4}$(*o*-NO$_2$)-N$_3$** (1 mg/mL in MeCN:H$_2$O/1:1) after irradiation with hυ = 365 nm over the course of 90 min at 23°C (at t = 0, 15, 30, 45, 60, 75, 90 min).

***ps*GSL$_{C4}$(*o*-NO$_2$)-CIP-N$_3$** was evaluated via LC-MS analysis for the controlled release of ciprofloxacin (**I-140**) under UV (365 nm). For this the compound was dissolved in MeCN:H$_2$O (1:1) for a final concentration of 1 mg/mL and irradiated with a LED laser at hυ = 365 nm for 15, 30, 45, 60, 75 and 90 min respectively (Figure I-24). A steady decrease in the amount of ***ps*GSL$_{C4}$(*o*-NO$_2$)-CIP-N$_3$** and a small increase in the amount of ciprofloxacin was observed over the course of 90 minutes including the formation of many light sensitive degradation products of ciprofloxacin. A detailed analysis of ***ps*GSL$_{C4}$(*o*-NO$_2$)-CIP-N$_3$** (Figure I-25, A: structure, B2: R_t = 3.01 min, and C3: mass 653.34 m/z for $[M+H]^+$) breakdown after irradiation with a LED laser at hυ = 365 nm for 90 min revealed the formation of ciprofloxacin degradation products as **I-153** (Figure I-25, A: structure, B2: R_t = 0.67 min, and C3: mass 334.19 m/z for $[M+H]^+$), **I-154** (Figure I-25, A: structure, B2: R_t = 1.00 min, and C3: mass 306.19 m/z for $[M+H]^+$) and **I-155** (Figure I-25, A: structure, B2: R_t = 1.53 min, and C3: mass 291.09 m/z for $[M+H]^+$) along with the release of the desired ciprofloxacin (**I-140**) product (Figure I-25, A: structure, B2: R_t = 1.34 min, and C3: mass 332.21 m/z for $[M+H]^+$). Although ciprofloxacin was unstable under UV 365 nm, there is clear evidence of the release of ciprofloxacin.

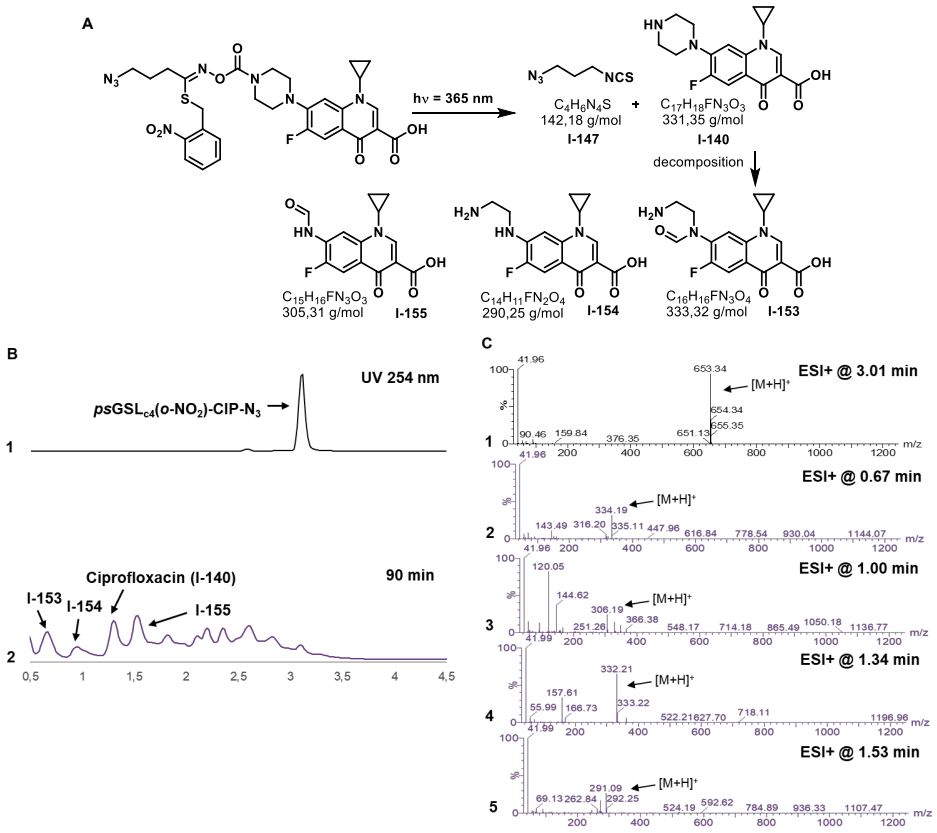

Figure I-25*:* LC-MS analysis of ***ps*GSL$_{c4}$(*o*-NO$_2$)-N$_3$** (1 mg/mL in MeCN:H_2O/1:1) after irradiation with hυ = 365 nm at 90 min at 23°C **A:** Structures of ***ps*GSL$_{c4}$(*o*-NO$_2$)-N$_3$**, ITC **I-147**, **I-152**, ciprofloxacin (**I-140**) and degradation products **I-153**, **I-154**, **I-155**. **B:** UV chromatogram at 254 nm of (B1) pure ***ps*GSL$_{c4}$(*o*-NO$_2$)-N$_3$** (1 mg/mL in MeCN:H_2O/1:1), (B2) irradiation of ***ps*GSL$_{c4}$(*o*-NO$_2$)-N$_3$** with hυ = 365 nm for 90 min at 23°C. **C:** ESI+ mass analysis at (C1) 3.01 min of B1, (C2) 0.67 min of B2, (C3) 1.00 min of B2, (C4) 1.34 min of B2 and (C5) 1.53 min of B2.

The controlled release of daptomycin from ***ps*GSL$_{c4}$(*o*-NO$_2$)-CIP-N$_3$** under irradiation with UV-light (365 nm) is currently being evaluated.

Additionally, it is planned to evaluate the NTR-responsive *ps*GSL based antimicrobial prodrugs in a MIC assay with *E. coli*. since they are well known to express NfsB. These assays would provide a preliminary proof of principle of the antibiotic release in a bacterial system and provide insight into the synergistic effect of the released antibiotic and ITC. This part of the work is in collaboration with the research group of Prof. Dr. Anne Farewell at the University of Gothenburg.

Further experiments are ongoing towards the immobilization of these probes onto resin beads utilizing a CuAAC with the terminal azide present in all probes and evaluation of the drug release in both enzymatic assay as well as MIC assays with *E. coli.*

I-3.3 Development of multivalent glucosinolates (mv-GSLs)

As discussed earlier in section I-2.3., the main aim of this work was to develop and study multivalent glucosinolates (mv-GSLs). These mv-GSLs were designed with additional β-D-pyranose moieties on bivalent or trivalent oxime-*O*-sulfonate backbones. Upon enzymatic cleavage by myrosinase, unstable aglycones were expected to undergo thio-*Lossen* rearrangements, generating multivalent isothiocyanates (ITCs) as active metabolites (Scheme I-20). The synthesis involved nucleophilic substitution with tetra-*O*-acetyl-1-thio-β-D-glucopyranose on intermediary chloro oximes derived from bis- or tri-aldehydes (Scheme I-21). Beyond validating enzymatic cleavage, the study aimed to evaluate the influence of nitrile specifier protein (AtNSP3) on nitrile formation and explore the antimicrobial and biofilm-inhibitory potential of multivalent ITCs, thereby broadening their potential applications.

I-3.3.1 Docking study of aliphatic bivalent mv-GSL (I-161b) with myrosinase from *Sinapsis alba*

The envisaged design of the mv-GSLs (Figure I-26A), particularly **I-161b** was evaluated for possible conversion by myrosinase as its monovalent counterpart, by docking **I-161b** into the active site of *Sinapis alba* myrosinase using the SeeSAR software[155]. Firstly, as a reference the co-crystal structure of the non-hydrolyzable carba-GSL **I-36j** with *Sinapis alba* myrosinase (PDB: 1W9B)[161] was used (Figure I-26B). Here it was observed that the glucose moiety of **I-36j** is deeply embedded in the binding pocket, forming a hydrogen bond network with Glu^{464}, His^{141}, Gln^{39}, Glu^{405}, and a water molecule (H_2O^{2742}). A second hydrogen bond network involves Gln^{187}, Ser^{190}. The thiohydroximate-*O*-sulfonate moiety of **I-36j**. interacts with another water molecule (H_2O^{2740}), and the guanidine groups of Arg459 and Arg194. Lastly, the lipophilic benzyl side chain of **I-36j** occupies a hydrophobic region within the pocket formed by Phe^{331}, Phe^{371}, and Ile^{382}.

Docking of aliphatic mv-GSL **I-161b** into the same myrosinase binding pocket (PDB: 1W9B) yielded a pose closely resembling that of **I-36j** (Figure I-26C). One glucose unit of **I-161b** was similarly embedded in the pocket, participating in a comparable hydrogen bond network with Glu^{464}, His^{141}, Gln^{39}, Glu^{405}, and the water molecule (H_2O^{2742}). The second hydrogen bond network, involving Gln187, Ser^{190}, the water molecule (H_2O^{2742}), Arg^{459}, and Arg^{194}, was also formed with the thiohydroximate-*O*-sulfonate group of **I-161b**. Additionally, the C5 carbon chain of **I-161b** occupied the lipophilic region of the pocket, interacting with Phe^{331}, Phe^{371}, and Ile^{382}. The second thiohydroximate-*O*-sulfonate moiety and glucose unit of **I-161b** extended outward from the binding pocket, forming two extra hydrogen bonds with Arg^{194} via a sulfonate oxygen and the C2 hydroxy group. The structural overlay of **I-36j** and **I-161b** showed minimal deviations in atomic positions for the glycosidic thiohydroximate-*O*-sulfonate moiety (Figure I-17D). Based on these docking results, we concluded that mv-GSL **I-161b** is likely a suitable substrate for *Sinapis alba* myrosinase.

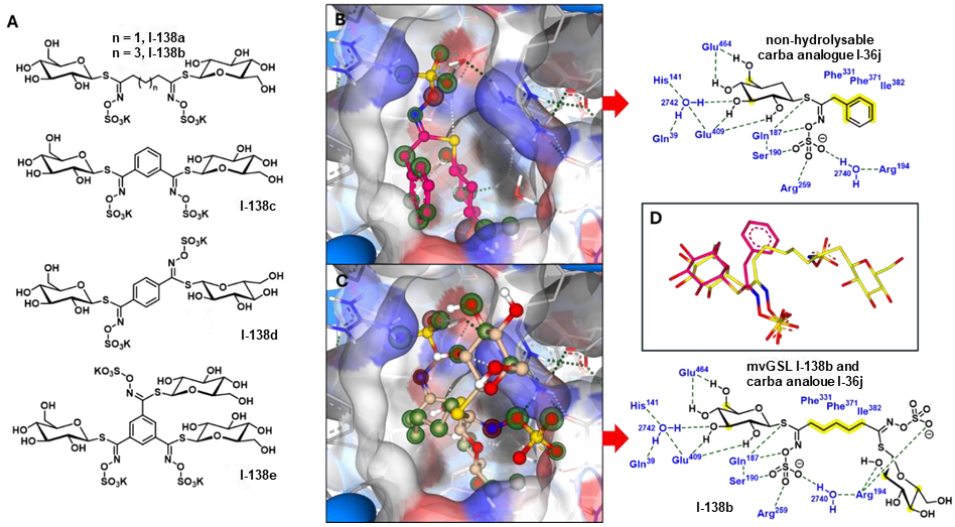

Figure I-26: A: Structures of artificial multivalent glucosinolates (mv-GSLs). **B**: 3D-illustration of the co-crystal structure and binding interactions of the non-hydrolyzable carba-GSL **I-36j** in the active center of myrosinase from *Sinapis alba* (PDB:1W9B).[161] **C:** Docking of mv-GSL **I-161b** onto myrosinase from *Sinapis alba* (PDB:1W9B)[161] **D**: 3D-overlay of **I-161b** and **I-36j** and 3D-illustrations of the binding interactions. The docking was performed and 3D-illustration were generated with SeeSAR version 14.0.0; BioSolveIT GmbH, 2024, www.biosolveit.de/SeeSAR.[155] Green spheres around atoms indicate overall favorable contributions to ΔG(Hyde), red spheres around atoms indicate overall unfavorable contributions to ΔG(Hyde).[157] Hydrogen bridges are indicated by dotted green lines. Light grey illustration represents surface of the binding pocket with elements surrounding the bound mv-GSL in red (oxygen), blue (nitrogen) and yellow (sulfur). Grey shadows represent unoccupied space in the binding pocket. D: overlay of the structures of carba-GSL **I-36j** (purple) and mv-GSL **I-161b** (yellow).

I-3.3.2 Synthesis of multivalent glucosinolates (mv-GSLs)

The aliphatic mv-GSLs **I-161a** and **I-161b** were synthesized using a classical chloroaldoxime approach,[136] (Scheme I-28). The bivalent alcohol **I-156** was oxidized in the presence of IBX to yield the corresponding bis-aldehyde **I-157b** with a yield of 99%. The commercially available aldehyde **I-157a** and synthesized aldehyde **I-157b** were then reacted with hydroxylamine in the presence of sodium acetate to produce the bis-oximes **I-158a** and **I-158b** in yields of 67% and 72% respectively, as a mixture of E:Z stereoisomers (99.9:0.1). The bis-oximes were then converted into bis-chloro oxime using NCS in DMF under light exclusion *in-situ* and immediately coupled with 2,3,4,6-tetra-O-acetyl-1-thio-β-D-glucopyranose (**I-57**) in the presence of triethylamine, resulting in the thiohydroximate **I-159a** and **I-159b** in yields of 86% and 91%, respectively. The *O*-sulfonate was installed as its potassium salt by treatment with the SO_3·Py complex followed by potassium hydrogen carbonate, yielding compounds I-160a and **I-160b** in 43% and 63% yields, respectively. Finally, the deprotection of acetates was performed using methanolic ammonia, affording the aliphatic mv-GSLs **I-161a** and **I-161b** in quantitative yields.

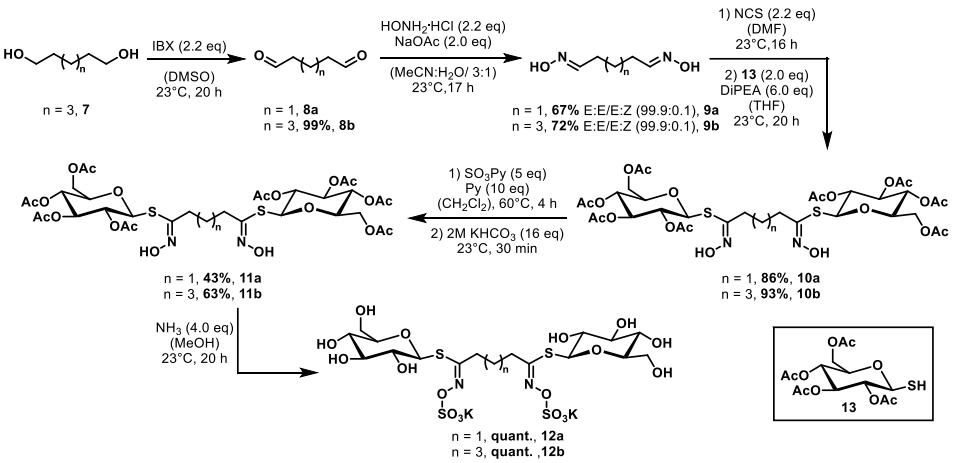

Scheme I-28: Synthesis of divalent aliphatic mv-GSLs.

The aromatic mv-GSLs **I-161c**, **I-161d** (Scheme I-29), and **I-161e** (Scheme I-30) were synthesized from their commercially available aldehyde precursors **I-157c**, **I-157d** and **I-157e**. The synthetic route followed was identical to the previously described method. The respective aromatic aldehydes **I-157c**, **I-157d** and **I-157e** were converted into oximes **I-158c, I-158d** and **I-158e** with quantitative, 50%, and 81% yield respectively. The *in-situ* formation of chloro oxime, followed by coupling with 2,3,4,6-tetra-*O*-acetyl-1-thio-β-D-glucopyranose (**I-57**) in the presence of triethylamine, yielded the aromatic thiohydroximates **I-159c**, **I-159d** and **I-159e** in 74%, 69%, and 70% yields, respectively. The *O*-sulfonation of the thiohydroximates resulted in **I-160c**, **I-160d** and **I-160e** with yields of 74%, 75%, and 45%, respectively. Finally, the removal of acetate groups on the glucopyranose under basic conditions afforded the final bivalent aromatic mv-GSLs **I-161c**, **I-161d** and **I-161e** in yields ranging from quantitative to high yields, specifically 98%, 99%, and 99%, respectively.

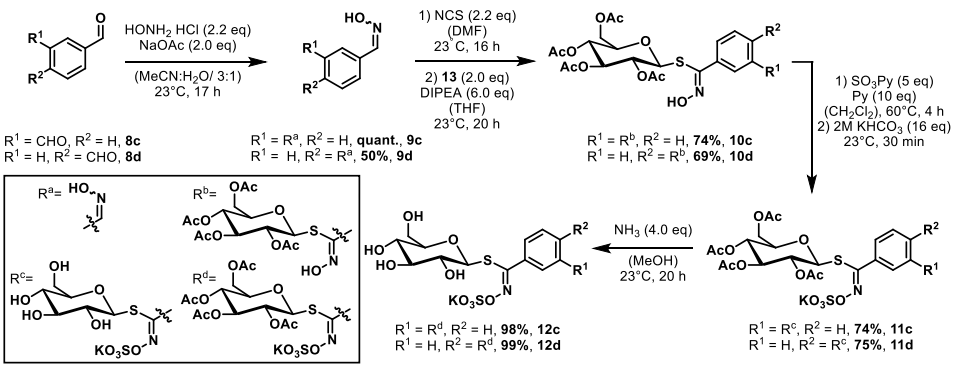

Scheme I-29: Synthesis of divalent aromatic mv-GSLs

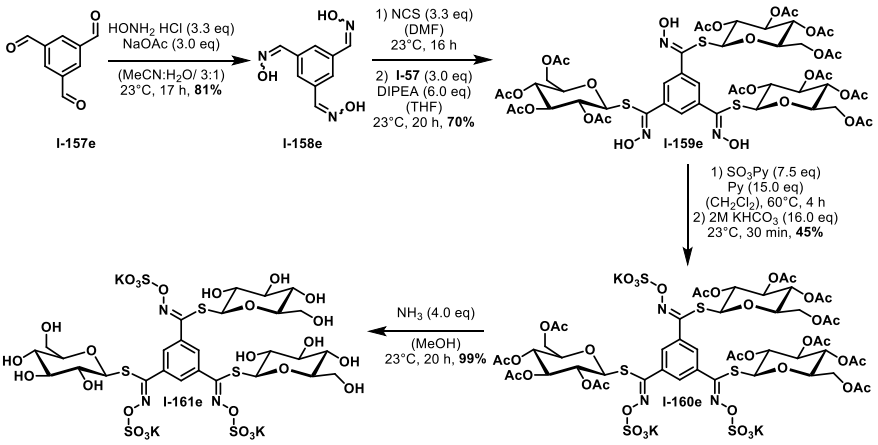

Scheme I-30: Synthesis of trivalent aromatic mv-GSL.

Finally, a monovalent aromatic GSL was synthesized to be used as a control for the enzymatic assays with myrosinase. The synthetic route was the same as the other aromatic mv-GSLs (Scheme I-31). benzaldehyde (**I-157f**) was converted to oxime **I-158f** in quantitative yield, followed by an *in-situ* formation of chloro oxime and immediate coupling with **I-57** gave thiohydroximate **I-159f** in 63% yield. Subsequent O-sulfonation gave **I-160f** in 90% yield and a final removal of the acetate groups provide the final compound **I-161f** in quantitative yield

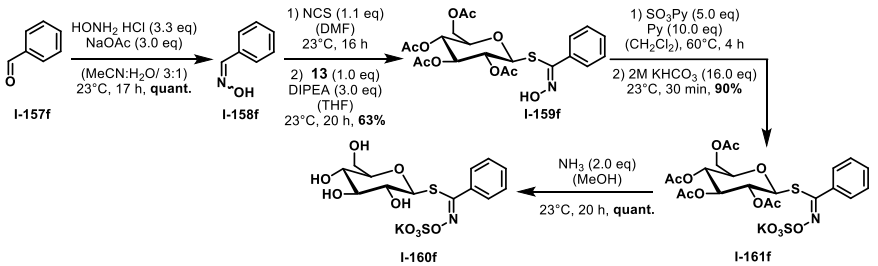

Scheme I-31: Synthesis of monovalent aromatic GSL

I-3.3.3 Evaluation of mv-GSLs

I-3.3.3.1 GC-MS analysis of ITC release from breakdown of mv-GSLs

With the synthesized mv-GSLs **I-161a-e** in hand, their conversion in the presence of myrosinase from *Sinapis alba* into the corresponding multivalent isothiocyanates (mv-ITCs) **I-162a-e** was investigated using qualitative GC-MS analysis (Scheme I-32, Table I-1). To this end, the compounds (2 mM) were incubated with 0.06 units/mL myrosinase from *Sinapis alba* in 50 mM MES buffer (pH 6.0) at 37°C for 24 hours. After incubation, benzonitrile was added as an internal standard, and the reaction mixtures were extracted with dichloromethane. The resulting extracts were then analyzed by GC-MS.

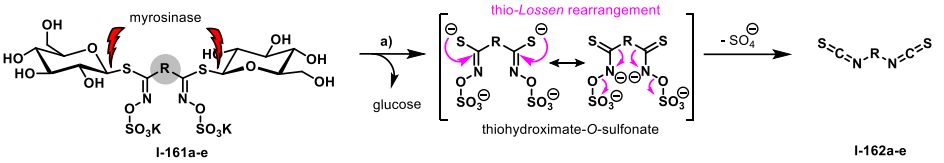

Scheme I-32: Schematic representation of ITC release from mv-GSLs

Table I-1: Qualitative GC-MS analysis of the hydrolysis of mv-GSLs in the presence of myrosinase from *Sinapis alba*.

Entry	Compound	Retention Time (min)	Structure of ITC	Mass of ITC	Fragmentation (m/z)
1	**I-161f**	13.1	 I-162f	135.01	135, 77, 51, 50
2	**I-161a**	17.4	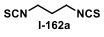 I-162a	158.00	158, 72, 44, 41, 40
3	**I-161b**	20.0	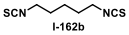 I-162b	186.02	186, 128, 72, 69, 44, 41
4	**I-161c**	20.1	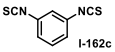 I-162c	191.98	192, 160, 134, 90, 44
5	**I-161d**	-	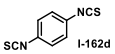 I-162d	191.98	-
6	**138e**	-	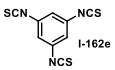 I-162e	248.94	-

- =no conversion, nt = not tested

The best conversion was observed for aliphatic bivalent mv-GSL **I-161b** (Table I-1, Entry 3) as observed in Figure I-27A. The corresponding mass fragmentation (Figure I-27B) confirmed the formation of ITC **I-162b**. A suitable mechanism for the mass fragmentation is shown in Scheme I-33, where the molecular ion (M^+) observed at m/z 186 undergoes fragmentation from the homolytic or heterolytic cleavage of bonds. α-Fragmentation results in a peak at m/z 128 corresponding to fragment **I-165**. From this fragment, two possible pathways lead to further fragmentation: either producing fragment **I-167** resulting in a peak at m/z 72 or yielding fragment **I-166** with a corresponding peak at m/z 69. Subsequently, the elimination of ethylene results in the final peak of the spectrum at m/z 41, corresponding to fragment **I-168**.

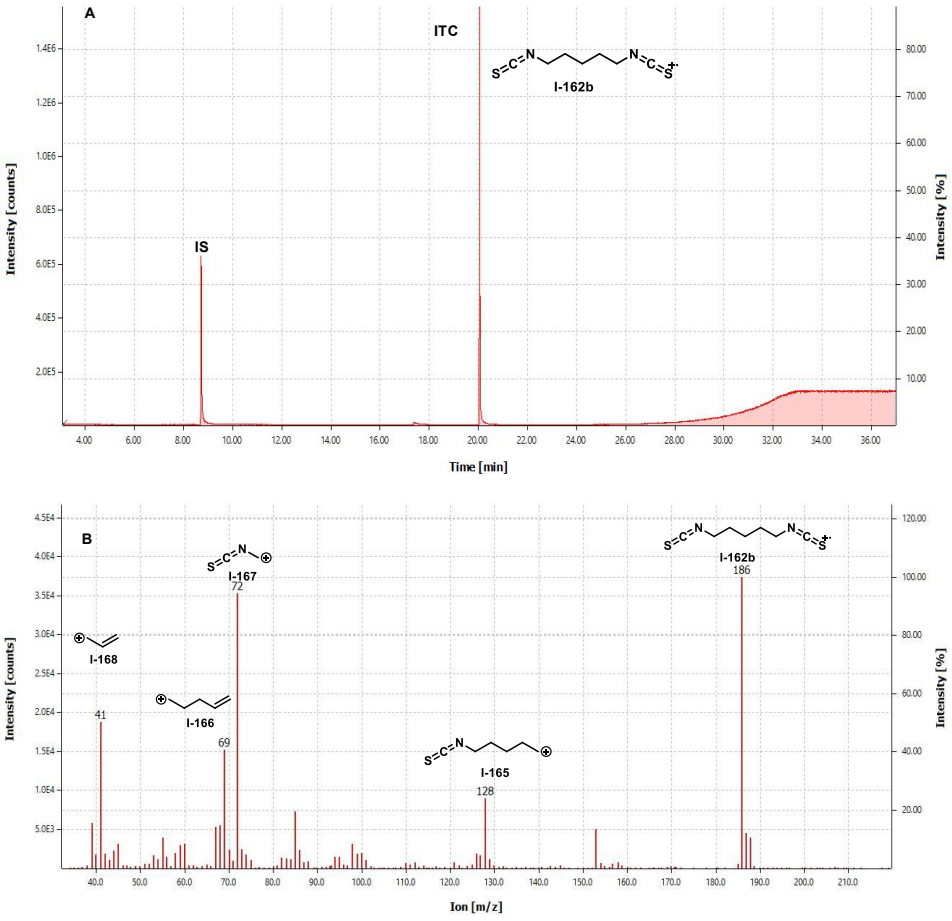

Figure I-27: GC-MS analysis of compound **I-161b**. A) Gas chromatogram of 2mM **I-161b** incubated with 0.06 units /mL myrosinase from *Sinapsis alba* in 50mM (pH=6.0) MES buffer for 24 h at 37°C; B): Mass fragmentation spectrum of ITC **I-162b**, R_t = 20.0 min.

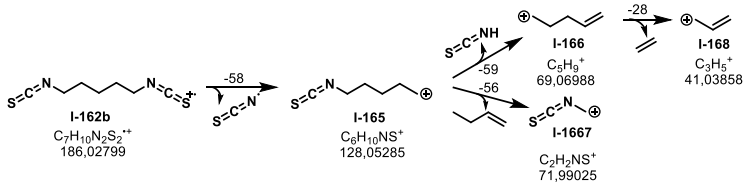

Scheme I-33: Proposed mechanism for mass fragmentation observed for **I-161b**.

Similarly, ITC formation was observed for aliphatic bivalent mv-GSL **I-161a** (Table I-1, Entry 2) and aromatic bivalent mv-GSL **I-161c** (Table I-1, Entry 4). In the case of **I-161c** the formation of ITC **I-162c** was very low as seen in Figure I-28. On the other hand, aromatic para substituted mv-GSL **I-161d** and

aromatic trivalent mv-GSL **I-161e** were not converted at all pointing to the fact that they were no longer substrates for myrosinase.

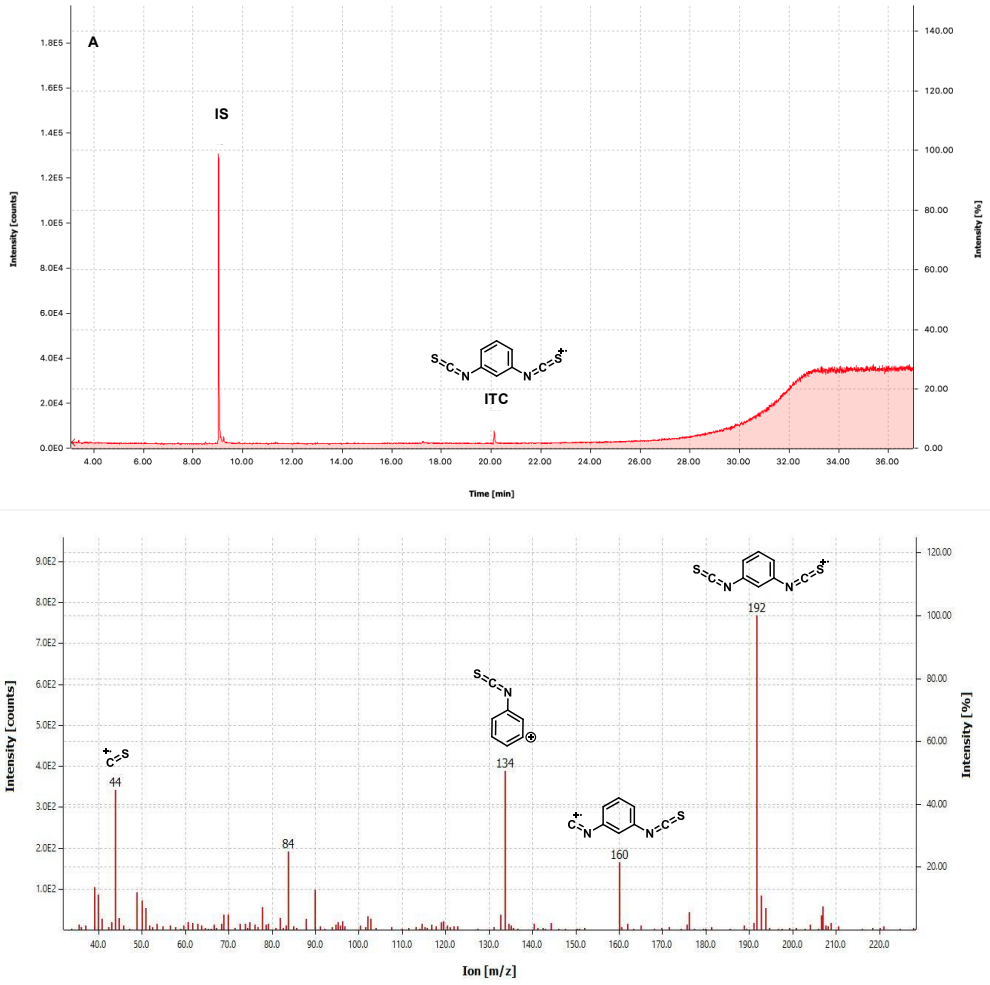

Figure I-28: GC-MS analysis of compound **I-161c**. Gas chromatogram of 2mM **I-161c** incubated with 0.06 units/mL myrosinase from Sinapsis alba in 50mM (pH=6.0) MES buffer for 24 h at 37°C; B): Mass fragmentation spectrum of ITC **I-162c**, R_t = 20.1 min.

Beyond that the mv-GSLs were evaluated to observe the formation of multivalent nitriles with NSP, AtNSP3 from *Arabidopsis thaliana*.as shown in Scheme I-34. Therefore, mv-GSLs (**I-161a-c**) were incubated for 24 h in presence of 0.06 units /mL myrosinase from *Sinapsis alba* in 50mM (pH=6.0) MES buffer, 0.01 mM $(NH_4)_2Fe(SO_4)_2$, and 5-10 µg of nitrile-specifier protein AtNSP3 from *Arabidopsis thaliana*, obtained from heterologous expression in *E. coli*.[162] After incubation, benzonitrile as internal standard was added and the mixtures were extracted with dichloromethane and the extracts were analyzed by GC-MS. Consistent with the prior results the mv-GSLs **I-161e** and **I-161f** were not converted. The results are compiled in Table I-2.

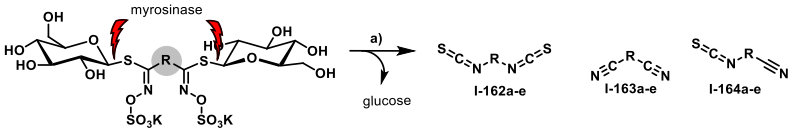

Scheme I-34: Schematic representation of release of breakdown products from mv-GSLs in presence of AtNSP3

Table I-II: Qualitative GC-MS analysis of the hydrolysis of mv-GSLs in the presence of myrosinase from *Sinapis alba* and AtNSP3 from *Arabidopsis thaliana*.

Entry	Compound	Retention Time (min)	Derivatization product	Structure	Mass of ITC	Fragmentation (m/z)
1	**I-161a**	17.4	ITC	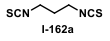 I-162a	158.00	158, 72, 44, 41, 40
2	**I-161a**	10.5	CN	 I-163a	94.05	103, 84, 54, 49, 41
3	**I-161a**	14.1	ITC/CN	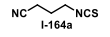 I-164a	126.03	126, 86, 72, 68, 41
4	**I-161b**	20.0	ITC	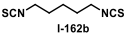 I-162b	186.02	186, 128, 72, 69, 44, 41
5	**I-161b**	14.4	CN	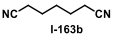 I-163b	122.08	82, 55, 54, 44, 41
6	**I-161b**	17.4	ITC/CN	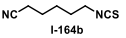 I-164b	154.06	154, 69, 55, 44, 41
7	**I-161c**	-	ITC	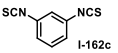 I-162c	191.98	-
8	**I-161c**	14.0	CN	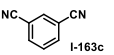 I-163c	128.04	128, 101, 84, 75, 40
9	**I-161c**	17.2	ITC/CN	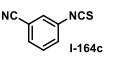 I-164c	160.00	160, 128, 84, 64, 44
10	**I-161d**	-	ITC	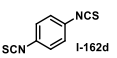 I-162d	191.98	-
11	**I-161d**	-	CN	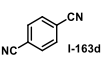 I-163d	128.03	-
12	**I-161d**	-	ITC/CN	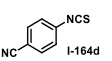 I-164d	160.00	-
13	**I-161e**	-	ITC	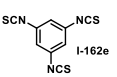 I-162e	248.94	-
14	**I-161e**	-	CN	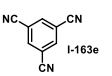 I-163e	153.03	-
15	**I-161e**	-	ITC/CN	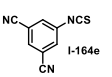 I-164e	185.00	-

- =not observed

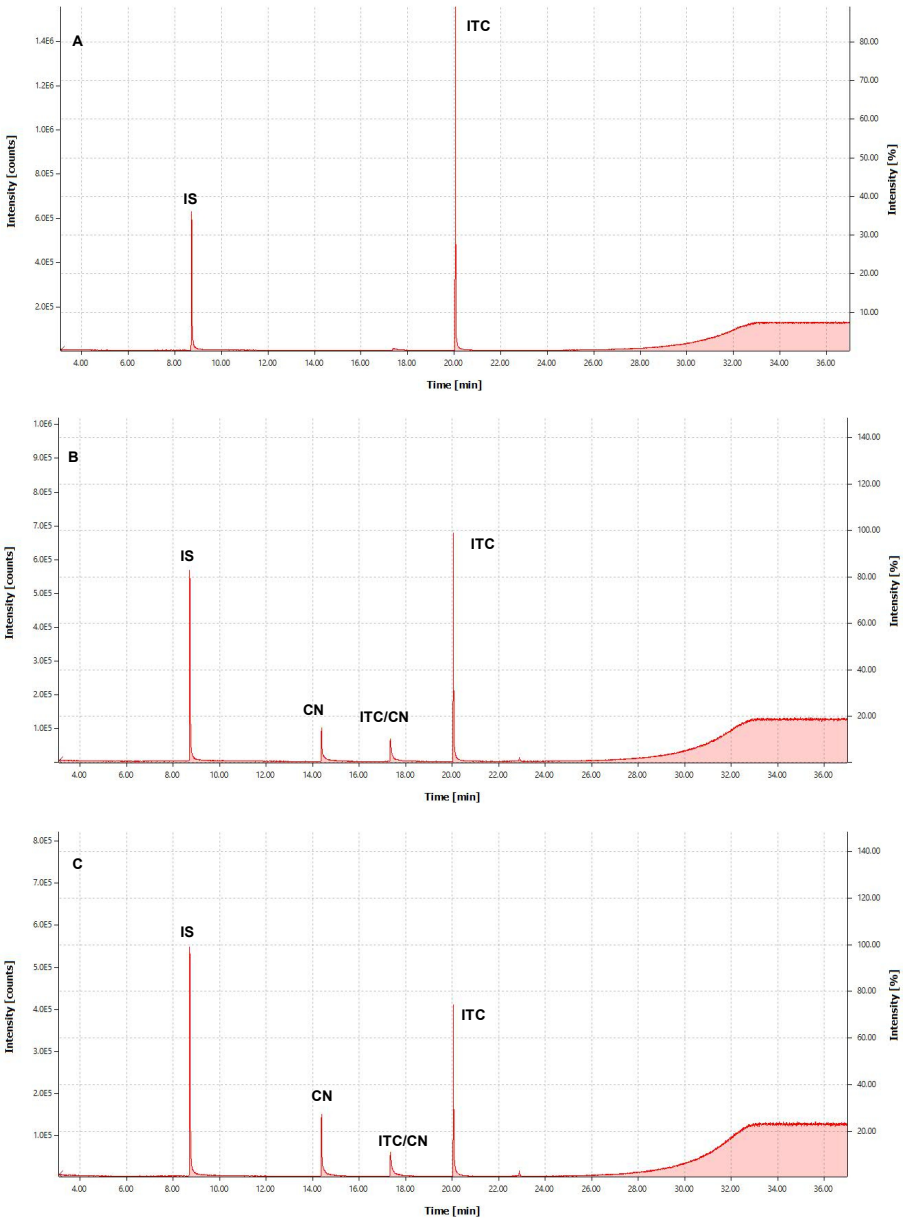

Figure I-29: Gas chromatogram of GC-MS analysis of compound **I-161b**. A) 2mM **I-161b** incubated with 0.06 units/mL myrosinase from *Sinapsis alba* in 50mM (pH=6.0) MES buffer, for 24 h at 23°C, B) 2mM **I-161b** incubated with 0.06 units/mL myrosinase from *Sinapsis alba* in 50mM (pH=6.0) MES buffer, 0.01 mM $(NH_4)_2Fe(SO_4)_2$, and 5 µg of nitrile-specifier protein AtNSP3 from *Arabidopsis thaliana* for 24 h at 23°C, C) 2mM **I-161b** incubated with 0.06 units/mL myrosinase from *Sinapsis alba* in 50mM (pH=6.0) MES buffer, 0.01 mM $(NH_4)_2Fe(SO_4)_2$, and 10 µg of nitrile-specifier protein AtNSP3 from *Arabidopsis thaliana* for 24 h at 23°C.

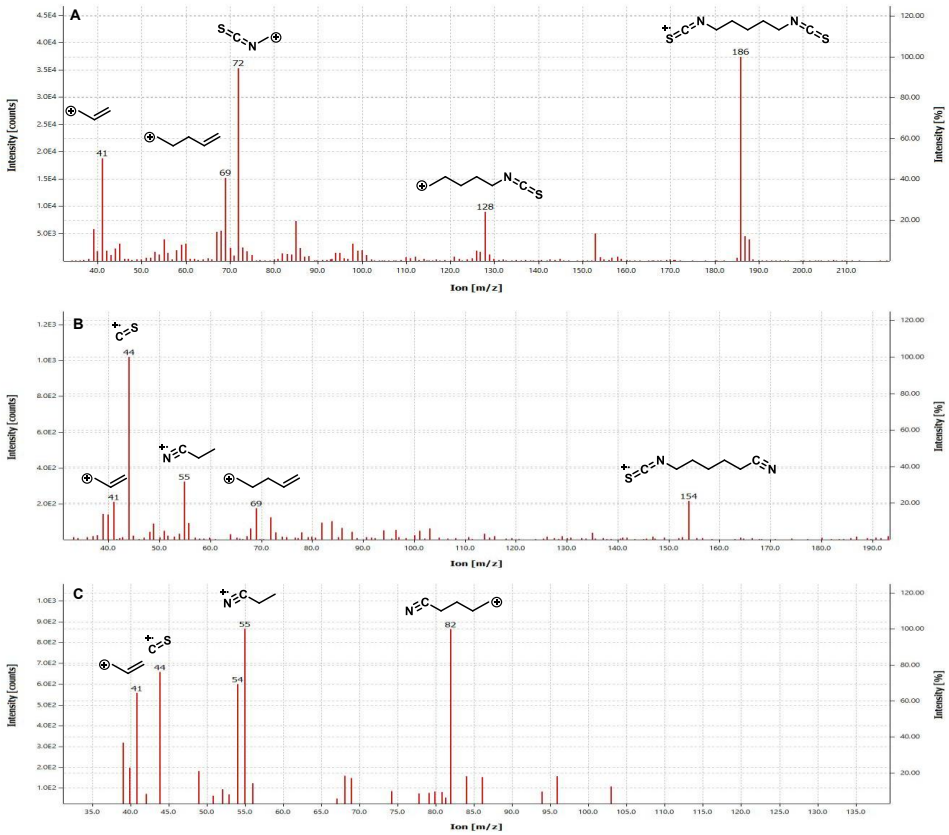

Figure I-30: Mass spectra. A) Mass fragmentation spectrum of ITC **I-162b**, (R_t = 20.0 min), C) Mass fragmentation spectrum of ITC/CN **I-164b**, (R_t = 17.4 min), C) Mass fragmentation spectrum of CN **I-163b**, (R_t = 14.4 min).

For aliphatic mv-GSL **I-161b** (Table I-2, Entry 5) only incomplete conversion to nitrile breakdown product was observed along with partial nitrile **I-164b** (Table I-2, Entry 6) as shown in Figure I-29B as compared to formation of only ITC in the control experiment as shown in Figure I-29A. The ITC was the major product which was observed (Table I-2, Entry 4) (Figure I-29B). Increasing the amount of AtNSP3 from 5 µg to 10 µg showed a small increase in the amount of nitrile formed (Figure I-29C). For the aromatic bivalent meta substituted mv-GSL **I-161d**, complete conversion to corresponding nitrile **I-163d** (Table I-2, Entry 8) and partial nitrile **I-164d** (Table I-2, Entry 9) breakdown products were observed as seen in Figure I-31B. The effect of increasing the amount of bivalent nitrile formed AtNSP3 from 5 to 10 µg could not be well quantified (Figure I-31C). The reason for complete conversion could be the small amount of ITC formation in the first place. Although the amount of ITC **I-162b** for aliphatic bivalent mv-GSL **I-161b** is reduced by 50% in presence of AtNSP3, it is not entirely depleted, meaning it could still function as a feeding deterrent in herbivores which utilize specifier proteins. However, this is not the case for compound **I-161c**. due to the low initial concentration of ITC **I-162c.** These findings suggest that the linear aliphatic mv-GSLs exhibit a stronger profile as feeding deterrents compared to aromatic its aromatic counterparts.

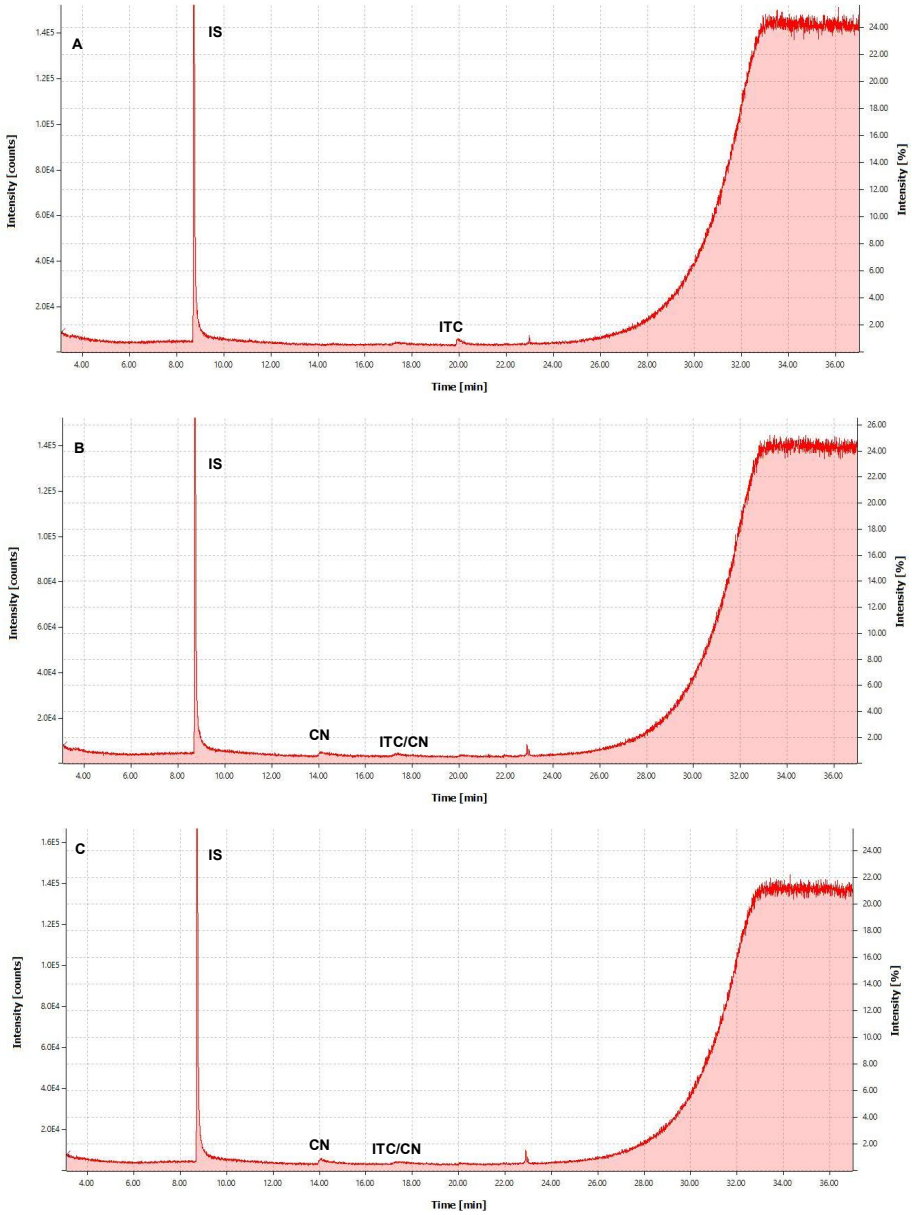

Figure I-31: Gas chromatogram of GC-MS analysis of compound **I-161c**. A) 2mM **I-161c** incubated with 0.06 units/mL myrosinase from *Sinapsis alba* in 50mM (pH=6.0) MES buffer, for 24 h at 23°C, B) 2mM **I-161c** incubated with 0.06 units/mL myrosinase from *Sinapsis alba* in 50mM (pH=6.0) MES buffer, 0.01 mM $(NH_4)_2Fe(SO_4)_2$, and 5 µg of nitrile-specifier protein AtNSP3 from *Arabidopsis thaliana* for 24 h at 23°C, C) 2mM **I-161c** incubated with 0.06 units/mL myrosinase from *Sinapsis alba* in 50mM (pH=6.0) MES buffer, 0.01 mM $(NH_4)_2Fe(SO_4)_2$, and 10 µg of nitrile-specifier protein AtNSP3 from *Arabidopsis thaliana* for 24 h at 23°C.

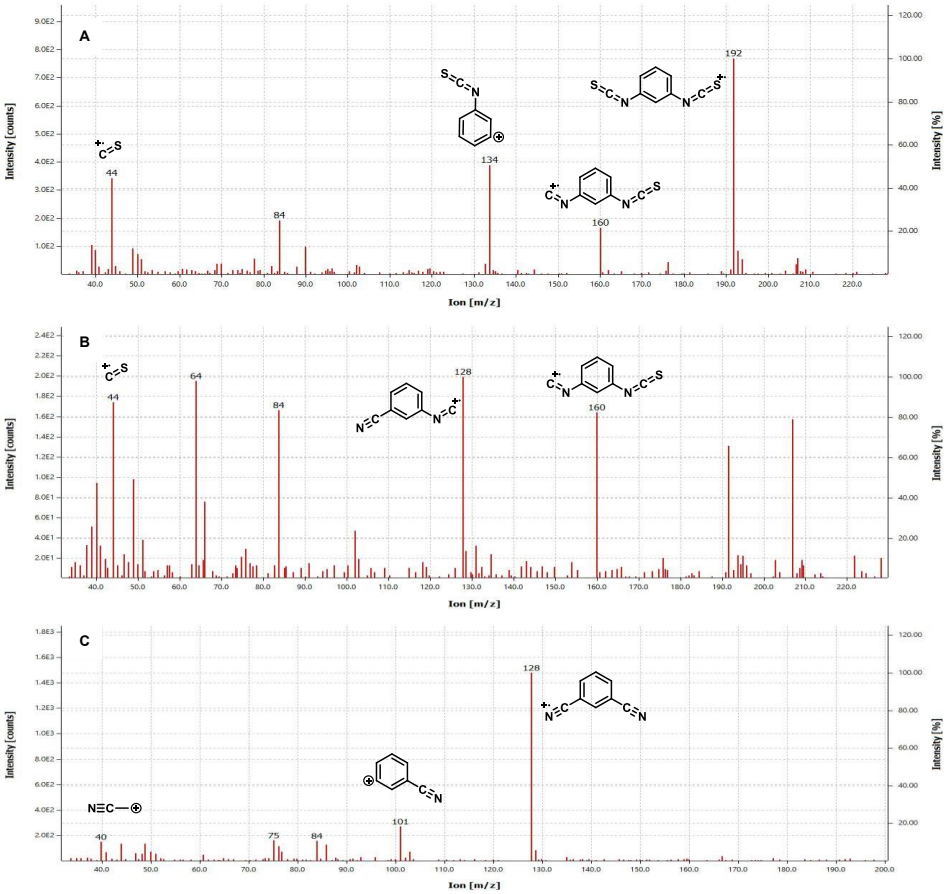

Figure I-32: Mass spectra. A) Mass fragmentation spectrum of ITC **I-162c**, (R_t = 20.1 min), C) Mass fragmentation spectrum of ITC/CN **I-164c**, (R_t = 17.2 min), C) Mass fragmentation spectrum of CN **I-163c**, (R_t = 14.0 min).

I-3.3.3.2 Quantitative GOD-PAP analysis of ITC release from breakdown of mv-GSLs

Additionally, the hydrolysis of mv-GSLs **I-161a-e** into mv-ITCs **I-162a-e** was evaluated using a glucose-oxidase-peroxidase-4-aminoantipyrine (GOD-PAP) assay by coworkers at the Klahn lab.[163,164] to indirectly measure the amount of released glucose (Scheme I-35, Table I-3). For this purpose, 1 µmol of the respective mv-GSLs was incubated with 0.03 units/mL of myrosinase from *Sinapis alba* in 50 mM MES buffer (pH 6.0) at 37°C for 4 hours and 24 hours respectively. An aliquot of the reaction mixture was subsequently incubated with glucose oxidase from *Aspergillus niger*, horseradish peroxidase, and o-dianisidine (**I-171**). The hydrogen peroxide produced during glucose oxidation enabled the peroxidase-catalyzed oxidation of **I-171** to its corresponding quinonimine **I-172**, which, upon the addition of sulfuric acid, formed a pink protonated complex **I-173**. This was then analyzed and quantified through UV-Vis spectroscopy at 540 nm. The amount of glucose determined was directly

proportional to the extent of hydrolyzed thiohydroximate-*O*-sulfonate moieties in the respective molecules.

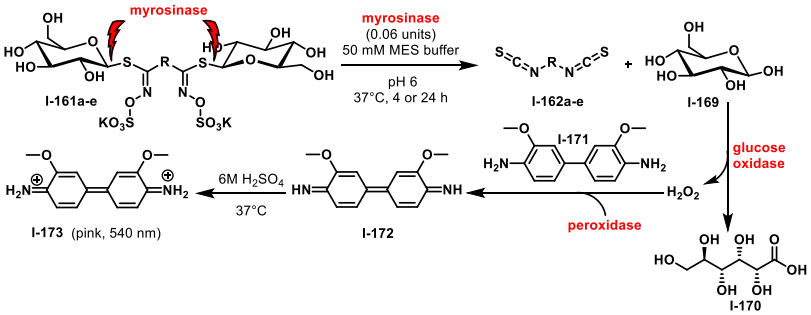

Scheme I-35: Schematic representation of GOD-PAP assay for mv-GSLs.

Table I-3: Quantitative analysis of the hydrolysis of mv-GSLs in the presence of myrosinase from *Sinapis alba*, based on hydrolyzed glucose content by GOD-PAP assay.[163,164]

Entry	Compound	Incubation time (4h)		Incubation time (24h)	
		Glucose (µmol)	Glucose %	Glucose (µmol)	Glucose %
1	**I-161f**	0.83	83	nt	nt
2	**I-161a**	0.37	19	0.75	38
3	**I-161b**	1.03	52	1.40	70
4	**I-161c**	0.13	6.5	0.63	32
5	**I-161d**	-	-	-	-
6	**I-161e**	-	-	-	-

nt = not tested, - = no conversion

Consistent with previous hydrolysis experiments, only mv-GSLs **I-161a**, **I-161b**, and **I-161c** exhibited conversion in the presence of myrosinase from *Sinapis alba*. The conversion of the aromatic mv-GSL **I-161c** proceeded the slowest, with only 6.5% after 4 hours and 32% after 24 hours (Table I-3, Entry 4). In contrast, mv-GSL **I-161a**, containing an aliphatic C3 core, reached 19% conversion after 4 hours and 38% after 24 hours (Table I-3, Entry 2). The fastest conversion was observed with mv-GSL **I-161b**, bearing an aliphatic C5 core, achieving 52% conversion after 4 hours and 70% after 24 hours. However, this conversion rate remained significantly slower than that of the naturally occurring monovalent GSL **I-161f**, which showed 83% conversion after just 4 hours (Table 3, Entry 1).

Overall, the qualitative and quantitative analysis of mv-GSLs (**I-161a-e**) provided proof of principle of conversion to corresponding mv-ITCs (I-162a-c) with myrosinase in the case of aliphaltic bivalent (**I-161a-b**) and aromatic bivalent (**I-161c**) mv-GSLs. The same compounds were also shown to convert to their corresponding mv-nitriles (**I-163a-c**) and mixed metabolites (**I-164a-c**) upon incubation with NSP (AtNSP3 from *Arabidopsis thaliana*).

I-3.3.3.3 Evaluation of mv-GSLs against microbial pathogens

The compounds were evaluated for antimicrobial and biodilm activity by our collaboration partners Prof. Dr. Marc Stadler, Dr. Hedda Schrey, Hoaxuan Zeng and Wera Collisi at the Helmholtz Centre for Infectious Research in Braunschweig, Germany. The mv-GSLs (**I-161 a-e**) were tested against a panel of Gram-positive and Gram-negative bacteria (*B. subtilis, S. aureus, M. Smegmatis, A. baumanni, C. violaceum, E. coli,* and *P. aeruginosa*) and different fungi (*M. hiemalis, P. anomala, R. glutinis*, *C. albicans* and *S. pombe*) but none of the compounds (**I-161 a-f**) showed antimicrobial activity up to a concentration of 66.7 µg/mL as shown in Table I-4.

Table I-4: MIC [µg/mL] assay data

		MIC [µg/mL]					
Tested organisms	**Strain No.**	**I-161a**	**I-161d**	**I-161c**	**I-161d**	**I-161e**	**Reference**
Bacteria							
Bacillus subtilis	DSM 10	–	–	–	–	–	4.2[a]
Staphylococcus aureus	DSM 346	–	–	–	–	–	0.4[a]
Mycobacterium smegmatis	ATCC 700084	–	–	–	–	–	1.7[c]
Acinetobacter baumannii	DSM 30008	–	–	–	–	–	0.5[d]
Chromobacterium violaceum	DSM 30191	–	–	–	–	–	0.4[a]
Escherichia coli	DSM 1116	–	–	–	–	–	1.7[a]
Pseudomonas aeruginosa	PA14	–	–	–	–	–	0.4[e]
Fungi							
Mucor hiemalis	DSM 2656	–	66.6	66.6	–	66.6	8.3[f]
Pichia anomala	DSM 6766	–	–	–	–	–	4.2[f]
Rhodoturula glutinis	DSM 10134	–	–	–	–	–	2.1[f]
Candida albicans	DSM 1665	–	–	–	–	–	8.3[f]
Schizosaccharomyces pombe	DSM 70572	–	–	–	–	–	4.2[f]

References: [a] oxytetracycline, [b] vancomycin, [c] kanamycin, [d] ciprobay, [e] gentamicin, [f] nystatin; –: not active.

Next a crystal violet assay was used for evaluation of the antibiofilm effects of the mv-GSLs. Although these compounds lack antimicrobial activity, they showed moderate to low biofilm dispersion in C. albicans with the highest activity for aliphatic bivalent mv-GSL bearing a C5 core of 56% biofilm dispersion (Table I-5). Both aliphatic mv-GSL **I-161a** and trivalent aromatic mv-GSL **I-161e** showed very poor anti-biofilm activity.

Table I-5: Inhibition of biofilm formation on *C. albicans* biofilms

Compound	Biofilm dispersion (C. albicans)[% ±SD]
I-161a	32 ± 10 (250 µg/mL) [a]
I-161b	56 ± 6 (250 µg/mL) [a]
I-161c	49 ± 11 (250 µg/mL) [a]
I-161d	43 ± 8 (250 µg/mL) [a]
I-161e	34 ± 10 (250 µg/mL) [a]

References [%]: [a] farnesol: 78 (250 µg/mL), 70 (31.3 µg/mL), 42 (15.6 µg/mL); SD: standard deviation

Finally, mv-GSLs (**I-161a-e**) were evaluated in a standard MTT antiproliferation assays assay against cervical adenocarcinoma (KB3.1) cell and mice fibroblasts (L929) not showing any cytotoxic activity.

GSLs are known to be transported throught GTR present in GSL rich plants. Therefore, it was planned to evaluate the synthesized mv-GSLs for uptake studies with GTRs expressed in *Arabidopsis thaliana*, and get an insight if they are still transported by the receptors. This work is currently ongoing in collaboration with the group of Prof. Dr. Hussam Hassan Nour-Eldin at the University of Copenhagen. For this expression plasmids containing genes for GTR1, GTR2, and GTR3 from *Arabidopsis thaliana* are generated and used for heterologous expressions in oocytes of *Xenopus laevis*. The oocytes are injected with cRNA transcribed from these plasmids, and the expressed proteins are localized to the plasma membrane, where they mediated the import of glucosinolates into the cytosol. This assay has been designed to evaluate transport specificity, substrate range, and efficiency of artificial GSLs.[141]

I-4. Conclusion and Outlook

I-4.1. Successful proof-of-principle for the concept of *ps*GSLs and potential future applications

The successful synthesis and evaluation of NTR responsive *ps*GSLs (***ps*GSL$_{PEG}$(NO$_2$)-N$_3$**, ***ps*GSL$_{PEG}$(NO$_2$)-DNSA** and ***ps*GSL$_{PEG}$(NO$_2$)-BODIPY**) and AzoR responsive *ps*GSL (***ps*GSL$_{PEG}$(Azo)-N$_3$**, ***ps*GSL$_{PEG}$(Azo)-BODIPY**) provide a significant foundation for their use as enzymatically activated tools for selective ITC release and biomolecular labeling. The developed probes demonstrated high sensitivity and specificity for enzymatic cleavage by NTR and AzoR, as confirmed by LC-MS, fluorescence spectroscopy, and SDS-PAGE analysis. Notably, the fluorescent ITCs (**I-131a, I-131b**) generated upon enzymatic activation covalently labeled key proteins such as NfsB and BSA, further demonstrating their potential for targeted labeling applications. Experiments in *C. elegans* validated the capability of the NTR-responsive probe (***ps*GSL$_{PEG}$(NO$_2$)-BODIPY**) to function *in vivo*, highlighting their potential as imaging and therapeutic tools. Furthermore, the incorporation of FRET-based fluorescent dyes, as seen in the AzoR-responsive probes, allowed for real-time monitoring of enzymatic activity, showcasing their utility in dynamic biochemical and cellular studies. Additionally, the ability to tune the probes' response and reactivity by modifying their core structures and masking groups further highlights their versatility.

These *ps*GSL probes show potential for application in a variety of fields such as targeted drug delivery for site-specific activation in disease environments, where the released ITC could also covalently bind to nucleophilic surroundings. Furthermore, similar FRET based probes like ***ps*GSL$_{PEG}$(Azo)-BODIPY** can be further optimized to serve as highly specific reporters of enzymatic activity in biological imaging, enabling the visualization of metabolic processes utilizing the fluorescence turn on effect. Their application in protein labeling and proteomics can enhance the study of enzyme-substrate interactions and protein function.

I-4.2. Successful drug release from *ps*GSLs and potential future application within antimicrobial prodrugs

The synthesis and evaluation of *ps*GSL-based antimicrobial prodrugs with both C4 and PEG linkers revealed their potential as substrates for NTR-mediated activation. However, the results demonstrated that these prodrugs exhibited slow and incomplete conversion by NfsB from *E. coli*, with limited release of the corresponding antibiotics via LC-MS analysis. The instability of some released β-lactam antibiotics, such as amoxicillin (**I-138**) and ampicillin (**I-143**), under the experimental conditions indicates that a proper selection of appropriate antibiotics need to be made in future studies. While hydroxylamine intermediates were identified for several compounds, the observed partial conversions highlight the need for optimization in both prodrug design and reaction conditions to enhance activation efficiency and drug release. Current ongoing studies aim to evaluate the antimicrobial efficacy of these prodrugs.

Furthermore, for the design of second generation *ps*GSL-based antimicrobial prodrugs, the *p*-nitrobenzyl thiol could be replaced by a more elongated thiol fragment to reduce possible steric hindrance and make the nitro trigger more accessible to NfsB. The design concept is mentioned in Figure I-27, where upon enzymatic activation the extended thiol moiety would undergo a double cascade to finally release the antibiotic and ITC via a thio-*Lossen* rearrangement. With the structure

optimized for enzymatic release, these prodrugs could be immobilized on resin beads and evaluated for antimicrobial activity as surface coatings. Currently, this is being explored in the Klahn lab.

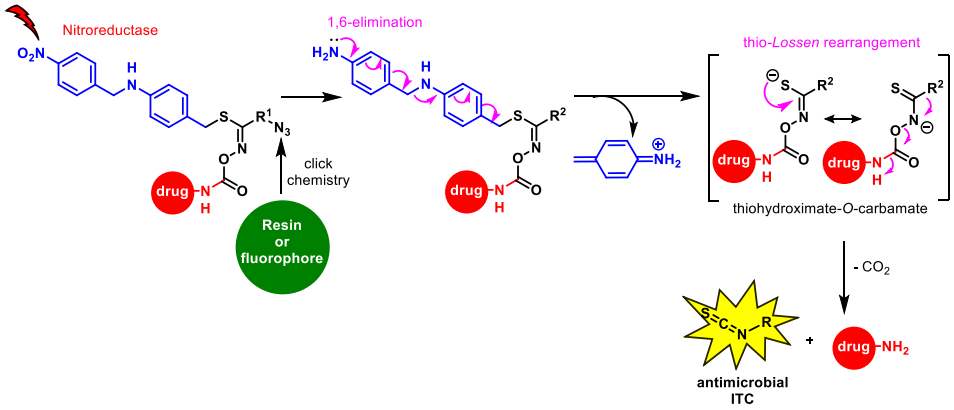

Scheme I-36: Design of second generation of *ps*GSL based antimicrobial prodrugs.

Additionally, UV-responsive *ps*GSL-based antimicrobial prodrugs bearing a C4 backbone were successfully synthesized in good to moderate yields. Evaluation of these probes successfully demonstrated the controlled release of ciprofloxacin (**I-140**) from ***ps*GSL$_{C4}$(*o*-NO$_2$)-CIP-N$_3$** under UV irradiation (365 nm). LC-MS analysis revealed a steady decrease in ***ps*GSL$_{C4}$(*o*-NO$_2$)-CIP-N$_3$** and the release of ciprofloxacin, along with the formation of photodegradation products of the attached drug ciprofloxacin. Although the design needs to be further improved, these preliminary results highlight the potential of UV-responsive *ps*GSL-based prodrugs for targeted drug release being independent of enzymes.

I-4.3. First-in-class multivalent glucosinolates (mv-GSLs) and potential future applications

In this work a small series of novel mv-GSLs (**I-161a-e**) were successfully synthesized in good yields. The subsequent qualitative and quantitative evaluation of these probes provided valuable insights into their chemical behavior, enzymatic conversion, and biological activities. Among the synthesized compounds, the aliphatic mv-GSL **I-161b** exhibited the most efficient enzymatic hydrolysis to its corresponding isothiocyanate ITC **I-162b** in the presence of myrosinase, highlighting the significant influence of core structure for efficiency of the enzymatic conversion. In contrast, the aromatic mv-GSLs like **I-161c** demonstrated either slower conversion rates or complete resistance to enzymatic hydrolysis in the case of **I-161d** and **I-38e**. These findings were corroborated by the GOD-PAP assay, which quantified glucose release as an indirect measure of hydrolysis. The mv-GSLs were further shown to be converted into nitriles in presence of AtNSP3. Despite their lack of antimicrobial activity against a range of pathogens, some mv-GSLs showed moderate biofilm dispersion effects, particularly **I-161b** with a C5 aliphatic core, suggesting limited biofilm-modulating potential.

Although proof-of-principle was obtained for the activity of selected mv-GSLs as substrates for myrosinase, the design of these probes needs to be improved for better conversion to their corresponding mv-ITCs in presence of myrosinase. With an improved structural hydrolytic efficiency against myrosinase, investigations into the environmental stability and controlled release of ITCs

derived from these mv-GSLs could also provide valuable insights for agricultural and pharmaceutical applications. Furthermore, based on this work, development of mv-GSLs responsive to enzymes like NTR, azoreductase or cytochrome P450s could open new routes to explore the effect of the controlled release of such multivalent ITCs in a physiological context.

II. Development of non-cytotoxic coumarins with antibiofilm activity

II-1. Antimicrobial resistance: Evolution, mechanisms and solutions.

II-1.2 Antimicrobial resistance

Antimicrobial resistance (AMR) posing as one of the greatest threats to public health continues to be a global burden. It has a huge impact on cost to healthcare systems, global population health and gross domestic product (GDP).[165,166] Antimicrobial resistance is defined as the ability of microorganisms to survive and be viable in the presence of antimicrobial agents such as antibiotics, food preservatives or disinfectants.[167] Widespread, prolonged and unchecked use of antimicrobials has given microbes an opportunity to grow resistance against them through natural evolution. Such newly emerging resistant strains make infections more persistent in patients, resulting in higher mortality rates, morbidity and clinical complications.[168–171] The general mistakes which have acted as contributors to the AMR problem can be simply classified as overuse of antibiotics in healthy livestock as prophylaxis,[172] treating infections of sick animals or even in animal food and drinking water in high volume livestock production on a global scale.[152] Unnecessary use or misuse of antimicrobials resulting from either self-medication,[173,174] improper prescribing patterns[175–177] or easier access to cheap drugs.[178] Furthermore, there is a lack of novel antibiotics and the ones being developed are in some form derived from existing antibiotics making it likely to develop resistance in the long run.[179] The lack of new drugs is particularly dangerous for infants and the geriatric populations due to their weaker immunity against aggressive infections.[180]

II-1.3 Bacterial resistance pathways

The escalating issue of bacterial resistance to antimicrobial drugs, must be recognized as a natural and inevitable aspect of bacterial evolution.[152] Microbes have developed several mechanisms of resistance towards antimicrobials. The most common is via inactivation of antibiotics. β-lactam antibiotics (penicillins, cephalosporins) prevent cross-linking of the glycan chain in bacterial cell wall by binding to penicillin binding proteins (PBPs). To combat this, resistant bacteria secretes β-lactamase enzymes which hydrolyze the amide bond of the β-lactam ring, thus rendering it ineffective.[181] In gram negative bacteria *Enterobacteriaceae*, the enzyme located in the periplasmic space deactivates the antibiotic before it reaches *the PBPs*. Similarly, in gram positive *Staphylococcus* sp. these enzymes make the antibiotic ineffective outside the cell wall.[182]

Aminoglycoside antibiotics (streptomycin, gentamycin) bind to ribosomal units of bacteria to prevent essential protein synthesis.[183] As seen in *Pseudomonas aeruginosa* the three enzymes secreted to inactivate aminoglycoside antibiotics are AG *O*-nucleotidyl transferases (ANTs), AG *N*-acetyl transferases (AACs), and AG *O*-phosphotransferases (APHs). They make chemical modifications to specific positions in the substrate. A family of AACs causes enzymatic *N*-acetylation of amino groups at specific positions. APHs, phosphorylate aminoglycoside antibiotics like neomycin, and streptomycin. For example, [APH (3')] in *Pseudomonas aeruginosa* modifies the 3'-OH of the antibiotic. While ANTs cause adenylation in aminoglycosides such as streptomycin, gentamycin and tobramycin.[184–190]

For macrolides, three possible enzymatic modifications are responsible for developing resistance. In *Enterococcus* sp., *Staphylococcus aureus* and *Streptococcus* sp., genes ereA or ereB cause ring cleavage via hydrolysis in erythromycin,[182,191] mgt gene causes glycosylation in macrolides[192,193] and mphA, mphB, and mphB genes cause macrolide phosphorylation.[194]

Resistance can also arise due to alteration in the target site. Bacteria resistant towards β-lactam antibiotics can alter the PBP structure, reducing attraction between the drug and target.[181] Vancomycin-resistant *Staphylococcus aureus* (VRSA) strains isolated in 2003,[195,196] use the pathway where they employ multiple proteins in order to recreate the peptidoglycan, inhibiting vancomycin binding, and simultaneously retaining cell wall integrity.[197] In *Mycobacteria tuberculosis*, a mutation in the rrs gene exerting an influence on the 16S in the A-site of the ribosome, leads to resistance against aminoglycoside antibiotics.[198] Additionally, ribosomal modifications can occur in the binding site of aminoglycosides by RNA methyltransferases (RMTases), which methylate a nucleotide in the 16S rRNA in presence of *S*-adenyosyl-L-methionine (SAM) as a coenzyme.[199] Furthermore, mutations in rRNA domains leads to decreased antibiotic affinity in *Staphylococcus aureus*[194] and *Escherichia coli*.[200] Resistance in *Streptococcus pneumonia* against fluroquinolones is observed via enzyme alteration in which DNA gyrase is mutated in quinolone resistance regions, thus decreasing the affinity towards the drug.[201–203] Trimethoprim resistant *Staphylococcus aureus*[204] and *Streptococcus pneumonia*[205] have a mutation in their dhfr gene through the substitution of one amino acid which leads to chromosomal alteration.

Another way of developing resistance is through decreasing permeability of the antibiotic where the antibiotic is removed from the bacterial cell. However, for aminoglycosides, efflux pumps are limited due to their polycationic structure. As observed in *Escherichia coli* the multidrug transporter efflux pump AcrAD is responsible for aminoglycoside resistance.[206] Macrolide efflux transporters can be classified as four main types like M-type associated with mefA and mef E genes as seen for *Streptococcus pneumonia*, MS-type associated with mrsA gene as seen for *Staphylococcus aureus*, Actinomycete-type associated with tlrC, carA, and srmB genes and Multidrug resistant-type associated with MdfA and unc genes.[194,207] Moreover, gram negative bacterial cell envelope is more resistant to drug diffusion because of lesser protein porins.[208,209]

II-1.3 Biofilms: Nature's slime

Apart from the intrinsic nature of microbes to mutate and disarm antimicrobials, biofilms are also a significant contributor to the AMR problem. In nature, bacteria and other microbes exist in structured aggregates within a self-produced matrix called biofilms.[210] They can be found in seawater, groundwater, ocean sediment, soil or other extreme environmental conditions.[211,212] Due to the protective nature of the matrix[213] and physiological changes producing more metabolically dormant cells,[211,214] biofilms are extremely tolerant to harsh conditions and physical stressors.[215] Biofilms lead to contamination of drinking water,[216] biomedical devices, prosthetics and implants,[217] thus making infections more persistent and recurrent.[211,218] Biofilm induced infections are especially difficult to tackle due to their innate antimicrobial resistance and their characteristic host immune response.[218] These chronic infections also cause an adaptive inflammatory response if case the biofilms are not cleared by the system.[219–221] In cystic fibrosis biofilm induced chronic infections limit life expectancy severely.[222] Chronically infected wounds also increase morbidity rates and puts a burden on the healthcare system.[223]

The formation of biofilm is a dynamic and complex process that involves physiological changes to the bacterial cell and formation of adhesins.[224,225] Biofilm formation is strain dependent and also influenced by the external environment, like in the case of *Pseudomonas aeruginosa* the shape of the biofilm depends on the external media.[226] In *Staphylococcus aureus* four different kinds of biofilms are found, namely polysaccharide biofilms dependent on *N*-acetylglucosamine and polysaccharide intercellular adhesin expression, extracellular (e-DNA) biofilm where the e-DNA is incorporated from

lysed cells through cell-to-cell communication via surface proteins, fibrin biofilms in which coagulase-mediated activation of plasminogen helps with fibrin incorporation into the matrix and amyloid biofilms where phenol-soluble molecules are utilized for the biofilm propagation.[227]

II-1.4 Formation and disruption of biofilms

The general process of biofilm formation includes five steps: preliminary attachment, irreversible attachment, formation of micro-colonies, maturation and dispersion (Figure II-1).[210,228] The first stage involves the reversible attachment of free flowing planktonic cells to biotic or abiotic surfaces.[213,229] It is also possible for a small aggregate of bacteria to initiate the first attachment, sometimes arising from pre-existing biofilms.[230] Under extreme conditions it is more likely that these self-aggregates attach onto a surface since they are more resilient to stress than planktonic cells.[230] Apart from direct surfaces, they can also attach to host proteins[231] as observed for *Staphylococcus aureus*, where it attaches to fibrin proteins present on catheter coatings.[232] The initial attachment is then followed by irreversible attachment.[212,233] Next, micro-colonies start forming resulting from the upregulation of a secondary metabolite, intracellular cyclic diguanylate monophosphate (c-di-GMP).[234] Synthesized by diguanylate cyclases (DGCs), c-di-GMP is broken down by phosphodiesterases (PDEs). High levels of c-di-GMP reduce cell motility, thus mutations in certain genes downregulate PDEs to increase aggregation and formation of larger matrices and biofilm mass.[235] The maturation process involves expansion of the micro-colonies[236] and secretion of extracellular matrix.[237] It contributes to the 90% of biofilm mass and is made up of a collection of biopolymers, known as extracellular polymeric substances (EPS). EPS includes polysaccharides, proteins, lipids and eDNA2.[213] The EPS however depends on different factors, like population of microorganisms, nutrient availability, and the environmental temperature.[211,213] At the maturation stage bacterial colonies employ cell to cell communication known as quorum sensing (QS), to respond to cell density, pH, signal flow rates in the surrounding community and change their behavior accordingly.[238–240]

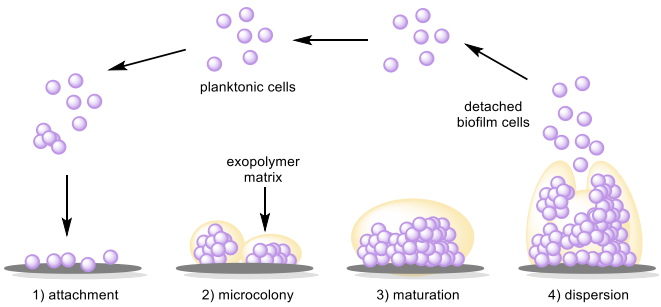

Figure II-1: Life cycle of biofilms.[224]

Signaling molecules called auto inducers, are detected, produced and released during the QS process.[239,241,242] This helps with formation and maintenance of biofilms as well as regulating virulence factors within the colony.[224,242,243] After maturation the last stage is biofilm dispersion, which can occur in various ways like seeding involving release large amounts of aggregates and EPS resulting in hollow cavities in the matrix, sloughing is a similar process involving abrupt detachment of substantial fragments.[244,245] In contrast, erosion involves passive detachment of smaller fragments over time, mostly due to external stress.[244,245] Furthermore, glycoside hydrolases, capable of breaking down glycosidic bonds within the EPS, can induce biofilm dispersal.[246,247]

Biofilm disruption for *Pseudomonas aeruginosa* was observed for compounds like acetylcholine or structurally similar compounds having a benzothiazole unit. They were reported to downregulate EPS producing genes, thus reducing cell adherence and expression of biofilm EPS.[247] Other EPS degrading enzymes such as glucanohydrolases, dispersin B, or DNAse can eliminate biofilms[248] Biofilm disrupting agents in combination with antimicrobials act synergistically and increases diffusion of antimicrobials into the matrix.[249] Bacteriophages in combination with ciprofloxacin has been shown to be effective for *Pseudomonas aeruginosa* biofilm associated infections.[250,251] Another strategy for biofilm disruption is to use efflux pump inhibitors like thioridazine, phenyl-arginine β-naphthylamide (PAβN), or the 1-(1-naphthylmethyl)-piperazine (NMP), which have been shown to inhibit biofilm formation in bacteria such as *Escherichia coli*, *Klebsiella pneumonia*, *Staphylococcus aureus*, and *Pseudomonas putida*.[238,252] Lastly, *N*-acylcyclopentylamides as quorum sensing (QS) inhibitors can also be used like *N*-(2-hydroxyphenyl)-3-oxododecanamide which is known to interfere with the rh1 QS system as well as las QS system. *N*-Octanoylcyclopentylamide moderately inhibits expression of transcriptional fusion genes in *Pseudomonas aeruginosa.*[253] Furthermore, twitching induced by lactoferrin causes bacterial cells to disperse than form biofilms in *Pseudomonas aeruginosa.*[254] Additionally, plant metabolites like coumarins have been reported to have antibiofilm activity[255–257] like coumarins isolated from *Mesua Ferrera* had an efflux pump inhibitory effect on *Staphylococcus aureus,*[255] which makes them interesting lead compounds to explore their antibiofilm effects.

II-1.5 Coumarins and their bioactivities

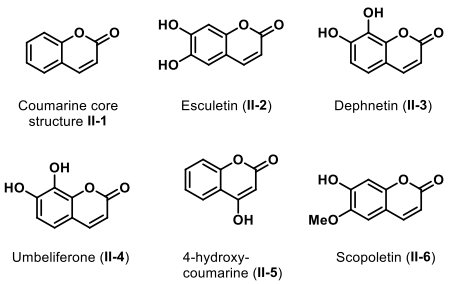

Figure II-2: Selected examples of biologically active coumarins.

Coumarins are a class of naturally occurring molecules biosynthesized by plant tissue.[258] They are also regarded as phytoalexins, produced as a response to pathogenic infection.[259] These compounds are found in various plant sources, including cinnamon oil, sweet clover, beans, and lavender.[260] They were also identified in bacteria and fungi *Streptomyces*[261] and different *Aspergillus* sp.[262] Structurally, they have both aliphatic and aromatic characteristic, the core structure consists of a benzene ring attached to an alpha-pyrone ring, also classified as benzopyrones (Figure II-2).[258] Plant families like *Umbelliferae*, *Rutaceae*, *Compositae*, *Leguminosae*, *Oleaceae*, *Moraceae*, and *Thymelaeaceae* produce high levels of these compounds.[263] These plant phenolic compounds (Figure II-2) show many interesting biological properties like anti-inflammatory for example escueletin (**II-2**) and umbelliferone (**II-4**) show inhibitory effects on toll-like receptors (TLRs) are receptors that recognize pathogen-associated (PAMPs) and damage-associated (DAMPs) molecular patterns.[264] 4-hydroxycoumarin (**II-5**) shows anti-coagulant activity inhibiting the vitamin K epoxide reductase complex.[265] 4-hydroxy coumarin (**II-5**) and it's analogues also act as a protease inhibitor for HIV.[266,267] Furthermore esculetin

(**II-2**) had a dose-dependent inhibition of hepatocellular carcinoma and was shown to inhibit migration and invasion of laryngeal cancer.[260,268]

Apart from this coumarins also show biofilm disruption activity against a plethora of pathogens like *Staphylococcus epidermidis, Porphyromonas gingivalis, Escherichia coli, Salmonella typhimurium, Candida albicans*, and *Pseudomonas aeruginosa*.[269,270] Furthermore, coumarins were reported to have antibiofilm activity against *Salmonella typhirium* by suppressing cellulose and curli fimbriae production in the EPS via downregulation of biofilm forming genes namely curlin subunit gene D (csgD), curlin subunit gene A (csgA), and adhesion related gene A (adrA).[271] The anti-QS activity of coumarins arise due to their effect on density dependent communication systems in biofilms as observed for gram positive *Pseudomonas aeruginosa.*[270] It is notable that coumarins predominantly show reduction of biofilm formation unlike antimicrobials that inhibit bacterial growth, thus they act well together with supplementary antibiotics synergistically to tackle infections.[272] An additive effect towards antibiofilm activity was observed when coumarins were paired with ampicillin and ceftazidime against *Pseudomonas aeruginosa* biofilms.[273] Umbeliferone was seen to differentially affect proteins involved in QS, virulence and stress response. It also regulates several genes in *Pseudomonas aeruginosa* responsible for different molecular processes and increases susceptibility to antibiotics.[263]

II-1.6 Metabolic pathways of coumarines

Although coumarins show antibiofilm properties among others, a main metabolic pathway carried out by the cytochrome (CYP) P450 family of enzymes (Scheme II-1),[274] generate cytotoxic intermediates leading to depletion of cellular glutathione levels,[275,276] thus limiting their pharmacological application. Coumarins can be metabolized through hydroxylation in all possible six positions yielding 3-hydroxycoumarin (**II-10**), 4-hydroxycoumarin (**II-17**), 5-, 6-, 8-hydroxycoumarin (**II-16**), or 7-hydroxycoumarin (**II-14**).

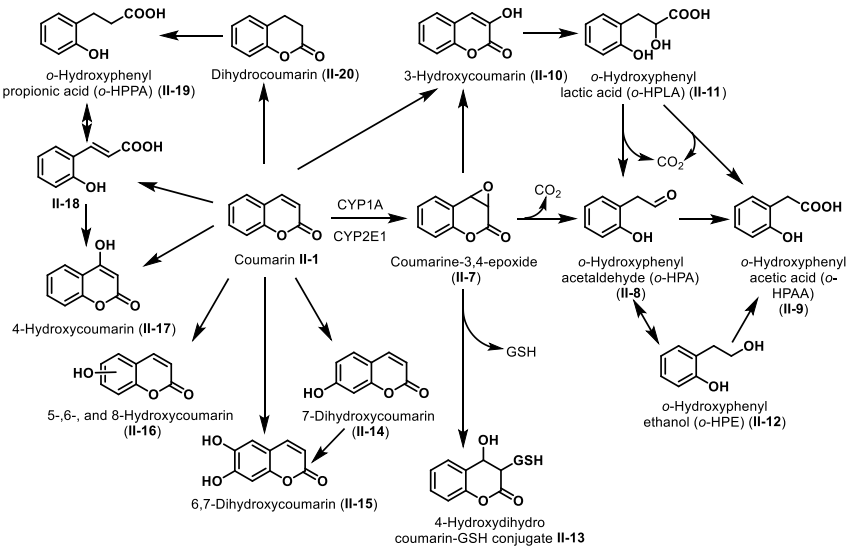

Scheme II-1: Metabolism pathway of coumarins.[276]

The opening of the lactone ring provides a series of other metabolites like **II-18** and **II-19**. There are several pathways of coumarin metabolism. The first one involves hydroxylation at C7 to form 7-hydroxy coumarin (**II-14**). Another pathway involves hydroxylation at C3 to form 3-hydroxy coumarin (**II-10**) followed by ring opening and cleavage at C2 releasing carbon dioxide.[277–279] Additionally hydrogenation at C3 and C4 gives dihydroxycoumarin (**II-20**) which can then be further metabolized to *o*-hydroxyphenyl propionic acid (*o*-HPPA) (**II-19**). Furthermore, coumarins can also be metabolized via formation of a 3,4-epoxide (**II-7**),[277,279–281] which decomposes under aqueous conditions[282] with the loss of carbon dioxide to form *o*-hydroxyphenyl acetaldehyde (*o*-HPA) (**II-8**) and further oxidation to *o*-hydroxyphenyl acetic acid (*o*-HPAA) (**II-9**). 3-hydroxyl coumarin (**II-10**) is also a minor metabolite of this pathway which further oxidizes to *o*-hydroxyphenyl lactic acid (*o*-HPLA) (**II-11**).[283–285]

II-2. Aims and Objectives

Microbial biofilms contribute to the AMR crisis by posing significant challenges for antimicrobial development, as bacterial[233,286–290] and fungal pathogens[291–293] often reside within these structures, hindering drug penetration and contributing to persistent and recurrent infections.[293] They contribute to the development of clinical infections in humans[292] and are present in numerous microbial pathogens, such as Methicillin-resistant *Staphylococcus aureus* (MRSA),[290,294] *Pseudomonas aeruginosa*,[286,295–298] and *Candida albicans*,[291,299,300] which can result in serious infections. Therefore, it is important to explore compounds showing antibiofilm activity to make pathogens more susceptible to antimicrobials. Coumarins are a class of plant metabolites that show antibiofilm activity like coumarin (**II-1**), esculetin (**II-2**), dephnetin (**II-3**), umbelliferone (**II-4**), 4-hydroxycoumarine (**II-5**), and scopoletin (**II-6**) (Figure II-2).[269,301–305] The biofilm-inhibitory properties of dihydroxycoumarins, including umbelliferone (**II-4**) and esculetin (**II-2**), have been attributed to their ability to inhibit efflux pumps and disrupt quorum sensing,[269,306] making them promising candidates for the development of new biofilm inhibitors. However, both compounds exhibit notable antiproliferative effects on human cells, which constrains their practical application.[307–310] Another hindrance to their pharmacological application is that , a main metabolic pathway carried out by the cytochrome (CYP) P450 family of enzymes (Scheme II-1),[274] generate cytotoxic intermediates especially coumarine-3,4-epoxide (**II-7**) leading to depletion of cellular glutathione levels.[275,276]

In this work, the aim was to design and develop new 6,7-dihydroxycoumarin-5-carboxylate derivatives. It was hypothesized that substituents at the 5-position would hinder the oxidative metabolism mediated by CYP450, thereby reducing the cytotoxicity of the corresponding 6,7-dihydroxycoumarins. The C5 carboxylate handle was also envisaged to facilitate attachment to other antimicrobial agents or siderophore units. This approach seeks to transfer the antibiofilm properties of 6,7-dihydroxycoumarins to these conjugated compounds, as shown in Figure II-3.

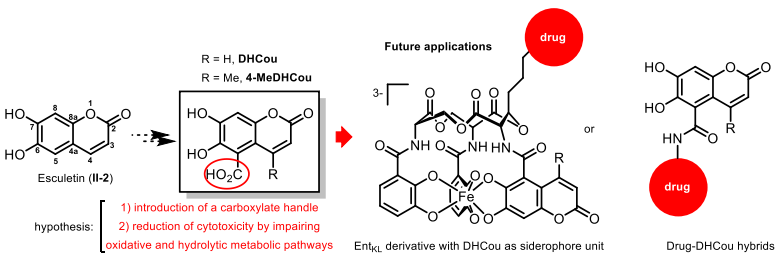

Figure II-3: Concept of 6,7-dihydroxcoumarin-5-carboxylates as potential antibiofilm compounds bearing a handle for conjugation to siderophores and antimicrobial drug moieties.

We proposed that incorporating a carboxylate group at the 5-position of the coumarin core could facilitate linking with artificial siderophores, like the enterobactin derivative Ent$_{KL}$,[311,312] or other antimicrobial drugs,[152] while maintaining antibiofilm efficacy.

II-3. Results and Discussion

II-3.1 Synthesis of novel 6,7-dihydroxcoumarin-5-carboxylates (DHCou and 4-MeDHCou)

The synthesis of **DHCou** as compiled in Scheme II-2, was started with esculetin (**II-2**), where the hydroxy group at C7 was protected with benzyl bromide (**II-27**) in presence of Na_2CO_3 to give **II-21** in 73% yield, followed by *O*-alkylation at the C6 position with propargyl bromide to give **II-22** in 91% yield. Next, *O*, *O*-dialkylated coumarin **II-22** was subjected to a [3,3] sigmatropic propargyl *Claisen* rearrangement, followed by a CsF mediated nucleophilic 5-exo dig cyclisation of the intermediate allenylphenolate to give **II-23** in 71% yield. The oxidative cleavage of the furan ring was facilitated via ozonolysis in a 1:1-mixture of CH_2Cl_2:MeOH followed by a reductive workup with triphenylphosphine to give the impure intermediary aldehyde **II-24** in roughly 61% yield. Next, the *Pinnick* oxidation of the impure aldehyde **II-24** gave the corresponding *O*-protected 6,7-dihydroxycoumarin-5-carboxylate **II-25b** in roughly 45% and 27% over two steps from furane **II-23**. A direct transformation from **II-23** to **II-25a** lacking the acetate moiety was also established in a one pot synthesis giving 48% yield of **II-25a**. Finally, the hydrogenolytic cleavage of the *O*-benzyl group in presence of palladium on charcoal (10 wt%) gave DHCou in 72% yield and an overall yield of 16% over 5 steps.

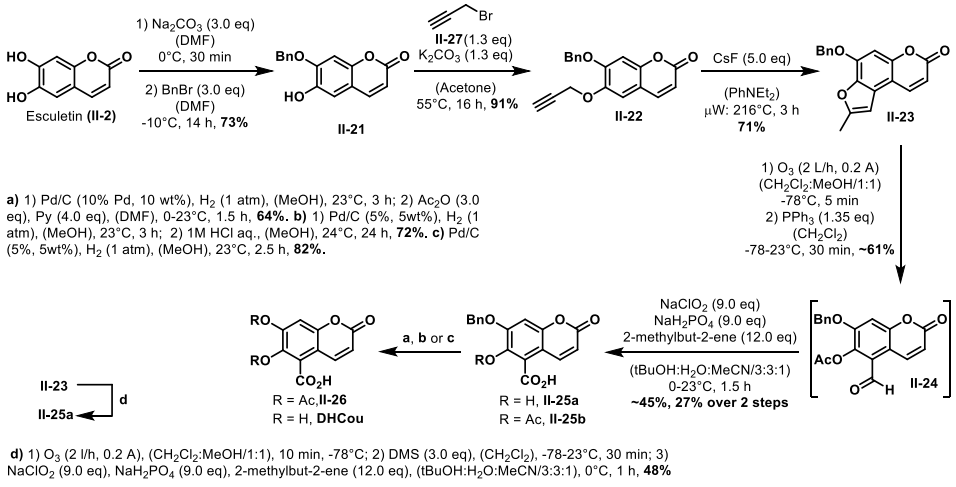

Scheme II-2: Synthesis of DHCou.

The synthesis for **4-MeDHCou** as compiled in Scheme II-3 was started with the *Pechmann* condensation of commercially available 1,2,4-trihydroxybenzene (**II-28**) with ethyl acetoacetate (**II-36**) in TFA to give 4-Methylescueletin (**II-29**) in 94% yield. 4-Methylescueletin (**II-29**) was selectively *O*-alkylated with benzyl bromide (**II-27**) at the C7 position to give **II-30** in 47% yield. **II-30** was then *O*-alkylated with propargyl bromide at the C6 position to give *O*, *O*-alkylated coumarin derivative **II-31** in 95% yield. Next, a [3,3] sigmatropic rearrangement of **II-31** followed by CsF mediated nucleophilic 5-exo dig cyclization at 216°C with microwave irradiation gave **II-32** in 55% yield. Next, ozonolysis of the furan ring in a 5:1-mixture of CH_2Cl_2:MeOH followed by a reductive workup with triphenylphosphine gave the intermediary aldehyde **II-33**. The intermediate **II-33** was difficult to isolate and obtained in very small amounts. Therefore, a sequence of ozonolysis and subsequent *Pinnick* oxidation gave **II-34** in 54% yield

over two steps. Finally, the hydrogenolytic cleavage of the benzyl group in presence of palladium on charcoal (5 wt%) followed by acidic cleavage of the acetate moiety gave **4-MeDHCou** in 72% yield.

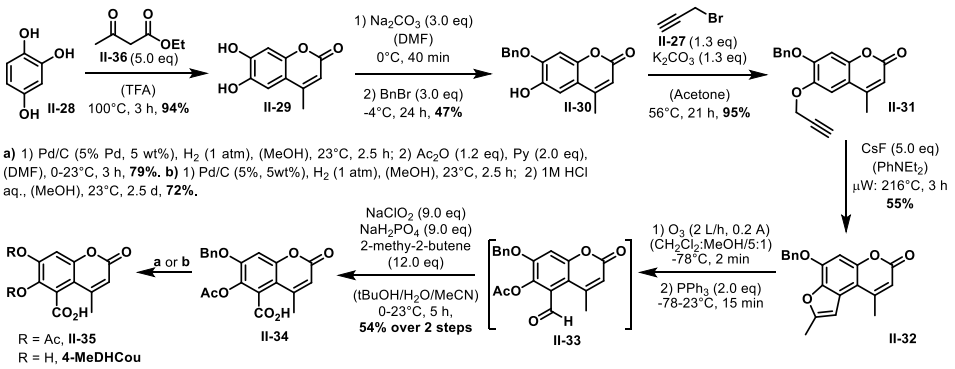

Scheme II-3: Synthesis of 4-MeDHCou.

II-3.2 Evaluation of novel 6,7-dihydroxcoumarin-5-carboxylates (DHCou and 4-MeDHCou)

The compounds were evaluated by our collaboration partners Prof. Dr. Marc Stadler, Dr. Hedda Schrey, Hoaxuan Zeng and Wera Collisi at the Helmholtz Centre for Infectious Research in Braunschweig, Germany.

A crystal violet assay was performed to evaluate the anti-biofilm activity of the synthesized compounds against gram positive *Staphylococcus aureus* and fungi *Candida albicans*.

Table II-1: Biofilm inhibition of *S. aureus* and biofilm inhibition of *C. albicans*

	Biofilm inhibition [% ± SD]	
Compound	S. aureus (DSM 1104)	C. albicans (DSM 11225)
Esculetin (**II-2**)	93 ± 2 (250 µg/mL)[a] 33 ± 6 (125 µg/mL)[a]	77 ± 7 (250 µg/mL)[c] 58 ± 17 (125 µg/mL)[c]
4-Methylesculetin (**II-29**)	94 ± 1 (250 µg/mL)[a] 48 ± 8 (125 µg/mL)[a]	76 ± 7 (250 µg/mL)[c] 48 ± 14 (125 µg/mL)[c]
DHCou	-[b]	62 ± 9 (250 µg/mL)[d]
4-MeDHCou	75 ± 5 (250 µg/mL)[b] 43 ± 11 (125 µg/mL)[b] 31 ± 15 (62.5 µg/mL)[b]	60 ± 2 (250 µg/mL)[d]

(–): no activity, SD: standard deviation, References [%]: [a] Microporenic acid A (MAA): 93 ± 0.3 (250 µg/mL), 93 ± 1 (62.5 µg/mL), 62 ± 6 (7.8 µg/mL); [b] MMA: 82 ± 6 (250 µg/mL), 81 ± 8 (62.5 µg/mL), 73 ± 17 (7.8 µg/mL); [c] Farnesol: 87 ± 3 (250 µg/mL), 79 ± 14 (31.3 µg/mL), 67 ± 11 (15.6 µg/mL). [d] Farnesol: 75 ± 6 (250 µg/mL), 58 ± 15 (31.3 µg/mL), 46 ± 14 (15.6 µg/mL).

It was observed that **DHCou** had no biofilm inhibitory activity at the highest concentration of 250 µg/mL, while esculetin (**II-2**) showed inhibition effects of 93% on the formation of *Staphylococcus*

aureus biofilms at the concentration of 250 µg/mL and of 33% at 125 µg/mL (Table II-1). On the other hand **DHCou** showed retention of biofilm inhibitory activity for *Candida albicans* of upto 62% for the highest concentration of 250 µg/mL, which was slightly lower than the inhibitory effect of its precursor escueletin (**II-2**) of77% for the same concentration of 250 µg/mL (Table II-1)

The other synthesized compound **4-MeDHCou** which was chemically a bit more lipophilic than **DHCou**, showed retention of biofilm inhibitory activity against both *Staphylococcus aureus* and *Candida albicans*. For *Staphylococcus aureus* it had 75% inhibition at 250 µg/mL and 43% at 125 µg/mL concentration, which were slightly lower than the inhibitory effect of its precursor 4-Methylescueletin (**II-29**) with 94% inhibition at 250 µg/mL and 48% at 125 µg/mL concentration (Table II-1). For *Candida albicans* the inhibitory effect of **4-MeDHCou** was comparable at 60% to that of 4-Methyescueletin (**II-29**) at 76% for 250 µg/mL (Table II-1). Although, a clear loss in antibiofilm activity against *Staphylococcus aureus* was observed, a significant portion of the initial antibiofilm activity against *Candida albicans* could be retained by C5 substitution in **DHCou**, and for its more lipophilic counterpart **4-MeDHCou** a retention of biofilm inhibition against both pathogens were observed.

Next, the cytotoxic activity of escueletin (**II-2**) and 4-Methylescueletin (**II-29**) were screened against various cell lines (Table II-2) and they were found to be cytotoxic against all cell lines for a maximum concentration of 1mg/mL. **DHCou** and **4-MeDHCou** on the other hand showed no cytotoxicity against mammalian cervical carcinoma cell line KB3.1 and the mouse fibroblasts cell line L929 at the highest concentration of 1 mg/mL.

Table II-2: Cytotoxic activity against several selected mammalian cell lines

	Cytotoxicity IC_{50} [µM]			
Cell line	**DHCou**	**4-MeDHCou**	Esculetin (**II-2**)	4-Methylesculatin (**II-29**)
KB3.1 (ACC158)	–	–	29.8	30.2
L929 (ACC2)	–	–	41.5	33.8
A549 (ACC107)	n.t.	n.t.	18.5	21.9
A431 (ACC91)	n.t.	n.t.	41.5	38.5
PC-3 (ACC465)	n.t.	n.t.	46.0	38.0
SKOV-3 (ATCC HTB 77)	n.t.	n.t.	45.5	42.7
MCF-7 (A115)	n.t.	n.t.	19.6	27.1

(–): no cytotoxicity or changed cells observed (max. concentration 1 mg/mL = 4.5 mM for **4-MeDHCou** and 4.2 mM for **DHCou**), n.t.: not tested

Thus, the installation of the carboxylate handle at C5 position made the synthesized compounds non cytotoxic against selected cell lines although there needs to be further studies towards the structure activity relationship.

In addition, none of the compounds (**DHCou**, **4-MeDHCou**, esculetin (**II-2**) or 4-Methylesculetin (**II-29**)) showed antimicrobial activity (Table II-3) against a panel of Gram-positive and Gram-negative bacteria (*B. subtilis, S. aureus, M. Smegmatis, A. baumanni, C. violaceum, E. coli,* and *P. aeruginosa*) and different fungi (*M. hiemalis, P. anomala, R. glutinis, C. albicans* and *S. pombe*) up to a concentration of 66.7 µg/mL.

Table II-3: MIC [µg/mL] assay data.

		Antimicrobial activity MIC [µg/mL]				
Organisms.	Strain No.	**DHCou**.	**4-MeDHCou**	Esculetin (**II-2**)	4-Me-Esculetin (**II-29**).	Ref.
Bacteria		-	-	-	-	
B. subtilis	DSM 10	-	-	-	-	8.3[a]
S. aureus	DSM 346	-	-	-	-	1.7[a]
M. smegmatis	ATCC 700084	-	-	-	-	1.7[b]
A. baumannii	DSM 30008	-	-	-	-	0.3[c]
C. violaceum	DSM 30191	-	-	-	-	0.4[a]
E. coli	DSM 1116	-	-	-	-	1.7[a]
P. aeruginosa	PA 14	-	-	-	-	0.4[d]
Fungi		-	-	-	-	
M. hiemalis	DSM 2656	-	-	-	-	4.2[e]
P. anomala	DSM 6766	-	-	-	-	8.3[e]
R. glutinis	DSM 10134	-	-	-	-	2.1[e]
C. albicans	DSM 1665	-	-	-	-	8.3[e]
S. pombe	DSM 70572	-	-	-	-	4.2[e]

-References: a oxytetracycline; b kanamycin; c ciprobay; d gentamicin; e nystatin; – : not active

From the results of the MIC assay, it can be concluded that the biofilm activity observed for the synthesized compounds was not influenced by any antimicrobial activity.

II-4. Conclusion and Outlook

With this work a proof-of principle for the design of non-cytotoxic dihydroxycoumarins retaining antibiofilm activity has been made. The coumarin based analogues **DHCou** and **4-MeDHCou** were successfully synthesized in overall yields of 11% and 8% over 6 steps. The lower yields could be attributed to the ozonolysis step, which was time sensitive, and the resulting intermediate aldehydes **II-24** (Scheme II-2) and **II-33** (Scheme II-3) were prone to decomposition and hard to purify. The subsequent *Pinnick* oxidation step when tried with either purified or crude aldehyde, resulted in poor yields of the 5-carboxylate coumarin derivatives **II-25** and **II-34**. There is a scope to improve the yields and explore more such analogues. Furthermore, a good retention of antibiofilm activity was observed for **4-MeDHCou** towards both *S. aureus* and *C. albicans* while the lesser lipophilic analogue **DHCou** only showed retention of antibiofilm activity against. Additionally, we observed a complete loss of cytotoxicity for **DHCou** and **4-MeDHCou** as compared to their parent compounds escueletin (**II-2**) and 4-Methylescueletin (**II-29**) respectively, against mammalian cervical carcinoma cell line KB3.1 and the mouse fibroblasts cell line L929 at the highest concentration of 1 mg/mL although there needs to be further study for understanding the structure-activity relationship of these compounds and improve their antibiofilm activity, the introduction of the carboxylate handle at C5 position is still a starting point for developing artificial siderophores with antibiofilm activity , which could be used to generate antimicrobial siderophore drug conjugates.

III. Studies towards the total synthesis of [13]-cytochalasans

This section has been incorporated into my PhD thesis to document the substantial effort and knowledge gained during the studies toward the synthesis of [13]cytochalasans, despite the overall lack of success in achieving the target molecule. While no publication or manuscript has been prepared based on this part of my work, it represents a significant portion of the research conducted during my doctoral studies. The decision to include these "negative" results and detailed experimental information is motivated by the importance of transparency in research. Documenting these findings ensures that the methodologies, challenges, and outcomes are accessible for future reference and can serve as a foundation for subsequent investigations or publications in this area. This approach highlights the scientific process, emphasizing that even unsuccessful outcomes contribute to the broader understanding and advancement of the field.

III-1. Cytochalasans - A diverse family of secondary fungal metabolites

Cytochalasans are biologically active fungal metabolites. These polyketide amino acid hybrids are part of a structurally diverse group showing a plethora of interesting biological activity.[313,314] The core structure of cytohalasans (Figure III-1) consists of a highly substituted isoindolone core having different oxidation states fused to a macrocycle, which is either a carbocycle, cyclic carbonate or a lactone, giving rise to a tricyclic structure. The side chain and the nitrogen of the of the perhydro isoindolone core is derived from amino acids.[315]

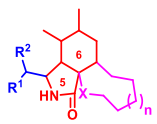

Figure III-1: Core structure of cytohalasans. Isoindolone core highlighted in red, macrocycle highlighted in pink and amino acid derived side chain highlighted in blue.

The structural diversity of cytochalasans is due to different factors such as the oxidation patterns of the highly substituted isoindolone core (Figure III-2), and every cytochalasan producing fungi can access most of these eight major oxidation states.

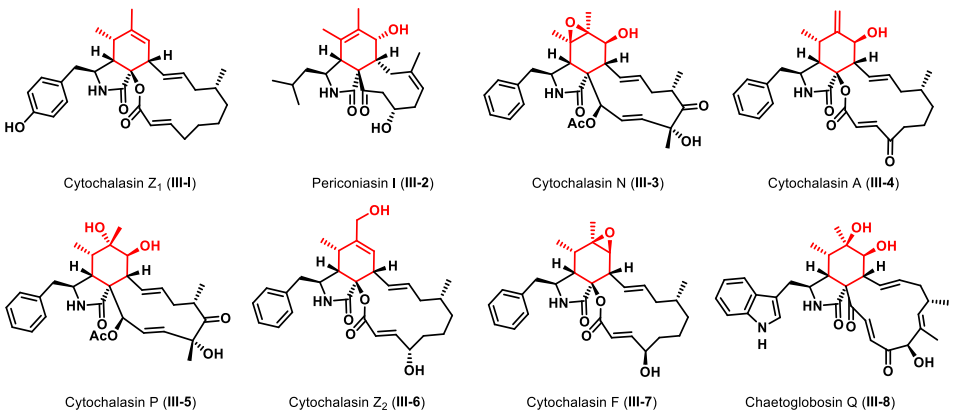

Figure III-2: Selected examples of different oxidation patterns in the isoindolone core (highlighted in red).

Another factor contributing to structural diversity is the amino acid derived side chain of the isoindolone core. However, the amino acid incorporated in the polyketide backbone is limited to the producer fungi and subclasses. A few examples (Figure III-3) are, phenylalanine containing cytochalasins (cytochalasan A-D) is obtained from *Phoma* sp[313] and (cytochalasin E (**III-9**)) from *Apergillus clavatus*,[316] tyrosine containing phenochalasins (phenochalasin A (**III-10**)) from *Phomopsis sp.*[316] and pyrichalasins (pyrichalasin H) from *Magnaporthe grisea*,[317] *Chaetomium globosum* produces tryptophan derived cytochalasans (chaetoglobosin A (**III-12**), cytoglobosin H-I, e.g. cytoglobosin H (**III-13**)),[318,319] *Trichoderma gamsii* produces valine derived trichalasin A (**III-11**),[320] leucine incorporated aspochalasins (aspochalasin A-D, e.g. aspochalasin D (**III-15**)) obtained from *Aspergillus microsysticus*[321] and (aspochalasin I-J) from *Trichoderma gamsii*,[320] *Stachybotrys charatum* produces alanine derives alachalasins (alachalasin A-G, e.g. alachalasin F (**III-16**)).[322]

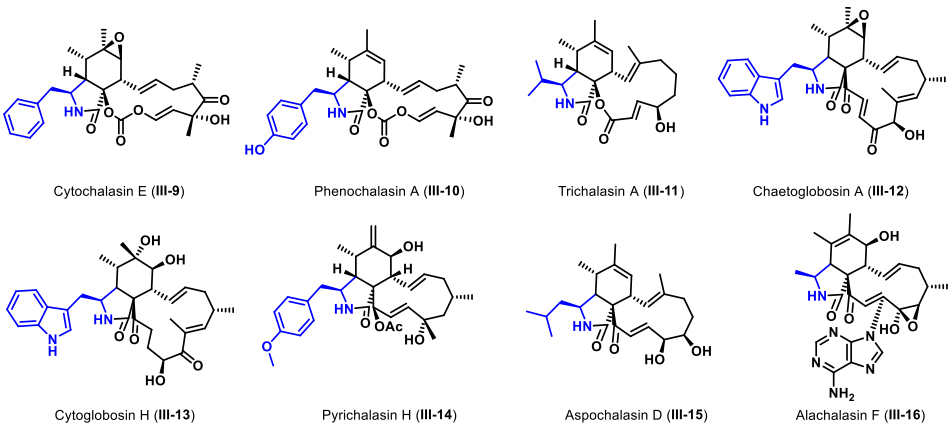

Figure III-3: Selected examples of examples of cytochalasans derived from different amino acids (highlighted in blue).

Initially cytochalasans were named after their source fungi, as phomins extracted from *Phoma* spp.[323] or zygosporins extracted from *Zygosporium masonii.*[324] Later, *Binder* and *Tamm* introduced a systematic method for cytochalasan nomenclature, where the number of atoms in the macrocycle, including those shared with the isoindole ring, would be specified by a numeral in square brackets that appears before the name "cytochalasan.". This led to differentiation of cytochalasans through the ring size of the macrocycle, thereby dividing it into various subclasses (Figure III-4).[325] The macrocycle also significantly contributes to the structural diversity. Usually, the macrocycle can either be a carbocycle (e.g. **III-20**, **III-24**, **III-25**), a cyclic lactone (e.g. **III-17**, **III-23**) or a cyclic carbonate (**III-21**).

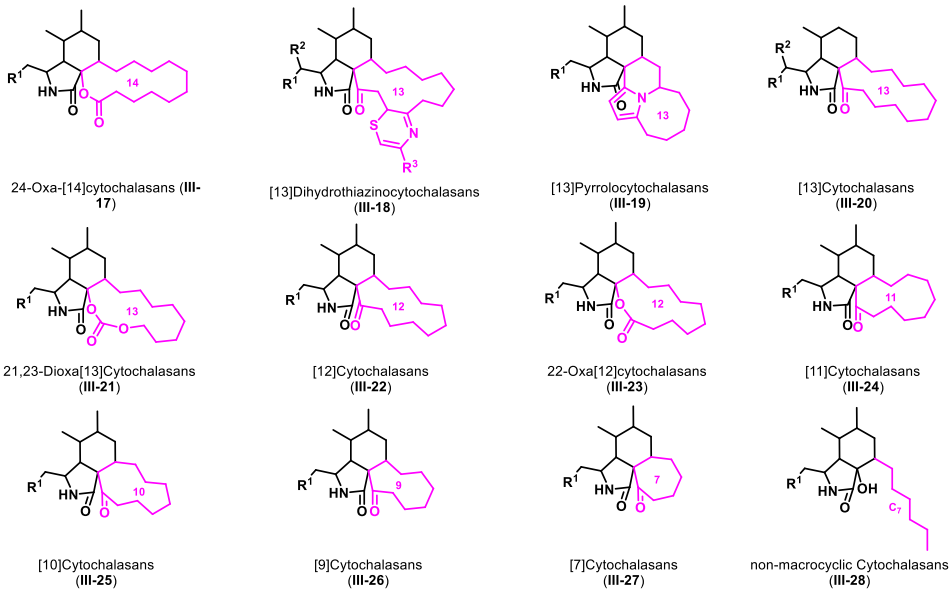

Figure III-4: Selected examples of cytochalasan subclasses based on the macrocyclic ring size (highlighted in pink).

More complexity is introduced in certain cases where the macrocycle has multicyclic fused ring systems or even open carbon chains attached to the isoindolone core due to post non-ribosomal peptide synthase-polyketide synthase (NRPS-PKS) modifications during the biosynthesis. Some of the examples highlighted in Figure III-5 are spiro-cytochalsans (trichodermone (**III-29**),[320] trichoderone B(**III-30**)[326]) both isolated from *Trichoderma gamsii*, which have a pentacyclic system. Phomopsichalasins (e.g. phompochalasin (**III-31**)) isolated from *Phomphosis sp*. ,have a fused tricyclic 13 membered macrocycle.[327] Penochalasin I (**III-32**) isolated from *Penicillium chrysogenum* has a unique 6/5/6/5/6/13 hexacyclic fused ring system.[328] Armochaeglobin A (**III-33**) having a 5/6/7/5 tetracyclic carbon skeleton bearing a peroxide functionality was isolated from *Chaetomium globosum*. Alachalasines (e.g. alachalasine F (**III-16**))isolated from *Stachybotrys charatum* have a adenosine moiety attached to the macrocycle.[322] Armochaetoglobin A (**III-34**) also isolated from *Chaetomium globosum* has a pyrrole moiety along with an open chain[329] and cytochalasins Z_{10}-Z_{15} isolated from *Spicaria elegans* (e.g. cytochalasin Z_{15} (**III-35**)) features an 8 carbon long open chain.[330]

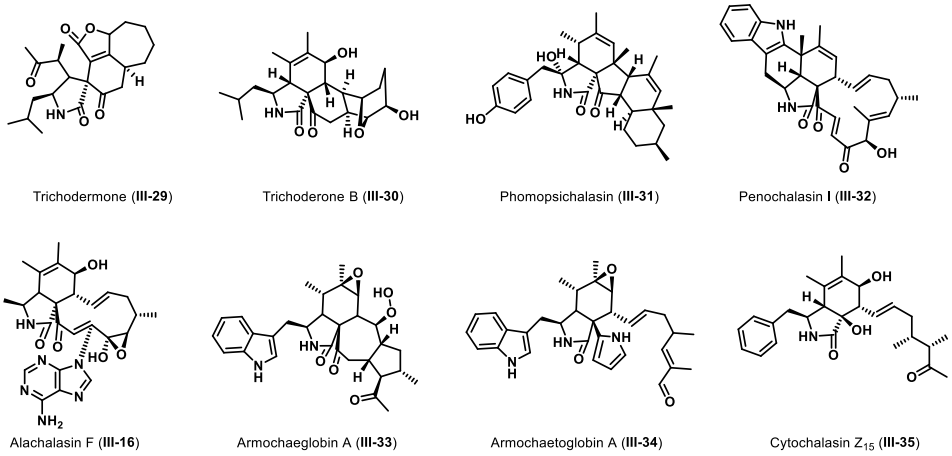

Figure III-5: Selected examples of multicyclic and non-macrocyclic cytochalasans.

Further complexity arises in the class of compounds known as merocytochalasans extracted from *Aspergillus flavipes* (Figure III-6). This occurs when two or more cytochalasan molecules dimerize with multiple eppicoccine (**III-41**) moieties via [4+2] *Diels–Alder* cycloadditions. Some examples are seen in epicochalasine A (**III-36**) and B (**III-37**) consisting of a cytochalasin fused to an epiccocine dimer.[331] Asperflavipine A (**III-38**) is a heterotetramer containing two cytochalasin and epicoccine molecule each.[332] Asperchalasine A (**III-39**) consists of a decacyclic ring system arising from the dimerization of two cytochalasins fused to an epicoccine moiety. On the other hand, asperchalasine B-D (e.g. asperchalasine B (**III-40**) contain a cytochalasin and epicoccine molecule each.[333]

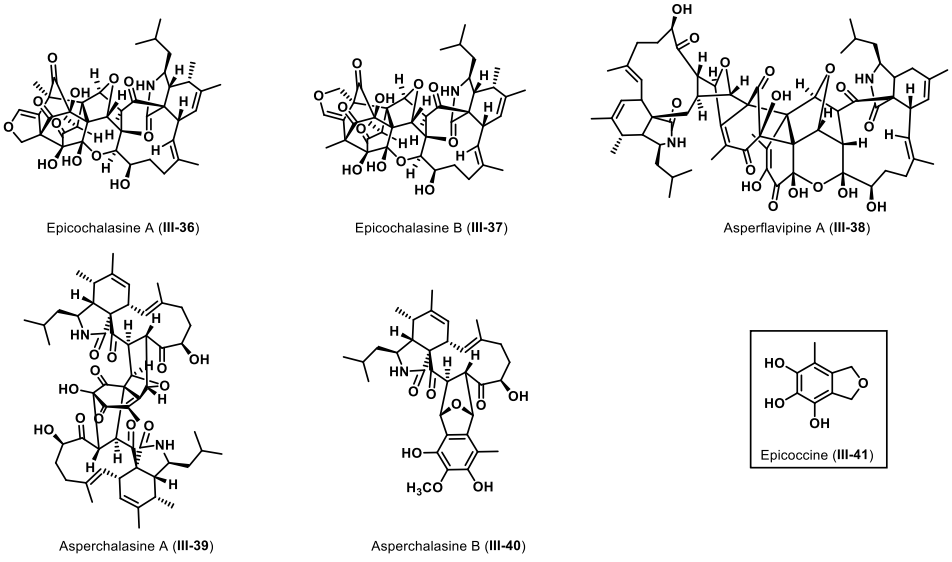

Figure III-6: Selected structures of merocytochalasans.

III-1.1. Bioactivity of cytochalasans

The broad structural diversity of cytochalasans is accompanied by a wide range of interesting biological properties. The principal biological activity of cytochalasans, observed across all subclasses, involves binding to actin filaments and disrupting actin polymerization dynamics. This interference affects cellular processes like intracellular motility, cytokinesis, exo- and endocytosis,[334–337] leading to cytotoxic effects with IC_{50} values in the range of sub-micromolar to double-digit nanomolar concentrations against various cancer cell lines.[315,338]

Actin is the most abundant protein in the cellular scaffold of eukaryotic cells, participating in the most number of protein-protein interactions than any other known protein.[339] Actin exists in two forms in the cell, the monomeric globular G-actin and the asymmetrical filamentous F-actin.[340] F-actin is produced through polymerization of G-actin.[340] Due to the instability of actin monomers the polymerization process is unfavorable but once started, the filaments grow rapidly.[341] F-actin is characterized by a barbed end, where G-actin polymerizes and a pointed end from where it depolymerizes back into G-actin.[342] Under physiological salt concentrations, ATP bound actin monomer attach to form F-actin on the barbed end. Hydrolysis of ATP to ADP brings about conformational changes in the filament resulting in unstable ADP bound G-actin at the pointed end which simultaneously depolymerizes (Figure III-7). Since the rate of polymerization is higher than depolymerization, under equilibrium the critical concentration of the barbed end is higher than the pointed end, which leads to a net flow of actin subunits through the filament.[341,343,344] Actin networks along with microtubules and intermediate filaments which are all a part of the cytoskeleton can respond to external stimuli, maintain spatial relationship and resist deformation.[345]. The cytoskeleton is responsible for regulating many cellular processes, like proliferation, motility, differentiation and apoptosis.[346–349]

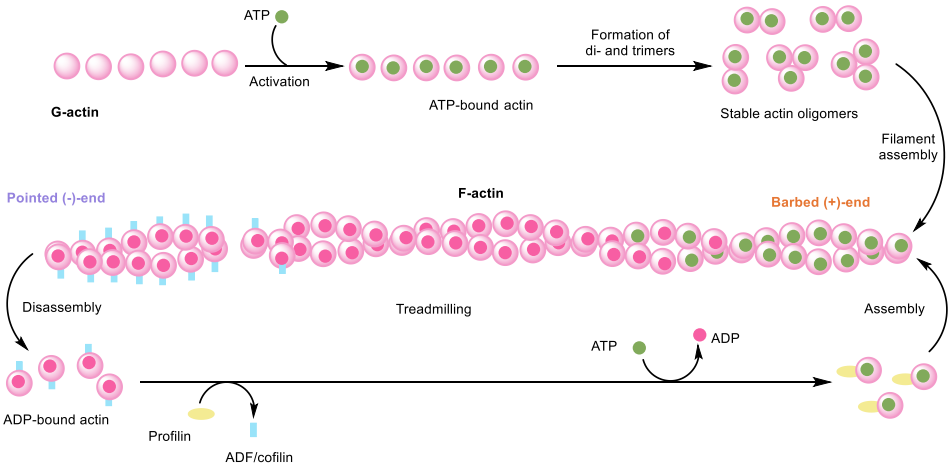

Figure III-7: Self-assembly of actin filaments

Cytochalasans interact with actin usually by binding the barbed ends and interfering with its dynamic properties and chain elongation.[350–354] Under cytotoxic conditions cytochalasans lead to cell denucleation.[336,355] Cytochalasin B (**III-45**) (Figure III-8) shows disruption in cell movement and formation of multinucleated cells in mouse fibroblasts[356] and human lymphocytes.[357] Studies with

Nitella pseudoflabellata showed that the effect of cytochalasans differ in their relative potency for cytoplasmic streaming and rearrangement of cytoskeleton on actin filament reorganization and cell motility [335] Hence, these compounds show potential for studying cell morphology and visualizing actin filaments.

Since cytochalasans interfere with important cellular activity they also show cytotoxic effects. chaetoglobosin A-G, and J have an IC_{50} values ranging from 3-20 µg/mL against HeLa cells,[358] while chaetoglobosin A, B, D, J, Q, T and prochaetoglobosins I (**III-49**) and II (**III-53**) extracted from *Chaetomium globosum* show significant cytotoxicity against P388 murine leukemia cell line.[359] Cytochalasin H shows antiangiogenic effect and inhibition of epithelial cell proliferation and mobility without altering cell viability.[360] Actin filaments have become interesting targets since they have an active role in alteration in cell motility and morphology [361,362] Therefore, cytochalasans have significant potential for anticancer therapy.[363,364]

Cytochalasans also show antifungal and antibacterial properties. One of the first reports was of cytochalasin A (**III-3**) (Figure III-2) having inhibitory effect on the growth of *Bacillus subtilis* and *Escherichia coli* and both cytochalasin A, D had antimycotic effect against *Botrytis cineria*.[365] Several cytochalasans including cytochalasin A, C, chaetoglobosin A (**III-42**) and phenochalasin D (**III-48**) showed potent antibiofilm activity against *Staphylococcus aureus*.[366] Chaetoglobosin B (**III-43**) showed weak inhibitory activity against *Staphylococcus aureus* but had comparatively higher bioactivity against MRSA and *Mycobacterium tuberculosis* H37Ra.[367] Cytochalasin A (**III-46**) inhibits a variety of physiological functions in gram positive bacteria like, transport ,respiration of exogenous substrates and enzyme induction.[368] The α,β-unsaturated carbonyl in the macrolide and an unsaturated lactam seems important for such activity.[369] Phomphopsichalasin (**III-31**) (Figure III-5) where the macrocycle is replaced with a tricyclic system showed antibacterial activity against *Bacillus subtilis*, *Salmonella gallinarum*, *Staphylococcus aureus* and antifungal activity against *Candida tropicalis*.[327] Scoparasins A (**III-50**) and B (**III-51**) had antifungal activity against dermatophyte *Microsporum gypseum*.[370] Furthermore, chaetoglobosin D (**III-44**) exhibited inhibitory activity against *Sclerotinia sclerotiorum*.[367] Cytochalasins B (**III-45**) (Figure III-8), D (**III-46**) (Figure III-8) and E (**III-9**) (Figure III-3) also show antiparasitic activity and prevents cyst wall formation of the parasite *Entamoeba invadens*.[371]

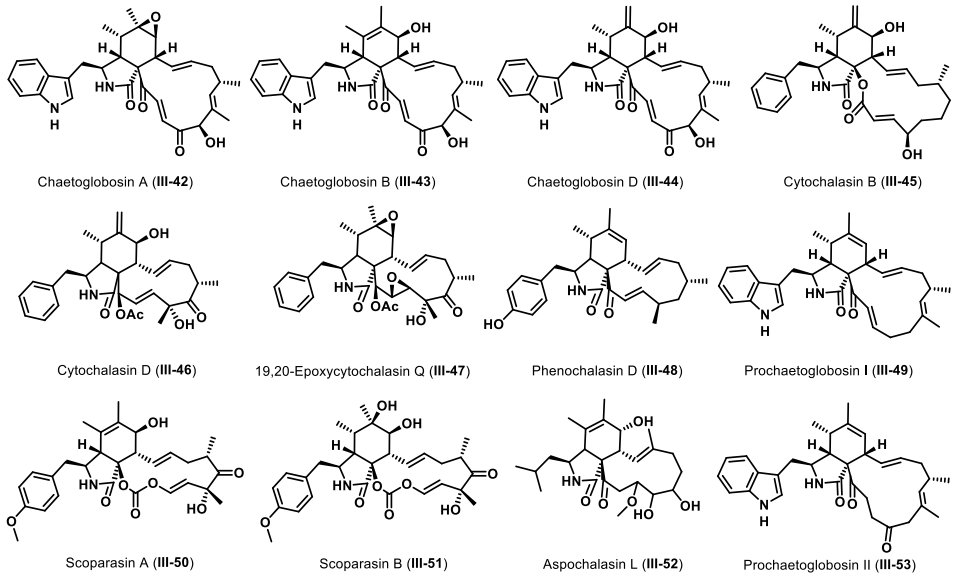

Figure III-8: Structures of selected bioactive cytochalasans.

Furthermore, cytochalasans also show other non-actin related bioactivities like binding to glucose transporter proteins and inhibiting monosaccharide transport systems.[372–376] Cytochalasin B (**III-45**) interfering with intracellular calcium levels and inhibits the biosynthesis of phosphatidylcholine and phosphatidylethanolamine.[377] Cytochalasans have also been shown to inhibit thyroid[378] and growth hormone secretion.[379] 19,20-epoxycytochalasin Q (**III-47**) had antagonistic effect against cytokine receptor (CCR5), which is connected with HIV infections.[380] Furthermore, aspochalasin L (**III-52**) showed inhibitory effect against HIV integrase enzyme.[381]

III-1.2. Biosynthesis of [13]cytochalasans: Chaetoglobosin A

Given the vast structural diversity of cytochalasans it is important to look into the biosynthesis of such compounds, especially for [13]cytochalasans because there is no formal synthesis known for such compounds. The elucidation of biosynthetic pathway for chaetoglobosin A was achieved through feeding experiments with isotope labelled precursors such as malonate, acetate, methionine, amino acid and oxygen, implying a NRPS-PKS pathway.[318,382–385] The first gene cluster for cytochalsans (Che) was reported from *Penicillium expansum*.[386] The gene clusters identified for biosynthesis of chaetoglobosin A comprises CheA (Figure III-9), hosting a number of enzymes like condensation (C), adenylation (A), peptidyl carrier protein (PCP) which constitute the NRPS part and ketosynthase (KS), acyltransferase (AT), dehydratase (DH), C-methyl- transferase (MT), inactive enoyl reductase (ERO), ketoreductase (KR), acyl carrier protein (ACP), reductase (R), which constitute the PKS part. It also employs other gene clusters like CheB which contains a trans enoyl esterase (ER), CheD and CheG encodes two P450 monooxygenase, CheE having a FAD-dependent monooxygenase and CheC and CheF encodes transcription factors.[314]

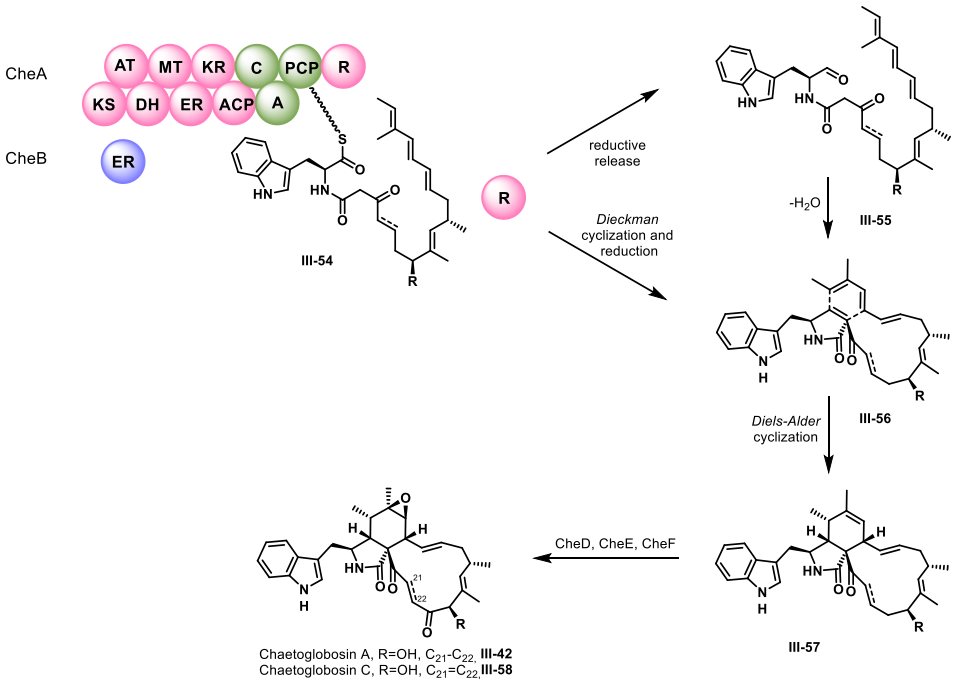

Scheme III-1: Proposed biosynthesis of Chaetoglobosin A by *Skellam et al*.[314]

The *N*-terminus of CheA belongs to a family of highly reducing PKS, such as nonaketide synthase, which lack an enoyl reductase.[387] The pathway proposed for the early-stage biosynthesis by *Skellam et al.* (Scheme III-1) suggests that the nonaketide backbone is synthesized by CheA and CheB acting together, followed by condensation with tryptophan to give intermediate **III-54**. [314] The next step involves the aminoaldehyde intermediate **III-54** undergoing a *Knoevenagel* condensation with subsequent reductive release to give a pyrrollilone intermediate **III-55**. The reductive release mechanism takes place due to the presence of a *C*-terminal reductase domain.[388] An alternate pathway was also proposed where the terminal NRPS-PKS domain would act as a *Dieckmann* cyclase and release a tetrameric acid derivative. Further reduction, dehydration would produce precursor **III-56** for an intramolecular *Diels-Alder* cycloaddition. intermediate **III-56** would then undergo an intramolecular [4+2] *Diels-Alder* cyclization, where the pyrrollilone terminal acts as a dienophile and the polyketide terminal acts as the diene to give an isoindolone fused macrocyclic structure **III-57** In the late-stage biosynthesis, the oxidizing gene clusters CheD, CheE and CheG catalyze oxidative modifications to afford Chaetoglobosin A (**III-42**) and its analogue chaetoglobosin C (**III-58**). Although a general pathway has been proposed, further insights into the individual transformations are missing.

Further insights into the late-stage biosynthetic modifications leading to Chaetoglobosin A (**III-42**) was provided by *Watanabe et al.* (Scheme III-2).[389] CHGG_01239 was identified as the gene encoding the NRPS-PKS, when targeted gene deletion of CHGG_01239 stopped the formation of **III-42**. Three different oxygenase genes CHGG_01242-1, CHGG_01242-2 and CHGG_01243 were also investigated via targeted gene deletion experiments. It was observed that CHGG_01242-1 catalyzes the epoxidation at C6-7 from the precursor prochaetoglobosin I (**III-49**) to prochaetoglobosin IV (**III-59**). CHGG_01243

also parallelly catalyzes the oxidation at both C19 and C20 of prochaetoglobosin I (**III-49**) to give cytoglobosin D (**III-61**) as well as oxidation of prochaetoglobosin IV (**III-60**) to 20-Dihydroxychaetoglobosin IV (**III-60**). Oxidation of **III-60** via oxidoreductase CHGG_01421-2 gives chaetoglobosin (**III-42**). Similarly, oxidation of **III-61** by CHGG_012421-2 to **III-62** followed by subsequent oxidation by CHGG_01241-1 gives **III-42**. This biosynthetic pathway highlights the non-linear nature of the formation of cytochalasans.

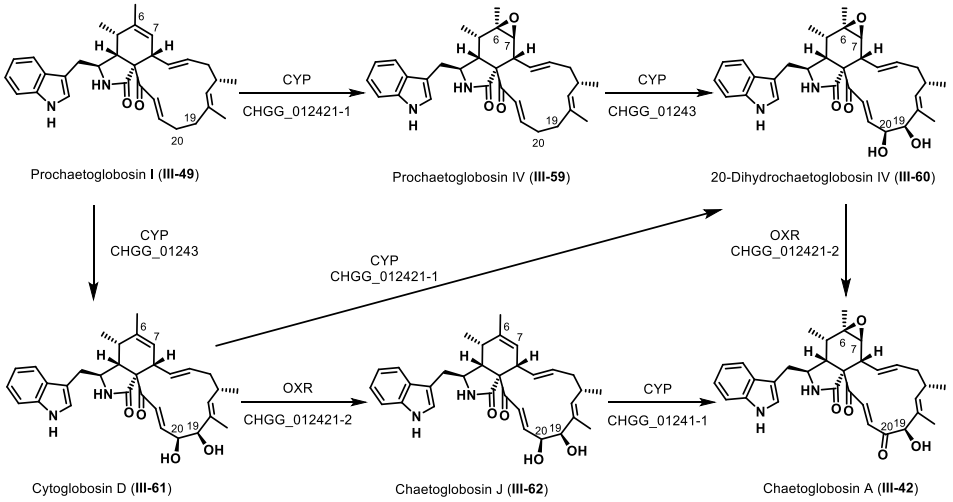

Scheme III-2: Advances in elucidation of late-stage biosynthesis of chaetoglobosin A by *Watanabe et al.*[389]

III-1.3. Total synthesis of [14]- and [11]cytochalasans

There has been some considerable effort towards the synthesis of these highly substituted complex tricyclic molecules. It could be concluded from the literature survey that there were two widely used approaches towards the retrosynthesis of cytochalasans. The first approach was a linear biomimetic pathway involving a late-stage *Diels-Alder* macrocyclization and the second approach was a more convergent route where the isoindolone core was built with an early-stage *Diels-Alder* and later attached to the macrocyclic fragment.

Stork and coworkers reported the first total synthesis of a [14]cytochalasan , cytochalasin B (**III-45**) in 1978 which also used the triene **III-64** (Scheme III-3) as an essential building block.[390] Improving on their existing synthesis they published a new synthetic strategy in 1983, having a [4+2] *Diels-Alder* cycloaddition as the key step (Scheme III-3).[391] The synthesis of the advanced building block **III-64** from (+)-citrollenol (**III-63**) over 13 linear steps was previously established by *Stork et al*.[390] *Mukaiyama* esterification of the triene **III-64** with *N*-acetyl hydroxypyrollone **III-65** gave the substrate **III**-67 for intramolecular *Diels-Alder*. The *Diels-Alder* required high temperatures up to 190°C and afforded the cytochalasan backbone **III-68** in a low yield of 30%. Subsequent epoxidation, deprotection of the *N*-acetyl moiety as well as the secondary alcohol of **III-68** gave the highly substituted intermediate **III-69**. An epoxide ring opening and subsequent oxidation gave the final compound cytochalasin B (**III-45**). This was a more biomimetic approach with 22 linear steps and 24 steps in total.

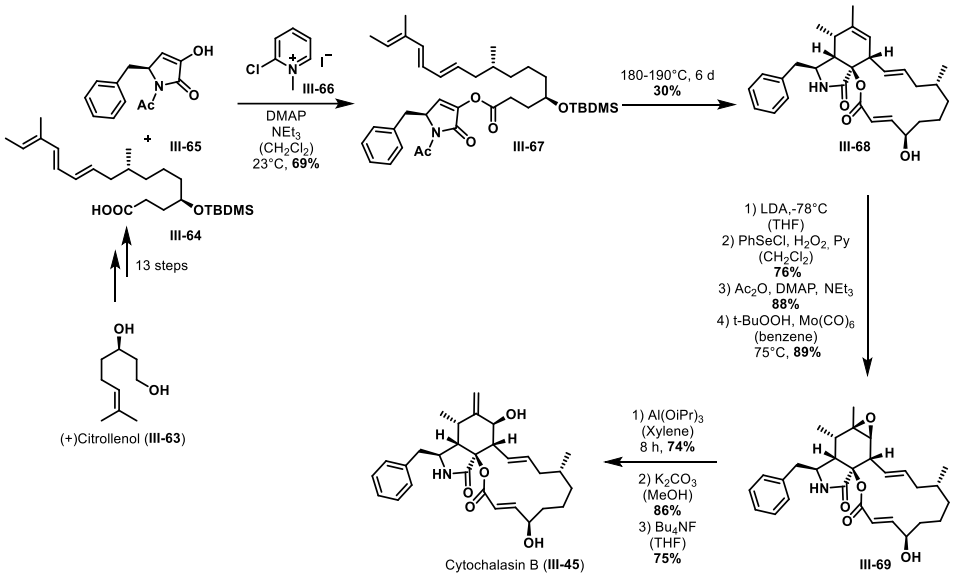

Scheme III-3: The total synthesis of cytochalasin B by *Stork et al.*[391]

Later a more convergent and highly modular synthesis for cytochalasin B by developed by *Haidle* and *Meyers* (Scheme III-4,5).[392] With this convergent approach, different cyctochalasans of varying ring sizes could be accessed with different macrocyclic fragments. As proof of principle, they synthesized the isoindolone building block **III-75** over 13 linear steps. They started with *N,N*-dibenzyl phenylalanal (**III-70**) which was converted to a diene **III-71** over 3 steps with a good overall yield of 74%. The installation of the dienophile **III-80** via an early-stage [4 + 2] intramolecular *Diels-Alder* giving the endo diastereomer product **III-72** in a good yield of 75% over two steps. The deprotection of the *N*-benzyl group of intermediate **III-72** with Pd/C followed by installation of a Boc protecting group and finally deprotection of the silyl enolate gave derivative **III-73**. Formation of a triflic enolate with *Comin's* reagent and strategic substitution of a methyl group via a *Grignard* reaction afforded **III-74** Finally, epoxidation of derivative **III-74** followed by lactone ring cleavage and subsequent oxidation of the resulting alcohol provided the isoindolone building block **III-75** over 9 linear steps in total. *Julia-Kocienski* olefination was utilized to couple **III-75** to the macrocyclic fragment **III-76**, which was separately synthesized over 9 steps from (1R,2R)-pseudoephedrine propionamide (**III-82**), to give the cytochalasan precursor **III-77**. Acylation of **III-77** gave phosphonate **III-78**, which underwent a macrocyclization via intramolecular *Horner-Wadsworth-Emmons* olefination. Further transformations afforded the final Cytochalasin B (**III-45**).

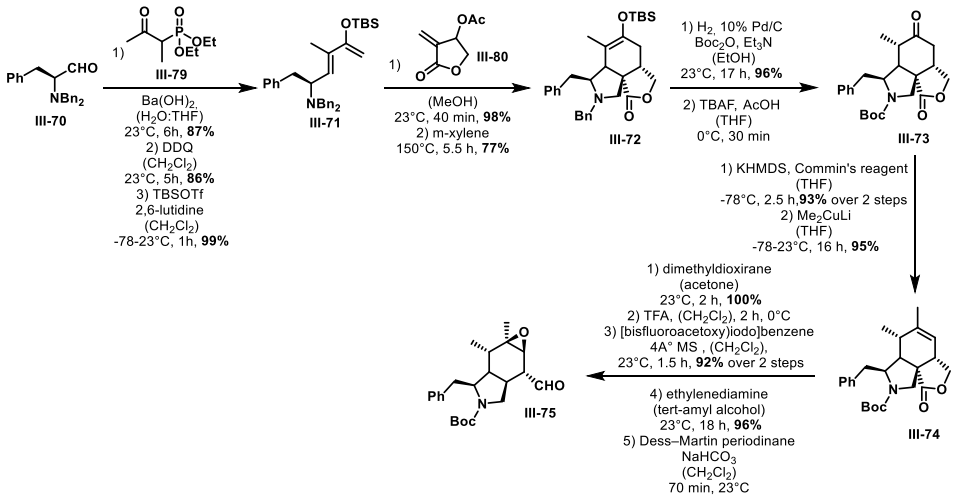

Scheme III-4: Synthesis of isoindolone building block for cytochalasin B by *Haidle* and *Meyers*.[392]

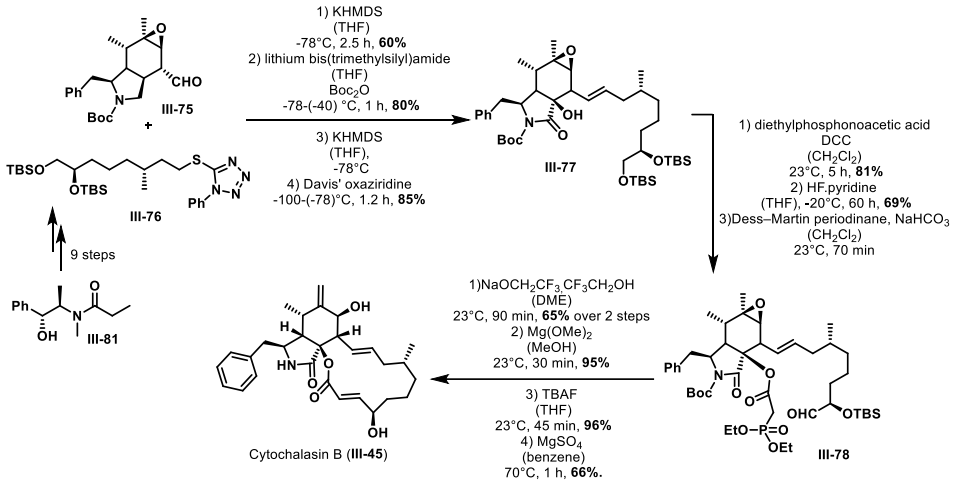

Scheme III-5: Synthesis of cytochalasin B by *Haidle* and *Meyers*.[392]

Thomas and coworkers utilized a biomimetic strategy utilizing a late-stage [4+2] *Diels-Alder* cycloaddition as the key step for the total synthesis of [11] cytochalasans, cytochalasin H, D, G and O.[393–396] For example, the total synthesis of cytochalasin H (**III-89**)[397] is depicted in Scheme III-6. They synthesized the early-stage *Diels-Alder* precursor (**III-85**) from aldehyde **III-82**, phosphonate **III-83** and benzoyl pyrrolidinone **III-84** over 18 steps. The intramolecular Diels-Alder cycloaddition and subsequent removal of the phenyl selenyl group provided the intermediate **III-86**. The α-deprotonation of **III-86** at C20, followed by phenylselenylation and subsequent elimination, facilitated the formation of the C18–C19 double bond to give **III-87**. Then the reduction of the ketone at C21 to a secondary alcohol and subsequent O-acetylation of the alcohol, followed by epoxidation gave cytochalasin H

precursor **III-88**. Finally, an epoxide opening and subsequent deprotection of the tertiary alcohol gave the cytochalasin H (**III-89**) in 29 linear steps overall.

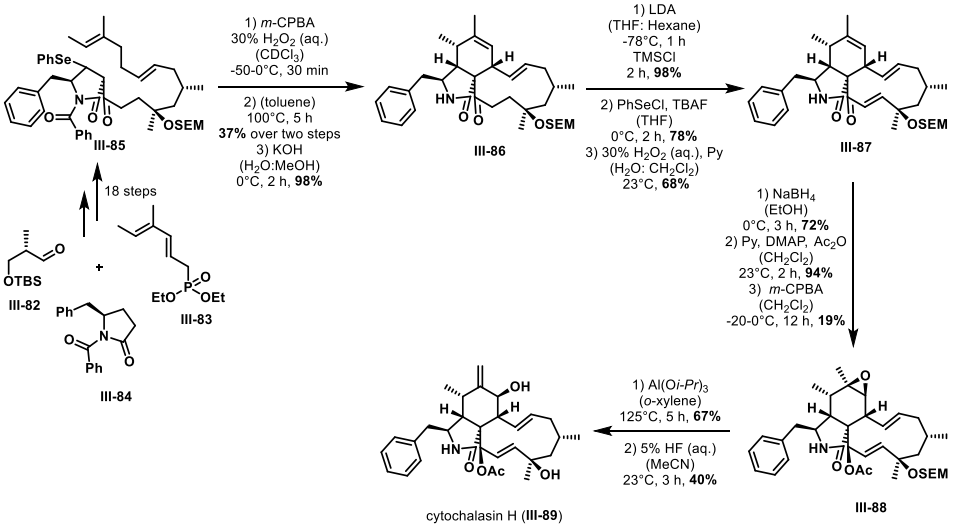

Scheme III-6: Total synthesis of cytochalasin H by *Thomas et al.*[397]

A very concise and relatively short palladium catalyzed synthesis of (-)-aspochalasin B (Scheme III-7), a [11]cytochalasan, was reported by *Trost* and coworkers which also approached the biomimetic route utilizing a late-stage palladium catalyzed macrocyclization (Scheme III-7).[398,399] The isoindolone core (**III-92**) was built via intramolecular *Diels-Alder* reaction from 4-methylsorbinol (**III-90**) and an alkylidene malonic ester (**III-91**), derived from a Cbz-protected isoleucine building block, as previously developed by *Tamm* and coworkers.[400] The lactone ring opening of **III-92** followed by *Swern* oxidation gave aldehyde intermediate **III-93**. The aldehyde side chain of **III-93** was extended through alkylation followed by *Claisen* rearrangement followed by formation into sulfonation to give sulfone **III-94**, A palladium catalyzed macrocyclization of **III-95** gave intermediate **III-96**. Finally, the conversion of the enol ether **in III-96** into a α-hydroxy ketone, followed by sulfoxide elimination gave (-)-aspochalasin B (**III-97**) in overall 13 linear steps.

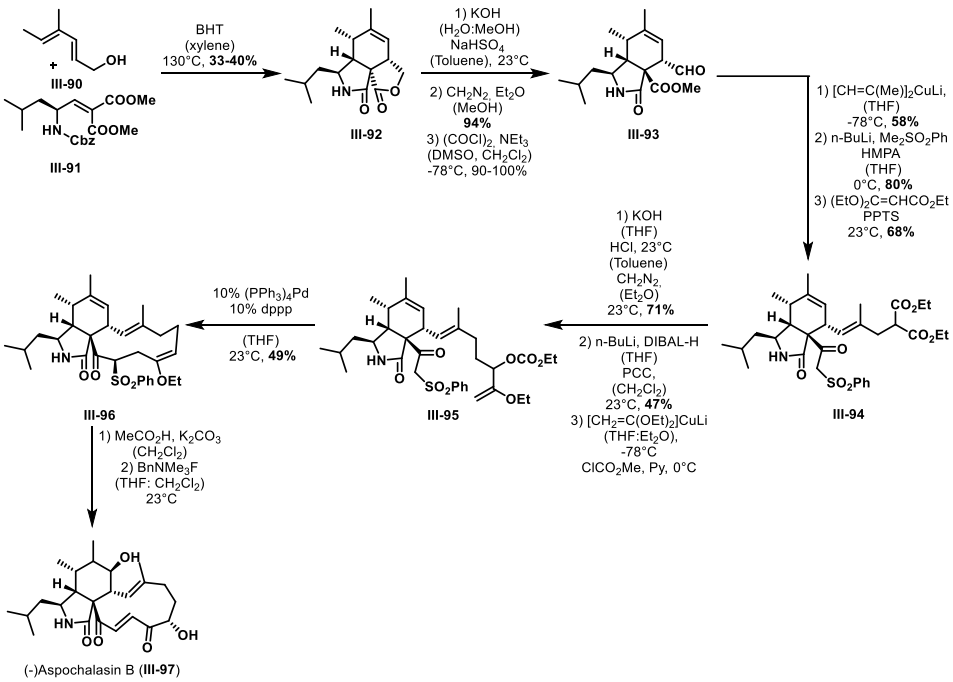

Scheme III 7: Total synthesis of (-)-aspochalasin B by *Trost* and coworkers.[398]

More recently, *Trauner* and coworkers also developed a similar biomimetic strategy for the total synthesis of (-)aspochalasin D and B (Scheme III-8) using an early stage intermolecular *Diels-Alder* to build the isoindolone core and late-stage macrocyclization to build the cytochalasan core.[401] The iodide **III-99** was obtained from epoxide **III-98** over 5 steps with an overall yield of 52%. A palladium catalyzed *Suzuki-Miyaura* cross coupling of iodide **III-99** with 1,3-dienyl boronate **III-105** to give the oxygenated polyolefin **III-100**. An intermolecular *Diels-Alder* cycloaddition with dienophile **III-106** with **III-100** gave the desired isoindolone core derivative **III-101** in 41% yield. Installation of a phosphonate gave **III-102** in 75% yield. Next, a selective deprotection of the primary alcohol of **III-102**, subsequent oxidation to an aldehyde and finally macrocyclization under *Masamune-Rousch* conditions afforded the aspochalasin D core over 3 steps with an overall yield of 46%. A final TBAF deprotection of the secondary alcohols gave aspochalasin D (**III-104**) over 11 linear steps. Semisynthetic modification of **III-104** provided aspochalasin B (**III-105**).

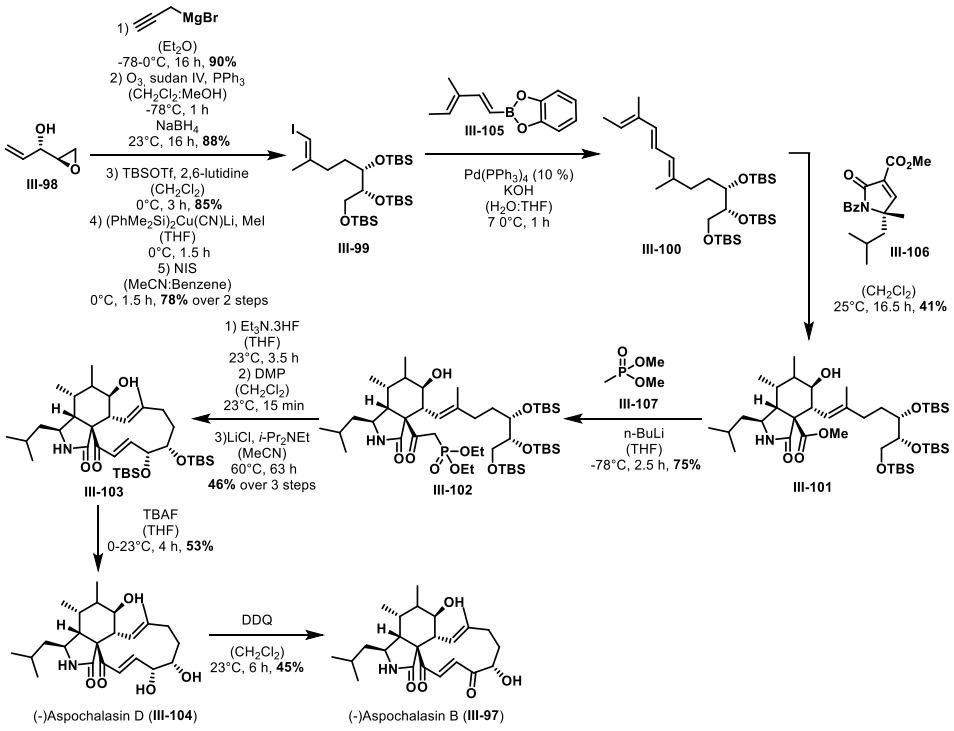

Scheme III-8: Total synthesis of (-)-aspochalasin D and B by *Trauner* and coworkers.[401]

Vedejs and coworkers developed an alternative pathway for the synthesis of zygosporin E.[402,403] They established a very high yielding intermolecular endo selective *Diels-Alder* of a doubly activated dienophile **III-109**, with a trimethylsilyl-substituted triene **III-108** which gave the isoindolone core **III-110** in 91% yield. The isoindolone core (**III-110**) was then subjected to a sulfur mediated substitution to give phenacyl sulfide **III-111** Then a photochemically generated thioaldehyde from the phenacyl sulfide (**III-111**), was trapped by a hetero *Diels–Alder* reaction with 2-(tert-butyldimethylsiloxy)-1,3-butadiene (**III-118**). Further modification provided intermediate **III-112**. Next, the formation of the allylic chloride provided substrate **III-113**, for a base-mediated macrocyclization which afforded the sulfur-bridged carbocycle **III-104**. Next, the methylation of **III-104** at C16 and C18 proved to be highly stereospecific, followed by an *S*–methylation and subsequent zinc mediated reduction cleaved the C16–S bond to afford selenide **III-115**. A highly selective [2,3] sigmatropic rearrangement followed by an oxidative sulfur elimination afforded zygosporin E (**III-116**) This approach allowed sulfur mediated late-stage stereospecific introduction of ring substituents to the isoindolone core.[404]

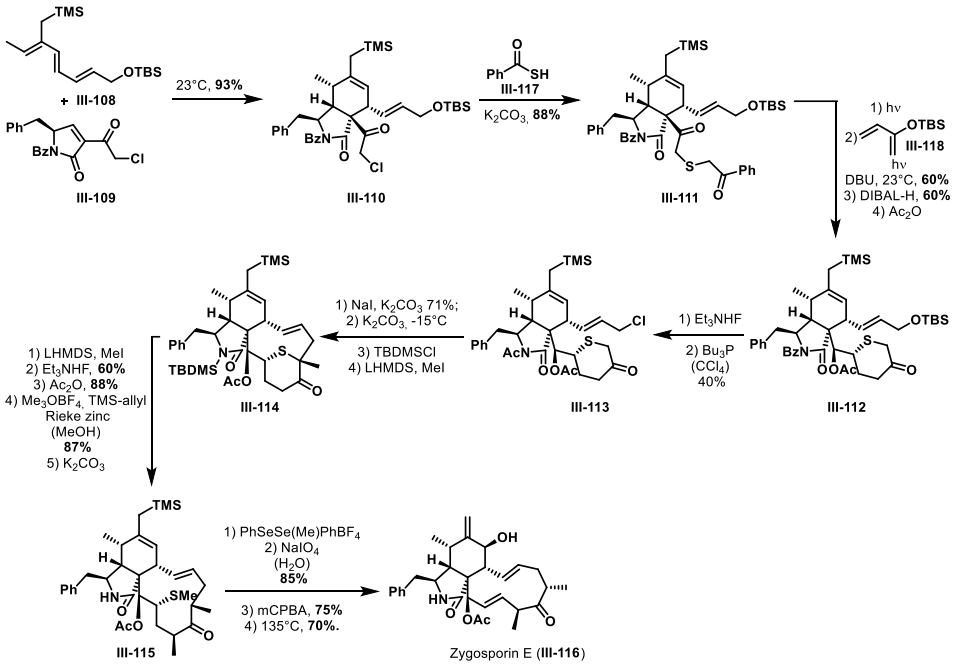

Scheme III-9: Total synthesis of zygosporin E by *Vedjes* and coworkers.[402,403]

From all the published total synthesis for different cytochalasan subclasses, it can be concluded that they are all compound specific and there is a lack of a synthetic approach that allows for an interchange of substituents in the isoindolone core. Furthermore, there is no known total synthesis for [13]cytochalasans, which include chaetoglobosins and armochaetoglobins. As a result, there is a lack of comprehensive studies towards understanding the structure-activity relationship of incorporation of specific amino acids in the isoindolone core or the influence of the macrocycle ring size on biological activity or target specificity.

III-2. Aims and Objectives

The aim of this work was to provide a highly convergent and modular synthetic route to access the [13]cytochalasan subclass. The first total synthesis of chaetoglobosin D (**III-44**) would be accessed via late-stage derivatization of the advanced key intermediate **III-150** via a decarboxylative *Negishi* and *Suzuki* cross-coupling as well as a late-stage biomimetic macrocyclization as shown in Scheme III-10. The key step to assemble the highly substituted key intermediate **III-50**, would be a *Julia-Kocienski* olefination reaction of the isoindolone building block **III-148** and macrocyclic fragment **III-149**. The isoindolone building block **III-48** could be synthesized via an early-stage intermolecular *Diels-Alder* cycloaddition reaction with diene **III-122** and dienophile **III-128**. The diene **III-122** would be synthesized from commercially available (*Z*)-but-2-ene-1,4-diol (**III-119**) and the dienophile **III-128** would be synthesized from an aspartic acid derivative **III-124**. The macrocyclic fragment would be assembled via *Scoopy-Schlosser-Wittig* olefination of *Wittig* salt **III-137** and aldehyde **III-146**. The *Wittig* salt would be synthesized from commercially available D-isoascorbic acid (**III-130**), and the aldehyde would be prepared from 1,3-propanediol (**III-139**).

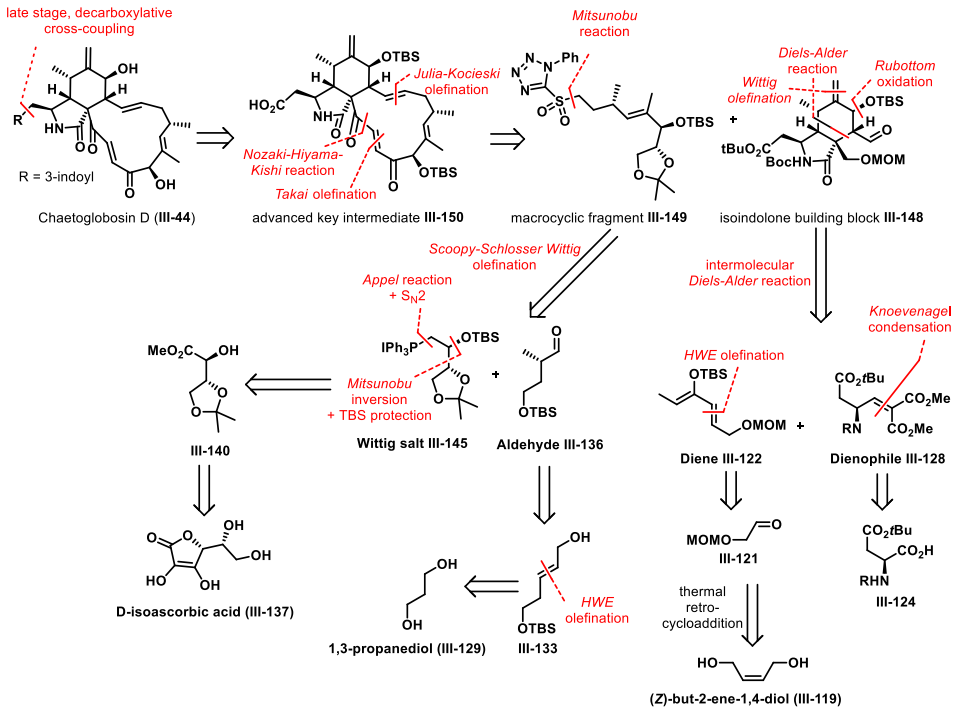

Scheme III-10: Retrosynthesis of chaetoglobosin D.

III-2.1. Preliminary, parallel studies towards the synthesis of isoindolone core of chaetoglobosin D

The synthesis of the isoindolone core for Chaetoglobosin D was studied in parallel by my colleague at the Klahn lab, Dr. Mervic D. Kagho. The synthesis of diene **III-12** was initiated from (*Z*)-but-2-ene-1,4-diol (**III-119**) (Scheme III-11), where both primary alcohol groups were protected in presence of MOMBr under basic conditions to give **III-120** in 82% yield. Ozonolysis of **III-120** followed by reductive workup with triphenylphosphine gave aldehyde **III-121** in 77% yield. *HWE* olefination of aldehyde **III-121** with phosphonate **III-123**, followed by enolate trapping by *O*-silylation in the presence of TBSOTf gave the final diene **III-122** ((Z,E):(E,E)/90:10) in 89% yield and an overall yield of 43% over 4 steps.

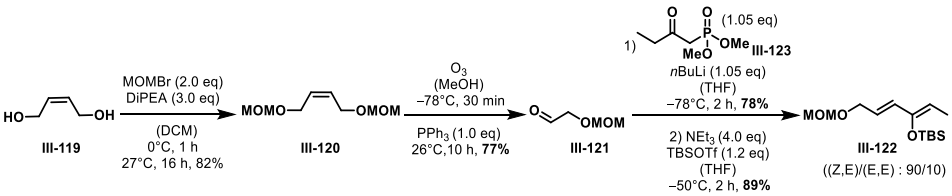

Scheme III-11: Synthesis of diene for the isoindolone building block of Chaetoglobosin D.

The synthesis of dienophiles **III-127a** and **III-127b** (Scheme III-12) was initiated by activation of aspartic acid derivatives **III-124a** and **III-124b** in presence of *N*-hydroxy succinimide to afford **III-125a** and **III-125b** in yields of 92% and 90% respectively. Reduction of the NHS-esters with sodium borohydride gave **III-126a** and **III-126b** in 80 % and 82% yields respectively. Subsequent *Swern* oxidation of the aminols, gave aldehydes **III-127a** and **III-127b** in 92% and 65% yields respectively. Finally, a piperidine catalyzed *Knoevenagel* condensation of **III-127a** and **III-127b** with methyl malonate (**III-129**) afforded the desired dienophiles **III-128a** and **III-128b** in 70% and 50% yields respectively.

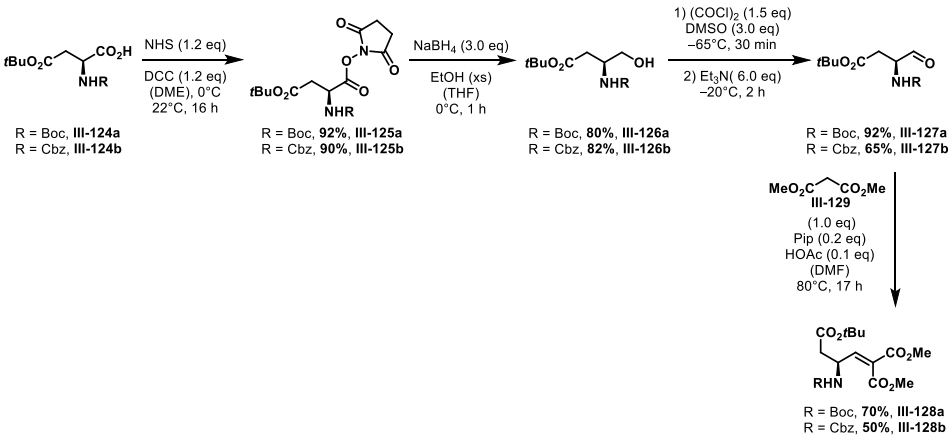

Scheme III-12: Synthesis of dienophile for the isoindolone building block of Chaetoglobosin D.

Next, different reaction conditions were used for the assembly of the isoindolone core backbones (**III-147a**, **III-147b**) via an early-stage intermolecular *Diels-Alder* cycloaddition (Scheme III-13). The results are compiled in Table III-1.

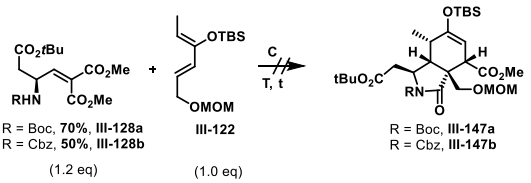

Scheme III-13: Attempts towards the assembly of the isoindolone building block for Chaetoglobosin D.

Table III-1: Reaction conditions and results for the attempts to the intramolecular DAR.

Entry	**Conditions (C)**	**Temperature (T)**	**Time (t)**	**Results**
1	BHT (0.2 eq) (toluene)	100°C (MW)	1 h	No reaction
2	BHT (0.2 eq) (toluene)	120°C (oil bath)	24 h	No reaction
3	BHT (0.2 eq) (toluene)	130°C (MW)	1 h	No reaction
4	BHT (0.2 eq) (toluene)	150°C (oil bath)	48 h	Decomposition of the diene
5	BHT (0.2 eq) neat	150°C (oil bath)	24 h	Decomposition of the diene
6	BHT (0.2 eq) (toluene)	150°C (MW)	45 min	No reaction
7	BHT (0.2 eq) (toluene)	200°C (MW)	1 h	Decomposition of both the diene and the dienophile
8	$BF_3{\cdot}Et_2O$ (0.05 eq) (CH_2Cl_2)	–78°C	17 h	Decomposition of the diene
9	Tf_2NH (0.05 eq) (toluene)	–40°C	5 h	Decomposition of the diene

It was observed that longer reaction times resulted in decomposition of the diene (**III-122**) (Entry 4, 5, 8, 9). While no reaction was observed for temperatures like 100-130°C (Entry 1, 2, 3), higher temperatures of 200°C resulted in decomposition of both diene and dienophile. In conclusion, although the diene (**III-122**) and dienophiles (**III-128a**, **III-128b**) were successfully synthesized, attempts towards the optimization of the intermolecular *Diels-Alder* cycloaddition were not successful.

III-3. Results and Discussion

III-3.1. Studies towards the synthesis of the macrocyclic fragment of chaetoglobosin D

In my first attempt to access the macrocyclic fragment of Chaetoglobosin D two smaller building blocks, the *Wittig* salt (**III-145**) and the aldehyde (**III-136**) were required. The synthesis of the aldehyde **III-136** was initiated from 1,3-propanediol (**III-129**) as shown in Scheme III-17. A selective protection of the one of the primary alcohol **III-129** in presence of TBSCl and sodium hydride gave **III-130** in 88% yield. Subsequent *Swern* oxidation gave corresponding aldehyde **III-131** in 77% yield. The aldehyde **III-131** was immediately subjected to a *HWE* olefination which gave **III-132** in 82% yield. Further reduction of **III-132** in presence of excess di*iso*butylaluminium hydride gave the corresponding alcohol **III-133**. Enantioselective *Sharpless* epoxidation of the olefin **III-133** gave epoxide **III-134** in 60% yield. Trimethylaluminium mediated epoxide ring opening provided the diol **III-135** in 90% yield. Finally, cleavage of the diol **III-135** with sodium periodate afforded the alcohol **III-136** in 70% yield and an overall yield of 18% over 7 steps. The aldehyde **III-136** was found to be sensitive to decomposition and therefore was not stored over long periods of time.

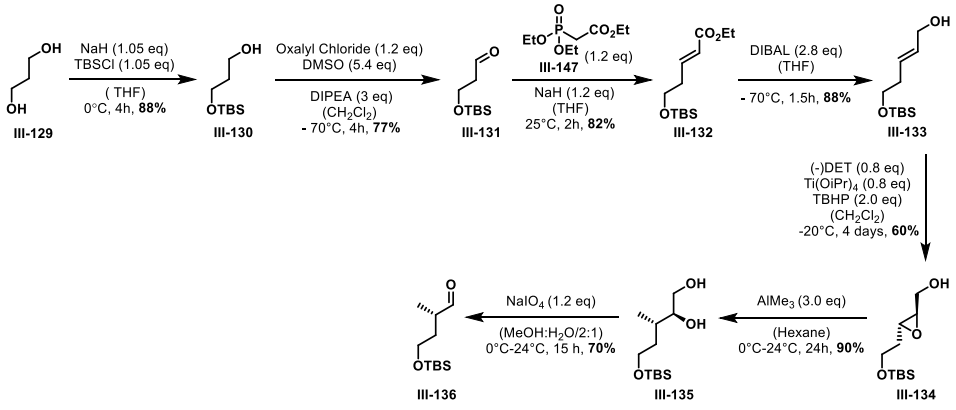

Scheme III-17: Synthesis of aldehyde for the macrocyclic fragment of chaetoglobosin D.

The synthesis of **III-145** (Scheme III-14) was initiated by subjecting D-isoascorbic acid (**III-137**) to an acetonide protection in presence of catalytic amounts of camphor sulfonic acid to afford **III-138** in 90% yield. Next a one pot decarboxylative cleavage of **III-138** and subsequent esterification in presence of dimethysulfate gave the methyl ester **III-139** in 73% yield. Next, a *Mitsunobu* inversion reaction provided the isomer **III-140** in 70% yield. Subsequent protection of the secondary alcohol in **III-140** in presence of excess TBSCl and imidazole afforded **III-141** in 90% yield. The methyl ester of **III-141** was reduced with di*iso*butylaluminum hydride to its corresponding alcohol **III-142** in 70% yield. The tosylation of the primary alcohol **III-142** provided **III-143** as a better substrate for iodination. Iodination of **III-143** in presence of sodium iodide gave **III-144** as the precursor for the *Wittig* salt.

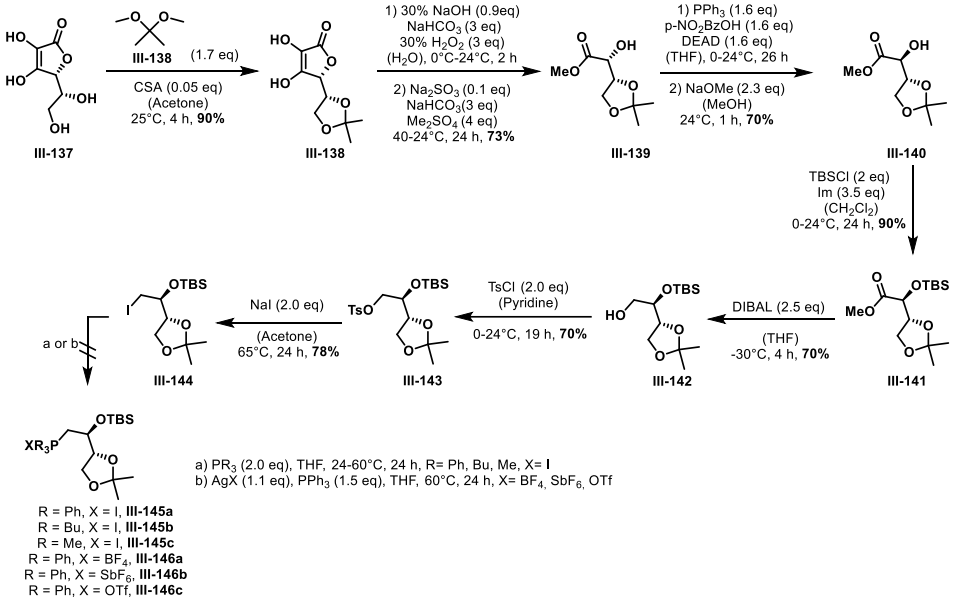

Scheme III-14: Synthesis of *Wittig* salt for the macrocyclic fragment of chaetoglobosin D.

Next, several attempts were made for the optimization of the *Wittig* salt formation (Scheme III-15) Addition of different phosphines like PPh_3, PBu_3, PMe_3or changing the solvent to THF, ACN or DMF did not result in any reaction under reflux conditions. Varying the time of the reaction was also unsuccessful.

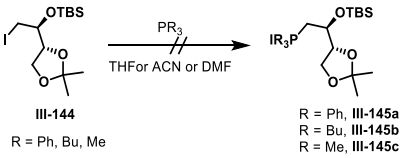

Scheme III-15: Attempts towards optimization of the synthesis of *Wittig* salt.

Table III-2: Attempts towards synthesis of *Wittig* salt with silver salts.

Entry	Silver salt (AgX)	Reaction conditions	Result
1	$AgBF_4$	PPh_3, THF, 65°C, 19h	Decomposition of **III-144**
2	$AgSbF_6$,		Decomposition of **III-144**
3	AgOTf		Decomposition of **III-144**
4	$AgBF_4$	PPh_3, Imidazole, THF, 65°C, 19h	No conversion
5	$AgSbF_6$,		No conversion
6	AgOTf		No conversion

Further attempts were made to increase the reactivity of the iodide *in situ* by introducing silver salts in the reaction mixture so that the precipitation of silver iodide could facilitate the overall reactivity (Scheme III-16). The results are shown in Table III-2.

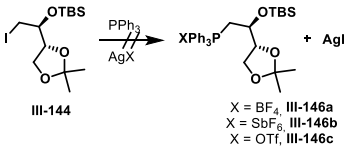

Scheme III-16: Attempts towards optimization of the synthesis of *Wittig* salt with silver salt.

The initial attempts of introducing various silver salts resulted in decomposition of the iodide **III-144** presumably due to the formation of an acidic solution during the reaction causing the deprotection of acid labile TBS group or even the acetonide in **III-144**. To counteract the acid, imidazole was added to the reaction mixture but in that case no reaction was observed. The overall attempts to synthesize the *Wittig* salt were unsuccessful. The absence of the required *Wittig* salt **III-145** for the *Scoopy-Schlosser-Wittig* olefination made the envisaged synthesis of the macrocyclic fragment impossible. Beyond that, as the synthesis attempt of the isoindolone cores **III-147a** and **III-147b** (work of my colleague Dr. Mervic D. Kagho, see section III-3.2) was not successful either it was decided to change the overall synthesis strategy and now target the synthesis of chaetoglobosin B (**III-43**) via an alternative approach.

III-3.2. Studies towards the synthesis of chaetoglobosin B

A new convergent synthetic route was proposed for chaetoglobosin B (**III-43**) (Scheme III-18), which now involved an early-stage intramolecular DAR following an approach by *Xu et al*.[405] The isoindolone core **III-180** was planned to be assembled from diene **III-163a** and dienophile **III-171**. Diene **III-163a** would be accessed from aldehyde **III-157** firstly via a *Wittig* reaction with ylide **III-164**, followed by another *Wittig* reaction with **III-165**. A Boc protection of **III-153** would give aldehyde **III-157**. **III-153** would be derived via a reductive amination of L-Tryptophane (**III-151**). Dienophile **III-171** would be accessed from fragment **III-169** by a *Wittig* reaction. Oxidation of secondary alcohol of **III-167** with TEMPO would give access to **III-167**. Dihydroxylation of *tert*-butylacrylate (**III-166**) followed protection of the primary alcohol would give fragment **III-167**. The new synthesis also proposed a different disconnection approach for the macrocyclic fragment where the previously built aldehyde **III-136** was incorporated but the synthesis of any *Wittig* salt could be avoided. Macrocyclic fragment **III-174** would be accessed from derivative **III-177** first via protection of the secondary alcohol followed by a *Mitsunobu* reaction with a tetrazole and subsequent oxidation of the resulting thioether. Substituted alkene **III-177** would be accessed from alkyne **III-176** through a *Grignard* reaction. Fragment **III-176** was planned to be accessed from previously synthesized aldehyde **III-146**, first via a *Bestmann-Ohira* reaction forming a terminal alkyne followed by a zinc mediated addition of aldehyde **III-182** to the terminal alkyne.

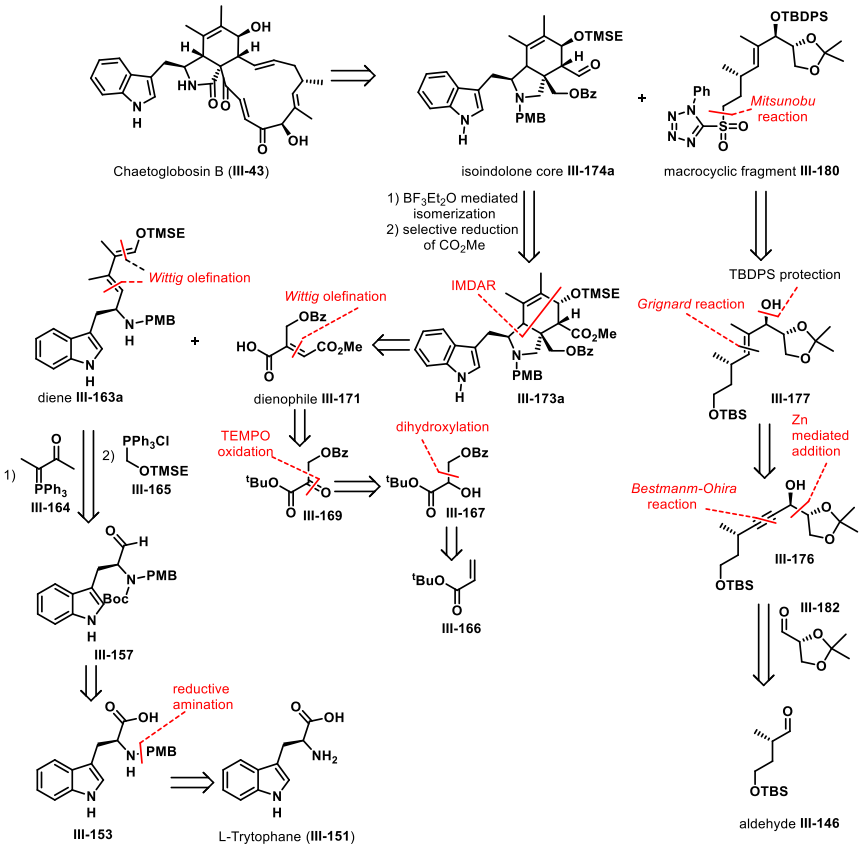

Scheme III-18: Retrosynthesis of chaetoglobosin B.

III-3.2.1 Studies towards the synthesis of the isoindolone core of chaetoglobosin B

The synthesis of diene **III-163** was initiated from L-tryptophane (**III-151**) as summarized in Scheme III-19. To III-151, a *para*-methoxybenzyl moiety was installed via a reductive amination to give **III-152** in 63% yield. Subsequent protection of the secondary amine of **III-152** in presence of Boc anhydride gave the double protected tryptophane derivative **III-153** in 31% yield. Attempts were then made to transform **III-153** to its corresponding *Weinreib* amide **III-154** in presence of coupling reagent EDC·HCl and *N*,*O*-dimethylhydroxylamine but no reaction was observed. Another attempt was made towards the synthesis of **III-154** by first making and acid chloride from **III-153** with thionyl chloride but even then, no product formation was observed. Next, the free carboxylic acid of **III-151** was first converted to the corresponding methyl ester derivative **III-155** in 90% yield. Then the primary amine in **III-155** was doubly protected to give **III-156** in an overall yield of 40% over 2 steps. Further attempts to convert **III-156** to the corresponding aldehyde **III-157** were unsuccessful. In fact, **III-156** could not be converted into the corresponding alcohol **III-158** as well. It could be concluded that the presence of both the Boc group and the *para*-methoxybenzyl moiety caused either steric influence or general low reactivity towards reduction.

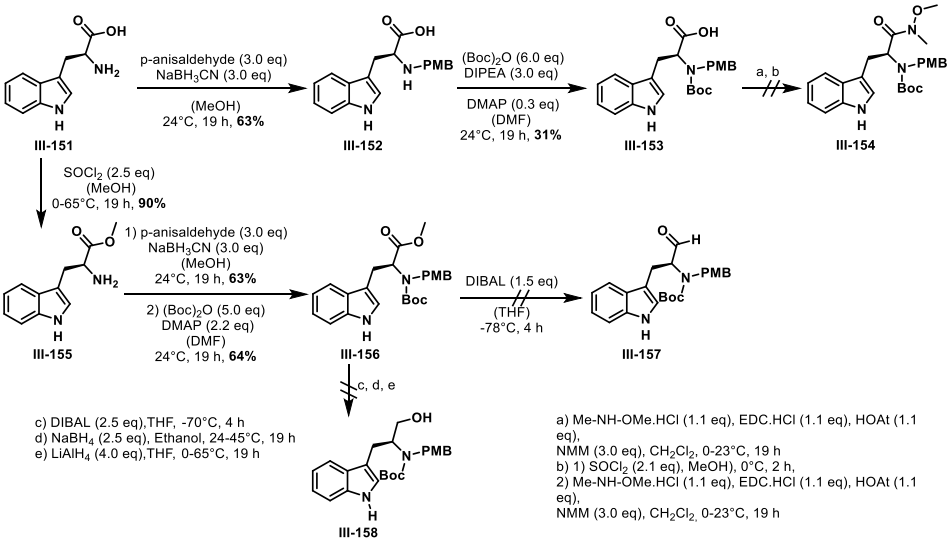

Scheme III-19: Initial attempts towards the synthesis of isoindolone building block for chaetoglobosin B.

In the next strategy for synthesis of the diene (Scheme III-20), only a Boc group was installed on tryptophane **III-151** which gave **III-159** in 70% yield. Next, a *Weinreib* amide **III-160** could be easily synthesized using *N,O*-dimethylhydroxylamine and EDC·HCl in 94% yield. Reduction of **III-160** with lithium aluminum hydride gave aldehyde **III-161**, which was swiftly converted to the *E*-isomer **III-162** via a *Wittig* olefination with ylide **III-164** under reflux conditions in toluene, in 68% yield. Another *Wittig* olefination of ketone **III-162** with *Wittig* salt **III-165** under basic conditions provided an inseparable (E:Z/1:1) mixture of **III-163** in 60% yield with an overall yield of 22%.

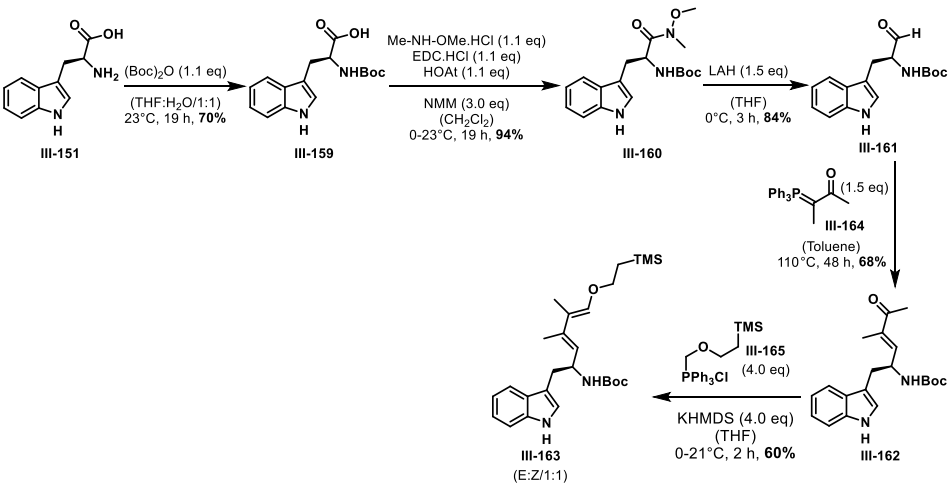

Scheme III-20: Synthesis of diene fragment of isoindolone core of Chaetoglobosin B.

For the synthesis of the dienophile **III-171** (Scheme III-21), tert-butyl acrylate (**III-166**) was subjected to an asymmetric dihydroxylation to give **III-167**, because initial attempts towards a non-asymmetric dihydroxylation failed. A selective installation of a benzoyl moiety on the primary alcohol gave **III-168** in only 33% yield. Subsequent, oxidation of the secondary alcohol of **III-168** with TEMPO provided **III-169** in 68% yield. The α-keto ester derivative **III-169** then underwent a *Wittig* olefination to give **III-170** in 39% yield. Finally selective deprotection of the tert-butyl group gave the dienophile **III-171** in 31% yield with a very poor overall yield of 1.5% over 5 steps.

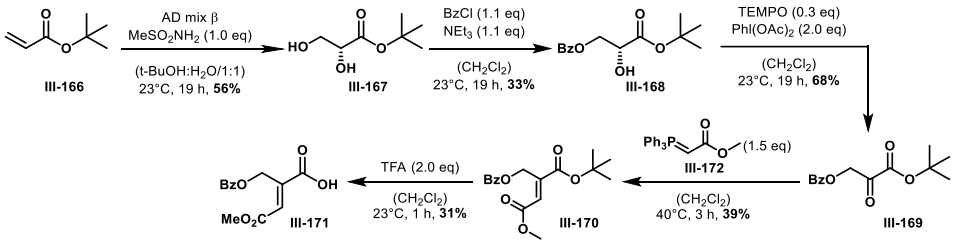

Scheme III-21: Synthesis of diene fragment for the isoindolone core of Chaetoglobosin B.

III-4. Conclusions and Outlook

Efforts toward the total synthesis of chaetoglobosin D focused on constructing key fragments, including the isoindolone core **III-148** and macrocyclic fragment **III-149**. The synthesis of diene **III-122** and dienophiles **III-128a** and **III-128b** was successfully accomplished using multistep synthesis. However, attempts to assemble the isoindolone backbone through intermolecular *Diels-Alder* reactions under various conditions were unsuccessful due to diene and dienophile decomposition. Parallel efforts to synthesize the macrocyclic fragment from aldehyde **III-136** and Wittig salt **III-145** encountered challenges, including decomposition of sensitive intermediates and unsuccessful Wittig salt formation despite optimization attempts using various phosphines and silver salts. The cumulative difficulties in assembling these building blocks necessitated a reevaluation of the synthetic strategy, redirecting efforts toward the synthesis of chaetoglobosin B using an alternative approach.

For the synthesis of chaetoglobosin B the precursors **III-163** and **III-171** for the isoindolone core **III-174** were successfully synthesized but there are a few drawbacks in these routes. For the synthesis of diene **III-163**, the *Wittig* olefination gives an inseparable mixture which brings further purification problems. The overall yield for the synthetic route for the dienophile can certainly be improved with further optimization. One drawback for that route is the loss of starting material during preparation of benzoyl protected alcohol **III-168** as the double protected substrate is the major product. The following *Wittig* reaction is also not very selective and gives an almost E:Z/1:1 for **III-170**. Further synthesis into the assembly of the isoindolone core **III-174** and macrocyclic building block **III-180** could not be explored due to the limited time left in my PhD.

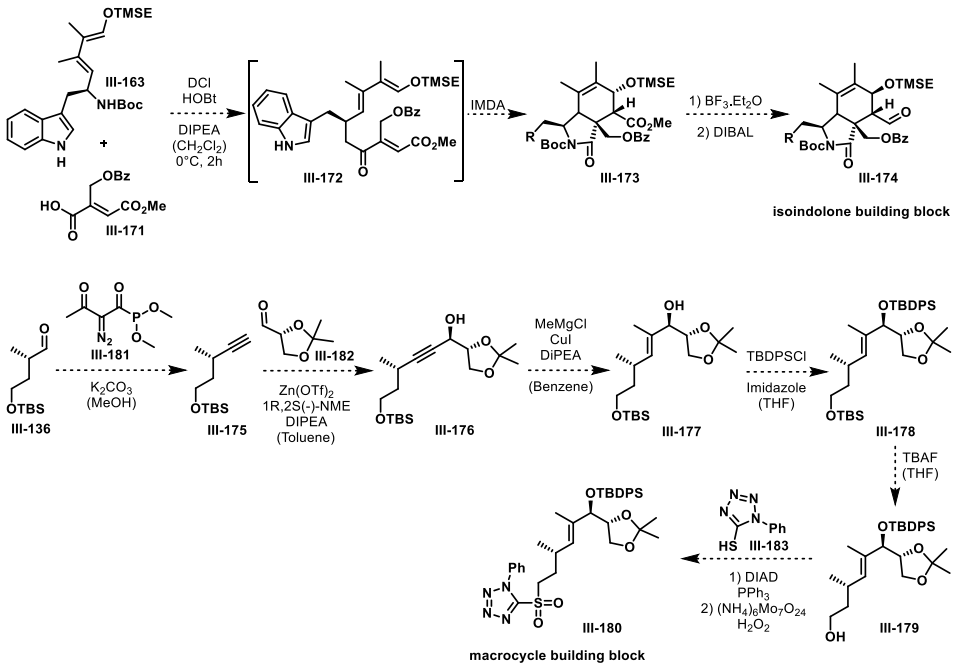

Scheme III-22: Proposed synthetic route for the assembly of isoindolone core and macrocyclic fragment.

There is potential to improve the synthesis, and the future work could be pursued according to the proposed route as shown in Scheme III-22. The isoindolone core **III-173** could be built by coupling the diene **III-163** and dienophile **III-171** in presence of DCI and HOBt to form an *in situ* intermediate **III-172**, which should rapidly undergo an intramolecular DAR. Further modifications would provide isoindolone building block **III-174**. For the macrocyclic fragment **III-180**, the previously synthesized aldehyde **III-136** could be utilized to make a terminal alkyne via *Bestmann-Ohira* reaction using reagent **III-181**. Then a zinc mediated attachment of **III-182** to the terminal alkyne of **III-175** would give a substituted alkyne **III-176**. A *Grignard* reaction followed by protection of the secondary alcohol with TBDPSCl would give **III-178**. Then selective deprotection of the primary alcohol and subsequent formation of the sulfone would provide the macrocyclic fragment **III-180**.

References

[1] C. P. Glindemann, A. Backenköhler, M. Strieker, U. Wittstock, P. Klahn, *ChemBioChem* **2019**, *20*, 2341–2345.

[2] J. W. Fahey, K. L. Wade, K. K. Stephenson, Y. Shi, H. Liu, A. A. Panjwani, C. R. Warrick, M. E. Olson, *Nutrients* **2019**, *11*, 1–14.

[3] R. F. Mithen, M. Dekker, R. Verkerk, S. Rabot, I. T. Johnson, *J. Sci. Food Agric.* **2000**, *80*, 967–984.

[4] M. A. Prieto, C. J. López, J. Simal-Gandara, *Adv. Food Nutr. Res.* **2019**, *90*, 305–350.

[5] B. A. Halkier, J. Gershenzon, *Annu. Rev. Plant Biol.* **2006**, *57*, 303–333.

[6] I. Blažević, S. Montaut, F. Burčul, C. E. Olsen, M. Burow, P. Rollin, N. Agerbirk, *Phytochemistry* **2020**, *169*, 112100.

[7] R. Kissen, Æ. J. T. Rossiter, Æ. A. M. Bones, *Phytochem. Rev.* **2009**, *8*, 69–86.

[8] P. D. Brown, J. G. Tokuhisa, M. Reichelt, J. Gershenzon, *Phytochemistry* **2003**, *62*, 471–481.

[9] P. Velasco, M. E. Cartea, C. González, M. Vilar, A. Ordás, *J. Agric. Food Chem.* **2007**, *55*, 955–962.

[10] A. L. Shelton, *J. Chem. Ecol.* **2005**, *31*, 1711–1732.

[11] S. Chhajed, I. Mostafa, Y. He, M. Abou-hashem, M. El-domiaty, *Agronomy* **2020**, *10*, 1–25.

[12] M. Shirakawa, H. Ueda, T. Shimada, I. Hara-nishimura, *Plant Signal. Behav.* **2016**, *11*, 1–6.

[13] L. Rask, E. Andr, B. Ekbom, S. Eriksson, B. Pontoppidan, J. Meijer, *Plant Mol. Biol.* **2000**, *42*, 93–113.

[14] Q. Lv, X. Li, B. Fan, C. Zhu, Z. Chen, *Int. J. Mol. Sci.* **2022**, *23*, 1577.

[15] A. R. Agnihotri, C. V. Hulagabali, A. S. Adhav, R. S. Joshi, *Phytochemistry* **2018**, *145*, 121–127.

[16] N. Aissani, P. Tedeschi, A. Maietti, V. Brandolini, V. L. Garau, P. Caboni, *J. Agric. Food Chem.* **2013**, *61*, 4723–4727.

[17] B. A. Halkier, L. Du, *Trends Plant Sci.* **1997**, *2*, 425–431.

[18] B. Activities, *Molecules* **2020**, *25*, 4537.

[19] I. E. Sønderby, F. Geu-Flores, B. A. Halkier, *Trends Plant Sci.* **2010**, *15*, 283–290.

[20] T. Knill, M. Reichelt, C. Paetz, J. Gershenzon, S. Binder, *Plant Mol. Biol.* **2009**, *71*, 227–239.

[21] Y. Sawada, A. Kuwahara, M. Nagano, T. Narisawa, A. Sakata, K. Saito, M. Yokota Hirai, *Plant Cell Physiol.* **2009**, *50*, 1181–1190.

[22] Y. He, T. P. Mawhinney, M. L. Preuss, A. C. Schroeder, B. Chen, L. Abraham, J. M. Jez, S. Chen, *Plant J.* **2009**, *60*, 679–690.

[23] M. Y. Hirai, K. Sugiyama, Y. Sawada, T. Tohge, T. Obayashi, A. Suzuki, R. Araki, N. Sakurai, H. Suzuki, K. Aoki, H. Goda, O. I. Nishizawa, D. Shibata, K. Saito, *Proc. Natl. Acad. Sci. U. S. A.* **2007**, *104*, 6478–6483.

[24] L. Du, B. A. Halkier, *Plant Physiol.* **1996**, *111*, 831–837.

[25] R. N. Bennett, G. Kiddle, R. M. Wallsgrove, *Phytochemistry* **1997**, *45*, 59–66.

[26] U. Wittstock, B. A. Halkier, *J. Biol. Chem.* **2000**, *275*, 14659–14666.

[27] J. Ludwig-Müller, W. Hilgenberg, *Physiol. Plant.* **1988**, *74*, 240–250.

[28] C. H. Hansen, U. Wittstock, C. E. Olsen, A. J. Hick, J. A. Pickett, B. A. Halkier, *J. Biol. Chem.* **2001**, *276*, 11078–11085.

[29] S. Chen, E. Glawischnig, K. Jørgensen, P. Naur, B. Jørgensen, C. E. Olsen, C. H. Hansen, H. Rasmussen, J. A. Pickett, B. A. Halkier, *Plant J.* **2003**, *33*, 923–937.

[30] M. R. Hemm, M. O. Ruegger, C. Chapple, *Plant Cell* **2003**, *15*, 179–194.

[31] P. Naur, B. L. Petersen, M. D. Mikkelsen, S. Bak, H. Rasmussen, C. E. Olsen, B. A. Halkier, *Plant Physiol.* **2003**, *133*, 63–72.

[32] S. Bak, R. Feyereisen, *Plant Physiol.* **2001**, *127*, 108–118.

[33] S. Bak, F. E. Tax, K. A. Feldmann, D. W. Galbraith, R. Feyereisen, *Plant Cell* **2001**, *13*, 101.

[34] C. D. Grubb, S. Abel, *Trends Plant Sci.* **2006**, *11*, 89–100.

[35] P. Bednarek, M. Pislewska-Bednarek, A. Svatos, B. Schneider, J. Doubsky, M. Mansurova, M. Humphry, C. Consonni, R. Panstruga, A. Sanchez-Vallet, A. Molina, P. Schulze-Lefert, *Science (80-.).* **2009**, *251*, 101–106.

[36] M. D. Mikkelsen, P. Naur, B. A. Halkier, *Plant J.* **2004**, *37*, 770–777.

[37] C. M. M. Gachon, M. Langlois-Meurinne, Y. Henry, P. Saindrenan, *Plant Mol. Biol.* **2005**, *58*, 229–245.

[38] C. D. Grubb, B. J. Zipp, J. Ludwig-Müller, M. N. Masuno, T. F. Molinski, S. Abel, *Plant J.* **2004**, *40*, 893–908.

[39] M. Piotrowski, A. Schemenewitz, A. Lopukhina, A. Müller, T. Janowitz, E. W. Weiler, C. Oecking, *J. Biol. Chem.* **2004**, *279*, 50717–50725.

[40] M. D. Mikkelsen, B. L. Petersen, C. E. Olsen, B. A. Halkier, *Amino Acids* **2002**, *22*, 279–295.

[41] B. G. Hansen, D. J. Kliebenstein, B. A. Halkier, *Plant J.* **2007**, *50*, 902–910.

[42] J. Li, B. G. Hansen, J. A. Ober, D. J. Kliebenstein, B. A. Halkier, *Plant Physiol.* **2008**, *148*, 1721–1733.

[43] D. J. Kliebenstein, V. M. Lambrix, M. Reichelt, J. Gershenzon, T. Mitchell-Olds, *Plant Cell* **2001**, *13*, 681–693.

[44] J. Kroymann, S. Textor, J. G. Tokuhisa, K. L. Falk, S. Bartram, J. Gershenzon, T. Mitchell-Olds, *Plant Physiol.* **2001**, *127*, 1077–1088.

[45] D. J. Kliebenstein, J. Kroymann, P. Brown, A. Figuth, D. Pedersen, J. Gershenzon, T. Mitchell-Olds, *Plant Physiol.* **2001**, *126*, 811–825.

[46] U. Wittstock, M. Burow, *IUBMB Life* **2007**, *59*, 744–751.

[47] J. C. Kuchernig, A. Backenköhler, M. Lübbecke, M. Burow, U. Wittstock, *Phytochemistry* **2011**, *72*, 1699–1709.

[48] W. P. Burmeister, S. Cottaz, H. Driguez, R. Iori, S. Palmieri, B. Henrissat, *Structure* **1997**, *5*, 663–676.

[49] S. Cottaz, B. Henrissat, H. Driguez, *Biochemistry* **1996**, *35*, 15256–15259.

[50] R. Bhat, D. Vyas, *Crit. Rev. Biotechnol.* **2019**, *39*, 508–523.

[51] U. Wittstock, N. Agerbirk, E. J. Stauber, C. E. Olsen, M. Hippler, T. Mitchell-Olds, J. Gershenzon, H. Vogel, *Proc. Natl. Acad. Sci. U. S. A.* **2004**, *101*, 4859–4864.

[52] U. Wittstock, M. Burow, *Arab. B.* **2010**, *8*, 1–14.

[53] H. L. Tookey, *Can. J. Biochem.* **1973**, *51*, 1654–1660.

[54] E. H. J. N.V. Matusheski, R. Swarup, J. A. Juvik, R. Mithen, M. Bennet, *J. Agric. Food Chem.* **2006**, *54*, 2069–2076.

[55] M. Burow, Z. Zhang, J. A. Ober, V. M. Lambrix, U. Wittstock, J. Gershenzon, D. J. Kliebenstein, *Phytochemistry* **2008**, *69*, 663–671.

[56] V. Lambrix, M. Reichelt, T. Mitchell-olds, D. J. Kliebenstein, J. Gershenzon, *Plant Cell* **2001**, *13*, 2793–2807.

[57] M. Burow, A. Losansky, R. Muller, A.

Plock, D. J. Kliebenstein, U. Wittstock, M. Burow, A. Losansky, *Plant Physiol.* **2009**, *149*, 561–574.

[58] R. Kissen, A. M. Bones, *J. Biol. Chem.* **2009**, *284*, 12057–12070.

[59] G. R. Fenwick, R. K. Heaney, *Food Chem.* **1983**, *11*, 249–271.

[60] R. Gmelin, A. I. Virtanen, S. Eriksson, C.-G. Hedén, B. Malmgren, H. Palmstierna, *Acta Chem. Scand.* **1959**, *13*, 1474–1475.

[61] M. Burow, A. Bergner, J. Gershenzon, U. Wittstock, *Plant Mol. Biol.* **2007**, *63*, 49–61.

[62] S. Maina, G. Misinzo, G. Bakari, H. Y. Kim, *Molecules* **2020**, *25*, 1–30.

[63] S. D. Johnson, M. E. Griffiths, C. I. Peter, M. J. Lawes, *Am. J. Bot.* **2009**, *96*, 2080–2086.

[64] S. L. F. Meyer, I. A. Zasada, S. B. Orisajo, M. J. Morra, *J. Nematol.* **2011**, *43*, 7–15.

[65] I. A. Zasada, J. E. Weiland, R. L. Reed, J. F. Stevens, *J. Agric. Food Chem.* **2012**, *60*, 339–345.

[66] L. J. Rivera-Vega, S. Krosse, R. M. de Graaf, J. Garvi, R. D. Garvi-Bode, N. M. van Dam, *Front. Plant Sci.* **2015**, *6*, 1–12.

[67] A. Borges, A. C. Abreu, C. Ferreira, M. J. Saavedra, L. C. Simões, M. Simões, *J. Food Sci. Technol.* **2015**, *52*, 4737–4748.

[68] A. Conrad, D. Biehler, T. Nobis, H. Richter, I. Engels, K. Biehler, U. Frank, *Drug Res. (Stuttg).* **2013**, *63*, 65–68.

[69] A. A. Al-Gendy, K. A. Nematallah, S. S. Zaghloul, N. A. Ayoub, *Pharm. Biol.* **2016**, *54*, 3257–3263.

[70] A. Radonić, I. Blažević, J. Mastelić, M. Zekić, M. Skočibušić, A. Maravić, *Chem. Biodivers.* **2011**, *8*, 1170–1181.

[71] J. Mastelić, I. Blažević, I. Kosalec, *Chem. Biodivers.* **2010**, *7*, 2755–2765.

[72] I. Blažević, A. Radonić, J. Mastelić, M. Zekić, M. Skočibušić, A. Maravić, *Food Chem.* **2010**, *121*, 1020–1028.

[73] I. Blažević, A. Đulović, A. Maravić, V. Čikeš Čulić, S. Montaut, P. Rollin, *Chem. Biodivers.* **2019**, *16*, DOI 10.1002/cbdv.201800661.

[74] M. S. Hifnawy, R. M. A. Salam, M. a Rabeh, M. a Aboseada, **2013**, *3*, 66–82.

[75] C. Dias, A. Aires, M. J. Saavedra, *Int. J. Mol. Sci.* **2014**, *15*, 19552–19561.

[76] V. Dufour, B. Alazzam, G. Ermel, M. Thepaut, A. Rossero, O. Tresse, K. L. Hiett, *Front. Cell. Infect. Microbiol.* **2012**, *2*, 1–13.

[77] S. J. Kaiser, N. T. Mutters, B. Blessing, F. Günther, *Fitoterapia* **2017**, *119*, 57–63.

[78] M. G. Kim, H. S. Lee, *J. Food Sci.* **2009**, *74*, 467–471.

[79] A. Bhattacharya, Y. Li, K. L. Wade, J. D. Paonessa, J. W. Fahey, Y. Zhang, *Carcinogenesis* **2010**, *31*, 2105–2110.

[80] Z. Y. Li, Y. Wang, W. T. Shen, P. Zhou, *Asian Pac. J. Trop. Med.* **2012**, *5*, 231–233.

[81] T. Kulisic-Bilusic, I. Schmöller, K. Schnäbele, L. Siracusa, G. Ruberto, *Food Chem.* **2012**, *132*, 261–267.

[82] S. B. Kntayya, M. D. Ibrahim, N. M. Ain, R. Iori, C. Ioannides, A. F. Abdull Razis, *Nutrients* **2018**, *10*, 1–15.

[83] M. S. Tafakh, M. Saidijam, T. Ranjbarnejad, S. Malih, S. Mirzamohammadi, R. Najafi, *Cells Tissues Organs* **2019**, *206*, 46–53.

[84] M. D. Ibrahim, S. B. Kntayya, N. Mohd Ain, R. Iori, C. Ioannides, A. F. A. Razis, *Molecules* **2018**, *23*, DOI 10.3390/molecules23123092.

[85] M. S. Dekić, N. S. Radulović, N. M. Stojanović, P. J. Randjelović, Z. Z. Stojanović-Radić, S. Najman, S.

Stojanović, *Food Chem.* **2017**, *232*, 329–339.

[86] F. A. Hashem, H. Motawea, A. E. El-Shabrawy, K. Shaker, S. El-Sherbini, *Phyther. Res.* **2012**, *26*, 743–747.

[87] T. S. Rajan, G. R. De Nicola, R. Iori, P. Rollin, P. Bramanti, E. Mazzon, *Fitoterapia* **2016**, *110*, 1–7.

[88] R. Arora, R. Kumar, J. Mahajan, A. P. Vig, B. Singh, B. Singh, S. Arora, *J. Food Sci. Technol.* **2016**, *53*, 3437–3445.

[89] J. Jakubikova, D. Cervi, M. Ooi, K. Kim, S. Nahar, S. Klippel, D. Cholujova, M. Leiba, J. F. Daley, J. Delmore, J. Negri, S. Blotta, D. W. Mcmillin, T. Hideshima, P. G. Richardson, J. Sedlak, K. C. Anderson, C. S. Mitsiades, *Haematologica* **2011**, *96*, 1170–1179.

[90] E. Antonini, R. Iori, P. Ninfali, E. S. Scarpa, *Nutr. Cancer* **2018**, *70*, 1159–1165.

[91] E. L. Connolly, M. Sim, N. Travica, W. Marx, G. Beasy, G. S. Lynch, C. P. Bondonno, J. R. Lewis, J. M. Hodgson, L. C. Blekkenhorst, *Front. Pharmacol.* **2021**, *12*, 1–12.

[92] C. Zhang, J. Zhang, Q. Wu, B. Xu, G. Jin, Y. Qiao, S. Zhao, Y. Yang, J. Shang, X. Li, K. Liu, *Cancer Cell Int.* **2019**, *19*, 4–13.

[93] A. Hać, J. Brokowska, E. Rintz, M. Bartkowski, G. Węgrzyn, A. Herman-Antosiewicz, *Eur. J. Nutr.* **2020**, *59*, 1421–1432.

[94] Q. V. Vo, C. Trenerry, S. Rochfort, J. Wadeson, C. Leyton, A. B. Hughes, *Bioorganic Med. Chem.* **2013**, *21*, 5945–5954.

[95] K. Mahéo, F. Morel, S. Langouët, H. Kramer, E. Le Ferrec, B. Ketterer, A. Guillouzo, *Cancer Res.* **1997**, *57*, 3649–3652.

[96] J. D. Brooks, V. G. Paton, G. Vidanes, *Cancer Epidemiol. Biomarkers Prev.* **2001**, *10*, 949–954.

[97] S. B. Jones, J. D. Brooks, *BMC Cancer* **2006**, *6*, DOI 10.1186/1471-2407-6-62.

[98] M. H. Traka, A. Melchini, J. Coode-Bate, O. Al Kadhi, S. Saha, M. Defernez, P. Troncoso-Rey, H. Kibblewhite, C. M. O'Neill, F. Bernuzzi, L. Mythen, J. Hughes, P. W. Needs, J. R. Dainty, G. M. Savva, R. D. Mills, R. Y. Ball, C. S. Cooper, R. F. Mithen, *Am. J. Clin. Nutr.* **2019**, *109*, 1133–1144.

[99] S. Tahata, S. V. Singh, Y. Lin, E. R. Hahm, J. H. Beumer, S. M. Christner, U. N. Rao, C. Sander, A. A. Tarhini, H. Tawbi, L. K. Ferris, M. Wilson, A. Rose, C. M. Dietz, E. Hughes, J. W. Fahey, S. A. Leachman, P. B. Cassidy, L. H. Butterfield, H. M. Zarour, J. M. Kirkwood, *Cancer Prev. Res.* **2018**, *11*, 429–437.

[100] Z. Bahadoran, M. Tohidi, P. Nazeri, M. Mehran, F. Azizi, P. Mirmiran, *Int. J. Food Sci. Nutr.* **2012**, *63*, 767–771.

[101] R. H. Brown, C. Reynolds, A. Brooker, P. Talalay, J. W. Fahey, *Respir. Res.* **2015**, *16*, 1–12.

[102] E. L. Carpenter, M. N. Le, C. L. Miranda, R. L. Reed, J. F. Stevens, A. K. Indra, G. Ganguli-Indra, *Front. Pharmacol.* **2018**, *9*, 1–10.

[103] Q. V. Vo, C. Trenerry, S. Rochfort, J. Wadeson, C. Leyton, A. B. Hughes, *Bioorganic Med. Chem.* **2014**, *22*, 856–864.

[104] A. Chimiak, W. Przychodzen, J. Rachon, *Heteroat. Chem.* **2002**, *13*, 169–194.

[105] S. R. Jensen, A. Kjaer, *Acta Chem. Scand.* **1971**, *25*, 3891–3893.

[106] G. Kumaran, G. H. Kulkarni, *J. Org. Chem.* **1997**, *62*, 1516–1520.

[107] B. Nitroethenes, O. S. Vasil, Y. A. Vereshchagina, E. S. Ostroglyadov, G. R. Fattakhova, D. V Beskrovnyi, S. M. Aleksandrova, **2004**, *74*, 1108–1114.

[108] A. A. B. Robertson, N. P. Botting, *Tetrahedron* **1999**, *55*, 13269–13284.

[109] L. Latxague, C. Gardrat, J. L. Coustille, M. C. Viaud, P. Rollin, *J. Chromatogr. A* **1991**, *586*, 166–170.

[110] M. H. Benn, *Can. J. Chem.* **1964**, *42*, 163–164.

[111] M. H. Benn, D. Meakin, *Can. J. Biochem.* **1965**, *43*, 1874–1877.

[112] M. H. Benn, *Can. J. Chem.* **1963**, *41*, 2836–2838.

[113] M. H. Benn, *Can. J. Chem.* **1965**, *43*, 1–5.

[114] S. Chevolleau, B. Joseph, P. Rollin, J. Tulliez, *J. Label. Compd. Radiopharm.* **1993**, *33*, 671–679.

[115] S. Chevolleau, N. Gasc, P. Rollin, J. Tulliez, *J. Agric. Food Chem.* **1997**, *45*, 4290–4296.

[116] H. Streicher, L. Latxague, T. Wiemann, P. Rollin, J. Theim, *J. Carbohydr. Res.* **1996**, *278*, 257–270.

[117] R. Iori, P. Rollin, H. Streicher, J. Thiem, S. Palmieri, *Fed. Eur. Biochem. Soc. J.* **1996**, *385*, 87–90.

[118] M. Blanc-Muesser, H. Driguez, B. Joseph, M. C. Viaud, P. Rollin, *Tetrahedron Lett.* **1990**, *31*, 3867–3868.

[119] F. Bertelsen, G. Gissel-Nielsen, A. Kjaer, T. Skrydstrup, *Phytochemistry* **1988**, *27*, 3743–3749.

[120] A. Kjaer, T. Skrydstrup, *Acta Chem. Scand.* **1987**, *41*, 29–33.

[121] B. Joseph, P. Rollin, *J. Carbohydr. Chem.* **1993**, *12*, 1127–1138.

[122] S. Lazar, P. Rollin, *Tetrahedron Lett.* **1994**, *35*, 2173–2174.

[123] A. Bourderioux, M. Lefoix, D. Gueyrard, A. Tatibouët, S. Cottaz, S. Arzt, W. P. Burmeister, P. Rollin, *Org. Biomol. Chem.* **2005**, *3*, 1872–1879.

[124] J. B. Lambert, S. M. Wharry, *J. Org. Chem.* **1981**, *46*, 3193–3196.

[125] G. Cutolo, F. Reise, M. Schuler, R. Nehmé, G. Despras, J. Brekalo, P. Morin, P. Y. Renard, T. K. Lindhorst, A. Tatibouët, *Org. Biomol. Chem.* **2018**, *16*, 4900–4913.

[126] D. Gueyrard, R. Iori, A. Tatibouët, P. Rollin, *European J. Org. Chem.* **2010**, 3657–3664.

[127] D. Nowicki, O. Rodzik, A. Herman-Antosiewicz, A. Szalewska-Pałasz, *Sci. Rep.* **2016**, *6*, 1–12.

[128] L. Ugolini, G. Cilia, E. Pagnotta, L. Malaguti, V. Capano, I. Guerra, L. Zavatta, S. Albertazzi, R. Matteo, L. Lazzeri, L. Righetti, A. Nanetti, *Biomolecules* **2021**, *11*, 1–22.

[129] A. Nanetti, L. Ugolini, G. Cilia, E. Pagnotta, L. Malaguti, I. Cardaio, R. Matteo, L. Lazzeri, *Microorganisms* **2021**, *9*, 1–19.

[130] A. Borges, A. C. Abreu, C. Ferreira, *J. Food Sci. Technol.* **2015**, *52*, 4737–4748.

[131] J. Melrose, *Biomedicines* **2019**, *7*, 1–28.

[132] P. Soundararajan, J. S. Kim, *Molecules* **2018**, *23*, DOI 10.3390/molecules23112983.

[133] F. S. Hanschen, E. Lamy, M. Schreiner, S. Rohn, *Angew. Chemie - Int. Ed.* **2014**, *53*, 11430–11450.

[134] G. Tian, P. Tang, R. Xie, L. Cheng, Q. Yuan, J. Hu, *Food Chem.* **2016**, *199*, 301–306.

[135] J. Zhang, X. Li, P. Ge, B. Zhang, L. Wen, C. Gu, X. Zhou, *Sep. Purif. Rev.* **2022**, *51*, 330–339.

[136] D. Cerniauskaite, J. Rousseau, A. Sackus, P. Rollin, A. Tatibouët, *European J. Org. Chem.* **2011**, 2293–2300.

[137] M. Mavratzotis, S. Cassel, S. Montaut, P. Rollin, *Molecules* **2018**, *23*, 1–15.

[138] M. S. C. Pedras, Q. H. To, G. Schatte, *Chem. Commun.* **2016**, *52*, 2505–2508.

[139] M. S. C. Pedras, Q. H. To, *J. Label. Compd. Radiopharm.* **2018**, *61*, 94–106.

[140] N. E. Davidson, T. J. Rutherford, N. P. Botting, *Carbohydr. Res.* **2001**, *330*, 295–307.

[141] C. Kanstrup, C. C. Jimidar, J. Tomas, G. Cutolo, C. Crocoll, M. Schuler, P. Klahn, A. Tatibouët, H. H. Nour-Eldin, *Int. J. Mol. Sci.* **2023**, *24*, DOI 10.3390/ijms24020920.

[142] C. C. Jimidar, L. Wiese, M. Stirz, U. Beutling, A. Schallmey, M. Brönstrup, P. Klahn, in *Poster 34. Irseer Naturstofftage*, **2022**.

[143] E. M. Williams, R. F. Little, A. M. Mowday, M. H. Rich, J. V. E. Chan-hyams, J. N. Copp, J. B. Smaill, A. V Patterson, D. F. Ackerley, *Biochem. J.* **2015**, *471*, 131–153.

[144] P. Eva, F. Castillo, C. Moreno-vivi, **2008**, *32*, 474–500.

[145] M. Yuan, Y. Wu, C. Zhao, Z. Chen, L. Su, H. Yang, J. Song, *Theranostics* **2022**, *12*, 1459–1485.

[146] J. Qiao, M. Wang, M. Cui, Y. Fang, H. Li, C. Zheng, Z. Li, Y. Xu, H. Hua, D. Li, *J. Pharm. Biomed. Anal.* **2021**, *203*, 114199.

[147] A. Ryan, *Br. J. Pharmacol.* **2017**, *174*, 2161–2173.

[148] N. Koppel, V. M. Rekdal, E. P. Balskus, *Science (80-.).* **2017**, *356*, 1–11.

[149] T. Sousa, R. Paterson, V. Moore, A. Carlsson, B. Abrahamsson, A. W. Basit, E. Development, R. Astrazeneca, D. Charnwood, L. Le, *Int. J. Pharm.* **2008**, *363*, 1–25.

[150] P. L. Carl, P. K. Chakravarty, J. A. Katzenellenborgen, *J. Med. Chem.* **1981**, *24*, 479–480.

[151] K. Knop, R. Hoogenboom, D. Fischer, U. S. Schubert, *Angew. Chemie - Int. Ed.* **2010**, *49*, 6288–6308.

[152] P. Klahn, M. Brönstrup, *Nat. Prod. Rep.* **2017**, *34*, 832–885.

[153] N. Schneegans, U. Wittstock, *plant J.* **2019**, *99*, 329–343.

[154] P. J. Shilling, K. Mirzadeh, A. J. Cumming, M. Widesheim, Z. Köck, D. O. Daley, *Commun. Biol.* **2020**, *3*, DOI 10.1038/s42003-020-0939-8.

[155] SeeSAR version 14.0.0; BioSolveIT GmbH, **2024**, www.biosolveit.de/SeeSAR.

[156] E. Johansson, G. N. Parkinson, W. A. Denny, S. Neidle, *J. Med. Chem.* **2003**, *46*, 4009–4020.

[157] N. Schneider, G. Lange, S. Hindle, R. Klein, M. Rarey, *J. Comput. Aided. Mol. Des.* **2013**, *27*, 15–29.

[158] C. C. Jimidar, C. S. G. Ganskow, M. D. Kagho, A. Chakrabarti, M. Zollo, U. Beutling, M. Brönstrup, S. A. Sieber, S. M. Hacker, P. Klahn, *ChemRxiv* **2024**, DOI: 10.26434/chemrxiv-2024-f8x8z.

[159] I. Gozlan, A. Rotstein, D. Avisar, *Chemosphere* **2013**, *91*, 985–992.

[160] Z. Yongxin, C. Hoogmartens, A. Van Schepdael, E. Roets, J. Hoogmartens, *J. Liq. Chromatogr. Relat. Technol.* **1999**, *22*, 1403–1415.

[161] A. Bourderioux, M. Lefoix, D. Gueyrard, A. Tatibouët, S. Cottaz, S. Arzt, W. P. Burmeister, P. Rollin, *Org. Biomol. Chem.* **2005**, *3*, 1872.

[162] A. Backenköhler, D. Eisenschmidt, N. Schneegans, M. Strieker, W. Brandt, U. Wittstock, *PLoS One* **2018**, *13*, 1–18.

[163] A. Basak, *Indian J. Clin. Biochem.* **2007**, *22*, 156–160.

[164] Á. L. García-Ponce, B. Martínez-Poveda, Á. Blanco-López, M. Á. Medina, A. R. Quesada, *Biochem. Mol. Biol. Educ.* **2019**, *47*, 341–347.

[165] P. Dadgostar, *Infect. Drug Resist.* **2019**, *12*, 3903–3910.

[166] N. R. Naylor, R. Atun, N. Zhu, K.

Kulasabanathan, S. Silva, A. Chatterjee, G. M. Knight, J. V Robotham, *Antimicrob. Resist. Infect. Control* **2018**, *7*, 1–17.

[167] M. A. Abushaheen, Muzaheed, A. J. Fatani, M. Alosaimi, W. Mansy, M. George, S. Acharya, S. Rathod, D. D. Divakar, C. Jhugroo, S. Vellappally, A. A. Khan, J. Shaik, P. Jhugroo, *Disease-a-Month* **2020**, *66*, DOI 10.1016/j.disamonth.2020.100971.

[168] F. C. Tenover, *Am. J. Infect. Control* **2006**, *34*, DOI 10.1016/j.ajic.2006.05.219.

[169] G. Zhou, Q. S. Shi, X. M. Huang, X. B. Xie, *Int. J. Mol. Sci.* **2015**, *16*, 21711–21733.

[170] B. Khameneh, R. Diab, K. Ghazvini, B. S. Fazly Bazzaz, *Microb. Pathog.* **2016**, *95*, 32–42.

[171] A. F. Read, R. J. Woods, *Evol. Med. Public Heal.* **2014**, *2014*, 147.

[172] H. Hao, G. Cheng, Z. Iqbal, X. Ai, H. I. Hussain, L. Huang, M. Dai, Y. Wang, Z. Liu, Z. Yuan, *Front. Microbiol.* **2014**, *5*, 1–11.

[173] C. L. Ventola, *Pharm. Ther.* **2015**, *40*, 277–283.

[174] A. Maguire, I. Douglas, L. Smeeth, M. Thompson, *Pharmacoepidemiol. Drug Saf.* **2007**, *16*, 228–228.

[175] N. Graetz, J. Friedman, A. Osgood-Zimmerman, R. Burstein, M. H. Biehl, C. Shields, J. F. Mosser, D. C. Casey, A. Deshpande, L. Earl, R. C. Reiner, S. E. Ray, N. Fullman, A. J. Levine, R. W. Stubbs, B. K. Mayala, J. Longbottom, A. J. Browne, S. Bhatt, D. J. Weiss, P. W. Gething, A. H. Mokdad, S. S. Lim, C. J. L. Murray, E. Gakidou, S. I. Hay, *Nature* **2018**, *555*, 48–53.

[176] A. L. Hersh, K. E. Fleming-Dutra, D. J. Shapiro, D. Y. Hyun, L. A. Hicks, *JAMA Intern. Med.* **2016**, *176*, 1870–1872.

[177] C. H. Lim, M. G. Choi, M. K. Baeg, S. J. Moon, J. S. Kim, Y. K. Cho, J. M. Park, I. S. Lee, S. W. Kim, K. Y. Choi, *Gut Liver* **2014**, *8*, 165–169.

[178] D. J. Morgan, I. N. Okeke, R. Laxminarayan, E. N. Perencevich, S. Weisenberg, *Lancet Infect. Dis.* **2011**, *11*, 692–701.

[179] M. Woolhouse, C. Waugh, M. R. Perry, H. Nair, *J. Glob. Health* **2016**, *6*, 1–5.

[180] J. G. Bartlett, D. N. Gilbert, B. Spellberg, *Clin. Infect. Dis.* **2013**, *56*, 1445–1450.

[181] A. Zapun, C. Contreras-Martel, T. Vernet, *FEMS Microbiol. Rev.* **2008**, *32*, 361–385.

[182] J. Silva, *Curr. Ther. Res.* **1996**, *57*, 30–35.

[183] B. Becker, M. A. Cooper, *ACS Chem. Biol.* **2013**, *8*, 105–115.

[184] E. Kharrhoubi, *Trends Microbiol.* **1994**, *2*, 347–353.

[185] I. Phillips, A. King, K. Shannon, *Am. J. Med.* **1986**, *80*, 48–55.

[186] J. W. Chow, V. Kak, I. You, S. J. Kao, J. Petrin, D. B. Clewell, S. A. Lerner, G. H. Miller, K. J. Shaw, *Antimicrob. Agents Chemother.* **2001**, *45*, 2691–2694.

[187] U. Över, D. Gür, S. Ünal, G. H. Miller, *Clin. Microbiol. Infect.* **2001**, *7*, 470–478.

[188] G. H. Miller, F. J. Sabatelli, R. S. Hare, Y. Glupczynski, P. Mackey, D. Shlaes, K. Shimizu, K. J. Shaw, *Clin. Infect. Dis.* **1997**, *24*, 46–62.

[189] K. Dornbusch, G. H. Miller, R. S. Hare, K. J. Shaw, *J. Antimicrob. Chemother.* **1990**, *26*, 269–278.

[190] K. Poole, *Antimicrob. Agents Chemother.* **2005**, *49*, 479–487.

[191] L. Wondrack, M. Massa, B. V. Yang, J. Sutcliffe, *Antimicrob. Agents Chemother.* **1996**, *40*, 992–998.

[192] E. Cundliffe, *Antimicrob. Agents Chemother.* **1992**, *36*, 348–352.

[193] C. Vilches, C. Hernandez, C. Mendez, J. A. Salas, *J. Bacteriol.* **1992**, *174*, 161–165.

[194] B. Weisblum, *Drug Resist. Updat.* **1998**, *1*, 29–41.

[195] L. M. Weigel, D. B. Clewell, S. R. Gill, N. C. Clark, L. K. McDougal, S. E. Flannagan, J. F. Kolonay, J. Shetty, G. E. Killgore, F. C. Tenover, *Science (80-.).* **2003**, *302*, 1569–1571.

[196] S. Chang, D. M. Sievert, G. R. Pupp, W. J. Brown, D. Ph, D. Cardo, S. K. Fridkin, *N. Engl. J. Med.* **2003**, *348*, 1342–1347.

[197] C. T. Walsh, S. L. Fisher, I. S. Park, M. Prahalad, Z. Wu, *Chem. Biol.* **1996**, *3*, 21–28.

[198] C. E. Maus, B. B. Plikaytis, T. M. Shinnick, *Antimicrob. Agents Chemother.* **2005**, *49*, 3192–3197.

[199] J. I. Wachino, Y. Arakawa, *Drug Resist. Updat.* **2012**, *15*, 133–148.

[200] S. Douthwaite, J. B. Prince, H. F. Noller, *Proc. Natl. Acad. Sci. U. S. A.* **1985**, *82*, 8330–8334.

[201] H. Yoshida, M. Bogaki, M. Nakamura, L. M. Yamanaka, S. Nakamura, *Antimicrob. Agents Chemother.* **1991**, *35*, 1647–1650.

[202] C. J. R. Willmott, A. Maxwell, *Antimicrob. Agents Chemother.* **1993**, *37*, 126–127.

[203] J. M. Blondeau, *Surv. Ophthalmol.* **2004**, *49*, 1–6.

[204] G. E. Dale, C. Broger, A. D'Arcy, P. G. Hartman, R. DeHoogt, S. Jolidon, I. Kompis, A. M. Labhardt, H. Langen, H. Locher, M. G. P. Page, D. Stüber, R. L. Then, B. Wipf, C. Oefner, *J. Mol. Biol.* **1997**, *266*, 23–30.

[205] A. Pikis, J. A. Donkersloot, W. J. Rodriguez, J. M. Keith, *J. Infect. Dis.* **1998**, *178*, 700–706.

[206] E. Y. Rosenberg, D. Ma, H. Nikaido, *J. Bacteriol.* **2000**, *182*, 1754–1756.

[207] M. Del Grosso, F. Iannelli, C. Messina, M. Santagati, N. Petrosillo, S. Stefani, G. Pozzi, A. Pantosti, *J. Clin. Microbiol.* **2002**, *40*, 774–778.

[208] L. J. V. Piddock, R. Wise, *J. Antimicrob. Chemother.* **1986**, *18*, 547–549.

[209] D. C. HOOPER, J. S. WOLFSON, *N. Engl. J. Med.* **2010**, *324*, 384–394.

[210] K. Sauer, P. Stoodley, D. M. Goeres, L. Hall-Stoodley, M. Burmølle, P. S. Stewart, T. Bjarnsholt, *Nat. Rev. Microbiol.* **2022**, *20*, 608–620.

[211] H. C. Flemming, J. Wingender, U. Szewzyk, P. Steinberg, S. A. Rice, S. Kjelleberg, *Nat. Rev. Microbiol.* **2016**, *14*, 563–575.

[212] C. Berne, C. K. Ellison, A. Ducret, Y. V. Brun, *Nat. Rev. Microbiol.* **2018**, *16*, 616–627.

[213] H. C. Flemming, J. Wingender, *Nat. Rev. Microbiol.* **2010**, *8*, 623–633.

[214] E. Trampari, E. R. Holden, G. J. Wickham, A. Ravi, L. de O. Martins, G. M. Savva, M. A. Webber, *npj Biofilms Microbiomes* **2021**, *7*, 1–13.

[215] B. Halan, K. Buehler, A. Schmid, *Trends Biotechnol.* **2012**, *30*, 453–465.

[216] J. Wingender, H. C. Flemming, *Int. J. Hyg. Environ. Health* **2011**, *214*, 417–423.

[217] Z. Khatoon, C. D. McTiernan, E. J. Suuronen, T. F. Mah, E. I. Alarcon, *Heliyon* **2018**, *4*, e01067.

[218] J. L. Del Pozo, R. Patel, *Clin. Pharmacol. Ther.* **2007**, *82*, 204–209.

[219] M. Burmølle, D. Ren, T. Bjarnsholt, S. J. Sørensen, *Trends Microbiol.* **2014**, *22*, 84–91.

[220] L. K. Vestby, T. Grønseth, R. Simm, L. L. Nesse, *Antibiotics* **2020**, *9*, DOI 10.3390/antibiotics9020059.

[221] L. Yang, Y. Liu, H. Wu, N. Høiby, S. Molin, Z. J. Song, *Int. J. Oral Sci.* **2011**,

3, 74–81.

[222] O. Guillaume, C. Butnarasu, S. Visentin, E. Reimhult, *Biofilm* **2022**, *4*, 100089.

[223] M. Cámara, W. Green, C. E. MacPhee, P. D. Rakowska, R. Raval, M. C. Richardson, J. Slater-Jefferies, K. Steventon, J. S. Webb, *npj Biofilms Microbiomes* **2022**, *8*, 1–8.

[224] H. Y. Liu, E. L. Prentice, M. A. Webber, *npj Antimicrob. Resist.* **2024**, *2*, 1–10.

[225] D. Dufour, V. Leung, C. M. Lévesque, *Endod. Top.* **2010**, *22*, 2–16.

[226] M. Klausen, A. Heydorn, P. Ragas, L. Lambertsen, A. Aaes-Jørgensen, S. Molin, T. Tolker-Nielsen, *Mol. Microbiol.* **2003**, *48*, 1511–1524.

[227] M. Zapotoczna, E. O'Neill, J. P. O'Gara, *PLoS Pathog.* **2016**, *12*, 1–6.

[228] S. Singh, S. Datta, K. B. Narayanan, K. N. Rajnish, *J. Genet. Eng. Biotechnol.* **2021**, *19*, DOI 10.1186/s43141-021-00242-y.

[229] T. Bjarnsholt, *APMIS. Suppl.* **2013**, 1–51.

[230] K. N. Kragh, J. B. Hutchison, G. Melaugh, C. Rodesney, A. E. L. Roberts, Y. Irie, P. Jensen, S. P. Diggle, R. J. Allen, V. Gordon, T. Bjarnsholt, *MBio* **2016**, *7*, 1–11.

[231] J. Kwiecinski, M. Peetermans, L. Liesenborghs, M. et. a. Na, *J. Infect. Dis.* **2016**, *213*, 139–148.

[232] T. Vanassche, M. Peetermans, L. N. L. Van Aelst, W. E. Peetermans, J. Verhaegen, D. M. Missiakas, O. Schneewind, M. F. Hoylaerts, P. Verhamme, *J. Infect. Dis.* **2013**, *208*, 92–100.

[233] M. H. Muhammad, A. L. Idris, X. Fan, Y. Guo, Y. Yu, X. Jin, J. Qiu, X. Guan, T. Huang, *Front. Microbiol.* **2020**, *11*, 1–20.

[234] M. Otto, *Annu. Rev. Med.* **2013**, *64*, 175–188.

[235] E. Mhatre, D. J. Snyder, E. Sileo, C. B. Turner, S. W. Buskirk, N. L. Fernandez, M. B. Neiditch, C. M. Waters, V. S. Cooper, *Proc. Natl. Acad. Sci. U. S. A.* **2020**, *117*, 21647–21657.

[236] R. M. Donlan, *Clin. Infect. Dis.* **2001**, *33*, 1387–1392.

[237] J. L. Lister, A. R. Horswill, *Front. Cell. Infect. Microbiol.* **2014**, *4*, 1–9.

[238] S. M. Soto, *Virulence* **2013**, *4*, 223–229.

[239] G. D. Geske, R. J. Wezeman, A. P. Siegel, H. E. Blackwell, *J. Am. Chem. Soc.* **2005**, *127*, 12762–12763.

[240] M. Martins, M. McCusker, L. Amaral, S. Fanning, *Lett. Drug Des. Discov.* **2011**, *8*, 114–123.

[241] P. Lembre, C. Lorentz, P. Di, *The Complex World of Polysaccharides* **2012**, DOI 10.5772/51213.

[242] I. Alav, J. M. Sutton, K. M. Rahman, *J. Antimicrob. Chemother.* **2018**, *73*, 2003–2020.

[243] A. Lal, *Resonance* **2009**, *14*, 866–871.

[244] J. B. Kaplan, *J. Dent. Res.* **2010**, *89*, 205–218.

[245] K. P. Rumbaugh, K. Sauer, *Nat. Rev. Microbiol.* **2020**, *18*, 571–586.

[246] W. K. Redman, G. S. Welch, K. P. Rumbaugh, *Front. Cell. Infect. Microbiol.* **2020**, *10*, 1–7.

[247] W. K. Redman, G. S. Welch, A. C. Williams, A. J. Damron, W. O. Northcut, K. P. Rumbaugh, *Biofilm* **2021**, *3*, 100061.

[248] P. Saxena, Y. Joshi, K. Rawat, R. Bisht, *Indian J. Microbiol.* **2019**, *59*, 3–12.

[249] R. Grande, V. Puca, R. Muraro, *Expert Opin. Ther. Pat.* **2020**, *30*, 897–900.

[250] P. Bowler, C. Murphy, R. Wolcott, *Antimicrob. Resist. Infect. Control* **2020**, *9*, 1–5.

[251] S. Hathroubi, M. A. Mekni, P.

Domenico, D. Nguyen, M. Jacques, *Microb. Drug Resist.* **2017**, *23*, 147–156.

[252] H. Van Acker, T. Coenye, *J. Biol. Chem.* **2016**, *291*, 12565–12572.

[253] T. Ishida, T. Ikeda, N. Takiguchi, A. Kuroda, H. Ohtake, J. Kato, *Appl. Environ. Microbiol.* **2007**, *73*, 3183–3188.

[254] P. K. Singh, M. R. Parsek, E. P. Greenberg, M. J. Welsh, *Nature* **2002**, *417*, 552–555.

[255] S. K. Roy, N. Kumari, S. Pahwa, U. C. Agrahari, K. K. Bhutani, S. M. Jachak, H. Nandanwar, *NorA Efflux Pump Inhibitory Activity of Coumarins from Mesua Ferrea*, Elsevier B.V., **2013**.

[256] J. H. Lee, J. H. Park, H. S. Cho, S. W. Joo, M. H. Cho, J. Lee, *Biofouling* **2013**, *29*, 491–499.

[257] M. G. da Cunha, J. de Cássia Orlandi Sardi, I. A. Freires, M. Franchin, P. L. Rosalen, *Microb. Pathog.* **2020**, *139*, 103855.

[258] A. S. Tajani, Z. A. Tehranizadeh, A. Pourmohammad, A. Pourmohammad, M. Iranshahy, F. Farhadi, V. Soheili, B. S. Fazly Bazzaz, *Iran. J. Basic Med. Sci.* **2023**, *26*, 445–452.

[259] L. Yang, S. Li, X. Qin, G. Jiang, J. Chen, B. Li, X. Yao, P. Liang, Y. Zhang, W. Ding, *Front. Microbiol.* **2017**, *8*, 1–10.

[260] N. Bhattarai, A. A. Kumbhar, Y. R. Pokharel, P. N. Yadav, *Anticancer Potential of Coumarin and Its Derivatives*, **2021**.

[261] K. Murase, K. L. Morrison, P. Y. Tam, R. L. Stafford, F. Jurnak, G. A. Weiss, *Chem. Biol.* **2003**, *10*, 161–168.

[262] P. Kumar, D. K. Mahato, M. Kamle, T. K. Mohanta, S. G. Kang, *Front. Microbiol.* **2017**, *7*, 1–10.

[263] E. R. El-sawy, M. S. Abdel-aziz, H. Abdelmegeed, G. Kirsch, *Molecules* **2024**, *29*, 1–21.

[264] B. Rostom, R. Karaky, I. Kassab, M. Sylla-Iyarreta Veitía, *Eur. J. Pharmacol.* **2022**, *922*, DOI 10.1016/j.ejphar.2022.174867.

[265] K. Kasperkiewicz, M. B. Ponczek, J. Owczarek, P. Guga, E. Budzisz, *Molecules* **2020**, *25*, 1–24.

[266] S. Mishra, A. Pandey, S. Manvati, *Heliyon* **2020**, *6*, e03217.

[267] M. Z. Hassan, H. Osman, M. A. Ali, M. J. Ahsan, *Eur. J. Med. Chem.* **2016**, *123*, 236–255.

[268] Y. Wu, J. Xu, Y. Liu, Y. Zeng, G. Wu, *Front. Oncol.* **2020**, *10*, 1–11.

[269] F. J. Reen, J. A. Gutiérrez-Barranquero, M. L. Parages, F. O'Gara, *Appl. Microbiol. Biotechnol.* **2018**, *102*, 2063–2073.

[270] J. A. Gutiérrez-Barranquero, F. J. Reen, R. R. McCarthy, F. O'Gara, *Appl. Microbiol. Biotechnol.* **2015**, *99*, 3303–3316.

[271] A. H. Elmaidomy, N. H. Shady, K. M. Abdeljawad, M. B. Elzamkan, H. H. Helmy, E. A. Tarshan, A. N. Adly, Y. H. Hussien, N. G. Sayed, A. Zayed, U. R. Abdelmohsen, *RSC Adv.* **2022**, *12*, 29078–29102.

[272] A. E. Clatworthy, E. Pierson, D. T. Hung, *Nat. Chem. Biol.* **2007**, *3*, 541–548.

[273] J. Zou, Y. Liu, R. Guo, Y. Tang, Z. Shi, M. Zhang, W. Wu, Y. Chen, K. Hou, *Nat. Prod. Commun.* **2021**, *16*, DOI 10.1177/1934578X20987744.

[274] D. F. V. Lewis, Y. Ito, B. G. Lake, *Toxicol. Vitr.* **2006**, *20*, 256–264.

[275] A. Stefanachi, F. Leonetti, L. Pisani, M. Catto, A. Carotti, *Coumarin: A Natural, Privileged and Versatile Scaffold for Bioactive Compounds*, **2018**.

[276] B. G. Lake, *Food Chem. Toxicol.* **1999**, *37*, 423–453.

[277] B. G. Lake, T. J. B. Gray, J. G. Evans, Et.al., *Toxicol. iand Appl. Pharmacol.* **1989**, *97*, 311–323.

[278] A. J. Cohen, *Food Chem. Toxicol.* **1979**, *17*, 277–289.

[279] J. H. Fentem, J. R. Fry, *Comp. Biochem. Physiol.* **1993**, *104C*, 1–8.

[280] B. G. Lake, D. G. Walters, S. D. Gangolli, *Toxicol. Lett.* **1989**, *45*, 299–306.

[281] B. G. Lake, H. Gaudin, R. J. Price, D. G. Walters, *Food Chem. Toxicol.* **1992**, *30*, 105–115.

[282] S. L. Born, A. S. Fix, D. Caudill, L. D. Lehman-McKeeman, *Toxicol. Appl. Pharmacol.* **1998**, *151*, 45–56.

[283] J. H. Fentem, J. R. Fry, *Xenobiotica* **1992**, *22*, 357–367.

[284] P. A. Gibbs, K. Janakidevi, G. Feuer, *Can. J. Biochem.* **1971**, *49*, 177–184.

[285] G. Feuer, *Chem. Biol. Interact.* **1970**, *2*, 203–216.

[286] A. Vetrivel, M. Ramasamy, P. Vetrivel, S. Natchimuthu, S. Arunachalam, G.-S. Kim, R. Murugesan, *Biologics* **2021**, *1*, 312–336.

[287] F. Hemmati, M. A. Rezaee, S. Ebrahimzadeh, L. Yousefi, R. Nouri, H. S. Kafil, P. Gholizadeh, *Mol. Biotechnol.* **2021**, *63*, 569–586.

[288] L. Hall-Stoodley, J. W. Costerton, P. Stoodley, *Nat. Rev. Microbiol.* **2004**, *2*, 95–108.

[289] N. Høiby, T. Bjarnsholt, M. Givskov, S. Molin, O. Ciofu, *Int. J. Antimicrob. Agents* **2010**, *35*, 322–332.

[290] V. Silva, L. Almeida, V. Gaio, N. Cerca, V. Manageiro, M. Caniça, J. L. Capelo, G. Igrejas, P. Poeta, *Pathogens* **2021**, *10*, DOI 10.3390/pathogens10080970.

[291] M. Gulati, C. J. Nobile, *Microbes Infect.* **2017**, *18*, 310–321.

[292] S. Fanning, A. P. Mitchell, *PLoS Pathog.* **2012**, *8*, 1–4.

[293] J. V Desai, A. P. Mitchell, D. R. Andes, *Cold Spring Harb Perspect Med* **2014**, *4*, 1–18.

[294] A. Boudet, P. Sorlin, C. Pouget, R. Chiron, J. P. Lavigne, C. Dunyach-Remy, H. Marchandin, *Front. Microbiol.* **2021**, *12*, DOI 10.3389/fmicb.2021.750489.

[295] F. F. Tuon, L. R. Dantas, P. H. Suss, V. S. Tasca Ribeiro, *Pathogens* **2022**, *11*, DOI 10.3390/pathogens11030300.

[296] E. Banin, M. L. Vasil, E. P. Greenberg, *Proc. Natl. Acad. Sci. U. S. A.* **2005**, *102*, 11076–11081.

[297] O. Ciofu, T. Tolker-Nielsen, *Front. Microbiol.* **2019**, *10*, DOI 10.3389/fmicb.2019.00913.

[298] M. T. T. Thi, D. Wibowo, B. H. A. Rehm, *Int. J. Mol. Sci.* **2020**, *21*, 1–25.

[299] C. Tsui, E. F. Kong, M. A. Jabra-Rizk, *Pathog. Dis.* **2016**, *74*, ftw018.

[300] T. Atriwal, K. Azeem, F. M. Husain, A. Hussain, M. N. Khan, M. F. Alajmi, M. Abid, *Front. Microbiol.* **2021**, *12*, DOI 10.3389/fmicb.2021.638609.

[301] J. H. Lee, Y. G. Kim, H. S. Cho, S. Y. Ryu, M. H. Cho, J. Lee, *Phytomedicine* **2014**, *21*, 1037–1042.

[302] Z. He, W. Jiang, Y. Jiang, J. Dong, Z. Song, J. Xu, W. Zhou, *J. Oral Microbiol.* **2022**, *14*, DOI 10.1080/20002297.2022.2055523.

[303] F. A. Qais, M. S. Khan, I. Ahmad, F. M. Husain, R. A. Khan, I. Hassan, S. A. Shahzad, W. Alharbi, *ACS Omega* **2021**, *6*, 18823–18835.

[304] K. Xu, J. L. Wang, M. P. Chu, C. Jia, *J. Mycol. Med.* **2019**, *29*, 28–34.

[305] Y. Zhang, A. Sass, H. Van Acker, J. Wille, B. Verhasselt, F. Van Nieuwerburgh, V. Kaever, A. Crabbé, T. Coenye, *Front. Microbiol.* **2018**, *9*, 1–10.

[306] R. M. Donlan, *ASAIO J.* **2000**, *46*, S47-52.

[307] C. Y. Chu, Y. Y. Tsai, C. J. Wang, W. L. Lin, T. H. Tseng, *Eur. J. Pharmacol.* **2001**, *416*, 25–32.

[308] G. A. Mohamed, S. R. M. Ibrahim, E. S. Elkhayat, R. S. El Dine, *Bull. Fac. Pharmacy, Cairo Univ.* **2014**, *52*, 269–284.

[309] S. M. Yu, D. H. Hu, J. J. Zhang, *Mol. Med. Rep.* **2015**, *12*, 3869–3873.

[310] J. L. Rodrigues, D. Gomes, L. R. Rodrigues, *Molecules* **2022**, *27*, 1–20.

[311] C. Rohrbacher, R. Zscherp, S. C. Weck, P. Klahn, C. Ducho, *Chem. - A Eur. J.* **2023**, *29*, DOI 10.1002/chem.202202408.

[312] R. Zscherp, J. Coetzee, J. Vornweg, J. Grunenberg, J. Herrmann, R. Müller, P. Klahn, *Chem. Sci.* **2021**, *12*, 10179–10190.

[313] D. C. Aldridge, W. B. Turner, *J. Chem. SOG.* **1967**, 923–928.

[314] E. Skellam, *Nat. Prod. Rep.* **2017**, *34*, 1252–1263.

[315] K. Scherlach, D. Boettger, N. Remme, C. Hertweck, *Nat. Prod. Rep.* **2010**, *27*, 869–886.

[316] T. Udagawa, J. Yuan, D. Panigrahy, Y. H. Chang, J. Shah, R. J. D'Amato, *J. Pharmacol. Exp. Ther.* **2000**, *294*, 421–427.

[317] M. Nukina, *Agric. Biol. Chem.* **1987**, *51*, 2625–2628.

[318] A. Probst, C. Tamm, *Helv. Chim. Acta* **1981**, *64*, 18–19.

[319] Z. Zhang, X. Min, J. Huang, Y. Zhong, Y. Wu, X. Li, Y. Deng, Z. Jiang, Z. Shao, L. Zhang, F. He, *Mar. Drugs* **2016**, *14*, DOI 10.3390/md14120233.

[320] G. Ding, H. Lou Wang, L. Chen, A. J. Chen, J. Lan, X. D. Chen, H. W. Zhang, H. Chen, X. Z. Liu, Z. M. Zou, *J. Antibiot. (Tokyo).* **2012**, *65*, 143–145.

[321] W. Keller-Schierlein, E. Kupfer, *Helv. Chim. Acta* **1979**, *62*, 1501–1524.

[322] Y. Zhang, R. Tian, S. Liu, X. Chen, X. Liu, Y. Che, *Bioorganic Med. Chem.* **2008**, *16*, 2627–2634.

[323] W. Rothweiler, C. H. Tamm, *Experientia* **1966**, *22*, 750–752.

[324] M. I. T. T. G. N. I. N. J. Lin, *Chem. Pharm. Bull.* **1973**, *21*, 2268–2277.

[325] M. Binder, C. Tamm, W. B. Turner, H. Minato, *J. Chem. Soc. Perkin Trans. 1* **1973**, 1146.

[326] G. Ding, H. Wang, L. Li, A. J. Chen, L. Chen, H. Chen, H. Zhang, X. Liu, Z. Zou, *European J. Org. Chem.* **2012**, 2516–2519.

[327] W. S. Horn, M. S. J. Simmonds, R. E. Schwartz, W. M. Blaney, *Tetrahedron* **1995**, *51*, 3969–3978.

[328] S. Huang, H. Chen, W. Li, X. Zhu, W. Ding, C. Li, *Mar. Drugs* **2016**, *14*, 1–12.

[329] C. Chen, J. Wang, J. Liu, H. Zhu, B. Sun, J. Wang, J. Zhang, Z. Luo, G. Yao, Y. Xue, Y. Zhang, *J. Nat. Prod.* **2015**, *78*, 1193–1201.

[330] R. Liu, Z. Lin, T. Zhu, Y. Fang, Q. Gu, W. Zhu, *J. Nat. Prod.* **2008**, *71*, 1127–1132.

[331] H. Zhu, C. Chen, Q. Tong, X. Li, J. Yang, Y. Xue, Z. Luo, J. Wang, G. Yao, Y. Zhang, *Angew. Chemie* **2016**, *128*, 3547–3551.

[332] H. Zhu, C. Chen, Q. Tong, J. Yang, G. Wei, Y. Xue, J. Wang, Z. Luo, Y. Zhang, *Angew. Chemie - Int. Ed.* **2017**, *56*, 5242–5246.

[333] H. Zhu, C. Chen, Y. Xue, Q. Tong, X. N. Li, X. Chen, J. Wang, G. Yao, Z. Luo, Y. Zhang, *Angew. Chemie - Int. Ed.* **2015**, *54*, 13374–13378.

[334] T. Hirose, Y. Izawa, K. Koyama, S. Natori, K. Iida, I. Yahara, S. Shimaoka, K. Maruyama, *Chem. Pharm. Bull.* **1990**, *38*, 971–974.

[335] I. Foissner, G. O. Wasteneys, *Plant Cell*

Physiol. **2007**, *48*, 585–597.

[336] J. R. Peterson, T. J. Mitchison, *Chem. Biol.* **2002**, *9*, 1275–1285.

[337] W. Berger, M. Micksche, L. Elbling, *Exp. Cell Res.* **1997**, *237*, 307–317.

[338] R. Kretz, L. Wendt, S. Wongkanoun, J. J. Luangsa-Ard, F. Surup, S. E. Helaly, S. R. Noumeur, M. Stadler, T. E. B. Stradal, *Biomolecules* **2019**, *9*, DOI 10.3390/biom9020073.

[339] R. Dominguez, K. C. Holmes, *Annu. Rev. Biophys.* **2011**, *40*, 169–186.

[340] L. A. Cingolani, Y. Goda, *Nat. Rev. Neurosci.* **2008**, *9*, 344–356.

[341] T. D. Pollard, G. G. Borisy, *Cell* **2003**, *112*, 453–465.

[342] W. Kabsch, J. Vandekerckhove, *Annu. Rev. Biophys. Biomol. Struct.* **1992**, *21*, 49–76.

[343] N. Selve, A. Wegner, *J. Mol. Biol.* **1986**, *187*, 627–631.

[344] C. Revenu, R. Athman, S. Robine, D. Louvard, *Nat. Rev. Mol. Cell Biol.* **2004**, *5*, 635–646.

[345] D. A. Fletcher, R. D. Mullins, *Nature* **2010**, *463*, 485–492.

[346] S. Huang, D. E. Ingber, *Exp. Cell Res.* **2000**, *261*, 91–103.

[347] K. Keren, Z. Pincus, G. M. Allen, E. L. Barnhart, G. Marriott, A. Mogilner, J. A. Theriot, *Nature* **2008**, *453*, 475–480.

[348] A. Zemel, F. Rehfeldt, A. E. X. Brown, D. E. Discher, S. A. Safran, *J. Phys. Condens. Matter* **2010**, *22*, DOI 10.1088/0953-8984/22/19/194110.

[349] M. Olausson, N. Esfahani, J. Östlin, C. Hägglin, *Swed. Dent. J.* **2016**, *40*, 91–100.

[350] M. D. Flanagan, S. Lin, *J. Biol. Chem.* **1980**, *255*, 835–838.

[351] S. S. Brown, J. A. Spudich, *J. Cell Biol.* **1981**, *88*, 487–491.

[352] D. W. Goddette, C. Frieden, *Biochem. Biophys. Res. Commun.* **1985**, *128*, 1087–1092.

[353] S. L. Brenner, E. D. Korn, *J. Biol. Chem.* **1980**, *255*, 841–844.

[354] S. MacLean-Fletcher, T. D. Pollard, *Cell* **1980**, *20*, 329–341.

[355] J. A. Cooper, *J. Cell Biol.* **1987**, *105*, 1473–1478.

[356] S. B. Carter, *Nature* **1967**, *213*, 261–264.

[357] G. F. Smith, M. A. C. Ridler, J. A. Faunch, *Nature* **1967**, *216*, 1134–1135.

[358] E. Furuya, *Chem. Pharm. Bull.* **2002**, *30*, 1609–1617.

[359] W. Jiao, Y. Feng, J. W. Blunt, A. L. J. Cole, M. H. G. Munro, *J. Nat. Prod.* **2004**, *67*, 1722–1725.

[360] J. Lee, J. M. Yi, H. Kim, Y. J. Lee, J. S. Park, O. S. Bang, N. S. Kim, *Biol. Pharm. Bull.* **2014**, *37*, 6–12.

[361] J. S. Allingham, V. A. Klenchin, I. Rayment, *Cell. Mol. Life Sci.* **2006**, *63*, 2119–2134.

[362] I. Spector, F. Braet, N. R. Shochet, M. R. Bubb, *Microsc. Res. Tech.* **1999**, *47*, 18–37.

[363] G. Yuebo, J. L. S. Au, L. Jie, M. G. Wientjes, *Pharm. Res.* **1998**, *15*.

[364] K. A. Alvi, B. Nair, H. Pu, R. Ursino, C. Gallo, U. Mocek, *J. Org. Chem.* **1997**, *62*, 2148–2151.

[365] V. BETINA, D. MICEKOVA, P. NEMEC, *J. Gen. Microbiol.* **1972**, *71*, 343–349.

[366] K. T. Yuyama, L. Wendt, F. Surup, R. Kretz, C. Chepkirui, K. Wittstein, C. Boonlarppradab, S. Wongkanoun, J. Luangsa-Ard, M. Stadler, W. R. Abraham, *Biomolecules* **2018**, *8*, 1–13.

[367] S. S. Zhao, Y. Y. Zhang, W. Yan, L. L. Cao, Y. Xiao, Y. H. Ye, *FEMS Microbiol. Lett.* **2017**, *364*, 1–6.

[368] D. Cunningham, D. Schafer, S. W. Tanenbaum, M. Flashner, *J. Bacteriol.* **1979**, *137*, 925–932.

[369] M. Flashner, J. Rasmussen, B. H. Patwardhan, W. Tanenbaum, *J. Antibiot. (Tokyo).* **2015**, *35*, 1345–1350.

[370] W. Pongcharoen, V. Rukachaisirikul, S. Phongpaichit, N. Rungjindarnai, J. Sakayaroj, *J. Nat. Prod.* **2006**, *69*, 856–858.

[371] A. Makioka, M. Kumagai, H. Ohtomo, S. Kobayashi, T. Takeuchi, *Parasitol. Res.* **2002**, *88*, 454–459.

[372] A. L. Rampal, H. B. Pinkofsky, C. Y. Jung, *Biochemistry* **1980**, *19*, 679–683.

[373] R. Bloch, *Biochemistry* **1973**, *12*, 4799–4801.

[374] P. G. W. Plagemann, D. P. Richey, *BBA - Rev. Biomembr.* **1974**, *344*, 263–305.

[375] J. F. Griffin, A. L. Rampal, C. Y. Jung, *Proc. Natl. Acad. Sci. U. S. A.* **1982**, *79*, 3759–3763.

[376] S. Lin, J. A. Spudich, *J. Biol. Chem.* **1974**, *249*, 5778–5783.

[377] D. Xu, M. Luo, F. Liu, D. Wang, X. Pang, T. Zhao, L. Xu, X. Wu, M. Xia, X. Yang, *Sci. Rep.* **2017**, *7*, 1–9.

[378] J. A. Williams, J. Wolff, *Biochem. Biophys. Res. Commun.* **1971**, *44*, 422–425.

[379] J. G. Schofield, *Nat. new Biol.* **1971**, *234*, 215–216.

[380] H. Jayasuriya, K. B. Herath, J. G. Ondeyka, J. D. Polishook, G. F. Bills, A. W. Dombrowski, M. S. Springer, S. Siciliano, L. Malkowitz, M. Sanchez, Z. Guan, S. Tiwari, D. W. Stevenson, R. P. Borris, S. B. Singh, *J. Nat. Prod.* **2004**, *67*, 1036–1038.

[381] S. Rochfort, J. Ford, S. Ovenden, S. S. Wan, S. George, H. Wildman, R. M. Tait, B. Meurer-Grimes, S. Cox, J. Coates, D. Rhodes, *J. Antibiot. (Tokyo).* **2005**, *58*, 279–283.

[382] J. -L Robert, C. Tamm, *Helv. Chim. Acta* **1975**, *58*, 2501–2504.

[383] M. Binder, J.-R. Kiechel, C. Tamm, *Helv. Chim. Acta* **1970**, *53*, 1797–1812.

[384] J. C. Vederas, C. Tamm, *Helv. Chim. Acta* **1976**, *59*, 558–566.

[385] H. Oikawa, Y. Murakami, A. Ichihara, *J. Chem. Soc. Perkin Trans. 1* **1992**, 2955–2959.

[386] J. Schümann, C. Hertweck, *J. Am. Chem. Soc.* **2007**, *129*, 9564–9565.

[387] J. Kennedy, K. Auclair, S. G. Kendrew, C. Park, J. C. Vederas, C. R. Hutchinson, *Science (80-.).* **1999**, *284*, 1368–1372.

[388] Z. Song, R. J. Cox, C. M. Lazarus, T. J. Simpson, *ChemBioChem* **2004**, *5*, 1196–1203.

[389] K. Ishiuchi, T. Nakazawa, F. Yagishita, T. Mino, H. Noguchi, K. Hotta, K. Watanabe, *J. Am. Chem. Soc.* **2013**, *135*, 7371–7377.

[390] G. Stork, Y. Nakahara, Y. Nakahara, W. J. Greenlee, *J. Am. Chem. Soc.* **1978**, *100*, 7775–7777.

[391] G. Stork, E. Nakamura, *J. Am. Chem. Soc.* **1983**, *105*, 5510–5512.

[392] A. M. Haidle, A. G. Myers, *Proc. Natl. Acad. Sci. U. S. A.* **2004**, *101*, 12048–12053.

[393] E. Merifield, E. J. Thomas, *J. Chem. Soc. - Perkin Trans. 1* **1999**, 3269–3283.

[394] H. Dyke, P. G. Steel, E. J. Thomas, *J. Chem. Soc. - Perkin Trans. 1* **1989**, 525–528.

[395] H. Dyke, R. Sauter, P. Steel, E. J. Thomas, *J. Chem. Soc. Chem. Commun.* **1986**, 1447–1449.

[396] E. J. Thomas, J. W. F. Whitehead, *J. Chem. Soc. Chem. Commun.* **1986**, 727–728.

[397] E. J. Thomas, J. W. F. Whitehead, *J. Chem. Soc. Perkin Trans. 1* **1989**, 507–518.

[398] B. M. Trost, M. Ohmori, S. A. Boyd, H. Okawara, S. J. Brickner, *J. Am. Chem. Soc.* **1989**, *111*, 8281–8284.

[399] B. M. Trost, F. W. Gowland, *J. Org. Chem.* **1979**, *44*, 3448–3450.

[400] T. Schmidlin, P. E. Burckhardt, N. Waespe-Šarčevič, C. Tamm, *Helv. Chim. Acta* **1983**, *66*, 450–465.

[401] J. R. Reyes, N. Winter, L. Spessert, D. Trauner, *Angew. Chemie - Int. Ed.* **2018**, *57*, 15587–15591.

[402] E. Vedejs, S. J. Wittenberger, *J. Am. Soc.* **1990**, *112*, 4357–4364.

[403] E. Vedejs, J. G. Reid, J. D. Rodgers, S. J. Wittenberger, *J. Am. Chem. Soc.* **1990**, *112*, 4351–4357.

[404] E. Vedejs, J. G. Reid, *J. Am. Chem. Soc.* **1984**, *106*, 4617–4618.

[405] J. Xu, B. Lin, X. Jiang, Z. Jia, J. Wu, W. M. Dai, *Org. Lett.* **2019**, *21*, 830–834.